National Library of Canada
Bibliothèque nationale du Canada

Canadian Theses Service
Services des thèses canadiennes

Ottawa, Canada
K1A 0N4

CANADIAN THESES

THÈSES CANADIENNES

NOTICE

The quality of this microfiche is heavily dependent upon the quality of the original thesis submitted for microfilming. Every effort has been made to ensure the highest quality of reproduction possible.

If pages are missing, contact the university which granted the degree.

Some pages may have indistinct print especially if the original pages were typed with a poor typewriter ribbon or if the university sent us an inferior photocopy.

Previously copyrighted materials (journal articles, published tests, etc.) are not filmed.

Reproduction in full or in part of this film is governed by the Canadian Copyright Act, R.S.C. 1970, c. C-30.

AVIS

La qualité de cette microfiche dépend grandement de la qualité de la thèse soumise au microfilmage. Nous avons tout fait pour assurer une qualité supérieure de reproduction.

S'il manque des pages, veuillez communiquer avec l'université qui a conféré le grade.

La qualité d'impression de certaines pages peut laisser à désirer, surtout si les pages originales ont été dactylographiées à l'aide d'un ruban usé ou si l'université nous a fait parvenir une photocopie de qualité inférieure.

Les documents qui font déjà l'objet d'un droit d'auteur (articles de revue, examens publiés, etc.) ne sont pas microfilmés.

La reproduction, même partielle, de ce microfilm est soumise à la Loi canadienne sur le droit d'auteur, SRC 1970, c. C-30.

THIS DISSERTATION
HAS BEEN MICROFILMED
EXACTLY AS RECEIVED

LA THÈSE A ÉTÉ
MICROFILMÉE TELLE QUE
NOUS L'AVONS REÇUE

NL-339 (r.86/06)

Canada

THE UNIVERSITY OF ALBERTA

NUMERICAL SIMULATION OF THE ELECTRIC PRE-HEAT AND STEAM DRIVE BITUMEN RECOVERY PROCESS FOR THE ATHABASCA OIL SANDS

by

ⓒ ALLAN DAVID HIEBERT

A THESIS
SUBMITTED TO THE FACULTY OF GRADUATE STUDIES AND RESEARCH
IN PARTIAL FULFILMENT OF THE REQUIREMENTS FOR THE DEGREE
OF DOCTOR OF PHILOSOPHY

DEPARTMENT OF ELECTRICAL ENGINEERING

EDMONTON, ALBERTA
SPRING, 1986

Permission has been granted to the National Library of Canada to microfilm this thesis and to lend or sell copies of the film.

The author (copyright owner) has reserved other publication rights, and neither the thesis nor extensive extracts from it may be printed or otherwise reproduced without his/her written permission.

L'autorisation a été accordée à la Bibliothèque nationale du Canada de microfilmer cette thèse et de prêter ou de vendre des exemplaires du film.

L'auteur (titulaire du droit d'auteur) se réserve les autres droits de publication; ni la thèse ni de longs extraits de celle-ci ne doivent être imprimés ou autrement reproduits sans son autorisation écrite.

ISBN 0-315-37848-4

THE UNIVERSITY OF ALBERTA

RELEASE FORM

NAME OF AUTHOR	ALLAN DAVID HIEBERT
TITLE OF THESIS	NUMERICAL SIMULATION OF THE ELECTRIC PRE-HEAT AND STEAM DRIVE BITUMEN RECOVERY PROCESS FOR THE ATHABASCA OIL SANDS

DEGREE FOR WHICH THESIS WAS PRESENTED DOCTOR OF PHILOSOPHY

YEAR THIS DEGREE GRANTED SPRING, 1986

Permission is hereby granted to THE UNIVERSITY OF ALBERTA LIBRARY to reproduce single copies of this thesis and to lend or sell such copies for private, scholarly or scientific research purposes only.

The author reserves other publication rights, and neither the thesis nor extensive extracts from it may be printed or otherwise reproduced without the author's written permission.

(SIGNED) Allan Hiebert

PERMANENT ADDRESS:

B402 - 1919 UNIVERSITY DR. N.W
CALGARY, AB
CANADA T2N 4K4

DATED April 8 1986

THE UNIVERSITY OF ALBERTA

FACULTY OF GRADUATE STUDIES AND RESEARCH

The undersigned certify that they have read, and recommend to the Faculty of Graduate Studies and Research, for acceptance, a thesis entitled NUMERICAL SIMULATION OF THE ELECTRIC PRE-HEAT AND STEAM DRIVE BITUMEN RECOVERY PROCESS FOR THE ATHABASCA OIL SANDS submitted by ALLAN DAVID HIEBERT in partial fulfilment of the requirements for the degree of DOCTOR OF PHILOSOPHY in ELECTRICAL ENGINEERING.

F.E. Vermeulen

F.S. Chute

Supervisors

....

....

....

....

Theodore

External Examiner

Date: April 7, 1986

Abstract

The electric pre-heat and steam drive bitumen recovery process has been proposed for oil reservoirs containing very viscous oil. In this process, the oil in a reservoir is first heated by direct application of electrical energy, then subsequently driven to a production well by the injection of steam. Pre-heating the reservoir lowers the viscosity of the oil contained therein, allowing higher injection and production rates during the subsequent steam drive than would be possible without pre-heating.

In this thesis, an existing mathematical model of the low frequency, single phase electrical heating of an oil reservoir is extended to two models, each allowing three dimensional, low frequency, multiple electrical phase heating, and with one model including the effects of fluid movement and expansion, while the other does not. Approximate solutions to the two models were obtained using the finite difference method, implemented in two flexible computer programs. The finite difference equations used to solve for the electrical potentials and the calculation of the electrical heating rates used in these computer codes are given in detail.

Simulation studies were conducted, using these two computer programs, which investigated both the effects of including fluid movement and expansion in the model of the electric pre-heat, and the viability of using an electric pre-heat to create a communication channel between an injection well and a production well in an Athabasca oil sand reservoir. In particular, one of the studies simulated a complete electric pre-heat and steam drive process for a five-spot well pattern in a realistic Athabasca oil sand formation.

In addition, this work reports a preliminary experimental investigation of the high temperature, high pressure, electrical conductivity of Athabasca oil sands. The variation of the electrical conductivity of repacked oil sand samples with temperature, pressure, current density, and the water content was studied. Several experimental difficulties encountered during the investigation are also described.

Acknowledgement

The author would like to thank his supervisors, Dr. F.S. Chute and Dr. F.E. Vermeulen, for their help with the studies reported in this work.

Thanks are also due to Jim Fearn for his fine work in preparing many of the figures presented in this thesis.

The author would also like to thank the Alberta Oil Sands Technology and Research Authority and the Natural Sciences and Engineering Research Council for financial support in the form of scholarships. In addition, the Alberta Oil Sands Technology and Research Authority provided financial support for the high temperature, high pressure electrical conductivity measurement program on oil sands, and the Natural Sciences and Engineering Research Council provided financial support for the development of the electrical heating rate calculation code, EPEIOS.

The author would like to thank the Alberta Research Council for making available its Two Component Thermal Model for use in this study, and the Computer Modelling Group for permitting the use of its thermal model, ISCOM.

Table of Contents

Chapter Page

1. Introduction and Literature Review 1

1.1 Statement of Problem 1

1.2 Literature Review 6

2. The Mathematical Model 15

2.1 The Electric Field 15

2.1.1 Anisotropic Electrical Conductivity 17

2.1.2 The Quasi-static Approximation 19

2.1.3 Current Continuity Equation 22

2.1.4 Electrical Boundary Conditions 24

2.2 Heat Generation from Ohmic Losses 29

2.3 The Mathematical Model Assuming No Fluid Flow ...29

2.4 The Mathematical Model for Fluid Flow 30

2.4.1 Conservation of Mass 32

2.4.2 Darcy's Law 34

2.4.3 Conservation of Energy 38

3. Solution of the Mathematical Model with No Fluid Flow 41

3.1 Overall Solution Algorithm 42

3.2 Solution of the Current Continuity Equation 47

3.2.1 A Conservative Finite Difference Formulation 47

3.2.2 Solving the Set of Finite Difference Equations 58

3.3 Calculation of the Electric Heating Rates 60

3.4 Solution of the Heat Conduction Equation 64

3.5 Electrode Current, Scaling, and Energy Balance Calculations 68

3.6 Testing of the Solution Method 72

3.7 Conclusions 72

4. Solution of the Electrical Heating and Fluid Flow Model 73

4.1 The Alberta Research Council Two Component Thermal Model 75

4.2 Calculation of the Electrical Conductivity 78

4.3 Calculation of Electrical Heating Rates 81

4.4 Treatment of the Electrical Conductivity as Either an Implicit or an Explict Property 83

4.5 Interfacing of EPEIOS and TCTM 86

4.6 Printing and Storage of Program Results 89

4.7 Testing of the Combined Code 90

4.8 Conclusions 91

5. Results from the Computer Simulation of the Electric Pre-heat and Steam Drive Process 92

5.1 Note Regarding Properties 93

5.2 Case 1 - A Simplified Homogeneous Reservoir 94

5.3 Case 2 - A Two Layer, Horizontal Well Study 106

5.4 Case 3 - A Realistic Five-Spot Pattern Flood ...121

5.5 Conclusions 146

6. The Electrical Conductivity of Oil Sand at 60 Hz. ..149

6.1 Introduction 149

6.2 Experimental Apparatus and Sample Preparation ...152

6.2.1 Sample Holder 152

6.2.2 Electrodes 154

6.2.3 Sample Preparation 156

6.2.4 Pressure Vessel 157

6.2.5 Data Logging System 160

6.3 Experimental Procedure 160

6.4 Problems Encountered with the Experimental Apparatus and Method 164

6.4.1 Fluid Expansion 164

6.4.2 Sample Preparation 165

6.5 Experimental Results 167

6.5.1 Results from the Rapid Measurement Procedure on Low and Medium Grade Oil Sand Samples 168

6.5.2 Results from the Constant Temperature Measurement Procedure on Low and Medium Grade Oil Sand 171

6.5.3 Results of Experiments using High Grade Oil Sands 177

6.5.4 The Variation of Electrical Conductivity with Pressure 180

6.5.5 The Variation of Electrical Conductivity with Current Density 181

6.5.6 The Variation of Electrical Conductivity at Ambient Temperatures with Water Saturation 182

6.5.7 The Variation of Electrical Conductivity with Temperature in the Range of 24°C to 100°C 185

6.6 Discussion of the Results 186

6.7 Electrical Conductivity Formulas for use in the Computer Simulation of Electrical Heating of Oil Sand Formations 196

6.7.1 Effect of the New Formulas 198

6.8 Conclusions and Recommendations for Further Study 201

7. Conclusions and Recommendations for Further Study ..203

Bibliography 207

Appendix I. Experimental Results 215

Appendix II. Details of the Computer Simulation Run used to Compare the Old and New Conductivity Equations ...251

Appendix III. EPEIOS User's Reference Manual 257

Appendix IV. TCTM-EPEIOS User's Reference Manual 278

Appendix V. Testing of EPEIOS and TCTM-EPEIOS 289

List of Tables

Table Page

5.1 Reservoir Properties for Case 1 96

5.2 Electrical heating rates and steam injection rates for Case 1. 98

5.3 A comparison of the temperature increases (in °C) predicted by three models, due to the electric pre-heating of the reservoir in Case 1. 100

5.4 Reservoir properties used by Model 1 in the simulation of the electric pre-heat of Case 2. 109

5.5 Reservoir properties for Case 2 used by Model 1 in simulating the steam drive and by Model 2 in simulating both the electric pre-heat and steam drive. 110

5.6 Details of the electric preheat and steam drive for Case 2 112

5.7 A comparison of the temperature increase (in °C) predicted by two models, due to the electric pre-heating of the reservoir in Case 2. 114

5.8 Reservoir properties used by Model 1 in the simulation of the electric pre-heat of Case 3. 124

5.9 A comparison of the temperature increases (in °C) predicted by two models, due to the electrical heating of the reservoir in Case 3. 127

5.10 Reservoir properties used in the simulation of the steam drive of Case 3 133

5.11 Initial temperatures (in °C) used at the start of the steam drive for Case 3. These values were obtained using Model 1 (EPEIOS). 135

A.1 Results of Experiment No. 4. 216

A.2 Results of Experiment No. 6. 217

A.3 Results of Experiment No. 7. 218

A.4 Results of Experiment No. 8. 219

A.5 Results of Experiment No. 11. 221

A.6 Results of Experiment No. 12. 222

A.7 Results of Experiment No. 16. 224
A.8 Results of Experiment No. 18. 225
A.9 Results of Experiment No. 19. 227
A.10 Results of Experiment No. 21. 228
A.11 Results of Experiment No. 22. 229
A.12 Results of Experiment No. 23. 230
A.13 Results of Experiment No. 24. 231
A.14 Results of Experiment No. 25. 232
A.15 Results of Experiment No. 26. 233
A.16 Results of Experiment No. 28. 234
A.17 Results of Experiment No. 29. 235
A.18 Results of Experiment No. 30. 236
A.19 Results of Experiment No. 31. 237
A.20 Results of Experiment No. 32. 238
A.21 Results of Experiment No. 33. 239
A.22 Results of Experiment No. 34. 240
A.23 Results of Experiment No. 35. 241
A.24 Results of Experiment No. 36. 242
A.25 Results of Experiment No. 37. 243
A.26 Results of Experiment No. 38. 244
A.27 Results of Experiment No. 39. 245
A.28 Results of Experiment No. 40. 246
A.29 Results of Experiment No. 42. 247
A.30 Results of Experiment No. 43. 248
A.31 Results of Experiment No. 44. 249
A.32 Results of Experiment No. 45. 250

A.33 A comparison of the analytically calculated potentials with EPEIOS results for Test Problem #2. Columns headed "AN" indicate analytic solution while thoses headed "EP" indicate EPEIOS result. 295

List of Figures

Figure Page

3.1 A flow chart showing the order of the major calculations in the program EPEIOS. 44

3.2 The dimensions and relative locations of an arbitrary grid block and the six adjacent blocks. 49

4.1 A flow chart showing the order of the calculation of the electrical heating rates in TCTM-EPEIOS. 83

5.1 The geometry and the dimensions of the reservoir for Case 1. This is a two dimensional problem. 95

5.2 A plot of the injection pressure versus time, for Case 1, comparing the results of simulations run using Model 1 (EPEIOS) and Model 2 (TCTM-EPEIOS). ...102

5.3 A plot of the oil production rate versus time, for Case 1, comparing the results of simulations run using Model 1 (EPEIOS) and Model 2 (TCTM-EPEIOS). ...103

5.4 A plot of cumulative oil production versus time, for Case 1, comparing the results of simulations run using Model 1 (EPEIOS) and Model 2 (TCTM-EPEIOS). The cumulative production is shown as a fraction of the original oil in place. 104

5.5 The geometry and dimensions of the reservoir and adjacent formations for Case 2. 108

5.6 A plot of the inter-electrode resistance versus time for the electric pre-heat phase of Case 2. 115

5.7 A plot of the oil production rate versus time, for Case 2, comparing the results of simulation runs using Model 1 (EPEIOS) and Model 2 (TCTM-EPEIOS). ...117

5.8 A plot of the cumulative oil production versus time, for Case 2, comparing the results of simulation runs using Model 1 (EPEIOS) and Model 2 (TCTM-EPEIOS). 118

5.9 A plot of cumulative oil production versus time for Case 2, and for a simulation similar to Case 2, but with increased electrical heating. 119

5.10 The reservoir dimensions and electrode and well locations for Case 3. The dashed lines in the areal view shows the simulation grid used in simulating the steam drive. 123

5.11 An isosurface plot of temperature, showing the portion of the simulation region (one quadrant of a five spot) that was heated to a temperature greater than 55 °C. 130

5.12 Inter-electrode resistance, versus time, for the pair of electrodes in one well. The resistances predicted by each of Model 1 and Model 2 are compared. 131

5.13 The temperature at the centers of the grid blocks on a vertical cross-section between the injection well and one of the production wells, at a time of 744 days after the start of the electric pre-heat. 139

5.14 The temperature at the centers of the grid blocks on a vertical cross-section between the injection well and one of the production wells, at a time of 1479 days after the start of the electric pre-heat. 140

5.15 The temperature at the centers of the grid blocks on a vertical cross-section between the injection well and one of the production wells, at a time of 2065 days after the start of the electric pre-heat. 141

5.16 Cummulative oil production versus time for the five spot pattern simulated in Case 3. 144

6.1 Cross section of the sample holder tube with the oil sand sample and electrodes in place. This sample holder is placed inside the pressure vessel shown in Figure 6.2. 153

6.2 Diagram of the pressure vessel, oven, pressure system, electrical system and data logging system for the experiment. 159

6.3 The electrical conductivity of oil sand versus temperature for Experiment No. 7. Two successive heating and cooling cycles were performed over two days. 169

6.4 The electrical conductivity of oil sand samples, and one water sand sample (#4), versus temperature for experiments where the samples were rapidly heated. The usual heating time for the samples was five hours. 170

6.5 The normalized electrical conductivity versus time for an oil sand sample held at 100°C. 172

6.6 The normalized electrical conductivity versus time for oil sand samples held at 150°C. The experiment number, weight percent of water, and electrode type are given for each set of results. ...173

6.7 The normalized electrical conductivity versus time for oil sand samples held at 200°C. The experiment number, weight percent of water, and electrode type are given for each set of results. ...175

6.8 The normalized electrical conductivity versus time for oil sand samples held at 240°C. The experiment number, weight percent of water and electrode type are given for each set of results. ...176

6.9 The normalized electrical conductivity versus time for oil sand samples with very low water contents. Three experiments, one each at 150°C, 200°C, and 240°C are shown. ...178

6.10 The initial electrical conductivity versus water saturation for oil sand samples. ...183

6.11 The normalized electrical conductivity of a mixture of sand and a 20 wt.% NaCl solution versus temperature, compared to the normalized results of Ucok. et al. for a 20 wt.% NaCl solution. ...191

A.1 The reservoir lithology and properties, and the electrode configuration for the simulation are shown 253

A.2 A plan view of the simulation electrode configuration ...254

A.3 A comparison between the temperature contours obtained using the old conductivity formula (solid lines) and those from the new formula (dashed lines). The horizontal dashed lines indicate the top and bottom of the oil sand zone. ...256

A.4 The geometries used by some of the test problems. Diagram (a) shows the geometry used for Tests #1 and #4. Diagram (b) shows the geometry used for Test #2. Diagram (c) shows the geometry used for Test #3. ...290

A.5 The geometry used by Test No. 5. ...301

Nomenclature

In this section the symbols used in the text are given, followed by the superscripts and subscripts.

Symbol	Units	Description
$\bar{a}_x$		Unit vector in X direction
$\bar{a}_y$		Unit vector in Y direction
$\bar{a}_z$		Unit vector in Z direction
$\bar{B}$	T	Magnetic Flux Density
$\bar{D}$	C/m^2	Electric Flux Density
$\bar{E}$	V/m	Electric Field Strength
$\bar{H}$	A/m	Magnetic Field Strength
$\bar{J}$	A/m^2	Electric Current Density
k	$W/m \cdot K$	Thermal Conductivity
K	m^2	Absolute Permeability
K_s		Water - Steam Equilibrium Ratio
Krg		Relative Permeability to Gas
Kro		Relative Permeability to Oil
Krw		Relative Permeability to Water
M	$J/m^3 \cdot K$	Volumetric Heat Capacity
Pcgo	kPa	Capillary Pressure from Gas to Oil Phase
Pcow	kPa	Capillary Pressure from Oil to Water Phase
Pg	kPa	Pressure of the Gas Phase
Po	kPa	Pressure of the Oil Phase
Pw	kPa	Pressure of the Water Phase

Q_l	W	Electrical Heating Rate
qg	m^3/s	Gas Production Rate
qo	m^3/s	Oil Production Rate
qw	m^3/s	Water Production Rate
Sg		Gas Saturation
So		Oil Saturation
Sw		Water Saturation
t	s	Time
T	°C	Temperature
Ug	J/kg	Internal Energy of Gas Phase
Uo	J/kg	Internal Energy of Oil Phase
Ur	J/kg	Internal Energy of Reservoir Rock
Uw	J/kg	Internal Energy of Water Phase
$\bar{v}_l$	m/s	Fluid Velocity
w		Weight percentage of water
α	$°C^{-1}$	Temperature dependence of Electrical Conductivity
ϵ	F/m	Electric Permittivity
ρ	C/m^3	Volume Charge Density
ρ_s	C/m^2	Surface Charge Density
ρ_m	kg/m^3	Mass Density
ρg	kg/m^3	Gas Phase Mass Density
ρo	kg/m^3	Oil Phase Mass Density
ρw	kg/m^3	Water Phase Mass Density
σ	S/m	Electrical Conductivity
σ_{24}	S/m	Electrical Conductivity at 24 °C
σw	S/m	Connate Water Electrical Conductivity

$\hat{\sigma}$	S/m	Tensor Electrical Conductivity
ϕ		Porosity
ψ	V	Scalar Electric Potential
ω	rad/s	Angular Frequency

1. Introduction and Literature Review

1.1 Statement of Problem

The Athabasca oil sand deposit, located in northeastern Alberta, contains well over one hundred billion cubic meters of bitumen (Camp 1976). Bitumen is a form of petroleum which is heavier and more viscous than conventional crude oil. The amount of bitumen in the Athabasca oil sands deposit is about one thousand times Canada's current yearly consumption of crude oil. Though the bitumen is both difficult to recover from oil sand, and must be upgraded before it is of the same quality as crude oil, the size of the Athabasca oil sand deposit, and it's potential for supplying much of Canada's long term petroleum needs, have resulted in a large amount of research into the development of the Athabasca deposit.

To date, the only commercial developments (by Suncor and Syncrude) have involved mining the oil sand in open pit mines, followed by separation of the bitumen from the sand in large extraction plants. The bitumen is upgraded to "synthetic crude", then piped to a refinery. However, as the thickness of the earth, or overburden, above the oil sand formation increases, open pit mining becomes uneconomical. Only about ten percent of the oil sand reserves are recoverable by surface mining (Outtrim and Evans 1977). Thus, there is considerable interest in developing in situ (in place) processes for recovering the bitumen. Many possible in situ processes have been suggested (Fitzgerald 1978).

If a well is drilled into a conventional oil reservoir, the oil in the reservoir will flow into the well and can be pumped to the surface. Unfortunately, the bitumen in the Athabasca oil sand deposit is so viscous that when a well is drilled into an oil sand reservoir, no bitumen flows into the well. However, the viscosity of bitumen decreases rapidly with increases in temperature (Nicholls and Luhning 1977). At natural formation temperatures Athabasca bitumen has a viscosity in the millions of centipoise. If this bitumen is heated to 80°C the viscosity drops to 1000 cp, and if heated to 200°C the viscosity will be about 10 cp. Most of the proposed in situ processes depend on this decrease in bitumen viscosity with temperature.

One of the proposed in situ processes is steamflooding. In the steamflood method an array of injection and production wells is drilled, then steam is injected down the injection wells and oil and water are pumped up the production wells. Two major problems with this method are firstly developing adequate steam injection rates, and secondly establishing communication between the injection and the production wells. The unheated bitumen is so viscous that it blocks the steam from entering the formation, and it stops the heated, mobilized bitumen from traveling to the production well. Various methods have been proposed to improve the initial steam injectivity and to develop communication between injection and production wells. These include the injection of solvents, the formation of emulsions and fracturing the formation (Redford and Cotsworth 1976).

Another method proposed to overcome the injectivity and communication problems involves heating the formation with an electrical current prior to steam injection (Nicholls and Luhning 1977; Flock and Tharin 1975; Towson 1979, 1982a, 1982b; Vermeulen and Chute 1983; Redford 1985). This method is known as the electric pre-heat process. The electrical current enters the oil sand formation from an electrode in one well, passes through the formation and heats it through Ohmic losses, and exits via another electrode in the same or a different well. The electric current flow in the formation is predominantly in the connate water surrounding the sand grains of the oil sand. The electric pre-heat process works by heating the bitumen, lowering it's viscosity, so that both initial steam injectivity and communication between injection and production wells may be established. It is estimated that the middle of the communication path should be raised from the initial value of 10°-15°C usual for Athabasca oil sand formations to 50°-90°C prior to the commencement of steam injection.

The patent literature reveals a large number of possible designs for electrically heating the oil sand formation pior to steam injection. There is a need for the ability to study and compare various designs prior to embarking on a costly field pilot plant based on a particular design implemented in a particular oil sand reservoir. A mathematical model of the various electric heating, fluid flow, and energy transport processes which would take place during an electric pre-heat and steam drive can be developed, but such a model would be difficult or impossible to solve analytically for a realistic, multilayered oil sand reservoir with a complex geometry of wells and electrodes. However, numerical techniques can be used to obtain approximate solutions to such a mathematical model. Numerical simulation, together with accurate property data, can provide a relatively low cost means to studying the electric pre-heat and steam drive method, both in determining the best design for an electric pre-heat in a particular formation, and in determining the economic feasiblity of the entire process.

The author, in a previous work (Hiebert 1981; Hiebert, Capjack, Chute, and Vermeulen 1983), developed a two dimensional numerical simulator of the electrical pre-heat process. In the present work the mathematical model of low frequency, single phase electrical heating of oil sand reservoirs, used in the previous work, is examined and extended to the three dimensional, multiple electrical phases, case. The reservoir may consist of multiple layers of materials (such as oil sand, shale and limestone) whose electrical conductivities may vary by orders of magnitude. This model of electrical heating is then coupled with each of two separate models for the change in temperature of the oil sand reservoir. The first of these models assumes that no significant fluid flow will occur during the electrical pre-heat, and that the only heat transport mechanism is thermal conduction. The second model allows fluid expansion and flow during the electrical pre-heat, and heat transport by convection as well as conduction. The fluid flow portion of this second model was developed by the Alberta Research Council, and was supplied to the author in the form of a computer code. The coupling of the Alberta Research Council's code to the electrical heating model is discussed.

Both of these two models for the electric pre-heat were solved numerically, using the finite difference method, in two flexible computer codes. Each of these two computer programs was used to run two realistic electrical pre-heat and steam drive simulations. The results obtained from each of the two models are compared and discussed.

A third simulation study was performed on the electric pre-heat and steam drive process for a five-spot pattern in an Athabasca oil sand reservoir. In this third study, the first model of the electric pre-heat process developed in this work was used to simulate the electric pre-heat. A commercial thermal reservoir simulator, the Computer Modelling Group's program ISCOM, was used to simulate the steam drive. The results of this third simulation study particularly illustrate how the electric pre-heat process may be used to develop a communication path within an oil sand reservoir, leading to the recovery of a large fraction of the oil in the reservoir.

One of the most important formation properties which must be known to accurately model the electrical heating of an oil sand reservoir is the electrical conductivity of the oil sand. In this study, the author reports on series of experiments measuring the low frequency electrical conductivity of various grades of oil sand. The variation of electrical conductivity with temperature, pressure, current density, time, and water saturation, was studied for the temperature range of 24°C to 240°C, with the fluid pressure of the oil sand samples maintained above the saturated steam pressure.

1.2 Literature Review

Electrical or electromagnetic energy may be used to heat the petroleum in the formation, lowering the viscosity of the fluid. Electrical conduction heating, induction heating, and heating with radio waves have all been proposed. A summary of these techniques and a survey of the literature are given in Vermeulen and Chute (1983) and in Chute, Vermeulen, and Cervenan (1978). As the current study will be limited to investigating low frequency electrical conduction heating of formations, the remainder of this literature review will be confined to low frequency heating only.

The low frequency, electrical conduction heating of oil-bearing formations to increase oil production is known as the electrothermic technique. The electrothermic system is described by Gill (1979) and the system and field tests have been described in various articles (Flock and Tharin 1975; Anon. 1969; Anon. 1970). Gill and Crowson, both of Electrothermic Co., have obtained several U.S. and Canadian Patents pertaining to the electrothermic process. The simplest form of the electrothermic process involves placing a single electrode downhole in contact with the oil-bearing formation and energizing this electrode with an A.C. voltage. The electrical current flows through the connate water in the oil-bearing formation, then upward through the overburden to a ground electrode at the surface. The current flow is concentrated near the downhole electrode and heats the fluid and the formation in the vicinity of this electrode. The electrical current flowing down the tubing to the bottom hole electrode will also provide some heating of the tubing string, maintaining the higher fluid temperature, and hence, lowering the energy required to pump the produced fluids to the surface. A D.C. bias may also be placed on the electrode to drive water away from the well via the electro-osmosis technique (Anbah et al. 1965; Sacuta 1981). Production and electrical heating normally occur simultaneously. Alternate configurations involve placing the ground electrode in another well in the formation. Water or brine may be injected into the electrode wells to prevent overheating near the electrodes.

The development of a two-dimensional, two-phase (oil and water), numerical reservoir simulator which includes electrical heating has been reported by El-Feky (1977) and Harvey, Arnold, and El-Feky (1978,1979). The program was used to study improvements in sweep efficiency and oil recovery in waterfloods due to formation heating by the electrothermic process. The simulator was compared to physical laboratory model experiments with good agreement.

The mathematical model used by El-Feky (1977) in the simulator contained several simplifying assumptions. The reservoir modelled was horizontal, uniform in thickness, and homogeneous with regards to porosity and permeability. No gas saturation was included in the model. The electrical current was confined to the reservoir (i.e. the adjacent formations were modelled as much more resistive than the reservoir), and the electrodes contacted the entire reservoir. The simulator geometry was limited to that of one quadrant of a five-spot pattern, and uniform grid spacing was used.

Additional analytic results for electrical heating using a radial model were reported by Harvey and Arnold (1980) and analytic work considering the effects of conductive adjacent formations was reported by Harvey (1982). Both of these works contain simplifying approximations which limit their usefulness and accuracy in modelling realistic oil sand reservoirs.

Pioneering work on electrical heating of Athabasca oil sands was done by the Atlantic Richfield Research Center. Atlantic Richfield Canada, together with Esso Resources and Canada-Cities Services, started work on development of a pilot project. Petro-Canada acquired Atlantic Richfield Canada and Japan Canada Oil Sands joined the group, which became known as the PCEJ group.

Two papers were published by the Atlantic Richfield Research group. The first, by Newbold and Perkins (1977), discusses the modelling and measurement of electrical losses for power flowing in the wellbore. These losses are due to both A.C. resistance and hysteresis effects in the casing. The paper includes a report on a shallow well test conducted by Atlantic Richfield.

The second paper, by Todd and Howell (1977), reports on a reservoir simulator which was developed to model electrical heating and production of fluids from a formation. The simulator first calculates the static electrical potential. The current flows and electrical energy dissipated are calculated from the electrical potential distribution. This heating is the source term for the temperature distribution calculation. The current flows are assumed fixed for the time step. Fluid expansion due to the temperature increase is calculated and used in the solution of the pressure distribution. Fluid flow and heat convection are calculated from the pressure distribution. The electrical conductivity and fluid viscosity are updated to account for temperature changes. The time step is completed and the next one begins. All finite difference equations are solved by the Extrapolated Liebmann method (a relaxation method) or by Gaussian Elimination.

This simulator was developed for two geometries. A radial, two-dimensional, one wellbore model was developed to study in detail the heating near the wellbore. Wellbore cooling and current limiting could be specified to prevent overheating and steam production near the wellbore. A three-dimensional model was also developed. This model had larger grid blocks than the two-dimensional wellbore model, and hence gave less detail of heating near the wellbore. Current distribution and heat removal terms from the radial model were input into the 3-D model to compensate for this lack of definition near the wellbores. The 3-D model had the ability to simulate three-phase heating.

Todd and Howell (in the same paper) present results from the simulator showing the effects of well radius, initial formation resistivity, wellbore cooling, and well spacing.

Numerous Canadian and U.S. patents dealing with electrical heating of oil sands have been granted to Petro-Canada or the PCEJ group (Kern 1977; Barnes 1978; Perkins 1978; Pritchett 1979; Todd 1980). These patents deal with such topics as methods of increasing the effective electrode size, which decreases the fraction of the total heating that is in the immediate vicinity of the wellbore, and with whether one should attempt to heat the entire oil sand formation uniformly, or only heat a communication channel between the injection and production wells. The question of whether a uniform pre-heat or a selective channel pre-heat is more efficient is one that has not been dealt with in the literature.

Towson (1979; 1982a; 1982b) has reported on the progress of an electrical pre-heat and steam drive pilot plant, operated by the PCEJ group in the Athabasca deposit, and has presented some details of its design. The pilot consisted of four wells in a square 30 m spacing. In addition, eight observation wells were drilled. The electrode wells were cooled during heating to prevent overheating near the electrodes. The pilot was electrically heated for about nine months. After five months, the temperature at a distance of 7.5 m from one of the electrodes had been raised to 78°C, while half way between the electrodes the temperature was 38°C. A recent paper by Khosla (1985) discusses the computer modelling of the pre-heat pilot. The computer models used were similar to those previously reported by Todd and Howell (1977).

Physical scale modelling of electrical and electromagnetic heating of oil sand over a broad range of frequencies has been discussed by Vermeulen, Chute and Cervenan (1979; 1982). Scaling criteria for physical models were developed for different frequency ranges. The author, in his M.Sc. thesis (Hiebert 1981; Hiebert et al. 1983), developed a simulator based on the low frequency, electrical conduction heating model used by Vermeulen et al.. This model includes quasi-static electric field calculations and heat transfer by conduction only. Results from the simulator were compared to results from physical models with good agreement, except in the immediate vicinity of the electrodes. This work differed from previous works in that sharp changes in electrical conductivity were taken into account by the finite difference equations, eliminating errors which will result if this is not done. The simulator was thus able to study the effects of different lithologies on the heating patterns of different electrode configurations. Some of these two dimensional studies are reported in a paper by Hiebert, Vermeulen, Chute and Capjack (1986 in print).

The only published studies on the electrical properties of oil sand are those of Chute, Vermeulen, and Cervenan (1978), Chute, Vermeulen, Cervenan, and McVea (1979), and McVea (1978). McVea discusses the apparatus and errors involved in measuring electrical properties for different frequency ranges. Chute et al. measured the electrical conductivity and permittivity of oil sand over the frequency range of 50 Hz to 1 GHz. They correlated these properties with temperature, water content, and density. Of particular interest to this study is the variation of electrical conductivity with temperature and water content at low frequencies. Chute et al. (1978) show a plot of conductivity vs. temperature for two grades of oil sand measured at 100 Hz between 3° and 150°C. The conductivity increases linearly with temperature until 90°C, then remains constant or declines. Only four runs were reported for this frequency and the data points show a fair scatter.

Some of the patent literature (originating from Atlantic Richfield) mentions 140 ohm-meters as a typical in situ resistivity. This value is in the middle of the resistivity values obtained for different grades of oil sand from the Suncor mine by Chute et al. (1979). Perkins (1976) suggests that the in situ electrical resistivity may be anisotropic, with 30 ohm-meters as a horizontal resistivity and 90 ohm-meters as a vertical resistivity. Anisotropic resistivities were not measured in the study done by Chute et al., because measurements were performed on oil sand samples which had been broken up during collection, mixed, and then repacked into measurement cells.

It is clear from this literature review that a body of previous work on electrical heating of oil sand reservoirs exists. However, there are several topics, important to the study of the electric pre-heat process and the engineering design of a large scale field test, which have not been discussed in the open literature. These topics include efficient methods of modelling in three dimensions the multi-phase electrical heating of an oil reservoir, the importance of including fluid movement and expansion in the mathematical model of the electric pre-heat process, and the electrical behavior of oil sand at higher temperatures and pressures. These topics will be addressed in this thesis.

2. The Mathematical Model

In this chapter, the set of equations used to model the various physical phenomona occurring during the pre-heat and steam drive recovery process are developed. In section 2.1 the equation used to calculate the electric potential field in the reservoir being heated is discussed in detail, with careful attention given to the assumptions made in deriving this equation. In section 2.2 the calculation of the electrical heating rates in the reservoir is discussed.

Two different models were used to calculate the temperature changes occurring in the oil sand formation during an electric pre-heat. In the first of these models, it was assumed that the effects of fluid expansion and flow could be neglected, and that the only heat transport mechanism was thermal conduction. In this model, the heat conduction equation, discussed in section 2.3, was used to calculate the temperature change. In the second model, the fluid flow equations for oil and water were included in the set of equations used, and fluid expansion, steam formation, and fluid movement were included in the model. This second model is discussed in section 2.4.

2.1 The Electric Field

The basic set of equations of classical electricity and magnetism, first developed by Maxwell in 1863 (Ramo, Whinnery, and Van Duzer, 1965), can be written as

$$\nabla\cdot\bar{J} = -\frac{\partial\rho}{\partial t} \tag{2.1}$$

$$\nabla\times\bar{E} = -\frac{\partial\bar{B}}{\partial t} \tag{2.2}$$

$$\nabla\times\bar{H} = \bar{J} + \frac{\partial\bar{D}}{\partial t} \tag{2.3}$$

where $\bar{J}$ is the electric current density (A/m^2), ρ is the volume charge density (C/m^3), $\bar{E}$ is the electric field strength (V/m), $\bar{B}$ is the magnetic flux density (T), $\bar{H}$ is the magnetic field strength (A/m), and $\bar{D}$ is the electric flux density (C/m^2). The term $\partial\bar{D}/\partial t$ is known as the displacement current density (A/m^2). Equation (2.1) is known as the current continuity equation and is the mathematical statement of the conservation of charge. Equations (2.2) and (2.3) are the generalized point forms of Faraday's Law and Ampere's Law.

These equations, together with the appropriate boundary conditions and material properties, may be used to find the electric field of any electrical heating configuration at any frequency. However, an analytic or numerical solution to Maxwell's equations is difficult, if not impossible, in all but the simplest cases. It is, therefore, desirable to simplify these equations, deleting terms which are negligible for the frequencies and electrode configurations of interest.

The following assumptions are made to simplify the modelling of the electric pre-heat process:

1. The electrical conductivity may be anisotropic, but only for the restricted case where the principal axes of the conductivity tensor are parallel to the coordinate axes.
2. The electrical conductivity, electrical permittivity, and magnetic permeability are not functions of the electric or magnetic field strengths.
3. Only low frequency sinusoidal excitations (voltages) are applied to the system, so that, for the given properties of the materials modelled, the conduction current predominates over the displacement current.
4. In addition, the frequency is low enough and the problem geometry is such that the electric fields associated with the time varying magnetic field are not important. This corresponds to the maximum dimension of the system being much less than a wavelength of the applied energy in the medium being modelled (Magid, 1972).

These assumptions are discussed in detail in the next two sections.

2.1.1 Anisotropic Electrical Conductivity

Some sections of the oil sand deposits consist of alternating layers of oil sand and silt, with layers up to one decimeter thick. These layers are continuous for tens of meters with a gradual slope to the layers (Mossop, 1980b). As there is a large difference in electrical conductivity between the silt layers and the oil sand, this type of formation would have an anisoptropic conductivity when viewed on a scale of the order of a meter.

This anisotropy may be dealt with in various ways. Each layer may be modelled separately as an isotropic media. This approach will lead to excessive calculations as there would be tens of separate layers to be included. One could neglect the anisotropy, and model the alternating silt and oil sand layers as one isotropic medium with some average conductivity. Finally, one could include the anisotropy as viewed on a scale of the order of a meter by replacing the scalar conductivity, σ, by a tensor, $\hat{\sigma}$ (S/m).

The author has chosen to use a simplified form of the last alternative. The conductivity may be specified in diagonal tensor form; that is, it is assumed that the coordinate axes are parallel to the principal directions of the conductivity tensor. Landau and Lifshitz (1960) show that for the static case in a material body the conductivity matrix must be symmetric. Any symmetric matrix may be put in diagonal form by an appropiate coordinate transformation (Sokolnikoff, 1964).

When using this approach, the conduction current, $\bar{J}$, becomes (for the three dimensional, cartesian case)

$$\bar{J} = \begin{vmatrix} \sigma_x & 0 & 0 \\ 0 & \sigma_y & 0 \\ 0 & 0 & \sigma_z \end{vmatrix} \begin{vmatrix} E_x\bar{a}_x \\ E_y\bar{a}_y \\ E_z\bar{a}_z \end{vmatrix}$$

$$= \sigma_x E_x \bar{a}_x + \sigma_y E_y \bar{a}_y + \sigma_z E_z \bar{a}_z \qquad (2.4)$$

where σ_x and E_x are the conductivity and electric field strength, respectively, in the x direction, and $\bar{a}_x$, $\bar{a}_y$ and $\bar{a}_z$ are unit vectors.

One of the weaknesses of using this approach is that it may not be convenient to use the principal directions of the conductivity tensor as the coordinate axes for the problem being modelled. The boundaries between different media may not be parallel to any of the principal directions, or different media may have different principal directions. One is then required to use average values for the diagonal terms of the conductivity tensor.

2.1.2 The Quasi-static Approximation

In their paper on physical scale modelling, Vermeulen et al. (1979) discuss the simplification of Maxwell's equations for various types of electrical heating. The discussion in this section (2.1.2) is drawn from the work of their paper, from a private communication (Chute and Vermeulen, 1985), and from Magid (1972).

If Ohm's law applies (i.e. $\bar{J} = \hat{\sigma}\bar{E}_0$), and the electric permittivity, ϵ, (F/m) is a scalar, and the system undergoes single frequency, sinusoidal excitation, then equations (2.1) to (2.3) may be rewritten as;

$$\nabla\cdot\hat{\sigma}\bar{E}_0 = -j\omega\rho_0 \qquad (2.5)$$

$$\nabla\times\bar{E}_0 = -j\omega\bar{B}_0 \qquad (2.6)$$

$$\nabla \times \bar{H}_0 = \hat{\sigma}\bar{E}_0 + j\omega\epsilon\bar{E}_0 \qquad (2.7)$$

where ω is the angular frequency of the excitation source (rad/s), j is equal to $\sqrt{-1}$, $\bar{B}_0$, $\bar{H}_0$, ρ_0, and $\bar{E}_0$ are phasors, ϵ is the electrical permittivity, and $\hat{\sigma}$ is the electrical conductivity tensor (limited to being in diagonal form).

As the frequency approaches zero the dominant r.m.s. currents that flow between the electrodes during any electric pre-heat are the same as those currents that would result if a static potential difference (equal to the r.m.s. applied voltage) were maintained between the electrodes. However, as the frequency is increased the magnetic fields associated with those currents induce additional electric fields, and hence currents, within the formation, and the heating distribution will be altered. To the extent that these additional currents are of negligible value in comparison to the primary currents, an electric pre-heat at power frequency can be analyzed by neglecting the time-variation of the magnetic field which implies replacing equation (2.6) by

$$\nabla \times \bar{E}_0 = 0 \qquad (2.8)$$

which is the same equation satisfied by static fields.

The resulting solution of equations (2.5), (2.7) and (2.8), known as the electro-quasi-static (or simply the quasi-static) approximation to the electromagnetic fields, is valid so long as the largest system dimension is much less than a wavelength as measured in any of the associated formation materials.

The wavelength in oil sand at 60 Hz is between 2000 m and 9000 m (Vermeulen et al., 1979), depending on the water content of the oil sand. Since electrode sizes and inter-electrode spacings will generally be less than some 200 m, the quasi-static approximation will satisfactorily describe the electric fields and currents associated with an electric pre-heat at power frequency.

Further simplification of the equations is possible upon consideration of the relative magnitudes of the conduction current and the displacement current terms. Consider one component of the displacement current term, say in the x direction, $j\omega\epsilon E_{0x}$, in equation (2.7). The ratio of the magnitude of the component of the conduction current in the x direction, $\sigma_x E_{0x}$, to the magnitude of the displacement current is given by $\sigma_x/\omega\epsilon$ for time harmonic solutions. If this ratio, known as the loss tangent, is much greater than one for all components (directions) of the current, then the displacement current may be neglected. For oil sand this ratio is typically greater than one hundred at power frequency (60 Hz), and does not fall to ten until frequencies of about one megahertz are reached. Thus, for lower frequencies the effect of the displacement current is negligible, and equation (2.7) becomes

$$\nabla \mathrm{x} \bar{H}_0 = \hat{\sigma} \bar{E}_0 \qquad (2.9)$$

This approximation is also generally applicable in the overburden and underburden materials at power frequency.

2.1.3 Current Continuity Equation

In phasor form the current continuity equation is given by equation (2.5). However, taking the divergence of both sides of equation (2.9) shows that

$$\nabla\cdot\hat{\sigma}\bar{E}_o = \nabla\cdot\bar{J}_o = 0 \tag{2.10}$$

Further, if a quasi-static approximation can be made, the electric field satisfies equation (2.8) which implies that the electric field can be expressed in terms of a scalar potential function ψ_o (V) as

$$\bar{E}_o = -\nabla\psi_o \tag{2.11}$$

where ψ_o is a phasor quantity. Using Ohm's Law and substituting this result into equation (2.10) gives

$$\nabla\cdot(\hat{\sigma}\nabla\psi_o) = 0 \tag{2.12}$$

which is the form of the current continuity equation valid whenever displacement currents are negligible and a quasi-static approximation is acceptable.

As the electrical conductivity $\hat{\sigma}$ in an oil reservoir will vary with the temperature and the amount of water present in a particular location, it will, in general, be a function of position, and equation (2.12) may not be simplified by moving the conductivity term outside the divergence operator.

For the three dimensional cartesian case, with a diagonal conductivity tensor, equation (2.12) becomes

$$\frac{\partial}{\partial x}\left[\sigma_x \frac{\partial \psi_0}{\partial x}\right] + \frac{\partial}{\partial y}\left[\sigma_y \frac{\partial \psi_0}{\partial y}\right] + \frac{\partial}{\partial z}\left[\sigma_z \frac{\partial \psi_0}{\partial z}\right] = 0 \qquad (2.13)$$

As $\psi_0 = \psi_1 + j\psi_2$ (i.e. the phasor has a real part, ψ_1, and an imaginary part, ψ_2) and as the gradient and divergence operators are linear and $\hat{\sigma}$ is entirely real, equation (2.13) may be separated into two equations, one which gives the real part of the potential and one which gives the imaginary part.

In summary, when using the quasi-static approximation the electric field is calculated by solving equation (2.13) for the scalar potential ψ_0. While calculating the real part of the potentials, the voltages (or boundary conditions) of the electrodes are fixed at the r.m.s. A.C. value of the real part of the electrode voltage. The imaginary part is similarly calculated. The time varying electric potential is then expressed as:

$$\psi(x,y,z,t) = \mathrm{Re}[\psi_0(x,y,z,t)\exp(j\omega t)] \qquad (2.14)$$

where $\psi_0(x,y,z,t)$ is a phasor which describes the spatial variation of the electric potential of the equivalent static problem, ω is the angular frequency of the applied voltage, and t is the time in seconds. It should be noted that the time dependence of the quasi-static electric potential, $\psi_0(x,y,z,t)$, is due to the variation of the electrical conductivity of the formation with temperature and water saturation changes during the heating process. This time dependence produces much slower changes than the time dependence due to the A.C. applied voltage (the $\exp(j\omega t)$ term). The variation of electrical conductivity with temperature and water saturation couples the electric field equation with the fluid flow and energy equations used in the model.

2.1.4 Electrical Boundary Conditions

Three different types of electrical boundaries will arise in the problem being modelled. They are: electrode - conducting material boundaries, insulator - conducting material boundaries, and boundaries between two conducting materials of different electrical conductivities.

Electrodes are modelled as perfect conductors. Thus, the boundary of a conductor is modelled as a constant potential surface. Electrode - oil sand contact impedances were noted by Chute et. al. (1979,1978) when measuring the electrical properties of oil sand. A major cause of contact impedance is poor physical contact between the oil sand and the electrode. In the mathematical model used it is assumed that contact impedance has been made negligible by a suitable technique such as the injection of a saline solution near the electrode.

Insulator - conducting material boundaries are modelled in electrostatics as surfaces at which there is no current flow normal to the surface (a homogeneous Neumann boundary condition). Having no current normal to the surface implies that the normal component of the electric field is zero just inside the conducting material. As well as modelling insulating boundaries, this type of boundary condition may be used to model planes of symmetry. Many of the electrode configurations of interest in electrical conduction heating of oil sand consist of large symmetric arrays of electrodes. The planes of symmetry in the electric field may be used to divide the large array into many small identical cells with no current flow between cells. The simulation of the heating in one of these small cells is all that is necessary to describe the heating in the entire array.

The interior of the electrical domain may contain interfaces between media with widely different conductivities. For example, the conductivities of oil sand and shale can differ by two or three orders of magnitude. It will be shown in the following paragraphs that, when displacement currents are negligible and a quasi-static approximation is used, both the current flow normal to the interface and the electrical potential will be continuous across the interface. This will lead to discontinuous changes in the magnitude of the electric field at the interface. These interfaces must be handled with special care when developing the finite difference schemes.

At a boundary between two media of finite conductivity the electric field boundary conditions are (Stratton, 1941);

$$\bar{n}\times(\bar{E}_1-\bar{E}_2) = 0 \tag{2.15}$$

$$\bar{n}\cdot(\bar{D}_1-\bar{D}_2) = \rho_s \tag{2.16}$$

where $\bar{E}_1$, $\bar{E}_2$, and $\bar{D}_1$, $\bar{D}_2$, are the fields and flux densities in the two media, and where ρ_s is the surface charge density at the interface (C/m^2) and $\bar{n}$ is a unit vector locally normal to the boundary and directed into region 1. These are general boundary conditions for Maxwell's equations and are valid for all frequencies. The boundary conditions may be expressed in terms of the normal and tangential components of the electric field.

The appropriate boundary conditions relating the currents at the interface between two media can be obtained from equation (2.1) for the conservation of charge. Writing this equation in its integral form and applying the Divergence Theorem gives

$$\int_s \bar{J}\cdot\bar{d}s = -\int \frac{\partial\rho}{\partial t}\, dv \tag{2.17}$$

To apply equation (2.17) to the boundary between two materials of finite conductivity, consider a small cylindrically shaped volume enclosing a portion of the boundary. One face of the cylinder, denoted S_1, is in material 1 and is parallel to the boundary. The second face, S_2, is in material 2 and is parallel to the boundary. The side of the cylinder, S_3, cuts across the boundary connecting the two faces. The left hand side of equation (2.17) is split into three integrals, one over each surface. Now, let the length of the side of the cylinder shrink toward zero. As both materials 1 and 2 are of finite electrical conductivity, the current density must remain finite, and the integral over S_3 goes to zero. For S_1 and S_2 sufficiently small (but an order larger than S_3), equation (2.17) becomes

$$(\hat{\sigma}_1\dot{\mathbf{E}}_1\cdot\bar{\mathbf{n}})\Delta S - (\hat{\sigma}_2\dot{\mathbf{E}}_2\cdot\bar{\mathbf{n}})\Delta S = -\frac{\partial\rho_s}{\partial t}\,\Delta S \qquad (2.18)$$

where ΔS is the area of a face of the cylinder, and ρ_s is the surface charge density on the interface. Dividing out the ΔS and assuming a time harmonic field (i.e. replacing the field vectors by phasors and the time derivative by $j\omega$) yields

$$\hat{\sigma}_1\bar{\mathbf{E}}_{o1}\cdot\bar{\mathbf{n}} - \hat{\sigma}_2\bar{\mathbf{E}}_{o2}\cdot\bar{\mathbf{n}} = -j\omega\rho_{os} \qquad (2.19)$$

From equation (2.16) and assuming that the electrical permittivity is uniform and isotropic in each material

$$\epsilon_1\bar{\mathbf{E}}_{o1}\cdot\bar{\mathbf{n}} - \epsilon_2\bar{\mathbf{E}}_{o2}\cdot\bar{\mathbf{n}} = \rho_{os} \qquad (2.20)$$

Substituting in equation (2.19) gives

$$(\hat{\sigma}_1 + j\omega\epsilon_1)\bar{\mathbf{E}}_{o1}\cdot\bar{\mathbf{n}} = (\hat{\sigma}_2 + j\omega\epsilon_2)\bar{\mathbf{E}}_{o2}\cdot\bar{\mathbf{n}} \qquad (2.21)$$

As pointed out in the previous section, displacement currents are negligible in comparison to conduction currents and $\sigma/\omega\epsilon$ is much greater than one for the materials and frequency of interest to this study. For the diagonal tensor conductivity case, which is assumed here, each component of the diagonal tensor must be much greater than $\omega\epsilon$ in each of the materials. Thus, neglecting displacement currents, the normal component of current is continuous across a boundary between two materials of finite electrical conductivity.

Treating the problem as quasi-static and assuming there are no double layers of charge at the interface, the electric potential must be continuous across the boundary. Thus the boundary conditions used are

$$\hat{\sigma}_1 \bar{E}_{01} \cdot \bar{n} = \hat{\sigma}_2 \bar{E}_{02} \cdot \bar{n} \qquad (2.22)$$

$$\psi_1 = \psi_2 \qquad (2.23)$$

In this discussion of the boundary between two materials of finite conductivity it was assumed that the conductivity was discontinuous at the boundary. In an actual oil sand formation the conductivity may change continuously between the oil sand and the overburden or underburden. The electric fields calculated assuming either a sharp, discontinuous boundary, or assuming a continuous transition over a short distance will be the same except in the transition region. As no data is available describing how the conductivity changes from the oil sand to the surrounding formations, and as the transition distance is likely small compared to the formation thickness or the thickness of the simulation grid blocks, it is assumed that a sharp, discontinuous change in conductivity occurs at the boundary.

2.2 Heat Generation from Ohmic Losses

The time average heating rate due to electrical conduction is given by

$$Q_1 = \hat{\sigma}\bar{E}_0 \cdot \bar{E}_0^* \tag{2.24}$$

where Q_1 is measured in watts (W/m^3), and r.m.s. values are used for the electric field. In terms of the electric potential and for the case of three dimensional, multiphase heating, with a real diagonal conductivity tensor, and assuming the quasi-static approximation, the average heating rate is

$$\begin{aligned} Q_1 = {} & \sigma_x\left[\frac{\partial\psi_1}{\partial x}\right]^2 + \sigma_y\left[\frac{\partial\psi_1}{\partial y}\right]^2 + \sigma_z\left[\frac{\partial\psi_1}{\partial z}\right]^2 \\ & + \sigma_x\left[\frac{\partial\psi_2}{\partial x}\right]^2 + \sigma_y\left[\frac{\partial\psi_2}{\partial y}\right]^2 + \sigma_z\left[\frac{\partial\psi_2}{\partial z}\right]^2 \end{aligned} \tag{2.25}$$

where $\psi_0 = \psi_1 + j\psi_2$ (i.e. ψ_1 is the real part of the potential and ψ_2 is the imaginary part of the potential).

2.3 The Mathematical Model Assuming No Fluid Flow

When it is assumed that no significant fluid flow will occur during the electrical heating, heat transport is limited to thermal conduction. The mathematical model consists of the electrical potential and electrical heating equations given above, and the conservation of energy equation,

$$M\frac{\partial T}{\partial t} = \nabla\cdot(k\nabla T) + Q_1 \qquad (2.26)$$

where M is the volumetric heat capacity of the material ($J/m^3\cdot K$), k is the thermal conductivity ($W/m\cdot K$), T is the temperature (°C) and Q_1 is the heat produced by electrical heating (W/m^3). In this work, both the thermal conductivity and the volumetric heat capacity are assumed to be constants (for a given material), even though Cassis et al. (1985) have recently reported on the temperature variation of the volumetric heat capacity of oil sands. This assumption of a constant thermal conductivity in each medium allows the removal of the thermal conductivity to outside of the divergence operator in equation 2.26. However, as different media in the problem domain may have different thermal conductivities, the thermal conductivity will be involved in the calculation of the boundary conditions at interfaces between different media.

2.4 The Mathematical Model for Fluid Flow

A petroleum reservoir consists of a rock matrix and several fluid components which will be mobile during the production of the reservoir. These mobile components could include different hydrocarbons (oil or bitumen, and natural gas), initial reservoir water, and injected fluids (such as water, steam, or various other gases). In some unconsolidated (uncemented) reservoirs, in particular the

Tia Juana field in Venezuela, formation compaction and/or sand production may contribute significantly to reservoir performance and must be included in the model (de Haan and van Lookeren, 1972).

The oil in a reservoir actually consists of a large number of different chemical compounds, with different fluid and thermodynamic properties (Hunt, 1979). To include each chemical separately in the model would necessitate an enormous amount of data collecting and computation. In general, it is possible to lump all of the components together into one or more pseudo-components. The bitumen in oil sand is usually modelled as one or two pseudo-components, while in a gas condensate reservoir it may be necessary to use six or seven hydrocarbon pseudo-components to obtain a good model (Coats, 1982). In the Alberta Research Council's Two Component Model, used in the present work, only two components are used to model the reservoir fluids, a non-volatile bitumen component and a water component.

The modelling of classical fluid dynamics is done by applying three conservation principles: conservation of mass, conservation of momentum, and conservation of energy (Potter, 1973). In modelling the flow of fluids through a porous media, however, the conservation of momentum equation is replaced by Darcy's Law. The application of conservation of mass, conservation of energy, and Darcy's Law to the modelling of oil sand reservoirs is discussed in the next three sections. This discussion is intended simply to provide an introduction to the modelling of fluid flow in petroleum reservoirs. For a more detailed and mathematically rigorous treatment of the volume averaging of the microscopic flow equations in a porous medium, the reader is refered to the works of de la Cruz and Spanos (1983) and Patel, Hegde, and Slattery (1972).

2.4.1 Conservation of Mass

The conservation of mass equation may be written in point form as

$$\nabla\cdot(\rho_{mi}\bar{v}_i) = -\frac{\partial\rho_{mi}}{\partial t} - q_i \tag{2.27}$$

where ρ_{mi} is the mass density (kg/m³) of a particular fluid component, $\bar{v}_i$ is the velocity (m/s) of the fluid component, and q_i is a local sink term. While equation (2.27) is correct for a fluid flowing in a petroleum reservoir, the solution of this equation, in the form given above, would be intractable. The manner in which equation (2.27) is altered to simplify the complex boundary conditions arising from the presence of the rock and other fluids in a petroleum reservoir is discussed in the next few paragraphs.

In general, a fluid component in a reservoir can exist in more than one phase. For example, water may exist as a liquid or a gas, depending on the temperature and pressure. While there may be mass transfer between the phases, the phases do not mix. In modelling an oil reservoir it is convenient to think of three phases existing, namely an oil phase, a liquid water phase, and a gas phase. Two liquid phases are used, as the water and the oil will generally be separate and not mixed. Each phase will have a mass density (denoted by ρw, ρo, and ρg for the water, oil and gas phases, respectively) which will depend on the temperature, pressure, and the components present in that phase. In the ARC Two Component Model the oil component is non-volatile, so only water vapour (i.e. steam) will be present in the gas phase.

In a reservoir, any component will occupy only a fraction of the total volume, with the reservoir rock and the other fluid components occupying the rest of the reservoir. The fraction of the reservoir not occupied by rock is known as the porosity, denoted by ϕ. The fraction of the reservoir occupied by the fluids is further subdivided to denote the fraction of the porosity which is occupied by each phase. In common practice Sg denotes the local gas saturation, or fraction of the porosity that is occupied by the gas phase. Similarly, So and Sw represent the fractions occupied by the oil phase and water phase respectively. Thus, the macroscopic average density of a fluid phase in the petroleum reservoir is the product of its microscopic density, the phase saturation, and the porosity of the reservoir rock. This average density may substituted into the right hand side of equation (2.27) in place of the microscopic component density. In the ARC Two Component

Thermal Model, only the water component can be present in the water phase and the gas phase and hence, in moving from a microscopic to a more macroscopic view, the water component density, ρ_{m1}, is replaced by the average water component density ($\rho w\ Sw\ \phi + \rho g\ Sg\ \phi$). Similarly, the oil component is the sole constituent of the oil phase, and hence the microscopic oil component density is replaced in the oil mass conservation equation by the average oil phase density ($\rho o\ So\ \phi$).

The sink (or source) term, q, in equation (2.27) is used to model a production (or injection) well. At such a well, fluid is taken from (or added to) the reservoir.

Now consider the left hand side of equation (2.27). The component velocity shown in the equation is for the microscopic level. At this level the velocity changes in magnitude and direction as the fluid moves around the rock and other fluids present in the reservoir. It is common practice in the modelling of petroleum reservoirs to replace this microscopic fluid velocity with a macroscopic average fluid phase velocity, calculated by the use of Darcy's Law.

2.4.2 Darcy's Law

In 1856, a monograph written by Henry Darcy (1856), concerning the modernization of the public water works in the city of Dijon, France, was published. One section of the monograph was entitled "Determination of the Law of Flow of Water through Sand", and reported a series of experiments which were performed to determine the rates of water flow through packed sand filters. The empirical formula was developed by Darcy in which the rate of water flow depended on the length and cross-sectional area of the sand pack, the difference in the head of water at the inlet and outlet ends, and an empirical constant.

Darcy's Law has evolved from this first expression. The water head has been divided up into a pressure term and a gravity term, the constant of proportionality has been divided into the fluid property of viscosity and the rock property of permeability and differential notation has been introduced. The form used in the ARC literature on the Two Component model is

$$\tilde{v} = -\frac{K}{\mu}(\nabla P - \gamma \nabla z) \qquad (2.28)$$

where $\tilde{v}$ is the apparent velocity (m/s), K is the absolute permeability (m^2), μ is the water viscosity (Pa-s), P is the water pressure (Pa), γ is the pressure gradient due to gravity (kPa/m) and is equal to the product of the mass density and the gravitational acceleration constant ($\gamma = \rho_m g$), and z is the depth (m) increasing downward.

Darcy's Law has been derived analytically by Hubbert (1940) for single phase flow. In his derivation he was forced to make the following assumptions:

1. The fluid velocity was low enough that the kinetic energy was always much less than the gravitational potential energy and the work done in compressing the

fluid to the reservoir presssure.

2. The frictional force term on the fluid was much greater than the inertial reaction term for the fluid.
3. The fluid density is only a function of the fluid pressure.

Further, El-Feky (1977) points out that Darcy's law implies that the flow potential field is conservative, or irrotational. He shows, for a non-isothermal reservoir, that if the flow potential gradient and the temperature gradient are not parallel, then this will not necessarily be the case. However, Darcy's Law has been used in all the thermal simulators discussed in the literature that the author has seen, and it is assumed that the error introduced by continuing to use Darcy's Law in the non-isothermal case is no bigger than the errors introduced by any of the other assumptions.

Equation (2.28) applies only to single phase flow. In a typical petroleum reservoir, however, there are two or three phases flowing. Each phase will interfere with the ability of the other phases to flow. In an attempt to model multi-phase flow with Darcy's Law, the concept of relative permeability was introduced. The effective permeability of the rock to a particular phase is equal to the rock permeability with just water present times a relative permeability factor, which is assumed to be a function of the saturations of all phases present.

Using the concept of relative permeability, Darcy's law (2.28) is substituted into the mass conservation equation (2.27) for each component. For the oil component the combined equation is

$$\frac{\partial}{\partial t}(\phi\ \rho o\ So) = \nabla\cdot\left[\frac{K\ Kro\ \rho o}{\mu o}(\nabla Po - \gamma o\nabla z)\right] - qo \qquad (2.29)$$

and for the water component the combined equation is

$$\frac{\partial}{\partial t}(\phi\ \rho w\ Sw + \phi\ \rho g\ Sg) = \nabla\cdot\left[\frac{K\ Krw\ \rho w}{\mu w}(\nabla Pw - \gamma w\nabla z)\right.$$

$$\left. + \frac{K\ Krg\ \rho g}{\mu g}(\nabla Pg - \gamma g\nabla z)\right] - qw - qg \qquad (2.30)$$

where Kro, Krw, and Krg are the relative permeabilities to the oil phase, water phase and gas phase, respectively, qo, qw, and qg are the oil, water and gas production rates, respectively, and Po, Pw, and Pg are the oil, water, and gas phase presssures, respectively. The bulk densities of the oil, water and gas phases are given by ρo, ρw, and ρg, respectively.

In addition, the local saturations at every point in the reservoir are constrained to add up to unity. (All of the pore space must be occupied by either gas, oil, or water phase.)

$$Sg + So + Sw = 1 \qquad (2.31)$$

Interfacial tensions between the different phases will result in slightly different pressures at the same point for the different phases. This introduces an additional two equations, known as the capillary pressure equations.

$$Pcgo = Pg - Po \tag{2.32}$$

$$Pcow = Po - Pw \tag{2.33}$$

where Pcgo and Pcow are the gas-oil and oil-water capillary pressures (Pa), respectively.

The phase behavior for water is modelled by a phase equilibrium equation when both liquid and gas phases are present. The equation used is

$$K_w = \frac{Y_w}{X_w} \tag{2.34}$$

where K_w is an equilibrium constant, Y_w is the mole fraction in gas and X_w is the mole fraction in liquid. K_w is a function of temperature and pressure.

2.4.3 Conservation of Energy

Energy can be present in a fluid and rock system in several forms.

1. **Thermal energy or heat.** In a petroleum reservoir, thermal energy may be transfered from point to point by thermal conduction, or by moving fluids (convection). Heat may be added to or subtracted from the reservoir by injecting or producing a fluid such as steam or oil. In the current work, heat will also be added by electrical heating. Thermal energy is accumulated in a reservoir volume by changes in the amounts and enthalpies of the components present in the volume. The enthalpies of the

different components depend on pressure, temperature, and phase.

2. **Chemical Energy.** As no chemical reactions are included in this model, the overall chemical energy of the system will not change.
3. **Kinetic Energy.** As the kinetic energy, as well as its rate of change, are small when compared to the thermal energy and its rate of change, kinetic energy is neglected when calculating the total energy of the system.
4. **Viscous Shear Heating.** The total amount of energy converted to heat by viscous shear heating is small and is neglected when calculating the total energy of the system.
5. **Potential Energy.** Potential energy is neglected when calculating the total system energy. A simple calculation shows that a drop of oil would have to fall over 150 m to gain enough energy to raise it's temperature one degree celsius.

As noted above, only thermal energy is included in the energy balance for the reservoir. The energy equation used in the ARC Two Component Model is

$$\begin{aligned} &\frac{\partial}{\partial t}[\phi(\rho w\ Sw\ Uw + \rho g\ Sg\ Ug + \rho o\ So\ Uo) \\ &+ (1 - \phi)\rho r\ Ur] = \nabla\cdot(k\ \nabla T) \\ &- \nabla\cdot(\rho w\ Uw\ \bar{v}w + \rho g\ Ug\ \bar{v}g + \rho o\ Uo\ \bar{v}o) + Q_l \end{aligned} \tag{2.35}$$

where Ug, Uo, Uw, and Ur are the internal energies of the gas, oil and water phases and of the reservoir rock (J/kg), k is the thermal conductivity of the reservoir (W/m·K), and Q_l is the heat added to the reservoir (W/m^3). Heat may be added by steam injection, subtracted by losses to the adjacent formation, and, in the case of the current study, added by electrical heating.

3. Solution of the Mathematical Model with No Fluid Flow

The analytic solution of the mathematical model developed in Chapter 2 is difficult even in the simplest of geometries. Solution of the model for the Electric Pre-heat and Steam Drive Process, for a case which realistically simulates an actual oil sand formation, is possible only when using a numerical solution method. In the present work, two FORTRAN language computer codes were written to numerically solve the mathematical model presented in Chapter Three. The first program, entitled EPEIOS, was written in its entirety by the author of this thesis, and solves the combined electrical heating and thermal conduction model (i.e. no fluid flow). This first program is discussed in the present chapter. The second program, entitled TCTM-EPEIOS, incorporates the Alberta Research Council's Two Component Thermal Model, sections of EPEIOS, and the necessary interface routines, to solve the combined electrical heating and fluid flow model. The methods used to calculate the electrical potentials and the electrical heating rates in the reservoir, once the electrical conductivities are known, are identical for both programs. These methods are discussed in detail in this chapter. The solution of the fluid flow equations, and the electrical and fluid flow models are discussed in the next chapter.

Three major techniques have been developed to numerically solve electromagnetic and electrostatic problems. These three techniques are the finite difference method, the finite element method, and the numerical integration method. The finite difference method was chosen as the means of numerical solution in EPEIOS for two major reasons. Firstly, the ARC Two Component Thermal Model is implemented using a finite difference method. If a method other than the finite difference method, such as the finite element method, had been used in the electrical part of the model, interfacing problems with the fluid flow part would have been greatly increased. Secondly, the group of people who are projected as the main users of EPEIOS are familiar with the finite difference method, and the problems and pitfalls associated with it.

A large number of texts exist which describe the finite difference method. In particular, the ones used by the author include Carnahan, Luther, and Wilkes (1969), Potter (1973), and Ames (1977). Resistivity modelling of arbitrary, three dimensional, structures is done in the area of geological prospecting, often using the finite difference method. In particular, two works in this field are those of Hermance (1982), and Dey and Morrison (1979).

3.1 Overall Solution Algorithm

An overall, schematic, flow chart for EPEIOS is given in Figure 3.1. A User's Reference Manual, detailing the various inputs needed for the program, is presented in Appendix III of this thesis. Most of the functional units present in the flow chart are discussed in detail in this

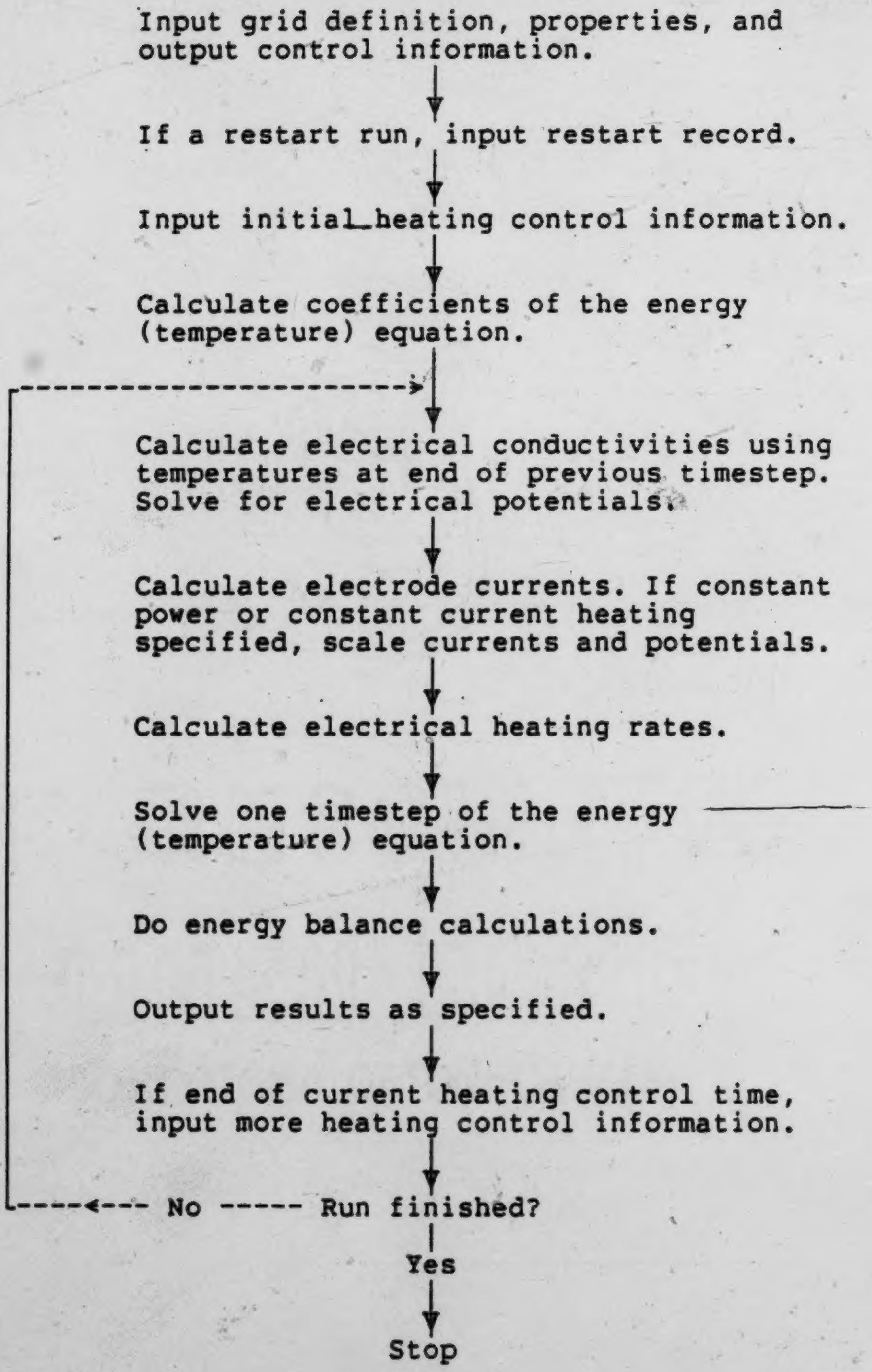

Input grid definition, properties, and output control information.

If a restart run, input restart record.

Input initial heating control information.

Calculate coefficients of the energy (temperature) equation.

Calculate electrical conductivities using temperatures at end of previous timestep. Solve for electrical potentials.

Calculate electrode currents. If constant power or constant current heating specified, scale currents and potentials.

Calculate electrical heating rates.

Solve one timestep of the energy (temperature) equation.

Do energy balance calculations.

Output results as specified.

If end of current heating control time, input more heating control information.

Figure 3.1 A flow chart showing the order of the major calculations in the program EPEIOS.

chapter.

As seen in Chapter 2, the electrical potential is found using the boundary conditions (including the voltages applied to the electrodes in the problem domain) and the electrical conductivities of the conducting regions of the problem domain. The heating rates are calculated from the potentials and the electrical conductivities. These heating rates are used either in the heat conduction equation (if the assumption of negligible fluid flow and expansion is made), or in a set of fluid flow and energy equations (if it is assumed that fluid flow and expansion are important). The temperature changes found in either of these two different models will result in changes to the electrical conductivities. Thus, the electrical heating rates are coupled to either of the energy equations used by the change in temperature (and the change in fluid saturations when using the fluid flow equations) which cause changes in the electrical conductivities throughout the problem domain.

In EPEIOS, the equations governing the electrical heating rates and the energy equation were coupled explicitly by first solving the electrical potential equation and calculating the heating rates, then holding the heating rates fixed for one timestep of either the heat conduction equation, or the set of fluid flow and energy equations. This method was developed by the author in previous work (1981,1983). It is stable, and provides results which are in good agreement with analytic and experimental results, if the maximum change of electrical conductivity in one time step is limited to some small value (approximately 5% of the electrical conductivity at the beginning of the timestep). Initially, the heating rates in TCTM-EPEIOS were also treated explicitly. However, a method was later developed to couple the heating rates to the energy and flow equations in a fully implicit manner. This method will be discussed in Chapter 4.

Thus, the overall solution algorithm is as follows. First, the electrical conductivity is found throughout the problem domain from the current values of the temperature, and the user specified electrical properties. In the explicitly coupled version of TCTM-EPEIOS, the current values of water saturation are also used in the electrical conductivity calculation. Once the electrical conductivity is known, the electrical potential is found. The potentials are used to calculate the heating rates. Once the heating rates have been found, they are used as inputs to either the heat conduction equation used in EPEIOS, or the set of fluid flow and energy equations used in TCTM-EPEIOS. These latter equations are advanced for one time step. The new values of temperature (and saturations for the fluid flow case in TCTM-EPEIOS) thus found are used to calculate new electrical conductivity values, and the cycle is repeated.

An extensive discussion of the electrical conductivity of oil sand, and its dependence on temperature and water saturation, is given in Chapter 6. In the computer program

EPEIOS (which includes only the heat conduction equation) the electrical conductivity is modelled as a continuous, piece-wise linear, function of temperature. For each medium in the reservoir being modelled (whether oil sand, shale or limestone) an electrical conductivity at 24°C, and several parameters defining the temperature function, must be input. The exact form of the equation used is given in Appendix III, which contains the EPEIOS reference manual. In TCTM-EPEIOS, the electrical conductivity varies not only with temperature, but also with water saturation and porosity. (The variation of electrical conductivity with water saturation and porosity is discussed in the next chapter.)

The solution of the current continuity equation to find the electrical potentials throughout the domain is described in Section 3.2 and its subsections. The solution method is common to both EPEIOS and TCTM-EPEIOS. The calculation of the heating rates, also common to both EPEIOS and TCTM-EPEIOS, is described in Section 3.3. The differencing and solution of the heat conduction equation, used only in EPEIOS, is discussed in section 3.4. Energy balance calculations, which give one indication of how well EPEIOS is working, are described in section 3.5. The testing of the computer program EPEIOS is described in section 3.6 and Appendix V. The implementation and testing of the combined electrical heating and fluid flow model (in TCTM-EPEIOS) is discussed in Chapter 4.

3.2 Solution of the Current Continuity Equation

The current continuity equation (Equation 2.13) may be separated into two equations, an equation involving the real part of the potential and an equation involving the imaginary part of the potential. These two equations will be identical in the domain of the problem, with the only differences between the two equations being the specific boundary conditions at the electrodes. (The equation involving the real part of the potential will have the real part of the electrode voltage as the boundary condition at the electrode, and, correspondingly, the equation for the imaginary part of the potential will have the imaginary part of the electrode voltage as the boundary condition at the electrode.) Other than the boundary conditions, the two equations have identical coefficients and are solved in an identical manner. If the boundary conditions are different, as is the case in a true multi-phase problem, different solutions will result for each equation.

3.2.1 A Conservative Finite Difference Formulation

A conservative, block centered, seven point, three dimensional formulation was used to difference the current continuity equation. The formulation allows for unequal and irregular grid block dimensions. The electrical conductivity is assumed to be known prior to the calculation of the electric potentials.

Using the finite difference method, in cartesian coordinates, the problem domain is divided into a three dimensional grid of rectangular prisms. Each grid block is denoted by a set of three indices which indicate its position, relative to the other grid blocks, in the X, Y, and Z directions. For an arbitrary grid block, denoted by indices (i,j,k), the grid block dimensions, and the indices of the adjacent blocks, are given in Figure 3.2. The potential at the center of grid block (i,j,k) is denoted by $\psi_{i,j,k}$, and the electrical conductivity at the center of the grid block by $\sigma_{i,j,k}$.

The current continuity equation (Equation 2.13) is integrated over the volume of each grid block. By means of the divergence theorem, the volume integrals are converted to surface integrals. Each surface integral is split into the sum of six separate integrals, one for each face of the rectangular prism grid block. Each of the surface integrals for one face is of the form

$$\int_{s} \left(\hat{\sigma}\cdot\frac{\partial\psi}{\partial n}\right) ds \qquad (3.1)$$

where $\bar{n}$ is the outward normal to the surface (face) of the grid block. The sum of the six integrals must be zero for each grid block, indicating that no charge is accumulated in the grid block.

The approximation is made that the normal electric field (potential derivative) and the electrical conductivity are constant over each particular face of each grid block.

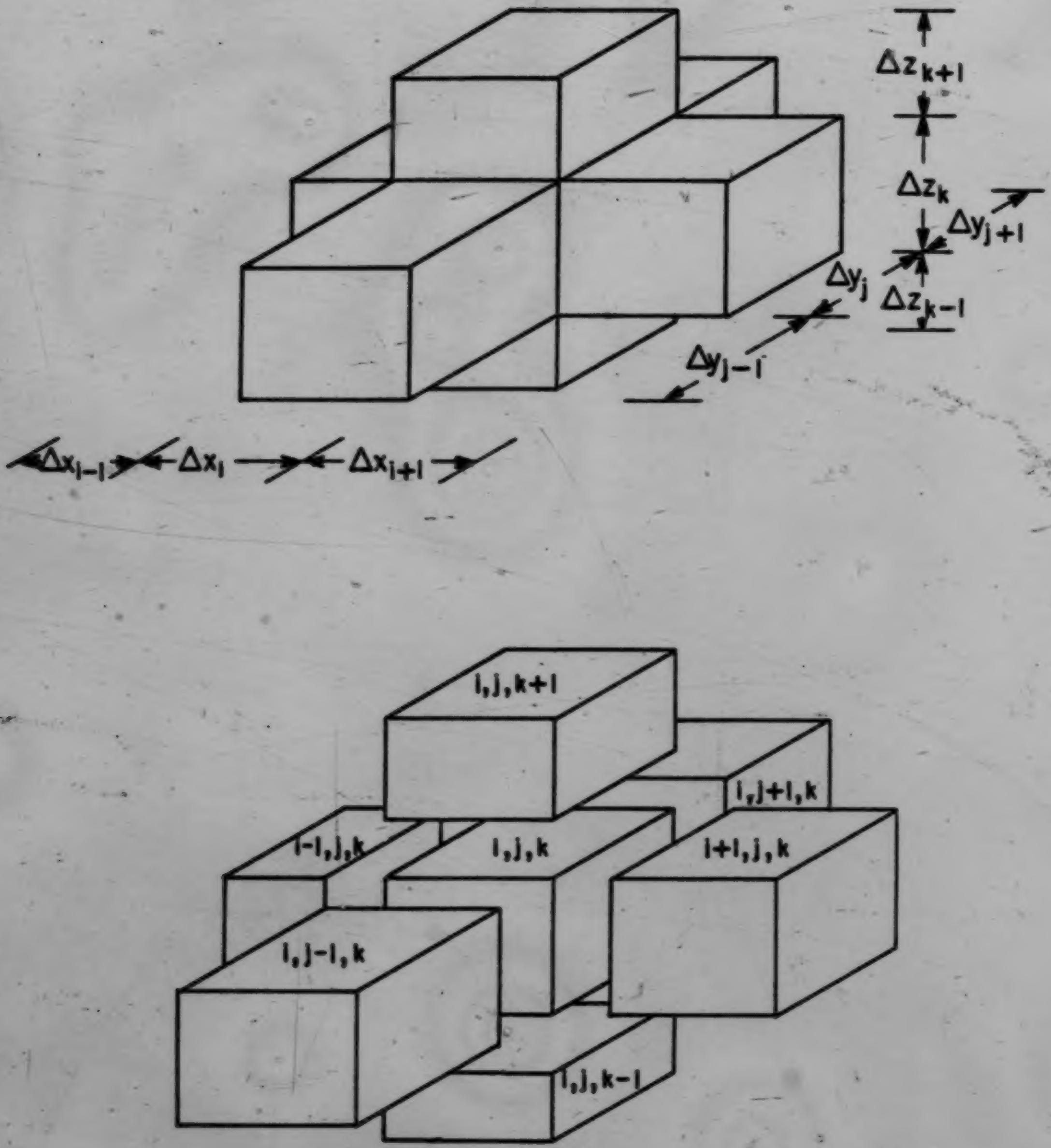
Δz k+1
Δz k
Δy j+1
Δy j
Δz k-1
Δy j-1
Δx i-1
Δx i
Δx i+1
i,j,k+1
i,j+1,k
i-1,j,k
i,j,k
i+1,j,k
i,j-1,k
i,j,k-1

Figure 3.2 The dimensions and relative locations of an arbitrary grid block and the six adjacent blocks.

As faces of the grid blocks are aligned with the coordinate axis, the six surface integrals for one grid block become

$$
\begin{aligned}
&- \Delta z_k \Delta y_j \left(\sigma_x \frac{\partial\psi}{\partial x}\right)\Bigg|_{-x} + \Delta z_k \Delta y_j \left(\sigma_x \frac{\partial\psi}{\partial x}\right)\Bigg|_{+x} \\
&- \Delta z_k \Delta x_i \left(\sigma_y \frac{\partial\psi}{\partial y}\right)\Bigg|_{-y} + \Delta z_k \Delta x_i \left(\sigma_y \frac{\partial\psi}{\partial y}\right)\Bigg|_{+y} \\
&- \Delta x_i \Delta y_j \left(\sigma_z \frac{\partial\psi}{\partial z}\right)\Bigg|_{-z} + \Delta x_i \Delta y_j \left(\sigma_z \frac{\partial\psi}{\partial z}\right)\Bigg|_{+z} = 0 \qquad (3.2)
\end{aligned}
$$

where "+x" indicates the face of the grid block in the positive X direction, "-x" indicates the face of the grid block in the negative X direction, and similarly for the Y and Z directions, and Δx_i, Δy_j, and Δz_k are the length, width, and height of the grid block, as shown in Figure 3.2. Equation 3.2 may be further simplified by dividing each term by $\Delta x_i \Delta y_j \Delta x_k$. Each term is then dependent only on the dimensions and properties in one direction.

Complex finite difference formulations have been developed which use twenty seven adjacent blocks in developing each finite difference equation. (See Hermance (1982) for an example of a nine point, two dimensional method which could be extended to three dimensions.) In these formulations, each grid block face is further sub-divided into four regions, each with a different surface integral. The center grid block and several of the adjacent blocks are used to calculate the approximations of the normal electric field and the electrical conductivity for each surface integral. While these more complex, twenty seven point formulations may be more accurate than the seven point formulation used in the present work, using more grid blocks adds to the complexity of the calculations in both setting up and solving the finite difference equations. Since sufficient accuracy was obtained using a formulation involving only seven adjacent grid blocks, the added cost of a twenty seven grid block formulation was not felt to be warranted.

Thus, in EPEIOS and TCTM-EPEIOS, the finite difference formulation approximates the electric field (negative of the potential gradient) at each face by using only the potential at the center of the grid block that the current integral is being performed on, and the potential at the center of the one other, adjacent, grid block that shares that block face. The value of the current integral for a particular face will depend linearly on the potentials involved in the calculation. The electric fields normal to each face of the grid block are calculated independently of the electric fields at the other faces. The properties of the other grid blocks, adjacent to the other faces of the grid block, do not affect the approximations made for a particular grid block face. Thus, the partial differential equation (Equation 2.13) is reduced first to a set of surface integrals (Equation 3.2, one for each grid block), and finally to a set of algebraic equations. Each algebraic equation has seven unknowns (the potentials at the centers of the grid blocks, used in approximating the electric fields, are unknown and are what is being solved for), and there is one equation for each grid block. The correct boundary conditions will reduce the number of unknowns and make the set of algebraic equations solvable. The algebraic equations resulting from the finite difference approximations will be of the form

$$
\begin{aligned}
&C_{-x}\psi_{i-1,j,k} + C_{-y}\psi_{i,j-1,k} + C_{-z}\psi_{i,j,k-1} \\
&- (C_{-x} + C_{-y} + C_{-z} + C_{+x} + C_{+y} + C_{+z})\psi_{i,j,k} \\
&+ C_{+x}\psi_{i+1,j,k} + C_{+y}\psi_{i,j+1,k} + C_{+z}\psi_{i,j,k+1} \\
&\quad = 0 \qquad (3.3)
\end{aligned}
$$

where the coefficients (C_{-x}, etc.) are calculated from the dimensions of the grid blocks and the known electrical conductivities at the centers of the grid blocks. (Note that the coefficients will, in general, be different for each equation, and should also have sets of indices indicating which grid block equation they are associated with. These have been omitted for clarity.) The calculation of these coefficients is discussed below.

There will be one equation, of the form given in Equation 3.3, for each grid block which is part of the problem domain. Some of the grid blocks may be designated as electrically insulating, and there would be no equations for such blocks. (The potentials of these grid blocks would be undefined. As they are considered to be perfect electrical insulators, no current will flow in them and no heat will be produced.) It is also necessary to use some of the grid blocks to indicate the positions of electrodes. Grid blocks which are parts of electrodes are assumed to be perfect conductors, and no heat is produced by the current flowing in them. There is no finite difference equation for grid blocks which are designated as parts of electrodes.

As previously mentioned, the calculation of each of the coefficients in the set of algebraic difference equations (each similar to Equation 3.3) is dependent only on the properties and dimensions of the center grid block and the grid block in the direction of interest for the particular coefficient being calculated. Depending on the properties of the two grid blocks in question, one of four different procedures is selected in EPEIOS for calculating the coefficient. These procedures, and the assumptions implicit in them, were developed with careful attention to the requirement that the current out of the grid block through a particular face of the grid block was equal to the current into the adjacent grid block through that same face. This may seem self evident. However, it is possible to develop some apparently correct finite difference formulations which do not follow this requirement.

In addition, it must be remembered that the values for the electrical field strength normal to the block boundary, and the electrical conductivity at the block boundary, are only approximated with the formulas used. For example, while the electrical potential may actually vary according to some arbitrary function between two grid points, the approximation of the field strength at the block boundary is, for evenly sized grid blocks, exact only if the potential may be exactly described by a second order polymonial. If the potential actually varies according to some higher order function, the higher order terms are lost in the approximations made. It is important, therefore, to have many small grid blocks in regions of the problem domain where the potential and/or electrical conductivity is varying rapidly in any direction.

The four different procedures used in calculating the the coefficients of the finite difference equations, and the selection criteria used for choosing a particular procedure, are as follows:

1. If the adjacent grid block in the direction of interest is of the same material as the center grid block (i.e. the input data indicates that the two blocks have the same electrical conductivity at 24°C and the same temperature dependence of electrical conductivity), the magnitude of the normal electric field component at the grid block face is calculated from the first order numerical derivative of the potentials at the centers of the grid block. (The difference of the potentials is divided by the distance between them.) Thus, the negative of the normal electric field component at the grid block face in the positive X direction is

$$\left.\frac{\partial\psi}{\partial x}\right|_{+x} = \frac{\psi_{i+1,j,k} - \psi_{i,j,k}}{\frac{\Delta x_i + \Delta x_{i+1}}{2}} \qquad (3.4)$$

The approximate electrical conductivity at the grid block face is found by linear interpolation of the known conductivities at the two centers of the grid blocks sharing the grid block face. Thus, at the face in the positive X direction,

$$\sigma_x\big|_{+x} =$$

$$\sigma_{x\,i,j,k}\left(1-\frac{\Delta x_i}{\Delta x_i+\Delta x_{i+1}}\right) + \sigma_{x\,i+1,j,k}\left(\frac{\Delta x_i}{\Delta x_i+\Delta x_{i+1}}\right) \qquad (3.5)$$

These two approximations are combined, and the terms involving the potentials at each of the grid block centers are separated, to find the coefficient in the positive X direction for equation 3.3.

$$C_{+x} =$$

$$\frac{2\left[\sigma_{x\,i,j,k}\left(1-\frac{\Delta x_i}{\Delta x_i+\Delta x_{i+1}}\right) + \sigma_{x\,i+1,j,k}\left(\frac{\Delta x_i}{\Delta x_i+\Delta x_{i+1}}\right)\right]}{(\Delta x_i+\Delta x_{i+1})\Delta x_i} \qquad (3.6)$$

2. If the adjacent grid block is an electric insulator, no current will flow across that face of the grid block. This case is modelled in the finite difference equation by setting the coefficient of the finite difference equation to zero. If the adjacent grid block in the positive X direction is an insulator, then

$$C_{+x} = 0. \qquad (3.7)$$

3. If the adjacent grid block is an electrode, the potential at the grid block face is the electrode potential. The distance used in calculating the electric field (potential derivative) at the grid block face must be adjusted appropriately. As the electrode block does not have a defined electrical conductivity, the conductivity at the block face is taken to be the same as at the center of the current grid block. For the positive X direction, the coefficient becomes

$$C_{+x} = \frac{2\sigma_{x\,i,j,k}}{\Delta x_i \cdot \Delta x_i} \tag{3.8}$$

The potentials of the electrode blocks are specified when setting up the problem.

4. In the final case, the adjacent grid block is composed of an electrically conducting material, but with a different electrical conductivity at 24°C, or a different temperature dependence of electrical conductivity, than the current grid block. In actual oil sand formations, adjacent oil sand, shale, or limestone layers may have electrical conductivities differing by over an order of magnitude. It is necessary to use a different formula in calculating the finite difference equation coefficients across such an interface, or the large discontinuity in the conductivity will lead to a large error in the calculated electrical field strength at the block face. The boundary conditions at an interface between two regions of different conductivity

are discussed in detail in section 2.1.4 of this thesis. Two boundary conditions, given by equations (2.22) and (2.23), are applied at the grid block face. These equations state that the electric potential is continuous across the interface, and that the current density is the same on both sides of the grid block face. When these two conditions are applied, if the electrical conductivity changes abruptly at the grid block face, so must the electric field. To preserve continuity of electrical current (i.e. to have the same current flow out of one grid block as flows into the adjacent grid block) a different electric field must be calculated for each side of the grid block face. The electric field and electrical conductivity are approximated as being constant in each grid block, between the grid block center and the grid block face in question (Hiebert, 1981; Hiebert et al., 1983). The coefficient of the finite difference equation, for the positive X direction, becomes

$$C_{+x} = \frac{2\sigma_{x\,i,j,k}}{\Delta x_i\left(\Delta x_i + \dfrac{\sigma_{x\,i,j,k}\Delta x_{i+1}}{\sigma_{x\,i+1,j,k}}\right)} \qquad (3.9)$$

Note that this formula and that of equation (3.6) will reduce to the same result for equal grid block sizes and equal conductivities.

Each of the finite difference equations (Equation 3.3), which together make up the matrix which must be solved to find the potentials, are linearly independent of each other. Thus, each may be multiplied by some arbitrary constant without affecting the solution of the matrix as a whole. This property may be used to normalize the diagonal of the matrix (making the coefficient of the center grid block potential equal to unity). This eliminates the need to store this coefficient for each equation, reducing the storage requirements for the program significantly.

3.2.2 Solving the Set of Finite Difference Equations

Once the matrix of finite difference equations has been set up, the matrix must be solved. To appreciate the size of this problem, consider the case where the problem domain has been divided up into twenty grid blocks in each direction. The total number of grid blocks is eight thousand (20x20x20), resulting in eight thousand finite difference equations. If the entire matrix of equations was stored, sixty four million words of storage would be required. As each equation (row of the matrix) has only seven non-zero elements, over 99.9 % of the matrix elements would be zeros.

A number of methods of solution of these types of matrices, known as spare matrices, have been developed. These methods can be divided into two major classes, direct solutions and iterative solutions. Direct solution methods have the advantage of being more reliable, consistent, and accurate than iterative methods. However, iterative methods require less storage, and less computer time on problems involving a large number of grid blocks (Hageman and Young, 1981).

In the particular case of the problem being considered, where successive solutions for the potential are required, iterative techniques have one additional advantage which further reduces the amount of computer time required to obtain a solution. This stems from the fact that iterative solution methods require that an "initial guess" at the solution be used at the start of the first iteration. The number of iterations required to obtain a satisfactory solution is related to the closeness of the "initial guess" to the solution to the problem. In the problem under study, the electric potentials will change only slightly from time step to time step. Thus, once the potentials have been found for the initial timestep, a very good "initial guess" at the solution is available (i.e. the solution for the potentials obtained the previous time step). The presence of this good "initial guess" significantly reduces the number of iterations, and hence computer time, required to obtain a satisfactory solution. When using a direct matrix solution method, the same amount of computer time would be required each time step (Nex, 1980).

Two common iterative methods of matrix solution were used in solving for the potentials in EPEIOS, the Alternating Direction Iterative Procedure (ADIP), and the Point-wise Successive Over-Relaxation method (PSOR). The ADIP method is a well known method (Carnaham et al., 1969) and was the method used by the author in his previous, two dimensional, computer program. The PSOR method used was a direct implementation of the algorithms described in Hagman and Young (1981), which includes automatic, adaptive relaxation parameter selection. After comparative tests using each of the solution methods on the same problems, it was found that the PSOR method required significantly less computer time and memory to obtain the same degree of accuracy when compared with the ADIP method. While the PSOR method required more iterations to achieve convergence, each iteration required fewer multiplications, and significantly fewer memory references than for the ADIP method.

The final computer program, EPEIOS, includes only the PSOR method for solving the electrical finite difference equations. The coding and design of the subroutines was such that alteration of the program to use the FPS-164 Attached Array Processor, available in the University of Alberta computer system, should be reasonably simple and straightforward.

3.3 Calculation of the Electric Heating Rates

After the complex electrical potential at the center of each grid block has been found, the electrical heating rates, at the center of each grid block, may be calculated from Equation 2.26. The calculation of the heating rates requires taking the numerical derivative, in each of the three cartesian directions, for both the real and the imaginary part of the potential, and multiplying the square of each derivative by the appropriate element of the electrical conductivity tensor.

The numerical derivative calculations, for a particular grid block and in a particular direction, involve the calculated potential at the center of that grid block, as well as the calculated potentials at the centers of the two grid blocks adjacent to the grid block of interest in the direction of interest. As in the calculation of the finite difference coefficients, the formula used will depend on the properties of the center grid block and the adjacent grid blocks. A major difference exists, however, between the approximation of the electric field strengths in finding the coefficients of the finite difference equation and their approximation when finding the electrical heating rate. In the calculation of the coefficients of the finite difference equation the electric field strengths at the block boundaries are needed, while in the calculation of the electrical heating rate the electric field strength at the block center is needed. In most cases a higher order approximation to the electric field strength can be used when calculating the electrical heating rates.

If all three grid blocks are composed of the same material, the second order formula for the numerical derivative, given by Dorn and McCracken (1972) may be used.

$$\frac{\partial\psi}{\partial x} = \frac{h_1^2\psi_{i+1,j,k} + (h_2^2-h_1^2)\psi_{i,j,k} - h_2^2\psi_{i-1,j,k}}{h_1h_2(h_1 + h_2)} \qquad (3.10)$$

where h_1 is the distance from the center of the grid block to the center of the adjacent grid block in the negative X direction and h_2 is the distance to the center of the adjacent grid block in the positive X direction (i.e. $h_1 = (\Delta x_i + \Delta x_{i-1})/2$ and $h_2 = (\Delta x_i + \Delta x_{i+1})/2$). This formula will work well as long as the electrical potential is varying smoothly between the three grid centers used in the calculation.

If one or both of the adjacent blocks is a boundary block, or has different electrical properties than the block of interest, different formulas must be used, as either all three block center potentials needed for equation (3.10) are not present, or the electrical conductivity undergoes a discontinuity between two of the block centers, increasing the error involved in using equation (3.10). In the formulas used for these special cases, the potential derivatives at each grid block face are calculated using the same approximations used in developing the finite difference formulation. Once the potential derivatives at the block faces are known, the electric field at the center of the block in a particular direction is the root mean square (r.m.s.) value of the two potential derivatives at the grid block faces in that direction. The r.m.s. value is used as the electric heating rate depends on the square of the electric field strength.

1. If the adjacent block to one of the faces is of the same material as the center block (and the grid block

adjacent to the opposite face is not), then the simple forward or backward difference formula is used to calculate the derivative at that face. For example, at the grid block face in the positive X direction,

$$\left.\frac{\partial\psi}{\partial x}\right|_{+x} = \frac{\psi_{i+1,j,k} - \psi_{i,j,k}}{h_2} \qquad (3.11)$$

where h_2 is the same as defined above ($h_2 = (\Delta x_i + \Delta x_{i+1})/2$).

2. If one of the adjacent blocks is an electrical insulator, the normal electric field, and hence the potential derivative, at that face is zero.
3. If one of the adjacent blocks is an electrode, the potential at the grid block face is the electrode potential. The simple forward or backward difference is used to calculate the potential derivative at the grid block face, however, the distance between the known potentials is equal to the distance from the center of the middle grid block to the grid block face. If the electrode is in the positive X direction, then

$$\left.\frac{\partial\psi}{\partial x}\right|_{+x} = \frac{\psi_{i+1,j,k} - \psi_{i,j,k}}{\frac{\Delta x_i}{2}} \qquad (3.12)$$

4. If the adjacent grid block is a conducting block, but with different electrical properties than the middle block, the electric field will be discontinuous at the grid block face. The potential derivative just inside

the grid block is found from (for the positive X direction)

$$\left.\frac{\partial \psi}{\partial x}\right|_{+x} = \frac{\psi_{i+1,j,k} - \psi_{i,j,k}}{\frac{\Delta x_i}{2} + \frac{\sigma_{x\,i,j,k}\,\Delta x_{i+1,j,k}}{2\,\sigma_{x\,i+1,j,k}}} \tag{3.13}$$

In summary, the real and imaginary electric fields, at the center of each grid block, are calculated by numerical differentiation once the real and imaginary potentials are known. The heating rate for the grid block is then found using Equation 2.25. The calculated heating rates are used as inputs to either the thermal conduction equation (EPEIOS) or to the energy equation in the model involving fluid flow (TCTM-EPEIOS).

3.4 Solution of the Heat Conduction Equation

The heat conduction equation (Equation 2.26) is solved using the finite difference method, with the Douglas-Rachford Alternating Direction Implicit Method used to solve the set of finite difference equations.

In the current version of EPEIOS, the thermal conductivity and volumetric heat capacity of each grid block is fixed for the duration of the simulation (i.e. EPEIOS does not account for the variation of these properties with temperature). This slightly simplifies the differencing of the thermal conduction equation (as compared to the current continuity equation) as, in a region containing a single medium, the thermal conductivity can be taken outside the divergence operator. In addition, as the thermal properties and the geometry of the problem do not change during the simulation, the coefficients of the thermal finite difference equations are constant throughout the simulation. Thus, these coefficients are calculated once at the beginning of the simulation, whereas the coefficients of the current continuity finite difference equation must be recalculated each timestep (due to the changes in electrical conductivity with temperature).

A seven point, block centered, finite difference formulation was used to difference the thermal conduction equation, with the same grid used as was used for the current continuity equation. However, the thermal conduction equation differs from the current continuity equation in that the latter is static (there is no variation with time included directly in the equation) while the former includes a first derivative of temperature with time. Thus, for the thermal conduction equation, the current temperatures are known, but the temperatures at the end of the incremental time period (referred to as the time step) are unknown. The finite difference equation for each grid block may be written as

$$M_{i,j,k}(T^{n+1}_{i,j,k} - T^{n}_{i,j,k})/\Delta t^{n+1} =$$
$$C_{-x}T^{n+1}_{i-1,j,k} + C_{-y}T^{n+1}_{i,j-1,k} + C_{-z}T^{n+1}_{i,j,k-1}$$
$$- (C_{-x} + C_{-y} + C_{-z} + C_{+x} + C_{+y} + C_{+z})\, T^{n+1}_{i,j,k}$$
$$+ C_{+x}T^{n+1}_{i+1,j,k} + C_{+y}T^{n+1}_{i,j+1,k} + C_{+z}T^{n+1}_{i,j,k+1}$$
$$+ Q^{n}_{i,j,k} \qquad (3.14)$$

where $M_{i,j,k}$ is the volumetric heat capacity of block (i,j,k), $T^{n+1}_{i,j,k}$ is the unknown temperature at the end of the timestep, $T^{n}_{i,j,k}$ is the known temperature at the beginning of the timestep, Δt^{n+1} is the length of the time step, C_{-x}, etc., are the coefficients (given in detail in the next paragraph) of the finite difference equation, and $Q^{n}_{i,j,k}$ is the electrical heating rate calculated at the beginning of the timestep. For a detailed discussion of the finite difference solution of the thermal conduction equation, see Carnahan, Luther and Wilkes (1969). A detailed description of the algorithm used is given on page 453.

In EPEIOS, there were four cases to consider when differencing the conduction term ($k\nabla^2 T$) of the heat conduction equation. In a manner similar to the differencing of the current continuity equation, each of the six coefficients of the temperatures of the adjacent grid blocks was calculated independently of the others.

1. If the adjacent block is of the same material, with the same thermal properties, as the center block, then the formula used for the coefficient is

$$C_{+x} = \frac{2k_{i,j,k}}{\Delta x_i(\Delta x_i + \Delta x_{i+1})} \qquad (3.15)$$

where $k_{i,j,k}$ is the thermal conductivity and $T_{i,j,k}$ is the temperature of the center grid block.

2. If the adjacent block is a thermal insulator, or if the current block is on the edge of the problem domain so the adjacent block would be outside of the grid block structure, then there is no heat flow through that face of the grid block. The coefficient is set to zero.
3. If the adjacent block is part of a constant temperature region (used, for example, to simulate a cooled wellbore) then the temperature of the constant temperature region is imposed at the grid block face. The coefficient becomes

$$C_{+x} = \frac{2k_{i,j,k}}{\Delta x_i \cdot \Delta x_i} \qquad (3.16)$$

4. If the adjacent grid block is thermally conducting, but of a different material, with a different thermal conductivity, than the current grid block, then the temperature gradient must change abruptly at the grid block face (to maintain a constant heat flux on either side of the face). In this case, the formula for the coefficient becomes (for the positive X direction)

$$C_{+x} = \frac{2k_{i,j,k}}{\Delta x_i\left(\Delta x_i + \frac{k_{i,j,k}}{k_{i+1,j,k}}\Delta x_{i+1}\right)} \qquad (3.17)$$

As neither the thermal conductivity nor the grid block sizes are allowed to change during a simulation run, these coefficients of the heat conduction equation do not change during the run. Thus, they are only calculated once, at the beginning of the simulation run.

3.5 Electrode Current, Scaling, and Energy Balance Calculations

In the formulation presented thus far, the electrical potentials are calculated from given electrode voltages. While these voltages are arbitrary in their real and imaginary components, they must be specified prior to the potential calculation. During the heating of an oil reservoir, the resistance of the reservoir will change. Thus, for a set of fixed electrode voltages, the electrode currents, and the total electrical power into the reservoir will change with time. However, when simulating the electrical heating of a reservoir, one may wish to specify a constant heating rate (i.e. constant electrical power level), or to specify the current flowing from a particular electrode. These specifications are possible in EPEIOS. The voltage of each electrode in the problem domain must be specified by the user of EPEIOS. However, if the problem involves a case where the current into the formation from a particular electrode, or the total power into the formation, is specified, then the voltages of the electrodes will be scaled by EPEIOS as follows:

1. First, the potentials are found, using the initially specified electrode voltages, by solving the current continuity equation.
2. Once the potentials are known, a numerical integration is performed to find the current flowing out of each electrode. The numerical integration uses the difference between the calculated values of the potentials in the grid blocks immediately adjacent to the electrodes and the known electrode voltages to calculate the potential gradient immediately adjacent to the electrode surface. This potential gradient is multiplied by the conductivity of the grid block, and the product is integrated over the entire electrode surface, giving the total current flowing out of the electrode.
3. The potentials are then scaled if the program user has specified either constant current, or constant power, heating. This scaling maintains the relative magnitudes of the initially specified electrode voltages, and the phase angles between these voltages. For constant current heating, the program user must specify the current flowing out of a specified electrode. All of the calculated potentials are scaled by the same multiplying factor necessary to produce the specified current. For constant power heating, all of the initially calculated potentials are scaled by the same multiplying factor necessary to produce the specified total power into the

problem domain.

4. When the scaled potentials have been calculated, these scaled potentials are used to find the electrical heating rates.

The total energy input to the problem domain is calculated in three different ways in EPEIOS, as outlined in the following paragraphs.

First, the scaled electrode voltages and electrode currents are used to find the total electrical power into the problem domain. In all problems solvable by EPEIOS, the sum of the complex electrode currents will be zero, as the outer boundaries of the problem domain must be either no-flow boundaries or electrodes and current continuity is solved within the problem domain. Where the sum of the electrode currents is zero, the power produced in a general, multiphase, electrical heating problem is the real part of the product of the complex r.m.s. electrode voltage and the complex conjugate of the r.m.s. electrode current, summed for each electrode. The electrode voltages are measured with respect to a single, but arbitrary, reference (Hayt and Kemmerly, 1978). To find the energy input to the problem domain for one time step, the power input is multiplied by the length of the time step (in seconds). The sum of the electrical energy input for each time step will give the total electrical energy input.

Second, the total energy produced by electrical heating within the domain being heated is found by summing, for all grid blocks, the product of the electrical heating rate and the volume of each grid block, then multiplying the sum by the length of the time step. In a manner similar to the calculation of the electrical energy, the heating energy for each timestep is summed to give the total heating energy for the simulation run.

Third, the cumulative energy change in the problem domain, reflected in the temperature change of the problem domain, is found by summing, for each grid block, the product of the volume, volumetric heat capacity, and temperature change from the initial temperature. The value for the cumulative energy change for the problem domain will differ from the total electrical energy input to the formation by the amount of energy which has been lost to constant temperature regions. The amount of this loss is found by performing a surface integration around each constant temperature region. When the energy lost to constant temperature regions is added to the calculated cumulative energy change the total energy input to the problem domain is found.

The three calculated amounts for the total energy input to the problem domain are printed out with the program results, and may be compared to one another. Such a comparison gives an indication of how well the numerical solution method is performing.

3.6 Testing of the Solution Method

Several simple problems, with known analytical solutions, were set up and run on EPEIOS. In all problems, good agreement between the analytic solution and the EPEIOS solution was obtained. These tests helped to find logical or other programming bugs which may have been present in EPEIOS. In addition, comparison of the EPEIOS solutions with the analytic solutions to these test problems gave an indication of the accuracy of the numerical solution techniques used and helped to develop an understanding of grid sensitivity and other considerations involved in using the finite difference method. The tests and test results are presented in detail in Appendix V.

3.7 Conclusions

A FORTRAN program, entitled EPEIOS, which uses the finite difference method to obtain approximate solutions to the first of the two mathematical models of the electric pre-heat presented in Chapter 2, was written. (This first model assumes that the effects of fluid flow and expansion may be neglected during the electric pre-heat.) The details of the program, in particular the finite difference operators used and the handling of the boundary conditions, were presented in this chapter. The program EPEIOS was tested by simulating several analytically solvable problems and comparing the answers produced by EPEIOS with the analytic solutions.

4. Solution of the Electrical Heating and Fluid Flow Model

In Chapter 2, two different mathematical models of electrical heating were presented. In the first of these models, no fluid flow or fluid expansion occurs during electrical heating. Approximate solutions to this first model were obtained by using the finite difference method, as implemented in the computer program EPEIOS, discussed in Chapter 3. The second mathematical model presented in Chapter 2 includes the possibility of fluid movement and expansion during electrical heating. Approximate solutions to this second model were obtained, again using the finite difference method, by a program entitled 'TCTM-EPEIOS' which is a combination of the Alberta Research Council's Two Component Thermal Model and sections of EPEIOS. The main subject of this chapter is the construction and details of TCTM-EPEIOS.

The calculations of the electrical potentials and heating rates are identical in both the first and the second models, once the electrical conductivities of the grid blocks have been specified. The electrical conductivity is calculated differently in the two models, varying only with temperature in Model 1 (EPEIOS), but varying with temperature, water saturation, and porosity in Model 2 (TCTM-EPEIOS). The calculations of the electrical potentials and heating rates were discussed in detail in Chapter 3. This chapter will be primarily concerned with the calculations which are different in the two models, namely the calculation of electrical conductivity, the solution of the fluid flow equations, and the changes in the energy equation necessary to account for both fluid flow and electrical heating.

It is not the purpose of this thesis to describe the current state-of-the-art in reservoir simulation (the solving of fluid flow equations in petroleum reservoirs). It will be assumed in this chapter that the reader is familar with the terms and definitions commonly used in the reservoir simulation field. Readers who are unfamilar with this field are referred to one of the standard, introductory works on reservoir simulation, such as Peaceman (1977), Aziz and Settari (1979), or Thomas (1982). Such introductory works do not deal with non-isothermal cases, such as when steam is injected into oil sand reservoirs. A good review of the work to 1981 on simulation of non-isothermal reservoir problems is given by Abou-Kassem (1981). Some more recent papers on thermal models include those of Rubin and Buchanan (1985), and Buchanan (1985).

It should be noted that this work does not present any changes or advancements in the art of reservoir simulation, except directly pertaining to the addition of an electrical heating source term in the energy equation. This additional term in one of the several nonlinear equations describing the petroleum reservoir does not require any change, whatsoever, in the methods used to solve this set of equations. The electrical heating source terms are simply calculated from the known reservoir properties, and added to the energy equations along with other heat source or sink terms. Thus, the reservoir simulator is largely treated as a black box, and requires only very minor modifications.

4.1 The Alberta Research Council Two Component Thermal Model

The reservoir simulator specifically used in this work was the Alberta Research Council's Two Component Thermal Model (hereafter refered to as TCTM). An agreement was reached between the ARC and the author permitting the author to use the source code for TCTM. This agreement imposed certain confidentiality restrictions. Thus, the author is not able to describe certain aspects of the solution algorithm used in the code. However, the code has been extensively tested by the Alberta Research Council, largely by comparing the predictions of this numerical simulator with the results of physical simulation experiments run by the ARC. In addition, these comparisons allowed the ARC to check the various physical properties used in the program. While TCTM was initially developed to simulate laboratory scale steam flood experiments, TCTM is also useful to simulate field scale steam floods. The TCTM was discussed in a paper by Reddy, Prowse and Redford (1980). The following quote is from that paper.

> The model used in the present study is multi-dimensional in cartesian and cyclindrical coordinates. It accounts for the flow of three phase (oil, water and steam) with viscous, gravity and [illegible]
> [illegible]

the oil phase and is applicable for steam flooding of oil sands when solution-gas drive and steam-distillation effects are negligible. The energy balance equation includes heat transfer by both conduction and convection. Viscous dissipation, kinetic energy and potential energy terms are neglected in the energy balance equation. Heat loss from the reservoir to the surrounding strata is computed from the solution of the heat conduction equation.

The material and energy balance equations, together with saturation and phase constraint equations are solved simultaneously with implicit pressure (P), temperature (T), water saturation (Sw) and gas saturation (Sg). Transmissibilities, capillary pressures, injection and production rates are also treated implicitly using the semi-implicit formulation. No-flow boundary conditions are imposed along the reservoir boundary. The heat conduction equation for the heat loss calculation is solved by the standard central-difference implicit method. The heat loss calculations in the model are implemented with two options.

Option 1: for reservoir-type problems, heat losses are calculated for the overlying and underlying strata by solving the heat conduction equation with semi-infinite boundary conditions; zero heat flux conditions are imposed along the lateral boundaries.

Option 2: for the 1.5 m physical simulator, heat losses are computed for the overburden, underburden and the peripheral packing by solving the heat conduction equation with a convection-radiation heat transfer boundary condition.

Relative permeabilities in the model are implemented as a function of fluid saturation and temperature. Three-phase oil relative permeabilities are calculated using Stone's method with normalization procedure suggested by Dietrich and Bondor.

The model program is written in FORTRAN IV for the Amdahl 470, operating under MTS at the University of Alberta. Operationally, the program is interactive, giving the user a great deal of flexibility. However, the program can be run in batch mode with no modifications.

The grid variables in the model are numbered sequentially in a linear fashion from the three-dimensional (i,j,k) notation and conversion of subscripted variables to sequential address is done within the program. Therefore, coding for one, two or three dimensional simulation is achieved with no [illegible] in the code. Dynami

> is also made possible by explicit addressing of array variables and is implemented by the first element pointers and equivalencing.
>
> The spatial variables in the partial differential equations are discretized using central-difference, finite difference approximations, with up-stream relative permeabilities, densities, viscosities, and enthalpies in the flow terms. The time derivatives in the accumulation terms are discretized using a backward time difference approximation. The discretized equations are solved simultaneously using a band-matrix direct solution algorithm.
>
> (Reddy et al., 1980)

The equations solved in TCTM are outlined in Chapter 2. These equations are similar to those commonly used in dead-oil type thermal simulators. In the experience of the author, there is nothing unusual about the finite difference approximation or the property calculations used in the program. The normalized permeability curves used in TCTM are directly contained in the program. These curves are shown in the paper by Reddy et al.(1980) and were obtained from ARC internal research reports. Similarly, all water and steam properties, and oil viscosities, are directly contained in the program, and do not need to be input by the program user. These internally contained properties were used to simulate, and match, experiments run by the ARC in their 1.5 m physical simulator. These experiments were run using repacked, high grade Athabasca oil sands. Thus, the oil properties contained in TCTM are those of Athabasca bitumen.

4.2 Calculation of the Electrical Conductivity

One of the major differences between the two mathematical models for the electric pre-heat is in the calculation of the electrical conductivity. In Model 1 (EPEIOS), the electrical conductivity changes only with temperature during the electrical pre-heat. In Model 2 (TCTM-EPEIOS), the electrical conductivity varies with changes in not only the temperature, but also with changes in the water saturation and the porosity. In each fluid flow grid block the water saturation, Sw, the porosity, ϕ, and the temperature, T, are known at the beginning of each timestep. The values of these variables will change during the simulation. The water saturation changes as fluid moves or expands, the porosity will change slightly with pressure changes, and the temperature will change as the formation is heated. These three variables, together with the specified electrical conductivity of the connate water, are used to determine the bulk conductivity of the grid block.

A form of Archie's equation is used to calculate the electrical conductivity (Wait, 1971). At the beginning of each timestep, the current values of Sw, ϕ and T, for a particular fluid flow grid block, are used in the following equation to calculate the electrical conductivity for that grid block.

$$\sigma = \frac{\phi^{1.37}\ Sw^{2}\ \sigma w\ f(T)}{0.88} \qquad (4.1)$$

Here, σw is the electrical conductivity of the connate water, and f(T) represents the functional dependence of the electrical conductivity of the connate water on temperature. Both of these are specified by the program input. The exponential dependences of the conductivity on the porosity and saturations, and the denominator of the equation were found empirically. See Chapter 6 for a more complete discussion on electrical conductivity.

In TCTM-EPEIOS, the functional dependence of the electrical conductivity on temperature is approximated with a three part, piece-wise linear, function. The slopes, and break-points of the function are specified as part of the program input. The form of the equations is given in Appendix IV, the TCTM-EPEIOS User's Reference Manual. However, if a better description of the functional dependence of electrical conductivity on temperature should become available, only minor modifications to TCTM-EPEIOS would be required to model the new functional dependence.

The program TCTM-EPEIOS was written so that different finite difference grids for the electrical potential and the fluid flow equations could be used. Computer costs limited the number of grid blocks that could be used for solving either the fluid flow equations or the electrical heating equations. A finer grid for the electrical equations was allowed for several reasons. First, an entire grid block or blocks, were used to model a single electrode. Unless a finer grid structure was allowed for this purpose, special electrode models, altering the electrical calculations in electrode blocks, would have to be developed. Secondly, as the heating rate is dependent on the square of the rate of potential change, a error in the potential will cause a larger error in the calculated heating rate. Thus, the electrical heating rate is more sensitive to spatial truncation errors, caused by the limited number of grid blocks, than are the fluid flow equations. When using two different grids, one for the electrical heating rate calculation, and one for the fluid flow and energy equations, the electrical conductivity will be the same for all the electrical grid blocks in one fluid flow grid block, as only one value of temperature and water saturation is available for that fluid flow grid block. Even though all the electrical (EPEIOS) grid blocks within a single fluid flow (TCTM) grid block have the same electrical conductivity, having a finer EPEIOS grid may still be justified in regions where the potential is changing rapidly.

One of the major differences between TCTM-EPEIOS and EPEIOS is that the connate water conductivity at 24°C, σw, is specified for each grid region, rather than the bulk conductivity at 24°C, σ_{24}. The literature, and the experiments described in Chapter 6 of this work indicate that values of connate water conductivity (at 24°C) between .5 S/m and 1.0 S/m are typical for Athabasca oil sand formations.

4.3 Calculation of Electrical Heating Rates

Once the electrical conductivity is known, the calculation of the potentials, and the heating rates, are unaltered from EPEIOS. The potentials are calculated, then the heating rates in the EPEIOS grid blocks are found from the potential gradients and the electrical conductivities. The detail on how this is done is described in Chapter 3 of this thesis. The current out of each electrode, and the total power input to the formation are also calculated in the same manner as in EPEIOS, with the same options for scaling the heating rates for constant power or constant current heating. The detailed steps of the heating rate calculation are given on Figure 4.1.

In passing the electrical heating rates back to TCTM, several conversions must take place. First, the units for the heating rates must be changed from watts per meter cubed to BTUs per day. Thus, while EPEIOS calculates rates on a per volume basis, TCTM must have the total rate (over the volume of each grid block). This conversion is accomplished as follows. The volumetric heating rate, with units of watts per meter cubed, is calculated by EPEIOS for a particular grid block. This volumetric heating rate is multiplied by the volume of the grid block to get the total rate for the block (in watts). This total heating rate for the grid block is multiplied by a conversion factor to get the total rate in BTUs per day. Finally, the total heating rates from all of the EPEIOS grid blocks in one TCTM grid block are summed

TCTM passes the current temperatures, porosities and water saturations to EPEIOS.

↓

Calculate electrical conductivities using Archie's Law and the temperature function.

↓

Solve for the electrical potentials.

↓

Calculate the electrode currents.

↓

If constant power or constant current heating specified, scale currents and potentials.

↓

Calculate the electrical heating rates.

↓

Perform unit conversion to units used in TCTM, and multiply by TCTM block volume.

↓

Return the heating rates to TCTM.

Figure 4.1 A flow chart showing the order of the calculation of the electrical heating rates in TCTM-EPEIOS.

to get the total heating rate for the TCTM grid block.

4.4 Treatment of the Electrical Conductivity as Either an Implicit or an Explict Property

To solve the set of material balance and energy equations given in section 2.4 of this thesis, the partial differential equations are approximated as a set of finite difference equations. (Details of these difference equations are given in the references listed at the beginning of this chapter.) The equations are differenced both in space, and in time. Thus, they contain properties both at their current, known, values and at their values at the end of the timestep. The values of the properties at the end of the timestep are usually found using some iterative technique, such as Newton's Method. (For those readers unfamilar with reservoir simulation, Newton's method of solving a non-linear set of equations is commonly used. In this method, the current values of primarly variables, and the derivatives of the equations with respect to these variables, are used to obtain new primary variable values which may solve the equation set. An iterative process is used to obtain successively better estimates of the new primary variables and other property values. For more details see Mathews and Walker (1970).) It is often possible to save some calculations by approximating the value of some property (say relative permeability or viscosity) at the end of the timestep by its current value at the beginning of the timestep. This is referred to as an "explicit formulation" of that property. In general, treating a property explicitly results in less required computation, but may lead to numerical instability in the solution method. The question therefore arises whether the electrical heating rate should be treated as an implicit or an explicit property.

Two formulations for the electrical heating rate in Model 2 were developed and implemented in TCTM-EPEIOS. The first formulation treats the electrical conductivity and heating rate as an explicit property of the temperature, porosity and water saturation of the reservoir. In other words, the values of the temperature, porosity, and water saturation at the end of the last timestep are used in the calculation of the electric conductivity, and hence the heating rate, for the next timestep of the fluid flow and energy equations. This new heating rate is then held fixed for the next timestep of the fluid flow equations. The second formulation treats the electrical conductivity and heating rates as implicit properties of the temperature, water saturation, and pressure. The electrical conductivity and heating rates are correct for the values of temperature, porosity and water saturation at the end of the timestep. Again, the heating rate is held fixed for the entire timestep. Thus, in the explicit formulation, the heating rates are calculated from the values of the reservoir properties at the beginning of the timestep, while in the implicit formulation the heating rates are calculated from the reservoir properties at the end of the timestep. The implicit formulation requires slightly more calculation than the explicit formulation.

In TCTM-EPEIOS, as in EPEIOS, the maximum allowable change in electrical conductivity in one timestep should be less than five percent. The TCTM allows the user to specify the maximum temperature change per timestep, the maximum pressure change per timestep, and the maximum saturation change per timestep. By specifying these maximums appropriately, the maximum electrical conductivity change per timestep may be controlled.

The maximum change in electrical conductivity per timestep is related to the maximum changes in temperature and water saturation by equation 4.1. By use of the product rule,

$$\Delta\sigma = \frac{\partial\sigma}{\partial P}\Delta P + \frac{\partial\sigma}{\partial Sw}\Delta Sw + \frac{\partial\sigma}{\partial T}\Delta T \qquad (4.2)$$

The partial derivatives may be calculated from equation 4.1. Such a calculation shows that, for the rock and fluid properties used in the simulation studies reported in this work, the changes in pressure may be neglected, the maximum change in water saturation should be restricted to less than ten percent of the mimimum initial water saturation, and the maximum temperature change per timestep should be restricted to about 5°F.

4.5 Interfacing of EPEIOS and TCTM

The guiding principle employed while designing the interface between TCTM and EPEIOS was to make as few changes as possible to either program. The TCTM is used as the main program and was altered the least. Only five lines of code were added to, or altered in, the TCTM. While this approach resulted in a less flexible code than may have resulted if the two programs had been more closely coupled, it greatly reduced both the design and programming time and the chance of introducing programming errors into a working code.

The two sections of the program use separate input files, grid structures, and systems of units. The TCTM input is unaltered from the Alberta Research Council's documentation, with the exception that a grid variable, "QE", which specifies the total heating rate of the grid block (in BTU/D), may be printed with the other grid variables. While no fluid injection should be specified during electrical heating (unless the fluid is of the same electrical conductivity as the connate water), fluid production may occur. All property values and units should be specified as in a regular input file for TCTM.

The input file used to control the electrical heating calculation is a reduced EPEIOS input file. The file has the same structure as a regular input file, but some of the variables, primarily those dealing with the thermal properties, restart and output control, and timestep control are removed. The electrical conductivity specified for each region is for the connate water, rather than the bulk conductivity as in EPEIOS. (This was discussed in detail in section 4.2.) Specific details on the input files for EPEIOS and for controlling the electrical heating in TCTM-EPEIOS may be found in Appendices III and IV, respectively.

A finer grid structure may be used for the electrical heating calculation than is used in TCTM, with one proviso. The boundaries of the EPEIOS grid must align with the boundaries of the TCTM grid blocks, so each EPEIOS grid block is entirely contained in a single TCTM grid block. No EPEIOS grid blocks can be located outside the TCTM grid structure. During the program data input, a matrix is established which maps each EPEIOS grid block, and the heating that occurs in that grid block, into a single TCTM grid. If a single EPEIOS grid block spans two TCTM grid blocks, an incorrect heating rate will be calculated for the two blocks.

As mentioned, the TCTM is used as the main program, and it controls the program flow. The alterations made to it are as follows:

1. A grid variable, "QE", was added to the TCTM grid variable array. This variable give the electrical heating rate, in BTU/D, for the TCTM grid block.
2. After the input of most of the TCTM data, and immediately prior to the calculation of the transmissibilities, a call is made to a subroutine which inputs the EPEIOS data, develops a matrix mapping the

EPEIOS grid blocks into the TCTM grid blocks, and inputs the EPEIOS electrical heating control information.

3. For the explicitly coupled version of TCTM-EPEIOS, at the start of each timestep, prior to the calculation of the new coefficients of the fluid flow and energy equations, a subroutine call is made which uses EPEIOS subroutines to calculate the current electrical heating rates, then returns these heating rates to the TCTM coefficient calculation subroutine. In the implicitly coupled version of TCTM-EPEIOS, the electrical heating rates are recalculated at the start of each Newton Iteration. The calculation is performed with the updated reservoir properties. In practise, this implicit scheme approximately triples the number of times the electrical heating rates are calculated. However, as the change in electrical conductivity is smaller between calculations, fewer iterations of the potential solver are required for each calculation.

4. One line of code in the coefficient calculation subroutine, used for calculation of the coefficient of the right hand side of the energy equation, is altered by the addition of the electrical heating rate for the gridblock.

5. The electrical heating rate for the grid block is subtracted from the heat lost through the boundaries of the simulation grid. The result is printed on the program output under the heading "TOTAL HEAT LOST". The

result will have a negative value if more electrical heating than heat loss has occured. The "ENERGY BALANCE" value printed out should be approximately one, as it is in the unaltered TCTM.

6. A line was added to the TCTM print subroutine to call an EPEIOS print subroutine. The electrode voltages, currents, surface voltages, and total power input will be printed if electrical heating is occuring.

Somewhat more extensive changes were made to EPEIOS than to TCTM. In particular, all calculations concerned with the heat conduction equation, timestep control, and data storage were removed, and the printing subroutine was substantially reduced. The main routines involving the calculation of the potentials and the heating rates are unchanged. Additional subroutines which transfer information between TCTM and EPEIOS, and perform the necessary unit conversion were also written.

4.6 Printing and Storage of Program Results

The printing of results and storage of restart records in TCTM were altered only slightly. As the total heating rate for each TCTM grid block was added to the TCTM variable array, it may be printed out by TCTM. A subroutine call from the TCTM print subroutine to the EPEIOS print subroutine was also added. This allows the electrode voltages and currents, and the total electrical power into the formation to be printed. Otherwise, the output routines in TCTM remain unaltered.

4.7 Testing of the Combined Code

As the electrical potential and heating rate calculations are done by subroutines which are identical to those in EPEIOS, rigorous testing of these routines in TCTM-EPEIOS was not required. As TCTM similarly underwent only minor modifications, the only testing required for the combined code was to ensure that the electrical conductivities were correctly calculated and passed from TCTM to EPEIOS, and that the unit and volume conversion of the heating rates was done correctly.

Thus, the TCTM-EPEIOS code was tested by simulating a simple, two dimensional case, involving one dimensional current flow through two, parallel porous media. The water saturations, connate water conductivities, and heat capacities of the two media were different, but they were calculated so that the temperature rise in both media would be identical. This problem was run using constant power scaling, for a uniform temperature rise in both media of 41°C. At the end of the simulation, the TCTM-EPEIOS calculated temperatures differed from the analytic solution by a maximum of 4%. This error may, in part, be due to the fact that TCTM-EPEIOS predicted that some fluid movement would occur during the heating. This fluid movement was not accounted for in the analytic model. For more details on this test, see Appendix V.

4.8 Conclusions

The Alberta Research Council's Two Component Thermal Model has been coupled to the electrical heating rate calculations in a manner which required a minimum of alterations to both codes. The coupling did not adversely affect the stability of the thermal model.

The combined model was tested for a simple, analytically tractable case to ensure that the interfacing of TCTM and EPEIOS was correct.

5. Results from the Computer Simulation of the Electric Pre-heat and Steam Drive Process

In this thesis, two different mathematical models for the electric pre-heat process have been presented. The first model, referred to as Model 1, neglects the movement and expansion of reservoir fluids during the electric pre-heat. The temperatures at the end of the electric preheat are input as initial conditions in a conventional numerical steam drive simulator. This mathematical model was implemented using two programs, EPEIOS to simulate the electric pre-heat, and the Alberta Research Council's Two Component Thermal Model (TCTM) to simulate the steam drive. The temperatures at the end of the electric pre-heat, calculated by EPEIOS, are used as initial conditions by TCTM. The second model, Model 2, includes the full fluid material balance equations during the electric pre-heat, as well as during the steam drive. This model was implemented in a single computer program, TCTM-EPEIOS, which was made up of the ARC Two Component Thermal Model and sections of EPEIOS. Two formulations for Model 2 were developed, one which treats the electrical heating rate as an explicit property, and the other which treats it implicitly. In both fomulations, all other properties are treated implicitly.

In order to compare these two different models of the electric pre-heat and steam drive process a series of three simulation studies were done. This chapter reports on these simulation studies. The first study, referred to as Case 1, considered a simplified two dimensional reservoir. The second study, Case 2, considered a two-layer, two-dimensional cross section of a reservoir containing horizontal wells. The third study, Case 3, involved the three-dimensional simulation of a five-spot pattern flood of a realistic Athabasca oil sand reservoir. In all three cases, the fluid, rock, and rock-fluid properties used were those typical of the Athabasca oil sand reservoirs.

The three simulation studies were run using both Model 1 and Model 2. A comparison of the results from both models gives some indication of the error introduced by the additional assumptions made in Model 1. In particular, the temperatures at the end of the electric pre-heat, the fluid production rates during the steam drive, and the cumulative oil recoveries, predicted by each of the two models, were compared. In addition, some comparisons of the implicit and explicit formulations of Model 2 were also made.

5.1 Note Regarding Properties

It was noted in Chapter 4 of this thesis that the oil and water viscosities, and the three phase relative permeabilities are contained internally in TCTM. These properties cannot be input (or printed). According to ARC literature, the properties used are the best available (from their research) properties for rich oil sands. Public information on these properties is contained in the paper by Reddy, Prowse, and Redford (1980). These properties, and the

TCTM code, were tested by history matching experiments run using the ARC 1.5 m physical simulator. It was assumed by the author that the fluid and rock-fluid properties contained in TCTM were accurate for high-grade Athabasca oil sand formations.

As no published work reporting the temperature dependence of the electrical conductivity of the shale and limestone layers adjacent to the oil sand was available, it was assumed that the conductivity increased linearly with temperature. The formulas used to calculate the electrical conductivities of the shale and limestone layers are given in the property tables (Tables 5.4, 5.5, and 5.8) for those case studies which modelled formations including shale or limestone.

5.2 Case 1 - A Simplified Homogeneous Reservoir

The first simulation study, hereafter referred to as Case 1, involved a reservoir with a simplified geometry. The reservoir consisted of a rectangular block of a single, homogeneous material, with the outer reservoir boundary thermally and electrically insulated. The reservoir geometry and dimensions are given in Figure 5.1, and the reservoir properties are given in Table 5.1. The rock, rock-fluid, and fluid properties used were those of a rich grade oil sand formation. As Case 1 was a two dimensional geometry, the electrodes and wells contact the entire thickness of the reservoir.

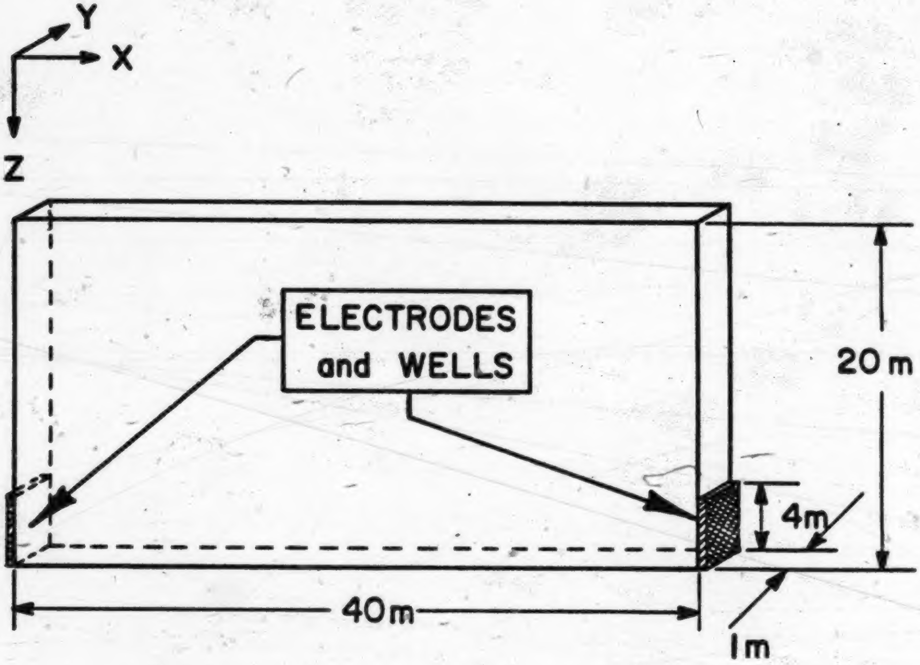
Y
X
Z
ELECTRODES and WELLS
20 m
4m
40m
1m

Figure 5.1 The geometry and the dimensions of the reservoir for Case 1. This is a two dimensional problem.

Table 5.1 Reservoir Properties for Case 1.

Data for Model 1 - Electric Preheat

Initial temperature	10.0	°C
Formation electrical conductivity		
$0.003188 \left[1+0.026(T-24)\right]$ S/m	$T \leq 100°C$	
$0.003188 \left[2.98+0.0022(T-100)\right]$ S/m	$T > 100°C$	
Thermal conductivity	1.65	W/m.K
Volumetric heat capacity	2.04	$MJ/m^3.K$

Data for Model 2 - Electric Preheat Only

Initial temperature	10.0	°C
Connate water electric conductivity		
$0.8 \left[1+0.026(T-24)\right]$ S/m	$T \leq 100°C$	
$0.8 \left[2.98+0.002(T-100)\right]$ S/m	$T > 100°C$	

Data for Model 1 - Steam Drive and Model 2 - Electric Preheat and Steam Drive

Initial Water Saturation	0.124	
Initial Oil Saturation	0.876	
Initial Gas Saturation	0.0	
Porosity at Reference Conditions	0.34	
Permeability (isotropic)	2.9	darcies
Oil Heat Capacity	1.71	kJ/kg·K
Water Heat Capacity	from steam tables	
Rock Heat Capacity	0.76	kJ/kg·K

Other Fluid and Rock-Fluid Properties as given in Reddy et al (1980)

This simple, if somewhat unrealistic, reservoir was chosen for the first study for several reasons. The outer boundary was chosen as insulated, so differences in boundary heat loss calculations for the different models would not cause differences in results. A simple, two dimensional problem was chosen so a relatively large number of grid blocks could be used, reducing spatial truncation error, while maintaining reasonable computer costs. As well, this simple example serves to illustrate how electrical pre-heating can establish a fluid communication path at the bottom of a reservoir. Neither a water zone nor a fracture is needed to establish steam injectivity once the formation has been heated.

The electric pre-heat consisted of passing an electrical current between the two electrodes for 180 days. The electrode voltages were constantly adjusted to maintain a constant heating rate of 6 kW. At the end of the electric pre-heat, steam injection was started at one well and oil and water production at the other well. The rate of steam injection was adjusted to maintain the injection pressure below 4.0 MPa. It is assumed that the formation fracture pressure is higher than this value. The injection rates used are given in Table 5.2.

The inclusion of thermal expansion in Model 2 results in increases in the reservoir fluid pressure during the electric pre-heat. In fact, if the reservoir is totally enclosed, the fluid pressure will exceed formation fracture

Table 5.2 Electrical heating rates and steam injection rates for Case 1. The same rates were used for both Model 1 and Model 2.

Electric Preheat

- 180 Days of Constant Power Heating at 6000 W
- Total electrical energy input 9.3 x 10^{10} J
- Initial formation resistance 1845 Ω
- Final formation resistance
  - Model 1 390 Ω
  - Model 2 - Implicit 366 Ω

Time after start of electrical preheat (Days)	Injection Rate (m^3/D)	Steam Quality
180-210	.15	0.7
210-260	.25	0.7
260-300	.40	0.7
300-565	.80	0.7

Total Energy Injected Steam 4.1 x 10^{11} J
Cumulative Injection 245 m^3 (cold water equivalent)

Cumulative Production	Model 1	Model 2
Oil	96 m^3	96 m^3
Water	245 m^3	246 m^3

pressure before the pre-heat is completed. To allow for thermal expansion, while maintaining the reservoir pressure below formation fracture pressure, some production of reservoir fluids was allowed during the electric pre-heat. Only a small amount of production was necessary to maintain the reservoir pressure below the fracture pressure.

A different finite difference grid was used in the solution of each of the electrical heating rates and the fluid flow equations. The grid used by Model 1 (EPEIOS) in the solution of the electrical potentials, electric heating rates, and temperatures during the electric pre-heat, consisted of 14 grid blocks in the horizontal direction and 10 grid blocks in the vertical direction. This same grid was used by Model 2 (TCTM-EPEIOS) in the solution of the electrical potentials and heating rates during the electrical pre-heat. A coarser grid, consisting of 6 grid blocks in the horizontal direction and 5 grid blocks in the vertical direction, was used to solve the fluid flow and energy equations. This second grid was used by Model 1 during the steam drive phase of the simulation, and by Model 2 during the entire simulation.

The increase in temperature at various points in the reservoir at the end of the 180 day electric pre-heat are shown in Table 5.3. Three different temperature increases for each point are shown. The first temperature increase is that predicted by Model 1. The second temperature increase shown is that predicted by Model 2 using the formulation

Table 5.3 A comparison of the temperature increases (in ^{o}C) predicted by three models, due to the electric pre-heating of the reservoir in Case 1. Initial reservoir temperature is $10^{o}C$.

For each grid block location:

the upper figure is for Model 1
the middle figure is for Model 2 - Explicit
the lower figure is for Model 2 - Implicit

X (m)→ Z (m)↓	2.0	8.0	16.0	24.0	32.0	38.0
2.0	7.9	14.3	23.5	23.5	14.3	7.9
	8.0	14.2	24.1	24.1	14.2	8.0
	7.8	14.0	23.8	23.8	14.0	7.8
6.0	18.7	23.4	30.5	30.5	23.4	18.7
	18.2	23.1	31.1	31.1	23.1	18.2
	17.9	22.7	30.7	30.7	22.7	17.9
10.0	48.1	44.2	42.7	42.7	44.2	48.1
	45.2	43.0	45.2	45.2	43.0	45.2
	44.7	42.7	44.9	44.9	42.7	44.7
14.0	112.9	77.9	63.5	63.5	77.9	112.9
	103.2	76.2	64.8	64.8	76.2	103.2
	103.2	76.1	64.8	64.8	76.1	103.2
18.0	187.0	108.5	78.0	78.0	108.5	187.0
	195.4	110.5	81.2	81.2	110.5	195.4
	196.6	110.6	81.4	81.4	110.6	196.6

which treats the electrical heating rate as an explicit property. The third temperature increase is that predicted by Model 2 when the heating rate is treated implicitly. An examination of this table shows that the maximum difference in the temperature increases predicted by the three models is 8.6 ~~per~~ cent. Over most of the reservoir, the difference in predicted temperature increases is less than five percent.

A further comparison was made of the results of the implicit and explicit formulations of Model 2. The pressure changes during the electric pre-heat, predicted by the two formulations, were compared. At the end of the electric pre-heat the formation pressures predicted by the two formulations agreed to within 1%, even though the formation pressure more than doubled. In addition, the two formulations were in almost exact agreement on the minor fluid saturation changes which occured during the electric pre-heat.

Immediately upon completion of the electric pre-heat, steam injection was started. The steam drive was simulated using each of Model 1 and the explicit formulation of Model 2. A comparison of the injection pressures, oil production rates, and cumulative oil productions, all versus time, predicted by the two models, are shown in Figures 5.2, 5.3, and 5.4. Note that all three of these graphs start at a time of 180 days after the start of the electric pre-heat, which corresponds to the start of the steam drive.

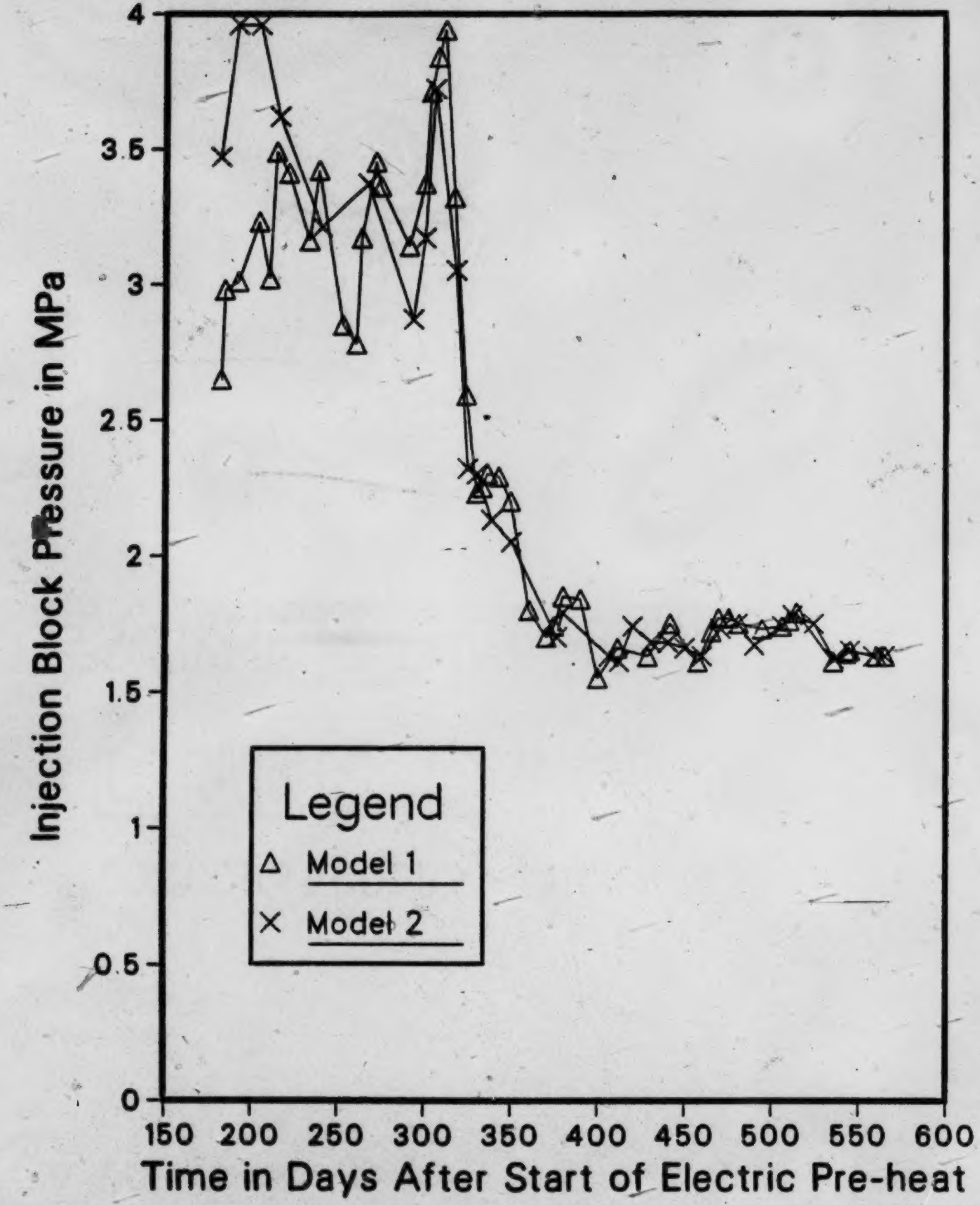

Figure 5.2 A plot of the injection pressure versus time, for Case 1, comparing the results of simulations run using Model 1 (EPEIOS) and Model 2 (TCTM-EPEIOS).

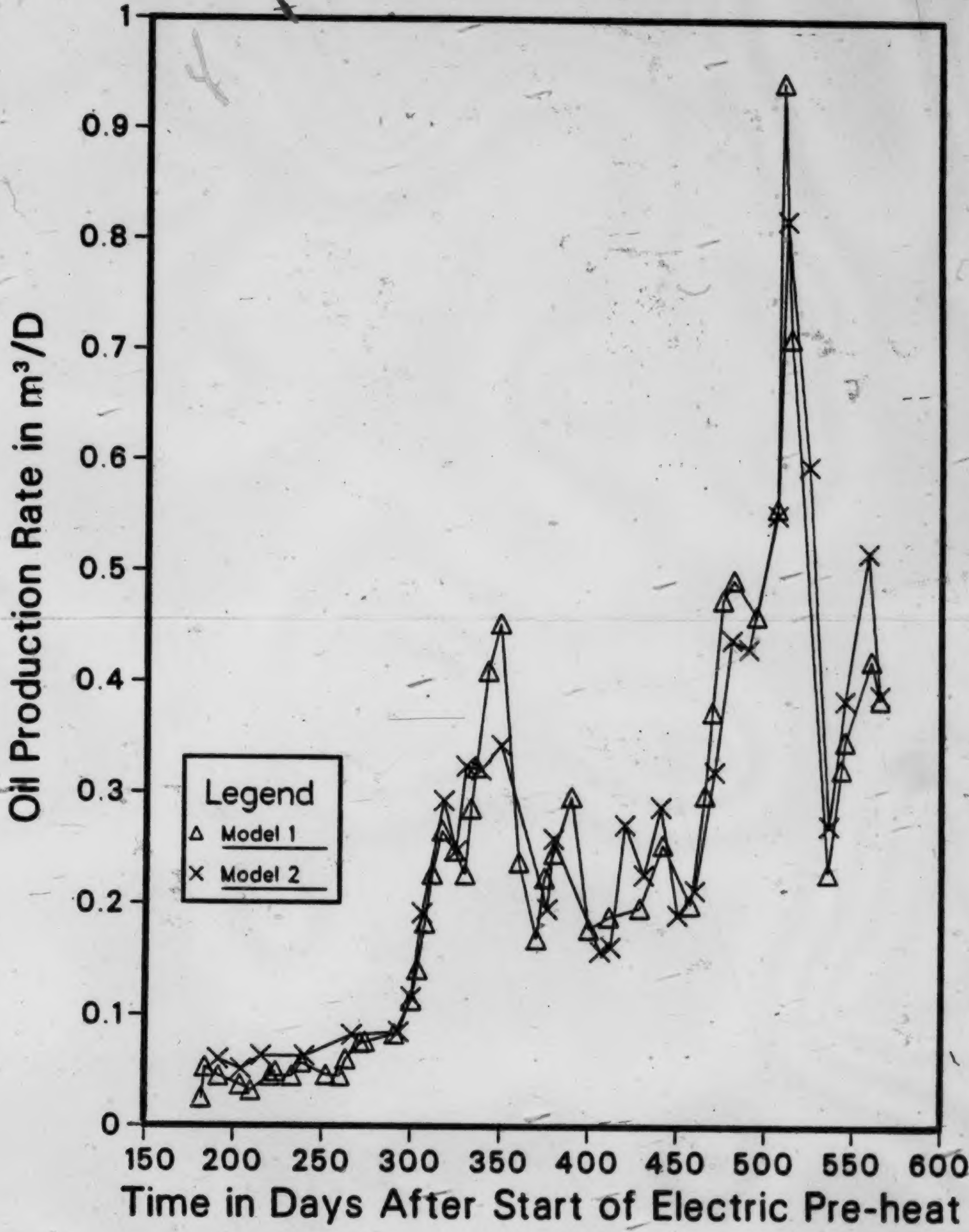

Figure 5.3 A plot of the oil production rate versus time, for Case 1, comparing the results of simulations run using Model 1 (EPEIOS) and Model 2 (TCTM-EPEIOS).

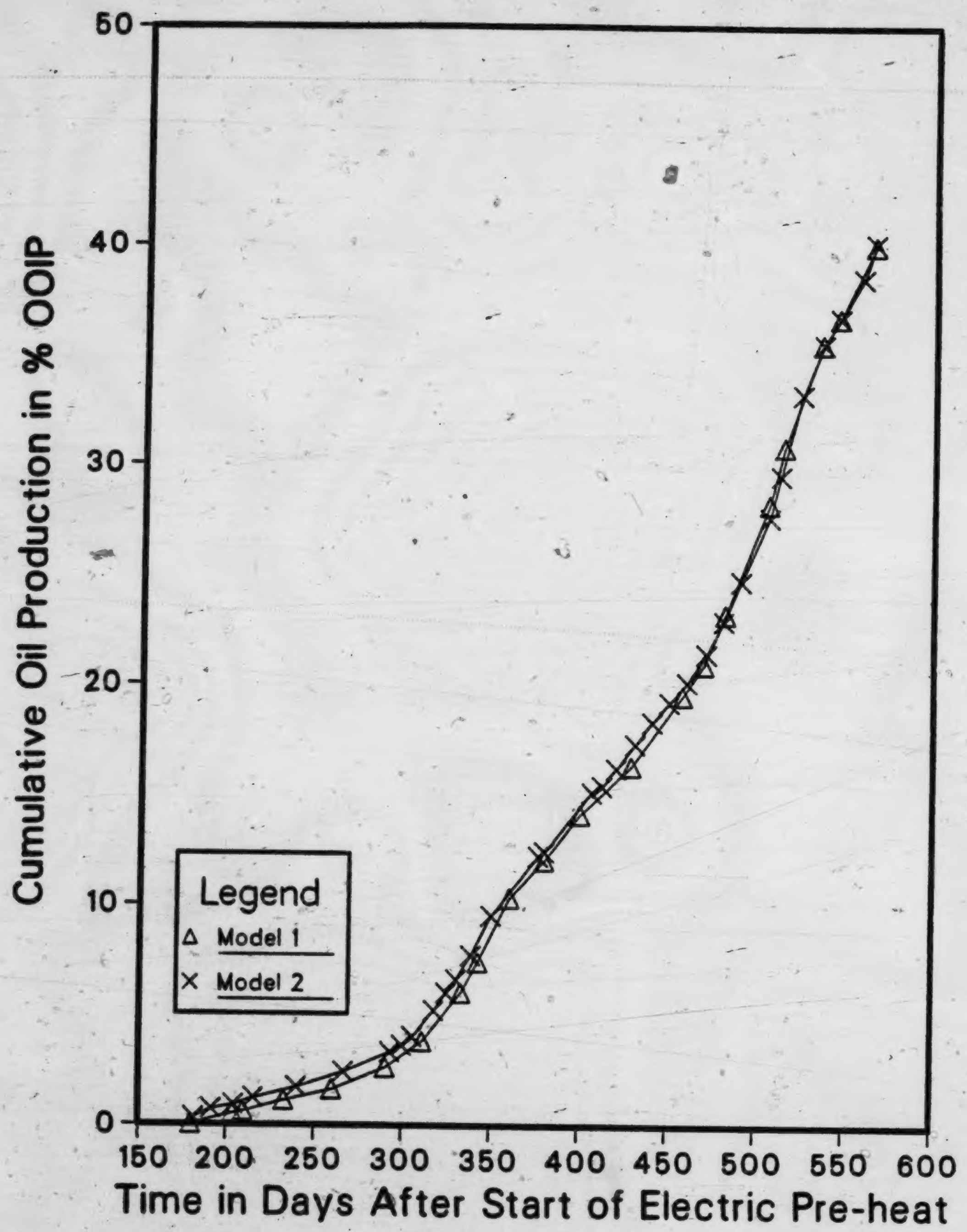

Figure 5.4 A plot of cumulative oil production versus time, for Case 1, comparing the results of simulations run using Model 1 (EPEIOS) and Model 2 (TCTM-EPEIOS). The cumulative production is shown as a fraction of the original oil in place.

The comparison of the injection pressures shows that, for the same specified steam injection rate, Model 2 initially predicted a higher injection pressure than was predicted by Model 1. This is due to the fact that thermal expansion had raised the pressure in the reservoir during the electric pre-heat. These increased pressures were used in Model 2 at the beginning of the steam drive. In simulations done with Model 1, where thermal expansion is neglected, the original reservoir pressure was utilized at the beginning of the steam drive. Thus, due to the higher pressures in the reservoir at the beginning of the steam drive, Model 2 initially predicted higher injection pressures. However, after fifty days of steam injection (about 12% of the total injection period) the injection pressures predicted by the two models nearly coincide.

The increased reservoir pressure, caused by the thermal expansion, also leads to a larger initial oil production rate predicted by Model 2 as compared to Model 1. However, this difference in oil production rate rapidly decreases so that, for the remainder of the steam drive the rates predicted by the two models substantially agree. Similarily, the cumulative oil production predicted by each of the two models substantially agrees after the initial period. At the end of the simulation, after 385 days of steam injection, both the cumulative oil production and cumulative water production predicted by the two models are nearly identical. (These figures are given in Table 5.2).

When the simulations were stopped, at a time of 385 days, the entire reservoir had been heated and steam was present throughout the entire reservoir. At this point, over 40 percent of the original oil in place had been produced. Further production was certainly possible. The simulation was stopped for two reasons. The first was the practical one of having only a finite supply of computer funds. The second reason is that the simulation to this point had already fulfilled its objectives. The simulation study had shown that the electric pre-heat provided a communications path between the wells allowing injection of steam. Injection of steam into this reservoir without the electric pre-heat would simply not be possible without fracturing the formation. The results predicted by each of Model 1 and Model 2 are very similar except in the prediction of formation pressure during the electric pre-heat and the initial period of steam injection.

5.3 Case 2 - A Two Layer, Horizontal Well Study

The second study, Case 2, involved the simulation of a two layer oil sand reservoir penetrated by four horizontal wells. A two dimensional cross section of the area in the middle region of the horizonal wells was simulated. The boundary conditions used in the simulation assume that the pattern of wells was repeated in each lateral direction; what was being simulated was part of a repeating pattern of wells, rather than an isolated set of four wells. The reservoir consisted of a layer of rich grade oil sand overlain with a layer of medium grade oil sand. The oil sand reservoir was surrounded above and below by layers of shale. The reservoir geometry, dimensions and well and electrode locations are shown in Figure 5.5. The reservoir properties used by Model 1 for the electric pre-heat simulation are given in Table 5.4, and the properties used by Model 1 for the simulation of the steam drive, and by Model 2 for simulation of both the electric pre-heat and the steam drive are given in Table 5.5.

A total of four horizontal wells were modelled in the simulation region. Two of these wells were electrode wells. These two electrode wells were drilled in each of the overlying shale formation and the underlying shale formation. The distance between the center of each of these electrode wells and the boundary between the shale layer and the nearest oil sand is 4 m. The electrode wells were assumed to have an effective radius of .25 m. The remaining two wells in the simulation area were used for steam injection and oil production. These two wells were located near the bottom of the rich oil sand, at the edges of the simulation region. As this was a simulation of part of a repeating pattern of wells, the simulation boundary passes through each of these injection or production wells. Only one half of each of these wells was included in the simulation area.

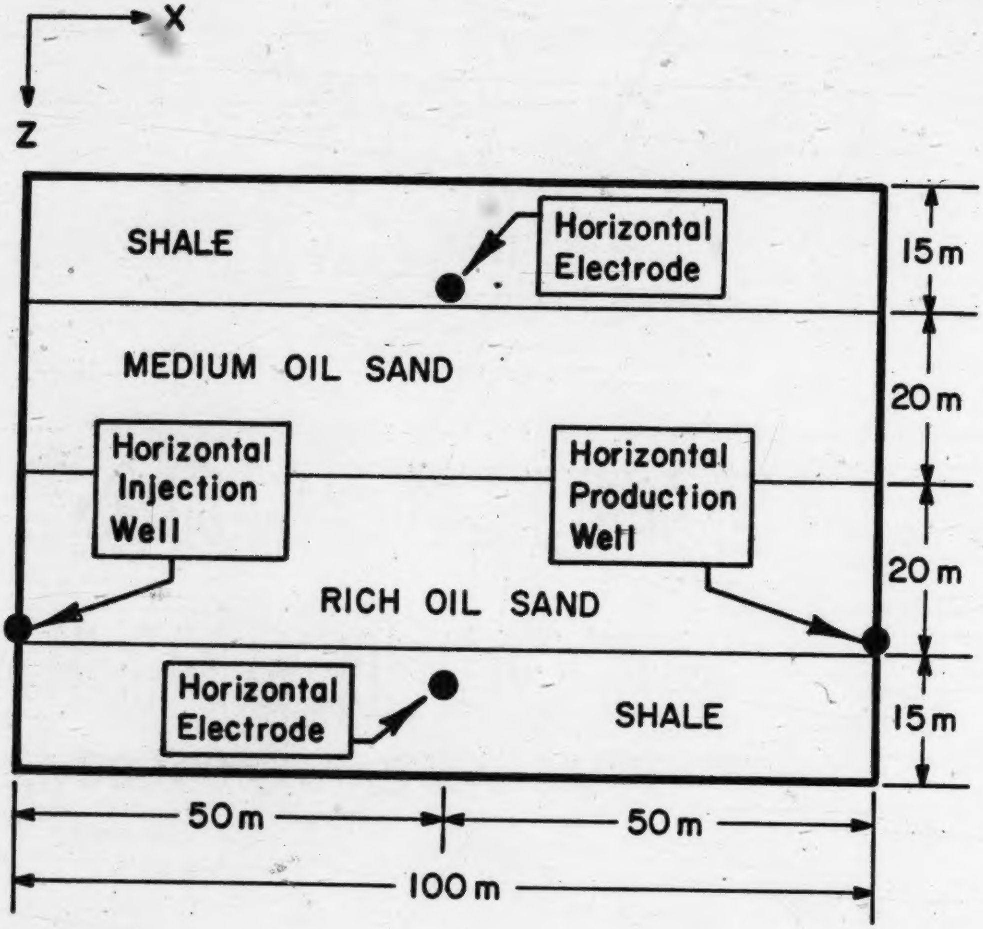
X
Z
SHALE
Horizontal Electrode
MEDIUM OIL SAND
Horizontal Injection Well
Horizontal Production Well
RICH OIL SAND
Horizontal Electrode
SHALE
15m
20m
20m
15m
50m
50m
100m

Figure 5.5 The geometry and dimensions of the reservoir and adjacent formations for Case 2.

Table 5.4 Reservoir properties used by Model 1 in the simulation of the electric preheat of Case 2.

Initial temperature	10.0	$^\circ C$
Shale		
Electrical conductivity		
$0.10 \left[1+0.025(T-24)\right]$ S/m		
Thermal conductivity	1.69	W/m·K
Volumetric heat capacity	2.13	$MJ/m^3 \cdot K$
Medium Oil Sand		
Electrical conductivity		
$0.022 \left[1+0.026(T-24)\right]$ S/m	$T \leq 100^\circ C$	
$0.022 \left[2.98+0.0022(T-100)\right]$ S/m	$T > 100^\circ C$	
Thermal conductivity	2.08	W/m·K
Volumetric heat capacity	2.20	$MJ/m^3 \cdot K$
Rich Oil Sand		
Electrical conductivity		
$0.0067 \left[1+0.026(T-24)\right]$ S/m	$T \leq 100^\circ C$	
$0.0067 \left[2.98+0.0022(T-100)\right]$ S/m	$T > 100^\circ C$	
Thermal conductivity	1.69	W/m·K
Volumetric heat capacity	2.06	$MJ/m^3 \cdot K$

Table 5.5 Reservoir properties for Case 2 used by Model 1 in simulating the steam drive and by Model 2 in simulating both electric preheat and steam drive.

For Model 2 Electric preheat only

Initial temperature	10.0	$^{\circ}C$
Connate water electrical conductivity		
Shale ($24^{\circ}C$)		
$0.8\left[1+0.025(T-24)\right]$ S/m		
Medium and Rich Oil Sand		
$0.89\left[1+0.026(T-24)\right]$ S/m		$T \leq 100^{\circ}C$
$0.89\left[2.98+0.0022(T-100)\right]$ S/m		$T > 100^{\circ}C$

For both Model 1 and Model 2

Shale		
porosity	0.20	
permeability (isotropic)	0.001	darcies
initial water saturation	0.999	
initial oil saturation	0.001	
Medium Oil Sand		
porosity	0.34	
permeability (isotropic)	2.90	darcies
initial water saturation	0.309	
initial oil saturation	0.691	
Rich Oil Sand		
porosity	0.34	
permeability (isotropic)	2.90	darcies
initial water saturation	0.17	
initial oil saturation	0.83	

Other fluid and rock-fluid properties as given by Reddy et al (1980).

The electric pre-heat for Case 2 consisted of two stages. In the first stage, lasting 365 days, the reservoir was electrically heated at a constant power rate of 13 kW per meter length of horizontal electrode. During the second stage, from 365 days to 547.5 days (a period of 182.5 days), the constant power heating rate was raised to 20 kW per meter length of horizontal electrode. The steam drive commenced at the end of the electric pre-heat. The steam drive occured in several stages, detailed in Table 5.6, where each well alternated between being an injection well and being a production well.

This simulation was run using each of Model 1 and the implicit formulation of Model 2. The finite difference grid used in the solution of the electrical potentials and electrical heating rates consisted of 37 grid blocks in the horizontal direction and 30 grid blocks in the vertical direction. This grid was also used by Model 1 in the solution of the temperatures during the electric pre-heat. Similarly to Case 1, a coarser grid was used in the solution of the fluid flow equations. The fluid flow grid consisted of 7 grid blocks in the horizontal direction and 6 blocks in the vertical direction. One layer of grid blocks was used to model each of the shale formations, and two layers of blocks were used to model each of the two oil sand zones. The use of two, different, finite difference grids allowed accurate solution of the electrical potentials and heating rates near the electrodes, while keeping the cost of solving the fluid

Table 5.6 Details of electric preheat and steam drive for Case 2.

Electric Preheat

Time (days)	Electrical Heating Rate
0-365	constant power heating 13kW per meter of electrode
365-547	constant power heating 20kW per meter of electrode

Total electrical energy input: 7.2×10^{11} J

Steam Drive

Time (days)	Well #1	Well #2
547-607	Prod @ 2070 kPa	Inj. @ 0.32 m^3/D
607-847	Inj. @ 0.32 m^3/D	Prod @ 1380 kPa
847-1147	Prod @ 1380 kPa	Inj. @ 0.95 m^3/D
1147-1207	Inj. @ 0.64 m^3/D	Prod @ 3450 kPa
1207-1247	Inj. @ 0.95 m^3/D	Prod @ 1380 kPa
1247-2047	Inj. @ 1.59 m^3/D	Prod @ 1380 kPa

Steam quality is 0.7, except for the period of 607-847 days, when the steam quality was 0.5.

Total volume injected	1729 m^3
Total energy in injected steam	2.8×10^{12} J
Total energy input to formation	3.55×10^{12} J

Cumulative Production (2047 days)

	Model 1	Model 2
Oil	511 m^3	528 m^3
Water	1832 m^3	1843 m^3

flow equations to an affordable level.

The predicted temperature increases, due to the electric pre-heat, are shown in Table 5.7. The temperature increases at the fluid flow grid block centers are shown. The upper figure at each grid block center is the temperature increase predicted by Model 1, while the lower figure is the temperature increase predicted by the implicit formulation of Model 2.

The use of two finite difference grids caused some of the variation in the results predicted by Model 1 and Model 2. While Model 1 and Model 2 used the same grid in the solution of the electrical potentials and heating rates, they used different grids in the solution of the temperatures. Model 1 used the finer 37x30 grid in the solution of the temperatures during the electric pre-heat, whereas Model 2 used the coarser 7x6 grid. Thus, Model 1 was better able to simulate the higher temperatures in the immediate area of the electrode. An examination of the plot of inter-electrode resistance versus time (Figure 5.6) shows that Model 1 predicted a lower resistance than Model 2. This was due to the higher temperatures, and hence lower resistance, of the formation near the electrode, which were predicted by Model 1. As the electrode occupied only a fraction of the larger grid block used in the solution of the temperature by Model 2, the predicted temperature increase (which is uniform for the entire block) is less than in Model 1.

Table 5.7 A comparison of the temperature increases (in ^{o}C) predicted by two models, due to the electric pre-heating of the reservoir in Case 2. Initial reservoir temperature is $10^{o}C$.

For each grid block location:

the upper figure is for Model 1
the lower figure is for Model 2 - Implicit

X (m)→ Z (m)↓	7.1	21.4	35.7	50.0	64.3	78.6	92.9
7.5	4.1 3.3	11.5 9.2	29.8 24.1	95.4 89.4	29.8 24.1	11.5 9.2	4.1 3.3
20.0	15.9 15.9	24.1 23.9	51.2 47.1	105.5 91.2	51.2 47.1	24.1 23.9	15.9 15.9
30.0	24.5 22.7	33.5 31.4	59.7 53.8	89.1 81.9	59.7 53.8	33.5 31.4	24.5 22.7
40.0	45.8 44.2	61.1 59.7	103.9 97.2	150.8 141.4	103.9 97.2	61.1 59.7	45.8 44.2
50.0	42.9 42.8	58.2 57.2	102.1 95.4	174.4 159.6	102.1 95.4	58.2 57.2	42.9 42.8
62.5	8.2 5.4	17.4 12.3	38.2 27.7	102.0 88.4	38.2 27.7	17.4 12.3	8.2 5.4

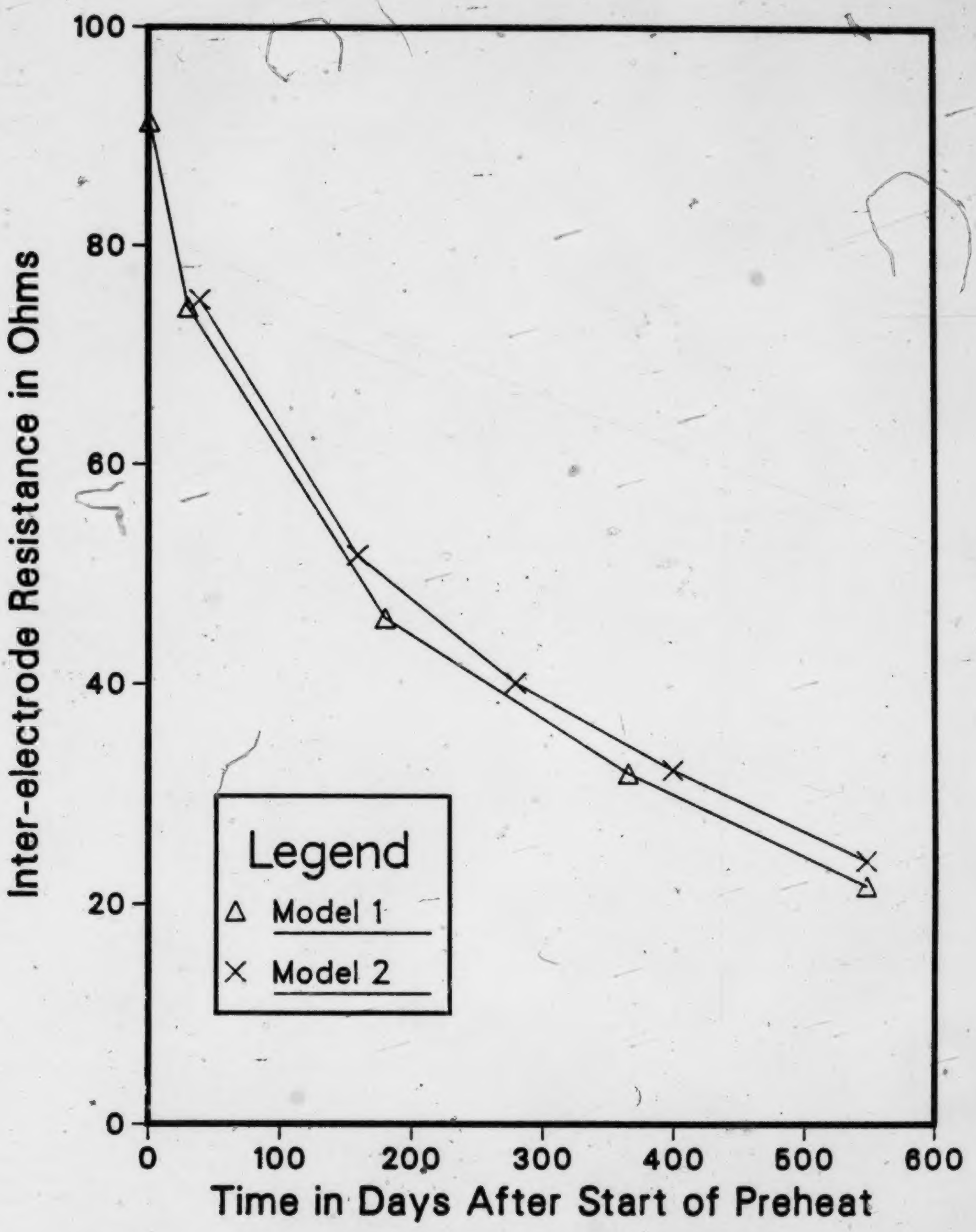

Figure 5.6 A plot of the inter-electrode resistance versus time for the electric pre-heat phase of Case 2.

The predicted oil rates, and the cumulative oil production, versus time, are shown on Figures 5.7 and 5.8. As may be seen from these figures, the simulation results from both models are nearly identical. Thus, though Model 1 predicted higher temperatures at the end of the electric pre-heat than were predicted by Model 2, particularly in the region midway between the injection and production wells, there is little difference in the cumulative oil production predicted by the two models.

A variation of Case 2 was simulated to further study the sensitivity of the steam drive performance to changes in the temperatures at the end of the electric pre-heat. This simulation run was done with a higher electrical heating rate than the other Case 2 runs, but with all other input data the same, including the length of the electric pre-heat. This resulted in higher initial temperatures at the start of the steam drive; the new run having temperatures 20 to 30°C higher than the base case in the rich oil sand layer. However, this higher temperature at the start of the steam drive did not lead to an improvement in the cumulative oil recovery, as shown in Figure 5.9. Thus, it appears that once sufficient electrical heating has taken place to allow the development of a fluid communication path, further electrical heating does not necessarily have beneficial results.

The CPU times required, to simulate Case 2, by the programs implementing Model 1 (EPEIOS) and Model 2

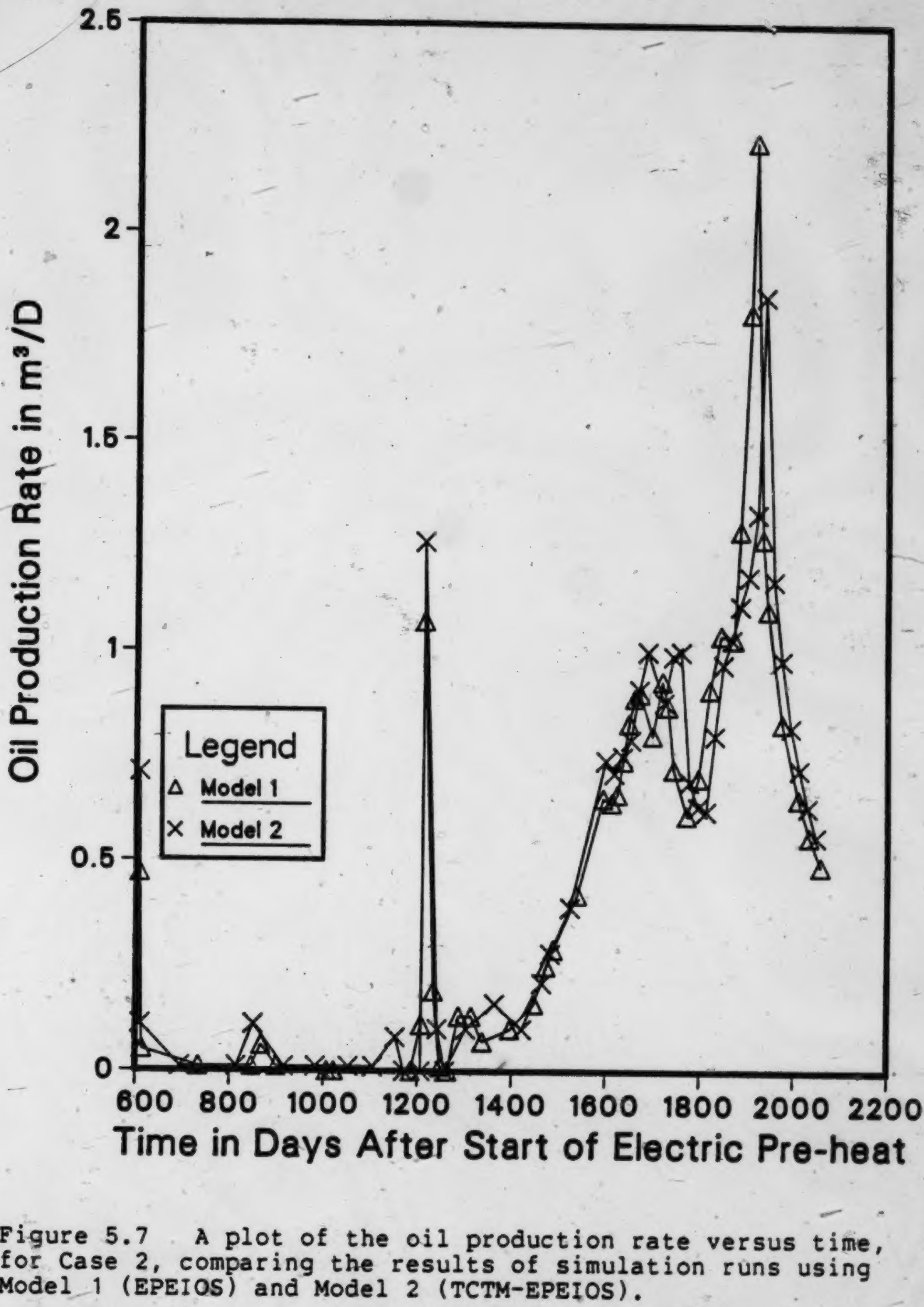

Figure 5.7 A plot of the oil production rate versus time, for Case 2, comparing the results of simulation runs using Model 1 (EPEIOS) and Model 2 (TCTM-EPEIOS).

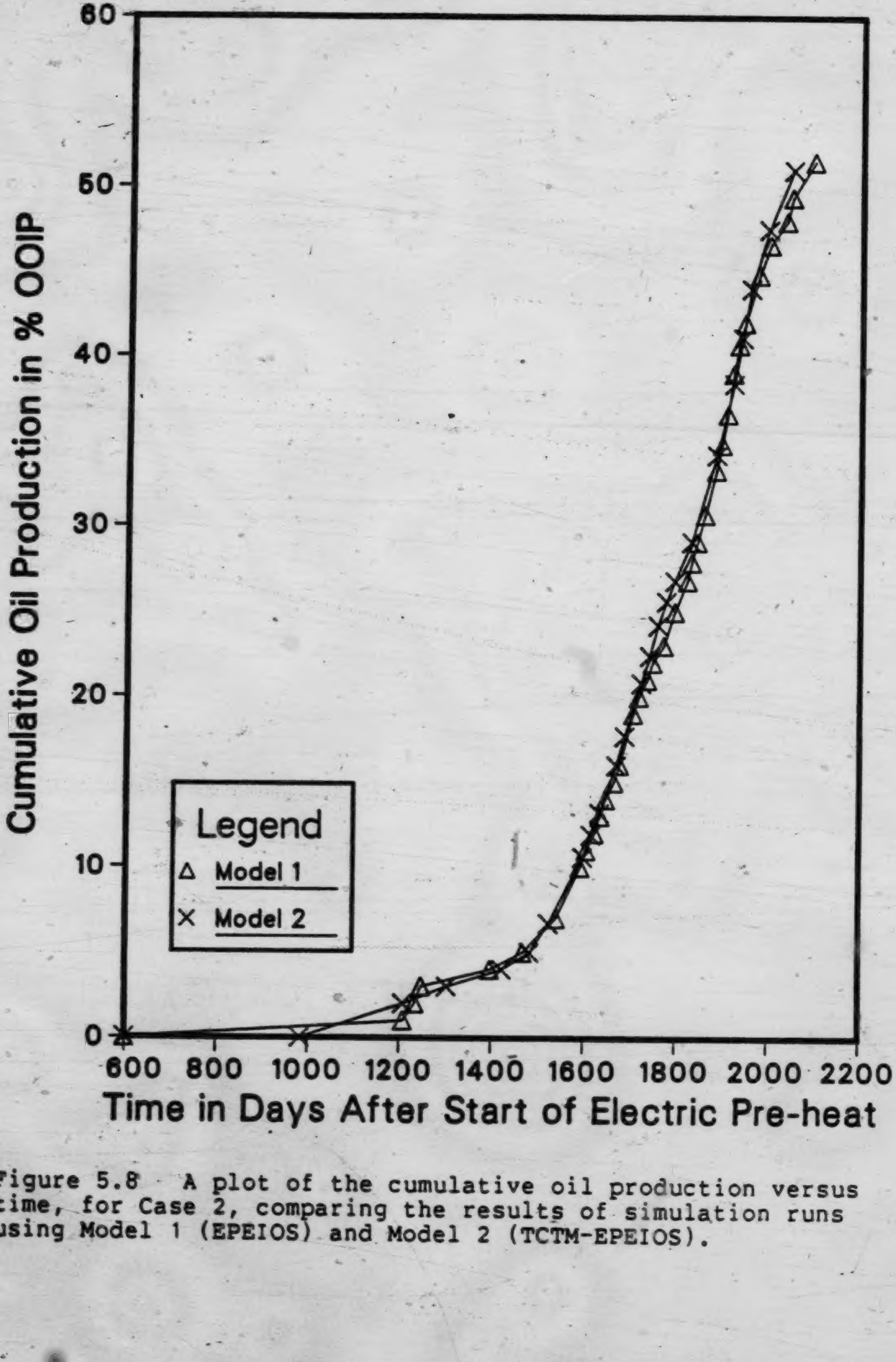

Figure 5.8 A plot of the cumulative oil production versus time, for Case 2, comparing the results of simulation runs using Model 1 (EPEIOS) and Model 2 (TCTM-EPEIOS).

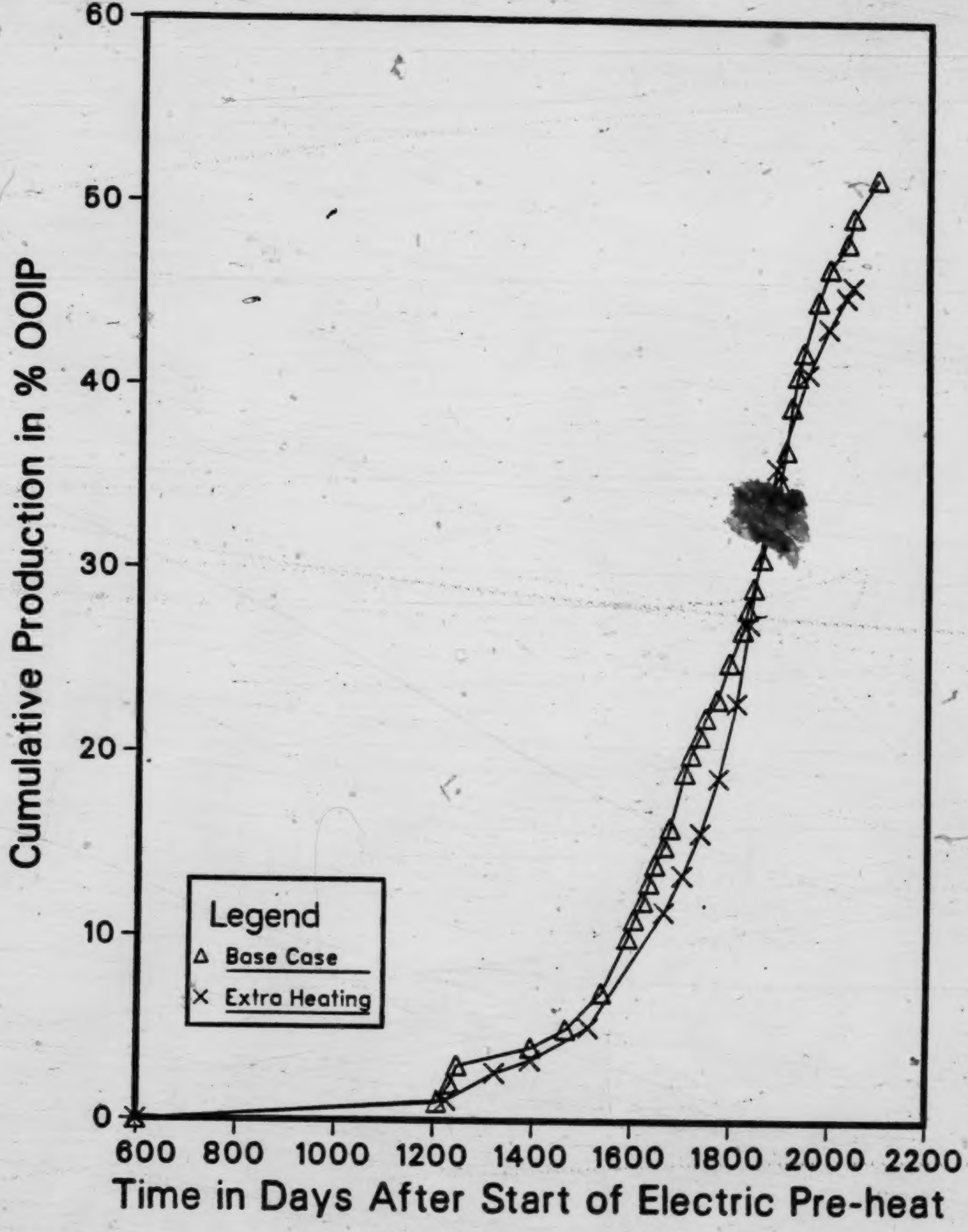

Figure 5.9 A plot of cumulative oil production versus time for Case 2, and for a simulation similar to Case 2, but with increased electrical heating.

(TCTM-EPEIOS) were recorded and compared for the simulation of the electric pre-heat. Model 1 (EPEIOS) took a total of 76 timesteps, requiring 626 seconds of CPU time on an Amdahl 5860. Model 2, using the same finite difference grid for the electrical potential calculation as Model 1, but a coarser grid for the fluid flow and energy calculations, required 759 seconds of CPU time. It must be noted in making this comparison that different compilers were used in compiling various portions of the two programs. As the optimizer of one of the compilers was unreliable, no optimization was used in compiling EPEIOS. This may affect the CPU comparison for the two models.

At the end of the simulations, a total of 2050 days after the start of the electric pre-heat, steam had broken through to the producer. The run was terminated at this point. Approximately 51% of the original oil in place was produced. The top half of the reservoir was at near residual oil saturation, but considerable oil remained in the bottom portion of the reservoir.

An equivalent oil steam ration (OSR) was calculated to this point of the combined electric pre-heat and steam drive. A total of 7.2 x 10^{11} Joules of electrical energy was input to the formation during the electric pre-heat, and a total of 2.8 x 10^{12} Joules of thermal energy was input during the steam drive, for a total energy input to the formation of 3.55 x 10^{12} J. This total input energy figure was converted to an equivalent amount of injected steam.

Typical injected steam may have a temperature of 240°C and a steam quality of 0.7. The energy required to raise one cubic meter of 13°C water to 240°C, 0.7 quality steam is 2.21×10^9 J. Thus, the energy input to the formation was the equivalent of 1610 m^3 of 240°C, 0.7 quality steam. As the total production to 2050 days was 511 m^3, the equivalent OSR was 0.32 (SOR = 3.13).

Recall that this simulation was for a two dimensional cross section in the mid well region of a horizontal well pattern. The energy and figures given are all per meter of horizontal well length. The two dimensional simulation presented would be accurate in the middle section of a pattern of long horizontal wells, but likely is not accurate near the ends of the wells.

5.4 Case 3 - A Realistic Five-Spot Pattern Flood

The third simulation study, Case 3, was the simulation of one quadrant of a five spot pattern in a realistic, if somewhat better than average, Athabasca oil sand reservoir. The objective of this simulation study was to accurately simulate a realistic, possible, electric pre-heat and steam drive project. To accomplish this objective, the reservoir chosen for the study was based on a very good Athabasca oil sand reservoir, and Athabasca oil sand property data was used. A one hectare (2.5 acre) five spot pattern was used in the study. While some aspects of the project being simulated are in need of further research, in particular the technological and economic feasibility of the well and electrode completion used, overall the simulation study accurately modelled a possible electric pre-heat and steam drive project.

The reservoir dimensions and well locations are given in Figure 5.10 and the reservoir properties are given in Table 5.8. A "Top-Bottom" electrode configuration was used, where electrical current was passed from an electrode located in the shale layer adjacent to the top of the oil sand layers, to an electrode located in the shale layer underlying the oil sand layers. Each well had two electrodes, one at the top and one at the bottom, which had different polarities. Single phase, alternating electrical current was passed between the electrodes. A discussion of the advantages of using this type of electrode configuration was given in Hiebert et al. (1986).

It was assumed that these electrodes were produced by underreaming or jet cutting the shale layers to a distance of three meters from the well, then filling the volume vacated with a conducting metal shot. Thus an electrode of 3 m radius was created. If research into electrode completion technology should show that such a large radius electrode is not economically feasible, a smaller radius electrode may be used. The use of a smaller radius electrode would require cooling of the electrodes, and possibly a lower electrical heating rate. A lower heating rate would increase the electrical heating time required to produce the

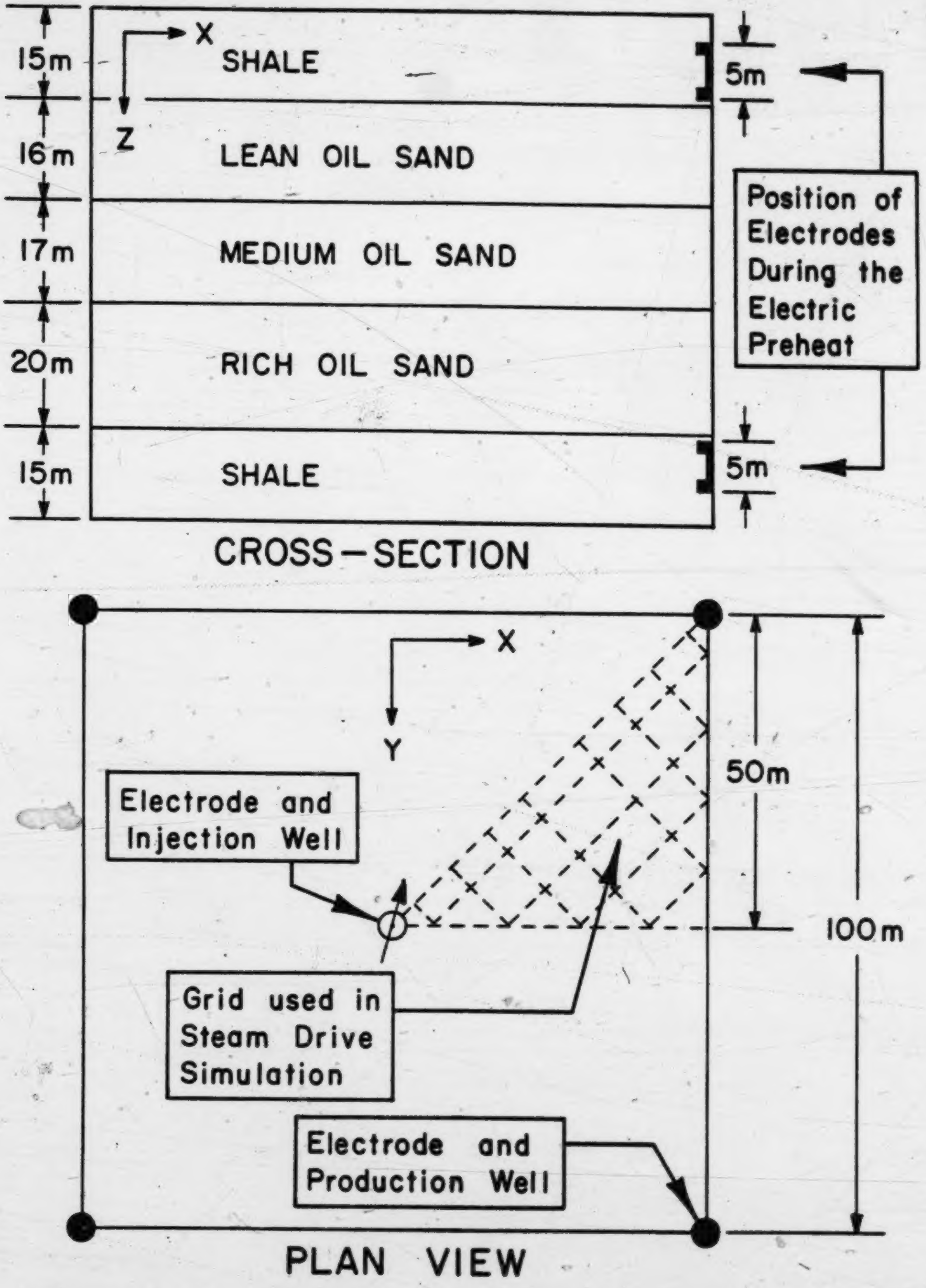
15m
16m
17m
20m
15m
X
Z
SHALE
LEAN OIL SAND
MEDIUM OIL SAND
RICH OIL SAND
SHALE
5m
5m
Position of Electrodes During the Electric Preheat
CROSS-SECTION
X
Y
Electrode and Injection Well
Grid used in Steam Drive Simulation
Electrode and Production Well
50m
100m
PLAN VIEW

Figure 5.10 The reservoir dimensions and electrode and well locations for Case 3. The dashed lines in the areal view shows the simulation grid used in simulating the steam drive.

Table 5.8 Reservoir properties used by Model 1 in the simulation of the electric preheat of Case 3.

Initial temperature	10.0	°C
Shale		
Electrical conductivity		
$0.10\left[1+0.025(T-24)\right]$ S/m		
Thermal conductivity	1.69	W/m·K
Volumetric heat capacity	2.13	$MJ/m^3 \cdot K$
Lean Oil Sand		
Electrical conductivity		
$0.043\left[1+0.026(T-24)\right]$ S/m	$T \leq 100$°C	
$0.043\left[2.98\right]$ S/m	$T > 100$°C	
Thermal conductivity	2.42	W/m·K
Volumetric heat capacity	2.28	$MJ/m^3 \cdot K$
Medium Oil Sand		
Electrical conductivity		
$0.022\left[1+0.026(T-24)\right]$ S/m	$T \leq 100$°C	
$0.022\left[2.98+0.0022(T-100)\right]$ S/m	$T > 100$°C	
Thermal conductivity	2.08	W/m·K
Volumetric heat capacity	2.20	$MJ/m^3 \cdot K$
Rich Oil Sand		
Electrical conductivity		
$0.00352\left[1+0.026(T-24)\right]$ S/m	$T \leq 100$°C	
$0.00352\left[2.98+0.0022(T-100)\right]$ S/m	$T > 100$°C	
Thermal conductivity	1.65	W/m·K
Volumetric heat capacity	2.04	$MJ/m^3 \cdot K$
Limestone		
Electrical conductivity		
$0.030\left[1+0.025(T-24)\right]$ S/m		
Thermal conductivity	3.55	W/m·K
Volumetric heat capacity	2.66	$MJ/m^3 \cdot K$

same oil sand formation temperatures.

The simulation study for Case 3 was carried out in two stages. In the first stage, ~~the~~ electric pre-heat was simulated using both Model 1 (EPEIOS) and the explicit formulation of Model 2 (TCTM-EPEIOS). An accurate simulation of the pre-heat was performed with Model 1, using a large number of finite difference grid blocks to accurately model the electrodes. The finite difference grid used by Model 1 (EPEIOS) consisted of 22 grid blocks in each of the horizontal directions, with 30 grid blocks in the vertical direction. Variable grid block sizes were used, with smaller grid blocks near the electrodes, where there are large electric potential gradients, and larger grid blocks in the regions away from the electrodes. The simulation of the electric pre-heat and a period of one week of well recompletion time after the pre-heat required over sixty minutes of CPU time on the Amdahl 5860. Cost considerations and storage requirements did not allow the use of the same finite difference grid when simulating the pre-heat with Model 2. The grid used by Model 2 for the solution of electrical potentials consisted of 12 grid blocks in each of the horizontal directions and 21 grid blocks in the vertical direction. For the solution of the fluid flow equations, a grid of 4 blocks in each of the horizontal directions and 5 blocks in the vertical direction was used.

The second stage of the Case 3 simulation study concerned the modelling of the steam drive part of the project. Excessive cost, limitations on the number of grid blocks, and lack of a sophisticated well model precluded the use of the TCTM in this stage of the study. Instead, the Computer Modelling Group's thermal reservoir simulator, ISCOM, was used. (For details of ISCOM, see Rubin and Buchanan, 1985). This second stage of the Case 3 simulation study will be discussed after the results of the first stage, the electric pre-heat simulation, have been presented.

The Case 3 electric pre-heat consisted of applying a constant power heating rate of 1.45 MW to the five spot pattern for a period of one year. A total of 4.58×10^{13} J of electrical energy was input to the five spot pattern during this period. Of the total input electrical energy, 76% remained as heat energy in the oil sand layers at the end of the electric pre-heat. The rest of the input energy was lost to the adjacent shale and limestone formations. At the end of the electric pre-heat a further one week period, with no electrical heating or steam injection, was simulated. This one week period accounts for the time necessary to recomplete the electrode wells as injection or production wells.

The temperatures at the start of the steam drive, predicted by both Model 1 and Model 2, are given in Table 5.9. The temperatures shown are those at the center of the grid blocks used in the solution of the fluid flow and temperature equations by Model 2. The temperatures given for

Table 5.9 A Comparison of the temperature increases (in ^{o}C) predicted by two models, due to the electrical heating of the reservoir in Case 3. The initial reservoir temperature was $10^{o}C$.

For each grid block location:

the upper figure is for Model 1
the lower figure is for Model 2

Plane of Z = 7.0 m — Upper Shale Layer

X (m)→ Y (m)↓	5.0	17.5	32.5	45.0
5.0	1.1 1.1	2.2 2.2	12.2 12.8	75.6 85.6
17.5	2.2 2.2	1.7 1.7	4.4 3.9	12.2 12.8
32.5	12.2 12.2	4.4 3.9	1.7 1.7	2.2 2.2
45.0	75.6 85.6	12.2 12.8	2.2 2.2	1.1 1.1

Plane of Z = 22.0 m — Lean Oil Sand Layer

X (m)→ Y (m)↓	5.0	17.5	32.5	45.0
5.0	4.4 5.0	6.1 6.1	13.9 12.8	42.8 37.8
17.5	6.1 6.1	4.4 6.1	8.3 7.8	13.8 12.8
32.5	13.9 13.3	8.3 7.8	4.4 6.1	6.1 6.1
45.0	42.8 38.3	13.9 13.3	6.1 6.1	4.4 5.0

Table 5.9 (Continued)

Plane of Z = 38.5 m Medium Oil Sand Layer

X (m)→ Y (m)↓	5.0	17.5	32.5	45.0
5.0	13.9 12.8	15.0 13.9	21.1 19.4	28.4 29.4
17.5	15.0 13.9	14.4 13.9	17.8 16.1	21.1 19.4
32.5	21.1 19.4	17.8 16.1	14.4 13.9	15.0 13.9
45.0	29.4 29.4	21.1 19.4	15.0 13.9	13.9 12.8

Plane of Z = 57.0 m Rich Oil Sand Layer

X (m)→ Y (m)↓	5.0	17.5	32.5	45.0
5.0	46.1 43.9	50.0 47.8	70.6 66.1	108.9 103.9
17.5	50.0 47.8	50.0 48.3	57.8 55.0	70.6 66.1
32.5	70.6 66.1	57.8 55.0	50.0 48.3	50.0 47.8
45.0	108.9 103.9	70.6 66.1	50.0 47.8	46.1 43.9

Plane of Z = 74.5 m Lower Shale Layer

X (m)→ Y (m)↓	5.0	17.5	32.5	45.0
5.0	4.4 2.8	6.1 5.0	21.7 22.2	75.6 103.9
17.5	6.1 5.0	5.6 3.9	10.6 8.9	21.9 22.2
32.5	21.7 22.2	10.6 8.9	5.6 3.8	6.1 5.0
45.0	75.6 103.9	21.7 22.2	6.1 5.0	4.4 2.8

Model 1, which used a finer finite difference grid, were obtained by interpolation. Examination of Table 5.9 shows that the two models are in good agreement in predicting the temperature increases during the electric pre-heat, particularly in the three oil sand layers. An isosurface plot of temperature is shown in Figure 5.11. This plot show that portion of one quadrant of the five spot that was heated to a temperature greater than 55 °C.

The inter-electrode resistance for each pair of electrodes is plotted versus time in Figure 5.12. Again note that Model 1 and Model 2 are in substantial agreement. As in Case 2, the lower resistance predicted by Model 1 is due to the larger number of grid blocks used by Model 1 in the solution of the temperature equation. This larger number of grid blocks allowed better resolution of the temperature near the electrodes, a region which is very important in the calculation of the inter-electrode resistance.

As mentioned above, limitations on TCTM, used to this point in the simulation study, precluded it's use in modelling the steam drive stage of Case 3. To accurately simulate this steam drive, more grid blocks and a better well model than were available in TCTM were needed. For these reasons, a commercial thermal reservoir simulator, the Computer Modelling Group's ISCOM, was used to conduct the simulation study of the steam drive portion of Case 3. In effect, a new implementation of Model 1 was created, using ISCOM instead of TCTM. ISCOM is a general purpose thermal

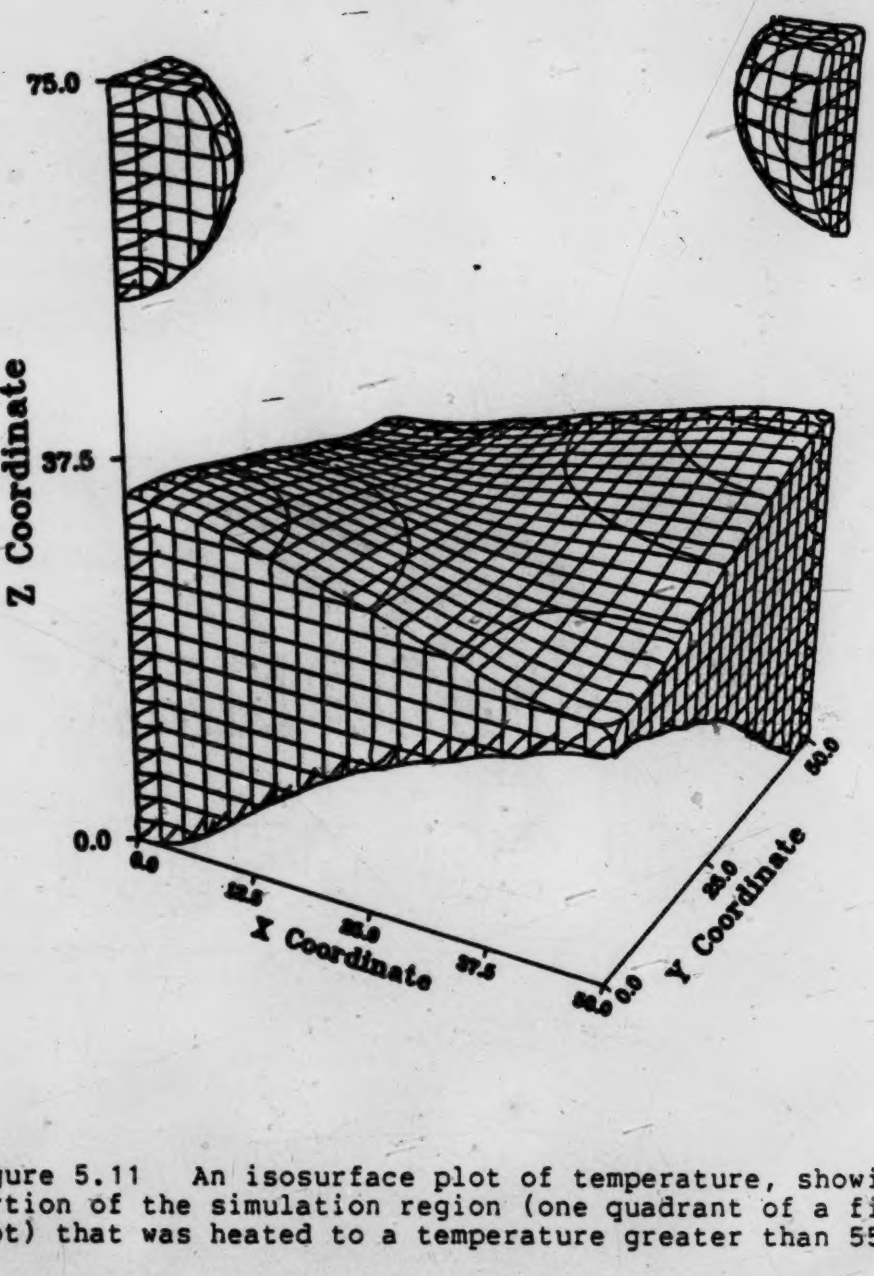
75.0
37.5
0.0
Z Coordinate
0.0
12.5
25.0
37.5
50.0
X Coordinate
0.0
25.0
50.0
Y Coordinate

Figure 5.11 An isosurface plot of temperature, showing the portion of the simulation region (one quadrant of a five spot) that was heated to a temperature greater than 55 °C.

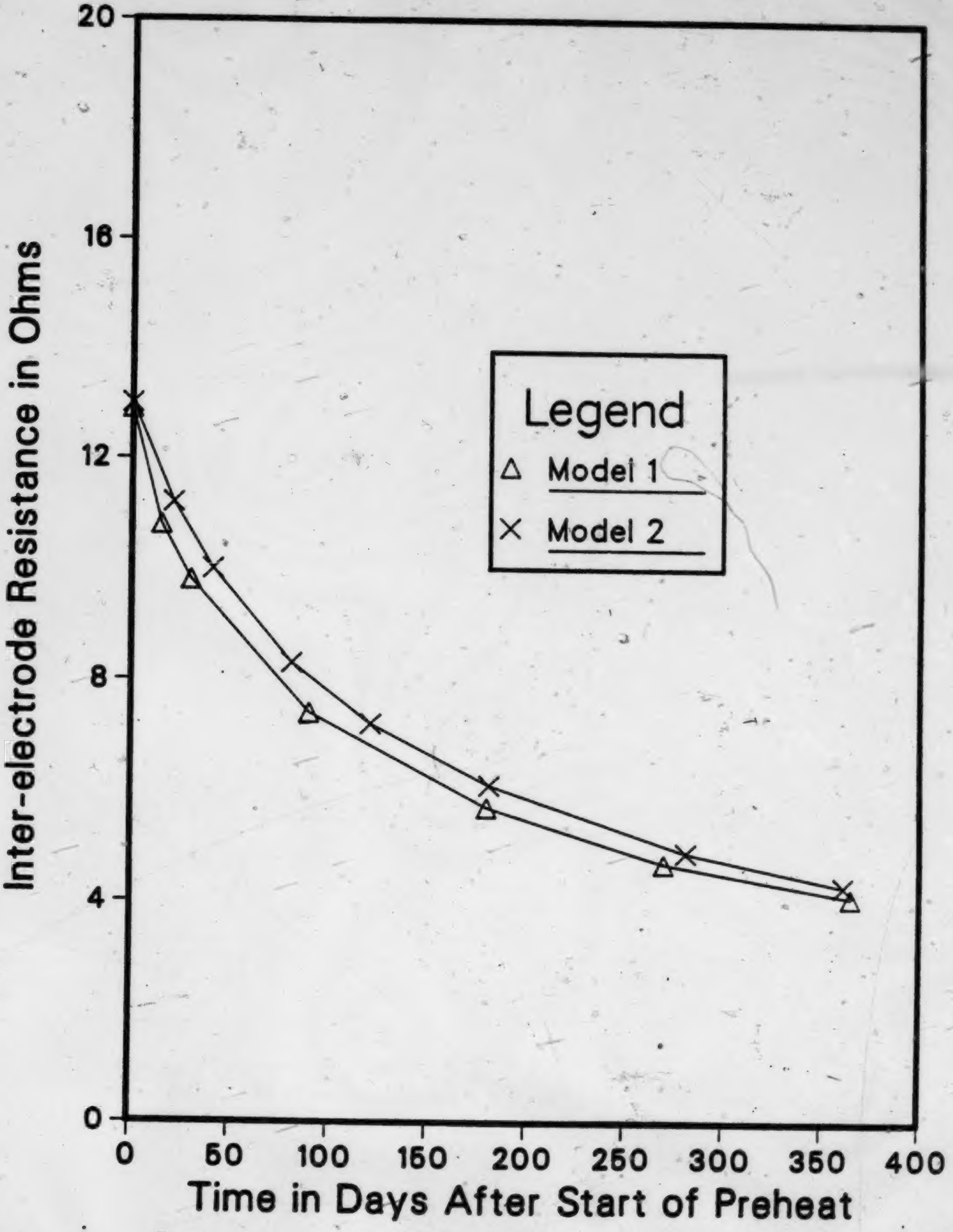

Figure 5.12 Inter-electrode resistance, versus time, for the pair of electrodes in one well. The resistances predicted by each of Model 1 and Model 2 are compared.

reservoir simulator, described in a paper by Rubin and Buchanan (1985). It does not have some of the limitations of TCTM, in particular it has a better, multi-block well model, and does not restrict the maximum number of blocks which may be used in the finite difference modelling of the problem domain.

An areal view of the simulation grid is shown on Figure 5.10. It may be shown by symmetry that it is only necessary to simulate one eighth of the five spot pattern. The simulation of this triangular area is allowed in ISCOM by the use of grid block volume modifiers. Vertically, six grid block layers were used, two layers for each of the three oil sand layers. A total of 150 grid blocks were used to model the one eighth of a five spot. A nine point differencing operator in the horizontal plane was used in ISCOM to reduce grid orientation effects which might otherwise affect the simulation results (Yanosik and McCraken, 1979).

The rock, rock-fluid, and fluid properties used in the simulation of the steam drive are given in Table 5.10. The relative permeability and viscosity data were obtained from a paper by Edmunds (1985). The specific heat capacity of the oil was obtained from a paper by Cassis, Fuller, Hepler, McLean, Skauge, Srinivasan, and Yan (1985). The initial temperatures of all the grid blocks used in the simulation of the steam drive are given in Table 5.11. These temperatures were obtained by interpolation of the results of the EPEIOS simulation of the pre-heat.

Table 5.10 Reservoir properties used in the simulation of the steam drive of Case 3.

Initial temperature - as given by Model 1 (EPEIOS) at the end of the electric preheat. See Table 5.11.

Initial pressure in bottommost layer	1934	kPa
Lean Oil Sand		
Porosity	0.33	
Horizontal permeability	1.0	darcies
Vertical permeability	0.5	darcies
Water saturation	0.443	
Oil saturation	0.557	
Medium Oil Sand		
Porosity	0.34	
Horizontal permeability	2.0	darcies
Vertical permeability	1.0	darcies
Water saturation	0.309	
Oil saturation	0.691	
Rich Oil Sand		
Porosity	0.34	
Horizontal permeability	3.0	darcies
Vertical permeability	1.5	darcies
Water saturation	0.13	
Oil saturation	0.87	

Water and Steam properties from ISCOM internal steam tables.

Oil Specific heat capacity

$$C_p = 0.055 + 6.818 \times 10^{-3} T - 4.464 \times 10^{-6} T^2 \quad \mathrm{J/K \cdot g}$$

Oil Compressibility 4.5×10^{7} kPa^{-1}

Pore Compressibility 3.45×10^{7} kPa^{-1}

Table 5.10 (Continued)

Oil Viscosity

Temperature	Viscosity (cp)
15	1 000 000
50	8 700
100	220
150	31
200	10
250	5
300	3.3

Water-oil Relative Permeability

S_w	k_{rw}	k_{row}
0.13	0.0	1.0
0.20	0.0002	0.98
0.30	0.0055	0.90
0.40	0.025	0.75
0.45	0.044	0.64
0.50	0.070	0.56
0.60	0.15	0.37
0.70	0.27	0.23
0.80	0.45	0.092
0.90	0.69	0.0
1.0	1.0	0.0

Gas-oil Relative Permeability

S_g	k_{rg}	k_{rog}
0.0		1.0
0.05	0.0	0.83
0.10	0.01	0.69
0.20	0.04	0.45
0.30	0.11	0.27
0.40	0.19	0.15
0.50	0.30	0.07
0.55	0.38	0.044
0.60	0.47	0.025
0.70	0.67	0.0055
0.80	0.90	0.0002
0.85	1.0	0.0

Table 5.11 Initial temperatures (in °C) at the grid block centers at the start of the steam drive for Case 3. These values were obtained using Model 1 (EPEIOS).

K=1 (Top Layer)

				13.8				
			14.3	14.0	14.3			
		18.0	15.2	14.4	15.2	18.0		
	40.5	22.7	16.2	14.8	16.2	22.7	40.5	
109.8	61.1	25.3	16.7	15.0	16.7	25.3	61.1	109.5

K=2

				16.3				
			16.8	16.5	16.8			
		19.8	17.7	17.0	17.7	19.8		
	31.3	22.8	18.7	17.6	18.7	22.8	31.3	
49.2	37.9	24.5	19.1	17.8	19.1	24.5	37.9	49.2

K=3

				20.9				
			21.5	21.2	21.5			
		24.6	22.6	21.8	22.6	24.6		
	32.7	27.2	23.7	22.6	23.7	27.2	32.6	
40.5	35.9	28.5	24.2	23.0	24.2	28.5	35.9	40.5

K=4

				28.6				
			29.5	29.0	29.5			
		33.5	30.9	30.0	30.9	33.5		
	42.9	36.8	32.5	31.1	32.5	36.8	42.9	
50.8	46.2	38.4	33.2	31.6	33.2	38.4	46.2	50.7

K=5

				52.6				
			54.5	53.5	54.5			
		63.7	57.6	55.4	57.6	63.7		
	87.8	71.5	61.1	57.8	61.1	71.5	87.8	
109.9	97.1	75.5	62.6	58.8	62.6	75.5	97.1	109.9

K=6 (Bottom Layer)

				50.4				
			52.4	51.2	52.4			
		63.9	55.8	53.2	55.9	63.9		
	105.8	75.1	59.6	55.4	59.7	75.1	105.8	
167.9	129.9	80.8	61.3	56.3	61.3	80.8	129.9	167.7

The steam drive started 379 days after the start of the electric pre-heat. Several injection and production strategies for the steam drive were simulated and the strategy with the best results is presented below. However, with limited computer funds available, only a few complete simulations of the steam drive could be conducted. Thus the strategy presented should not be regarded a fully optimized plan for the steam drive.

While only one eighth of the five spot pattern was simulated, all figures given in the following paragraphs are for the full pattern.

The first stage of the steam drive consisted of injecting steam into the "producers" to further heat the reservoir near these wells. Steam with an enthalpy of 2.45×10^9 J/m^3 was injected into the production wells for a period of 75 days. (This corresponds to 240°C, 0.8 quality steam. All steam volumes are given in cold water equivalents.) The injection rate was controlled by a maximum injection pressure constraint of 4.0 MPa. This maximum pressure was chosen as it is less than the formation fracture pressure for the reservoir, assuming a depth of greater than 330 m. While the injection rate varied over the 75 day period, a total of 7712 m^3 of steam was injected into the pattern, for an average injection rate of 103 m^3/D.

During this initial 75 days period, the central "injector" was allowed to produce reservoir fluids, subject to a minimum bottom hole pressure (BHP) constraint of

1.5 MPa. A total of 1120 m^3 of oil were produced during this period.

The second stage of the steam drive consisted of 290 days of low quality steam injection. Steam at a temperature of 240°C and with a steam quality of 0.10 was injected into the "injector". (The steam enthalpy was 1.21×10^9 J/m^3.) The injection rate was controlled by either a maximum injection pressure contraint of 4.0 MPa or a maximum injection rate constraint of 240 m^3/D. A total of 54056 m^3 of steam were injected during this period, for an average rate of 186.4 m^3/D. The "producers" were allowed to produce, subject to a minimum BHP constraint of 500 kPa. A total of 2664 m^3 of oil was produced during this stage, for an average oil production rate of 9.2 m^3/D.

The purpose of this second stage of the steam drive was to further heat the bottom oil sand layer. While the bottom, rich oil sand layer was heated to an average temperature of about 60°C during the electric pre-heat, the average bitumen viscosity in this layer is still several thousand centipoise, too high for a good communication path. The second stage of the steam drive was completed at a time of 744 days after the start of the electric pre-heat or 365 days after the start of the steam drive. The average bitumen viscosity in the heated zone at this time was only a few hundred centipoise, over an order of magnitude lower than at the end of the electric pre-heat.

The temperature profile, at the end of the second stage of the steam drive, of a vertical cross-section between the injection well and one of the production wells is shown on Figure 5.13. Note that the cross-hatched area indicates the steam zone.

The third stage of the steam drive consisted of 1947 days (5.3 years) of constant rate steam injection. Steam, with an enthalpy of 2.39×10^9 J/m^3 (corresponding to 240°C, 0.7 quality) was injected into the central injection well at a constant rate of 48 m^3/D. A total of 93 456 m^3 of steam was injected. Production during this stage of the steam drive amounted to 59 858 m^3 of oil, for an average oil production rate of 30.7 m^3/D. Temperature profiles between the injection and a production well, for two particular times during this stage, are shown in Figures 5.14 and 5.15.

During this third stage of the steam drive the injection rate is lowered and the injected steam quality is raised, when compared to the second stage of the steam drive. This was done to counterbalance two mechanisms controlling the flow of fluids in the reservoir. In the absence of gravity, the injected steam would simply travel through the heated channel in the bottom layer of the reservoir, directly to the production wells. Heating of the remainder of the reservoir would occur only by thermal conduction from the heated channel, and would occur very slowly. It would be difficult to recover the bitumen in most of the reservoir. However, with gravity present the bitumen

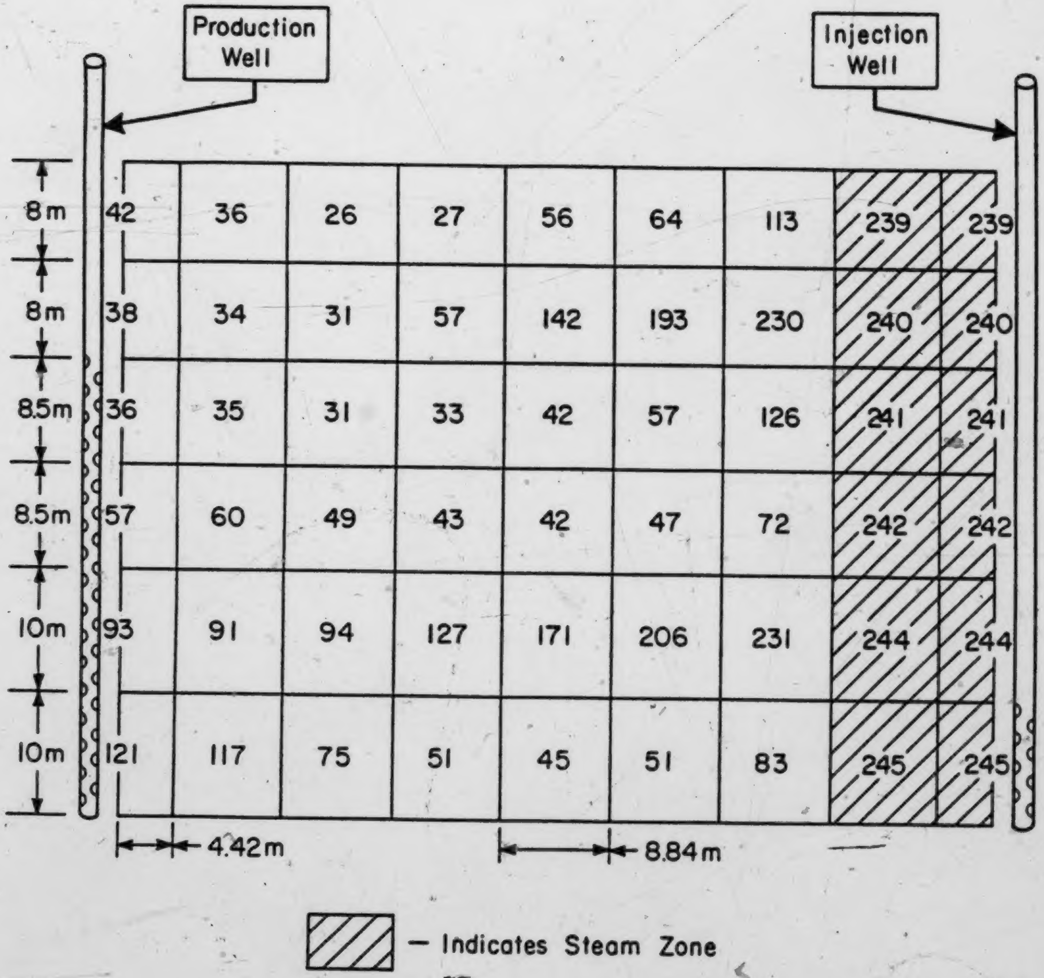
Production Well
Injection Well
4.42m
8.84m
▨ — Indicates Steam Zone

8m	42	36	26	27	56	64	113	239	239
8m	38	34	31	57	142	193	230	240	240
8.5m	36	35	31	33	42	57	126	241	241
8.5m	57	60	49	43	42	47	72	242	242
10m	93	91	94	127	171	206	231	244	244
10m	121	117	75	51	45	51	83	245	245

Figure 5.13 The temperature at the centers of the grid blocks on a vertical cross-section between the injection well and one of the production wells, at a time of 744 days after the start of the electric pre-heat.

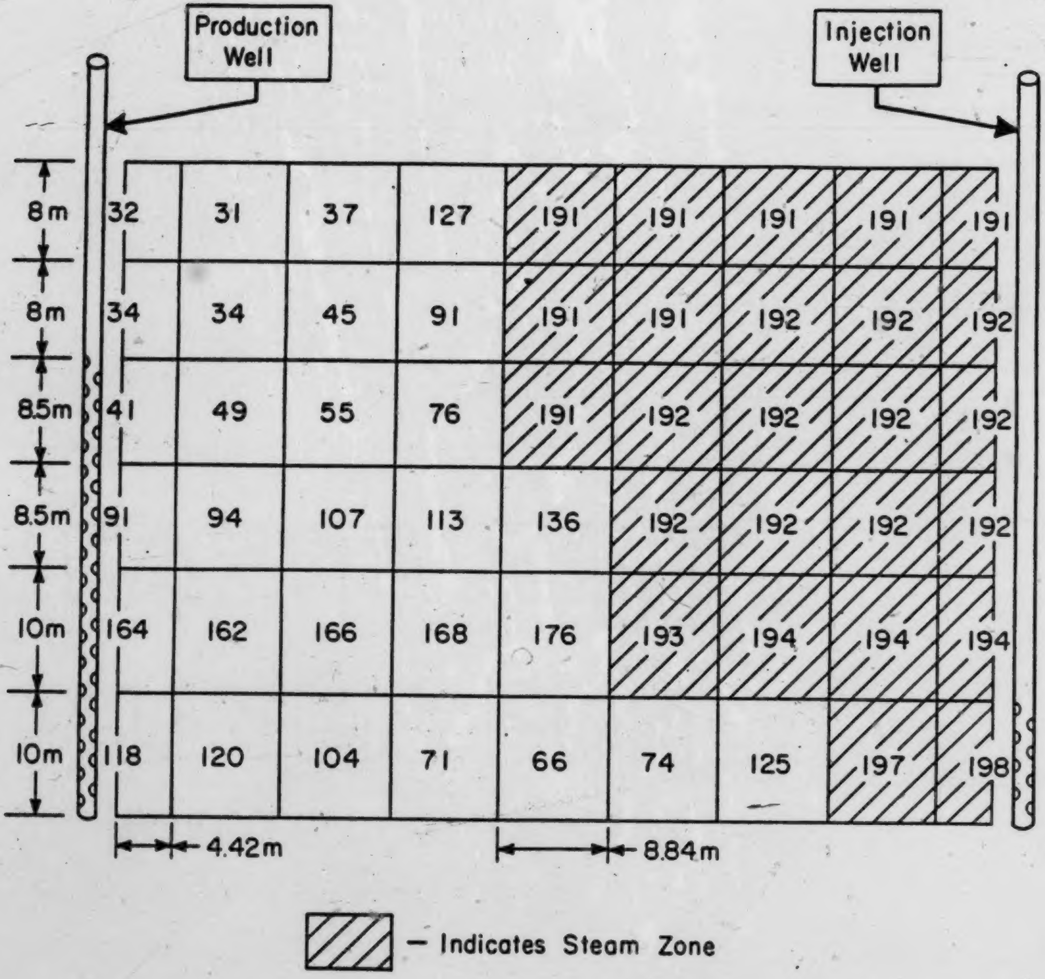
Production Well
Injection Well
8m
8m
8.5m
8.5m
10m
10m
32 31 37 127 191 191 191 191 191
34 34 45 91 191 191 192 192 192
41 49 55 76 191 192 192 192 192
91 94 107 113 136 192 192 192 192
164 162 166 168 176 193 194 194 194
118 120 104 71 66 74 125 197 198
4.42m
8.84m
▨ — Indicates Steam Zone

Figure 5.14 The temperature at the centers of the grid blocks on a vertical cross-section between the injection well and one of the production wells, at a time of 1479 days after the start of the electric pre-heat.

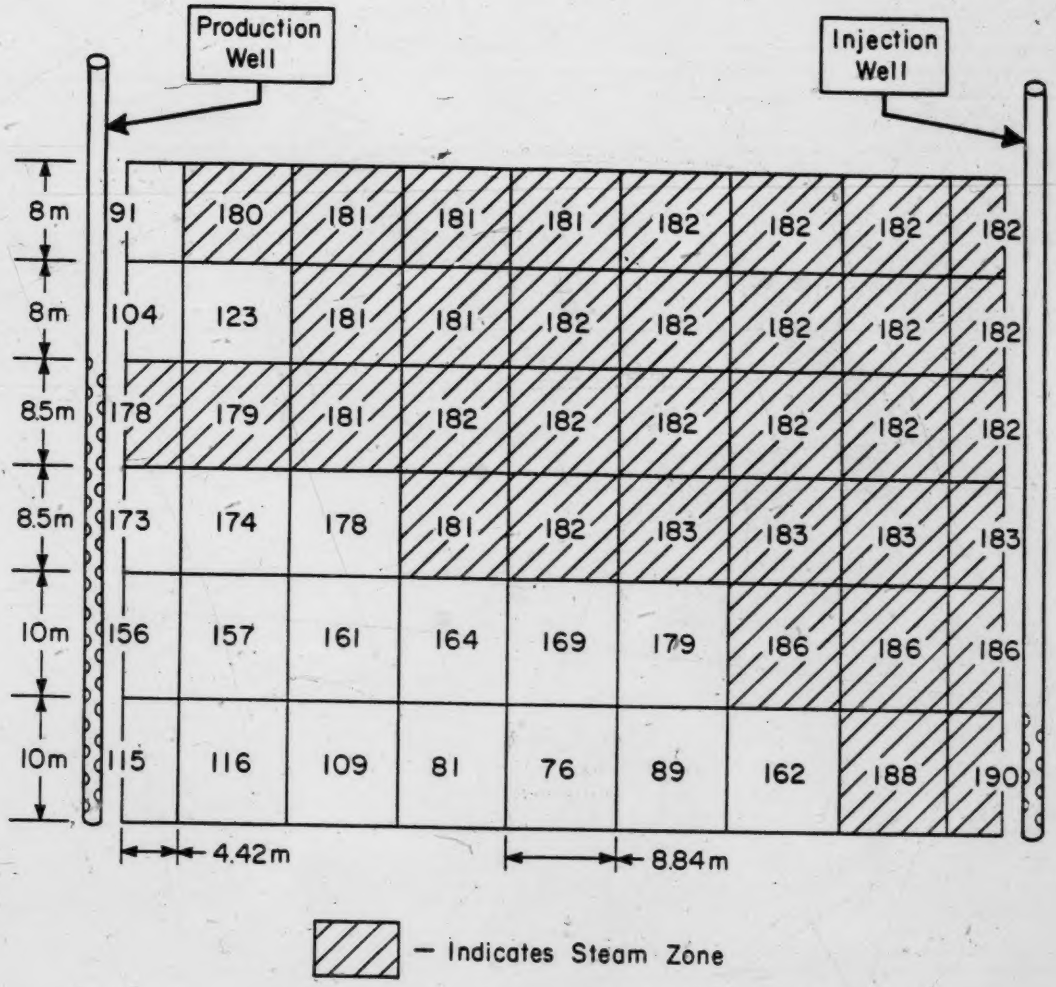
Production Well
Injection Well
8m
8m
8.5m
8.5m
10m
10m
91 180 181 181 181 182 182 182 182
104 123 181 181 182 182 182 182 182
178 179 181 182 182 182 182 182 182
173 174 178 181 182 183 183 183 183
156 157 161 164 169 179 186 186 186
115 116 109 81 76 89 162 188 190
4.42m
8.84m
— Indicates Steam Zone

Figure 5.15 The temperature at the centers of the grid blocks on a vertical cross-section between the injection well and one of the production wells, at a time of 2065 days after the start of the electric pre-heat.

at the top of the heated channel drops downward, displacing the less dense steam. Thus, the steam zone moves upward in the reservoir. Without the heated channel at the bottom of the reservoir most of the steam would rise to the top of the reservoir leading to the phenomina of steam override. Again, only a small fraction of the total bitumen in the reservoir would be produced.

As both a heated channel at the bottom of the reservoir and steam override due to density differences and gravity exist, these two mechanisms can be counterbalanced against each other. Steam is injected at a low rate, rises in the reservoir heating and displacing bitumen, which drops down to the heated channel and is swept to the producing wells. The result, as shown in Figure 5.14, is a near vertical boundary between the heated region (which contains mostly steam and has little bitumen) and the unheated region. If steam were injected at a higher rate, the steam would have less time to rise in the reservoir and would simply pass through the heated channel to the production wells. On the other hand, if the injection rate is too low, a large amount of steam override would occur, resulting in a lower overall bitumen recovery. Lower injection rates would also lead to lower production rates, which in general would result in less attractive project economics.

Steam breakthrough to the production wells occured at a time of 2065 days (see Figure 5.15). When this occured, the production wells were recompleted so that production occurred only in the bottom-most layer of grid blocks, rather than in the four bottom layers. Due to the low steam injection rate, the steam did not immediately channel down to the bottom layer after this recompletion. Another 247 days of steam injection passed before the steam again broke through to the producing well. At this point in time the final stage of the steam drive was started.

The final stage of the steam drive consisted of a hot water flood of the reservoir for a period of 689 days. Water, with a temperature of 240°C (enthalpy of 1.04×10^{9} J/m^3), was injected at a rate of 80 m^3/D. During this period a total of 12 080 m^3 of oil was produced, for an average rate of 17.5 m^3/D.

The simulation study was terminated at a simulation time of 3379 days after the start of the electric pre-heat. The total predicted oil production was 75 722 m^3 and the total predicted water production was 218 664 m^3. A plot of the cumulative oil production versus time is shown in Figure 5.16.

An equivalent Oil Steam Ratio (OSR) for the entire project may be calculated as follows. A total of 4.58×10^{13} J of electrical energy was input to the five spot pattern during the electric pre-heat. The total of 3.4×10^{14} J of energy would be required to change 13°C water to the steam input to the five spot during the steam drive. If it is assumed that electrical energy is produced at half of the efficiency of steam energy, the total equivalent steam

3

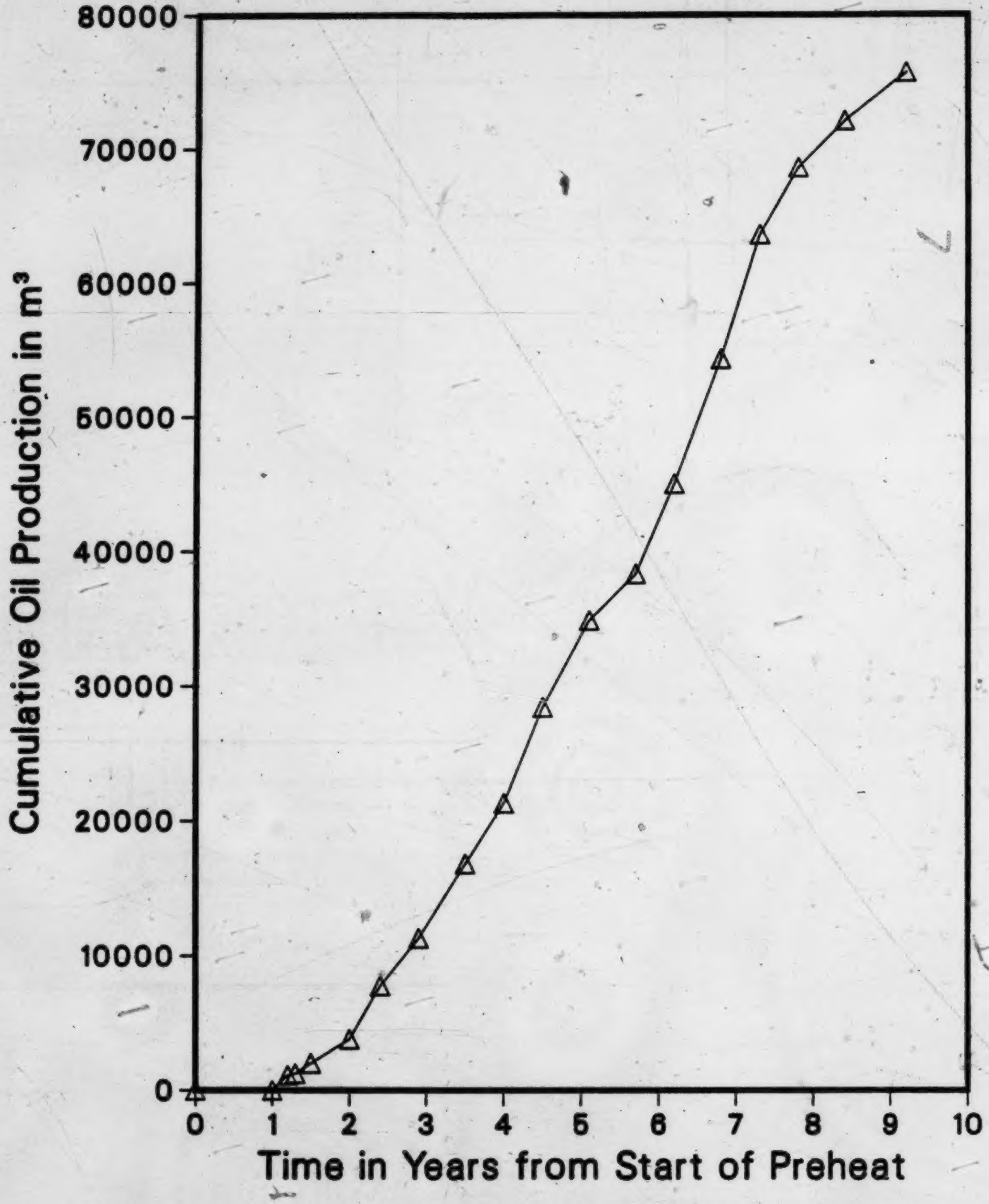

Figure 5.16 Cummulative oil production versus time for the five spot pattern simulated in Case 3.

energy used during the electric pre-heat and steam drive amounts to $4.32 x 10^{14}$ J. This is equivalent to the amount of energy necessary to produce 180 753 m^3 of 240°C, 0.8 quality steam from 13°C water. As the total production was 75 722 m^3, the equivalent OSR for the entire project was 0.42 (SOR=2.38).

At the end of the simulation run, a total of 59% of the original oil in place had been produced. With the relative permeability curves used as property data in the simulation, the residual oil saturation was 0.13. This amount of oil saturation will remain in the reservoir, unless a chemical flood of the reservoir is done. When this unrecoverable oil is considered, 72% of the recoverable oil in place was produced by the end of the simulation.

As previously mentioned, limitations on the amount of computer funds available prevented the development of a fully optimized steam drive strategy. Thus, it may be possible to improve the figures for cumulative oil production or oil steam ratio which have been given for Case 3. Different lengths and rates of electrical heating, different steam injection rates, and even different pattern types (such as seven spot or nine spot patterns) could be simulated. This work has been left to future studies.

5.5 Conclusions

In all three simulation studies presented, excellent agreement between the results predicted by Model 1, which neglects fluid expansion and flow during the electric pre-heat, and Model 2, which accounts for these two phenomena, was obtained. In particular, the variation of the inter-electrode resistances with time during the electric pre-heat, the temperatures at the end of the electric pre-heat, and the cumulative oil production during the steam drive, predicted by each of the two models, were compared for the three simulation studies. The good agreement between the two models for these important results indicates that the use of Model 1, which is less computationally expensive than Model 2, is justified in future studies. These results also add a measure of confidence to any previous studies which used a model for the electric pre-heat similar to the Model 1 presented in this work.

The simulation study Case 2 was run for two different amounts of electrical heating, but the same amount of steam injection. The cumulative oil production was nearly identical for both amounts of electrical heating, even though the temperatures at the end of the electric pre-heat for the two runs varied by 20 to 30 °C. This indicates, for at least this case, that the overall performance of the electric pre-heat and steam drive project does not continue to improve with increased amounts of electrical heating. A much larger study to determine the optimal amount of electrical heating is needed. While the optimal amount of electrical heating will likely depend on the particular reservoir geology and the pattern chosen for the steam drive, a general study of the problem may be able to provide a starting point from which to begin a simulation study on a particular project.

Some insight into the numerical approximations made by both of the models was provided by the comparison of the results of the two formulations of Model 2. In both of the mathematical models presented, the electrical potentials and heating rates were found by solving a static partial differential equation. This equation was resolved every timestep, with the updated electrical conductivities provided by the solutions of the other equations in the models. One of the formulations of Model 2 used the electrical heating rates calculated from the reservoir conditions at the beginning of the timestep, while the other formulation calculated the electrical heating rates from the conditions at the end of the timestep. When simulations were run using each of the formulations, and the maximum timestep size criteria developed in earlier work, the results of both formulations were in good agreement. This agreement between these two formulations indicates that the maximum timestep size criteria previously developed is conservative enough.

The three simulation studies themselves indicate that electrical heating can be used to establish a communication path in an Athabasca oil sand formation. None of these three studies should be regarded as establishing the ultimate or maximum cumulative oil production which could be obtained from their respective formations using the electric pre-heat and steam drive process. Only a limited amount of manpower and computer time was put into the studies. A much larger commitment would be necessary to establish the optimal amount of electrical heating, and the best steam injection strategy for any of the reservoir geologies and well configurations presented.

6. The Electrical Conductivity of Oil Sand at 60 Hz.

6.1 Introduction

This chapter reports on a set of experiments which constituted a preliminary study into the electrical conductivity of oil sand at the higher reservoir temperatures and pressures which would occur during the electric pre-heat process. In these experiments the electrical conductivity of oil sand samples was measured, with sample temperatures in the range of 24°C to 240°C. Measurements were taken at an excitation frequency of 60 Hz, with fluid pressures maintained above the saturated steam pressures. Four different grades of oil sand were used in the experiments. The variations of the electrical conductivity with weight percentage of water, current density and fluid pressure are also discussed. This study also identified some of the experimental difficulties which arise when trying to duplicate in the laboratory the in situ conditions of the oil sand during the electric pre-heat of an oil sand formation.

In low frequency, ohmic heating, of a material, the electrical conductivity is the sole property of the material which determines the heating rate in the material. The electrical conductivity appears both in the current continuity equation, used to calculate the electrical potentials, and in the equation used to find the heating rates once the potentials are known. Thus, for accurate simulation of any electric pre-heat it is necessary to understand and to be able to represent, at least empirically, the variation of the electrical conductivity with temperature (and other properties) for all formation materials.

An extensive study on the electrical properties of oil sand was carried out by Chute, Vermeulen, Cervenan, and McVea (1979,1978). This study was primarily concerned with establishing the behaviour of the electrical conductivity and dielectric constant as a function frequency at an ambient temperature of about 24°C. Some measurements of the variation of electrical conductivity with temperature were made. These measurements indicated that the electrical conductivity varies linearly in the temperature range from the initial formation temperature of 10°C-15°C to 100°C. The formula used to describe the temperature variation was

$$\sigma(T) = \sigma_{24}[1 + \alpha(T - 24)] \qquad T<100^\circ\mathrm{C} \qquad (6.1)$$

where T is the temperature, σ_{24} is the conductivity at 24 °C, and α is the temperature coefficient of conductivity. At 100 Hz, Chute et al. reported a value for α of $2.3 \times 10^{-2}\ ^\circ\mathrm{C}^{-1}$. As may be seen from Equation 6.1, the electrical conductivity of ~~oil~~ sand will increase by a factor of three as the temperature changes from the initial formation temperature to 100°C. At temperatures above 100°C the results indicated that the rate of increase of conductivity was significantly lower, but insufficient data was available to permit complete characterization of the conductivity at these elevated temperatures.

For a typical electrical heating process, most of the formation being electrically heated will not reach a temperature above 100°C. However, computer simulation studies have indicated that the oil sand, in the near electrode regions, may reach over 200°C. While the near electrode regions are only a small fraction of the total formation volume, the conductivity in this region can have a large effect on the total inter-electrode resistances and potential differences of the electrical heating system. As little published data is available on the electrical conductivity of oil sand for the temperature range above 100°C, a need existed to obtain such data so that accurate computer simulation studies could be performed.

The objective of the study described in this chapter was to characterize the variation of the electrical conductivity with temperature in the range of 24°C to 240°C. However, the variation of conductivity above 100°C proved to be more complex than at first anticipated. The conductivity of the oil sand samples exhibited dependence on not only temperature but also on the time each sample was held at temperatures above 100°C. Investigation of this time dependence required individual sample runs extending over periods of several hundred hours. The series of experiments described should be viewed as preliminary, with more data needed to fully characterize the variation of conductivity with temperature at elevated temperatures.

6.2 Experimental Apparatus and Sample Preparation

The experimental apparatus consisted of several parts. At the core was a sample holder, which held a sample of oil sand or other material, and two electrodes. The sample holder and sample were placed in a pressure vessel. The pressure vessel was placed in an oven with accurate temperature control, which was used to heat the pressure vessel, sample holder, and sample, and to maintain them all at a constant temperature for days or weeks if necessary. A computer, with an attached data aquisition system, was used to moniter the experiment, and measure and calculate experimental results.

6.2.1 Sample Holder

As shown in Figure 6.1, the sample holder consisted of a hollow, cylindrical, electrically insulating tube, and two metal electrodes. The sample holder tube was 15.2 cm (6 in.) long and had an inside diameter of 8.9 cm (3.5 in.). Initially, the insulating tube was made of thick glass. This, however, proved to be too fragile, and later a machined teflon tube, within an outer steel jacket, was used. Three small holes were spaced along the tube so that thermocouple temperature probes could be placed inside the sample. A clamp, which is not shown in Figure 6.1, was attached to the pressure vessel on one side and used to

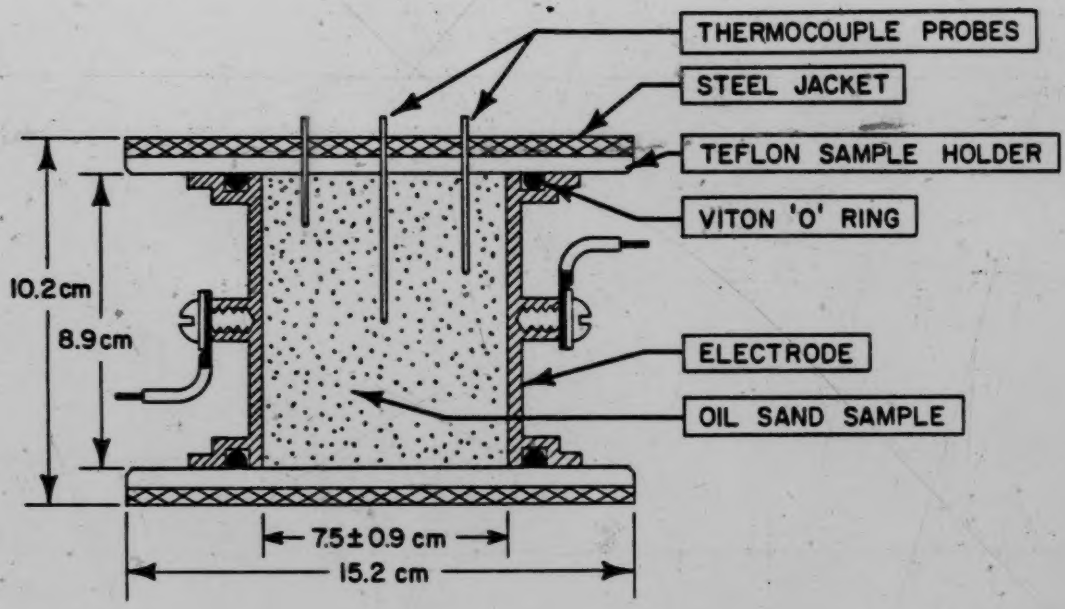
THERMOCOUPLE PROBES
STEEL JACKET
TEFLON SAMPLE HOLDER
VITON 'O' RING
ELECTRODE
OIL SAND SAMPLE
10.2 cm
8.9 cm
7.5 ± 0.9 cm
15.2 cm

Figure 6.1 Cross section of the sample holder tube with the oil sand sample and electrodes in place. This sample holder is placed inside the pressure vessel shown in Figure 6.2.

position and hold the sample holder tube, as well as to push the electrodes against the sample being studied. One of the electrodes was electrically grounded to the vessel, while the other was insulated from the clamp and the pressure vessel by machined ceramic rings.

6.2.2 Electrodes

The electrodes were cylindrical in shape, having a diameter slightly less than the inside diameter of the sample holder tube and a maximum thickness of 2.5 cm (1 in.). A Viton 'O' ring was used to maintain a seal between the sample holder tube and the electrode, preventing fluid loss from the sample. One face of each of the cylindrical electrodes was machined flat. These faces were pressed against the sample being studied. The other faces contained the screws for attaching the electrical conductor leads to the electrodes. The electrodes were recessed on this face to lower their thermal mass. The bodies of the electrodes were machined from stainless steel.

To study possible corrosion and electrode - oil sand contact problems, three different metal surfaces were used, in turn, on the electrode faces which contacted the sample. The first pair of electrodes, hereafter referred to as the copper electrodes, had a 2 mm thick copper sheet soldered onto the stainless steel body. These electrodes were found to react with the oil sand at the high temperatures and pressures used in the experiment. A dark layer formed on the surface of the electrodes during the experiment. This layer was removed before each experiment by cleaning the copper surface using nitric acid and steel wool.

A second pair of electrodes was made entirely of stainless steel, but with a nickel alloy surface applied by the 'Electroless Nickel' process. This nickel alloy surface is used in the oil industry as it is resistant to sulfur corrosion. The surface of these electrodes discolored somewhat during their first use, but did not appear to change after that.

The last pair of electrodes, hereafter refered to as the gold electrodes, were the same as the copper electrodes, except that a layer of gold was electroplated onto the copper face. The approximate thickness of the gold layer was 2 μm (.0001 in.). This gold surface also suffered from corrosion if the sample was held in the higher temperature range (200°C to 240°C) for extended periods of time. The surface had to be replated after every five experimental runs, due to abrasion during the packing of the sample.

It was noted that for comparable experiments, the measured electrical conductivity was always as high or higher when using the gold electrodes than when using the nickel electrodes or the copper electrodes. Towards the end of the current study, the gold electrodes were used exclusively, and it is recommended, in future high temperature studies, that gold electrodes be used. These electrodes must be cleaned after each run, and replated when the underlying copper begins to show through the gold layer.

6.2.3 Sample Preparation

Different grades of oil sand, obtained from the Alberta Research Council's sample bank, were used in the study. This oil sand was originally obtained from the Suncor open pit oil sand mine, in the winters of 1982 to 1984. After the samples were obtained from the Alberta Research Council, they were stored in air tight five gallon containers at room temperature. The drums were labelled as to bitumen content (5 wt.%, 7 wt.%, 8 wt.%, 11 wt.%, and 14 wt.%) and the year mined. Hereafter, the 5 wt.% bitumen oil sand is referred to as low grade oil sand, the 7, 8, and 11 wt.% bitumen oil sand is referred to as medium grade oil sand and the 14 wt.% bitumen oil sand is referred to as high grade oil sand.

The sample holder tube was prepared as follows. One electrode, with it's "O" ring in place, was positioned in the sample holder tube. The sample holder tube was then placed vertically on the floor. About two hundred grams of loose oil sand was removed from the airtight container and placed in the sample holder tube. Rocks larger than about 1 cm in diameter were removed from the oil sand. The oil sand in the sample holder tube was packed, by physical pounding with a metal packing tool, to approximately the in situ density of oil sand formations. Additional oil sand was then placed in the tube and the entire sample was again pounded. While packing the sample, some of the same oil sand would be removed from the container and a Toluene extraction would later be performed to determine the weight percentages of bitumen, water and sand in the sample. This procedure of adding some oil sand, then pounding the sample, was repeated until the sample had the desired thickness. All the samples used in the study were cylindrical in shape with a diameter of 8.9 cm (3.5 in.) and had thicknesses varying from 6.6 to 8.4 cm (2.6 to 3.3 in.). For most experiments a sample density of 2.0 to 2.1 g/cm³ was achieved. The in situ density of oil sand formations is about 2.1 g/cm³.

After the sample was packed, the second electrode was pressed against the remaining face of the cylindrically shaped sample. The sample holder was mounted in the pressure vessel, and three thermocouple probes were placed radially into the sample through holes in the sample holder tube. One of the electrodes was grounded to the pressure vessel, while the other electrode was connected to the 'hot' wire feedthrough in the pressure vessel.

6.2.4 Pressure Vessel

The author designed a pressure vessel which was used to maintain the fluid pressure of the sample at a pressure greater than the saturated steam pressure at the temperature of the sample. Maintaining this high fluid pressure prevented the water in the sample from flashing to steam, which would have severely altered the electrical, and other, properties of the sample. The pressure was maintained in the pressure vessel by a system of valves and a regulated Nitrogen gas supply. The pressure could be varied from atmospheric pressure to 4.8 MPa. An accurate gauge displayed the vessel pressure at all times during the experiment. The pressure system, and other connections to the pressure vessel, are shown in Figure 6.2.

The gas pressure in the pressure vessel was communicated to the fluid in the sample via the three holes in the sample holder tube. These holes were used to admit the thermocouple temperature probes to the sample, but there was sufficent space around the probes to permit gas to enter the sample or fluid to escape from the sample. Thus, the fluid in the sample was assumed to be at the same pressure as the gas in the pressure vessel.

In order to maintain a high partial pressure of water inside the pressure vessel, and thus retard evaporation from the sample, approximately 30 g of water was placed in the bottom of the pressure vessel, outside the sample holder, before each experiment. This water would evaporate during the heating of the vessel, maintaining the partial pressure of H_2O inside the vessel near the saturated steam pressure.

Three feed-throughs existed in the pressure vessel. One was for the Nitrogen gas pressure system. A second sealed feed-through in the pressure vessel permitted the passage of the wires for the six thermocouple temperature probes which were inside the pressure vessel. These thermocouple probes were used to measure the temperature within the sample, and

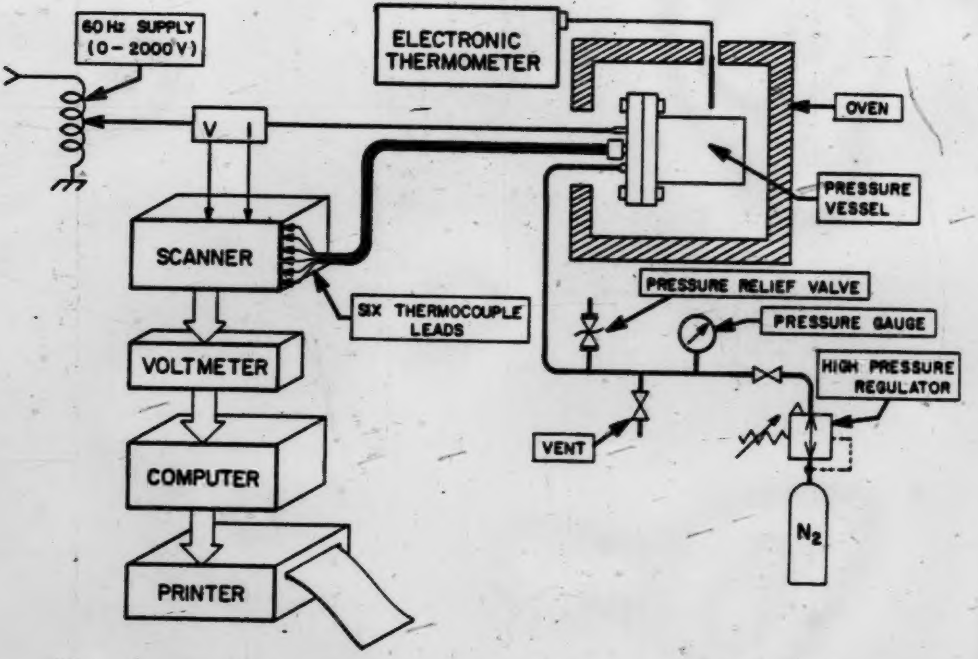
60 Hz SUPPLY (0-2000 V)
ELECTRONIC THERMOMETER
OVEN
V
I
PRESSURE VESSEL
SCANNER
SIX THERMOCOUPLE LEADS
PRESSURE RELIEF VALVE
PRESSURE GAUGE
VOLTMETER
HIGH PRESSURE REGULATOR
VENT
COMPUTER
N_2
PRINTER

Figure 6.2 Diagram of the pressure vessel, oven, pressure system, electrical system and data logging system for the experiment.

outside the sample but within the pressure vessel. The third feed-through allowed the passage of the 'hot' electrical lead into the pressure vessel.

6.2.5 Data Logging System

A Hewlett-Packard data logging system was used to calculate and record the experimental variables. This system consisted of a computer which controlled a scanner, a voltmeter and a printer. A program was written which requested that the sample thickness be input. On command it would then read the thermocouple voltages and calculate their temperatures, and read both the voltage applied across the electrodes and the current passing between them. Then, using the sample thickness, the known sample holder tube diameter, and the measured voltage and current, it would calculate the electrical conductivity. The date, time, temperatures, voltage, current, and electrical conductivity would then be printed. The pressure in the pressure vessel was manually entered into the computer and printed with the other results.

6.3 Experimental Procedure

During the current set of experiments, forty five oil sand samples were packed and placed in the measurement cell. The initial experimental procedure, hereafter refered to as the rapid measurement procedure, was as follows:

1. The loose oil sand was taken out of the storage drums

and packed into the sample holder, using the procedure outlined in the section on sample preparation (6.2.3). The results of the weight analysis (giving the weight percentages of sand, bitumen and water for the sample) and the density of the sample were recorded.

2. The sample holder was placed in the pressure vessel, with three of the thermocouples positioned in the sample and the other three placed around the sample holder. Approximately 30 g of water was placed in the bottom of the vessel. The electrical connections were made to the electrodes and the pressure vessel was bolted shut. The pressure vessel was placed in the convection oven and the thermocouple leads, electrical leads and Nitrogen gas tubing were attached.
3. The electrical conductivities of the sample at room temperature and both at atmospheric pressure and at an initial pressure of between 1.0 MPa and 1.3 MPa were measured.
4. The temperature of the sample and measurement cell was raised to approximately 50°C and allowed to stabilize so that all thermocouples were at the same temperature (to within 3 Celsius degrees). The heating of the sample, sample holder, and pressure vessel, was accomplished, as previously mentioned, by supplying heat from the oven. As well, an electrical current was passed through the sample producing additional heat. The heating and stabilization took about one half hour. Once the

temperatures were all about equal the electrical conductivity was measured for three different voltages between the electrodes. The voltages usually used were 50, 100 and 150 volts.

5. After the measurement had been taken, the temperature was raised to the next value. Measurements were taken at 25 degree intervals up to 240°C. This procedure usually took about five hours. During the heating period, care was taken to ensure that the pressure in the pressure vessel remained at least 1 MPa above the saturated steam pressure for the current temperature.
6. After the measurement at 240°C was taken, the sample was allowed to cool. From time to time during the cooling the oven was switched back on and the temperature throughout the sample was equalized. The conductivity of the sample was measured, then the cooling was continued. The cooling process was slower than the heating, and there was a greater temperature interval between measurments. The cooling procedure usually required nineteen hours to complete.
7. Normally a similar second set of measurements was carried out on the same sample within a day or two.
8. When the experiment was completed, a final measurement was taken at room temperature, and the pressure vessel was unpacked. A part of the oil sand sample was removed and a final weight analysis was done.

After several experiments were performed using the above procedure, it was noted that the electrical conductivity of the oil sand sample would decline with time when the temperature was held constant at some elevated value. This decline appeared to follow an exponential decline curve until some steady state value was obtained. Accordingly, a second experimental procedure, of significantly longer duration than the previous, rapid measurement procedure, was developed. This new procedure, known as the constant temperature measurement procedure, was as follows:

1. The sample holder tube was packed and the density and weight analysis were recorded as before. The pressure vessel was prepared and measurements of the electrical conductivity were taken at room temperature.
2. The cell was heated to a particular temperature and held at that temperature. (The temperatures used were 100°C, 150°C, 200°C, and 240°C). Measurements of the electrical conductivity were taken from time to time, with the length of time between measurements determined by how fast the conductivity was changing. The interval between readings varied in length from thirty minutes to one day.
3. When the electrical conductivity appeared to have stopped declining and have reached some steady state value, the measurements were stopped and the cell cooled. A final conductivity measurement was taken at

room temperature and a weight analysis was done on part of the sample as before.

6.4 Problems Encountered with the Experimental Apparatus and Method

6.4.1 Fluid Expansion

One of the major problems encountered in designing the experiments was caused by the expansion of the fluids in the sample holder. The fluids in the oil sand (bitumen and water) expand when heated, and further, they expand at a significantly greater rate than the sand grains.

A sample holder tube was constructed which completely sealed in the sample, allowing no fluid loss. It was found that as the sample was heated, the bitumen in the sample expanded and was forced out of the sample towards the electrodes. There it coated the surface of the electrodes, stopping or greatly reducing the current flow through the sample. The measured electrical conductivity no longer represented the true electrical conductivity of the sample.

If, however, the sample holder tube had three small holes in one side, used to admit the thermocouple probes into the sample, the expanding bitumen escaped from the sample holder tube by flowing past the thermocouple probes. This bitumen was now lost from the sample, but no electrode coating was observed. The amount of fluid loss increased with the temperature at which the sample was held, and also with the weight percentage of bitumen in the sample. The worst losses were about one eighth of the fluids in a 200°C experiment and one third of the fluids in a 240°C experiment. The losses appeared to be mainly bitumen.

Expansion of the formation fluids, due to an increase in temperature, will also occur in an actual field electric pre-heat. The pressures created by expanding fluids can be very high, and in a field operation a significant amount of bitumen may move into the wellbore as electrical heating occurs. Steps will have to be taken to ensure that the electrodes used in the well do not become coated with bitumen.

6.4.2 Sample Preparation

An additional problem with the experimental procedure involves the sample preparation and the use of loose mined oil sand in the samples. When using oil sand which has been broken up, mixed, and then repacked, the original grain to grain contact of the oil sand has been disturbed, and some of the lighter gaseous components of the bitumen are lost. The density of the repacked samples may not be as high as that of the original oil sand, and some of the sand grains may be broken or crushed during the packing of the sample holder tube. Any anisotropy of the in situ oil sand is lost in breaking up, mixing, and repacking the oil sand. However, the values of electrical conductivity of the oil sand which are measured for the repacked samples appear to agree with the values of electrical conductivity for the in situ formations which are measured by electric logging (when differences in density and temperature are taken into account).

Core samples of oil sand formations may be obtained where the original sand grain to sand grain contact is largely preserved. There are, however, difficulties in handling these cores and preparing them for use in the electrical conductivity experiments. A single core sample was obtained by the author from the Oil Sands Geotechnical Group of the Department of Civil Engineering at the University of Alberta. This core had been obtained by coring a surface outcrop near Fort McMurray. The sample was stored at about -40°C, and was machined, while frozen, to fit into the sample holder tube used in the electrical conductivity experiments. The core was placed in the sample holder tube, thawed, and electrical conductivity measurements were performed. It was found that something had disturbed the water in the sample so that the sample had an extremely low electrical conductivity (less than 10^{-8} S/m). This low conductivity occurred throughout the length of the core, and for frequencies up to at least 1 MHz. When a weight analysis was performed on the sample it was found that it contained the expected amount of water (2.6 wt.%). An oil sand sample with this amount of water should have a conductivity of about 6×10^{-3} S/m.

It is possible that, as the core was obtained from near the surface, the sample had undergone several freeze-thaw cycles. The freezing and thawing of the sample may affect the thin layer of water which covers the sand grains in the oil sand. If the water layer on the sand grains was no longer continuous, this would reduce the electrical conductivity of the sample. If, in the future, core samples are to be used in electrical conductivity measurements, a record of any freezing and thawing that the core undergoes should be kept. In particular, a comparison between the conductivities of cores which have been frozen and those cores which have not been frozen should be done to determine if freezing the cores substantially alters their conductivities.

6.5 Experimental Results

The results of the experiments are given in Tables A.1 to A.32 in Appendix I. The runs were numbered consecutively. The results of those runs where there was equipment failure, or where the experimental method was being developed, are not included. The date of sample packing, analysis of the sample material taken during sample packing, analysis of the sample material after the run was completed, packed sample density, sample thickness, initial conductivity at 24°C, electrode surface material, and whether the glass, or the teflon, sample holder tube was used, are all given with the tables.

6.5.1 Results from the Rapid Measurement Procedure on Low and Medium Grade Oil Sand Samples

Initially, experiments were performed using the Rapid Measurement Procedure, as outlined in section 6.3. Typical results from an experiment performed using this procedure are given in Figure 6.3. The measured electrical conductivities of medium grade oil sands versus temperature, for the heating phase of several experiments, are shown on Figure 6.4.

Several features, common to all the experiments using the Rapid Measurement Procedure, may be noted on Figure 6.3. The conductivity increased nearly linearly with temperature as the sample was heated to about 100°C, with all samples increasing at about the same rate. Above 100°C, the rate of conductivity increase decreases, with some variation in rate between samples. The peak of the electrical conductivity versus temperature curve usually occured between 200°C and 225°C. For most samples, a marked hysteresis occurs between the heating and cooling portions of the conductivity versus temperature curves, but the electrical conductivity returns to it's initial value at 24°C.

In order to further understand the "hysteresis" phenomenon observed in experiments using the Rapid Measurement Procedure, a series of experiments was conducted where an oil sand sample was heated to a particular temperature, then the sample was held at that temperature for an extended period of time. These experiments are

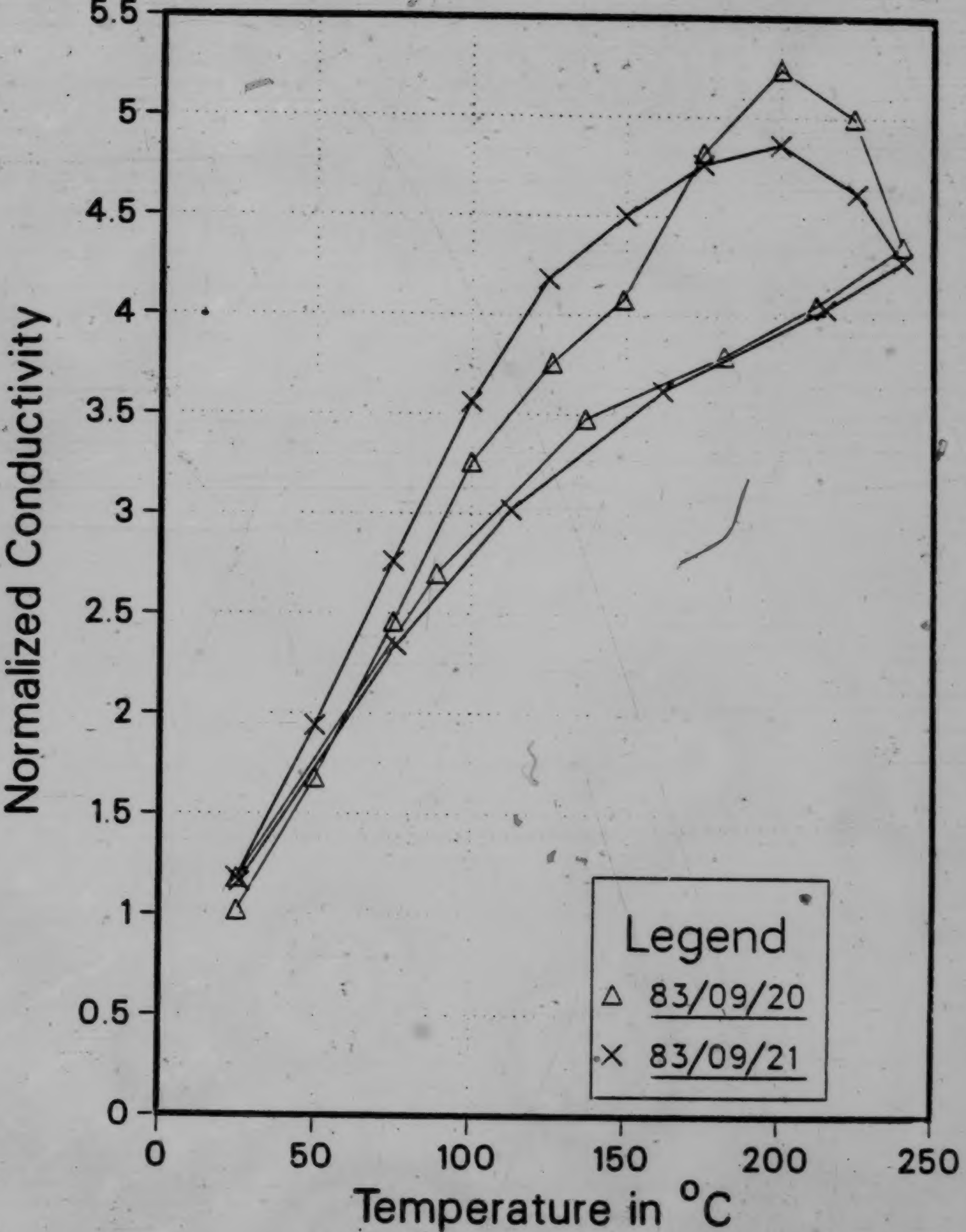

Figure 6.3 The electrical conductivity of oil sand versus temperature for Experiment No. 7. Two successive heating and cooling cycles were performed over two days.

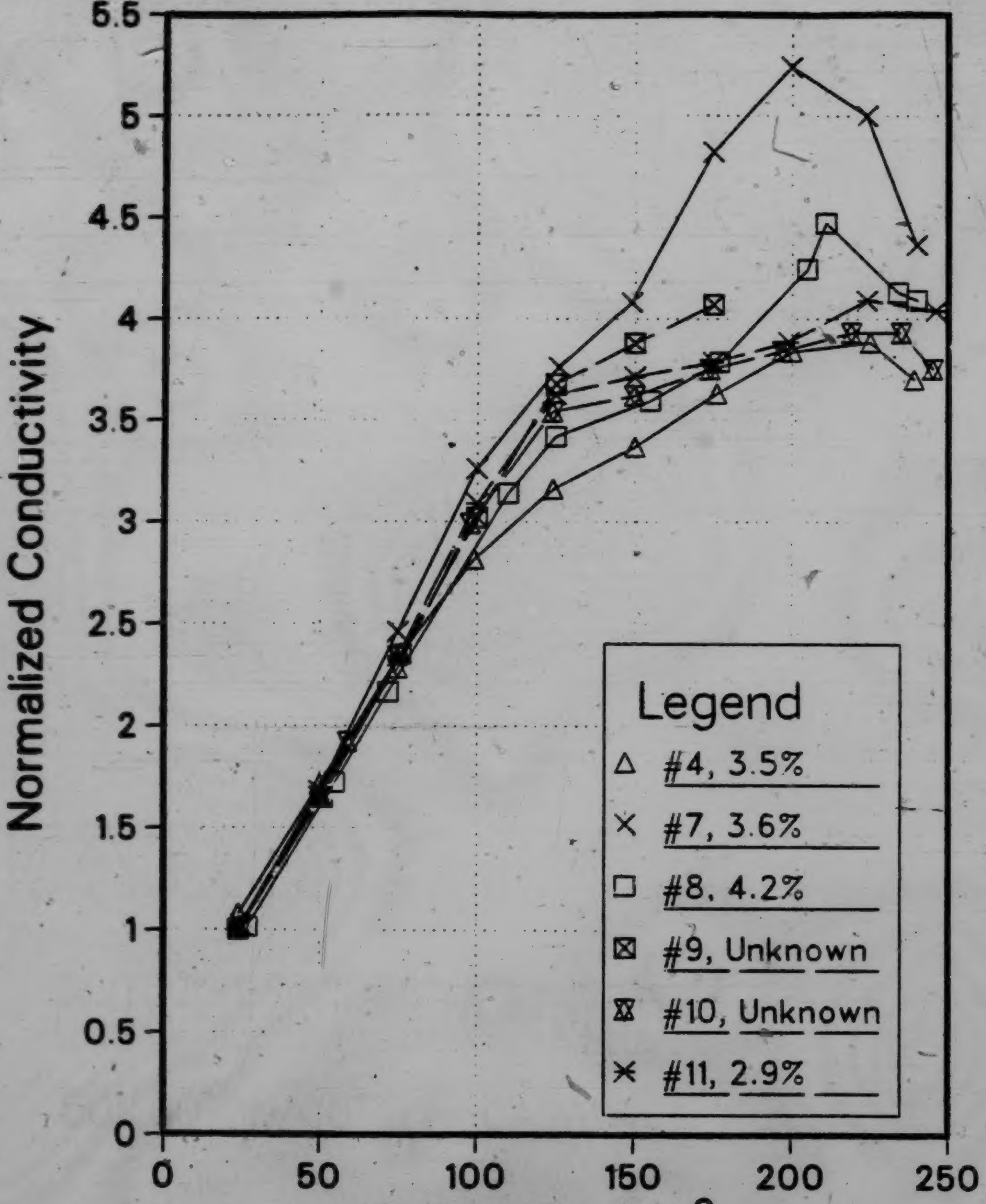

Figure 6.4 The electrical conductivity of oil sand samples, and one water sand sample (#4), versus temperature for experiments where the samples were rapidly heated. The usual heating time for the samples was five hours.

reported in the next section.

6.5.2 Results from the Constant Temperature Measurement Procedure on Low and Medium Grade Oil Sand

After several experiments had been performed using the Rapid Measurement Procedure, a second experimental procedure was developed where the sample was raised to, then held at, a certain temperature. This second procedure is outlined in the second part of section 6.3. The temperatures at which samples were held for extended periods of time were 100°C, 150°C, 200°C, and 240°C.

As shown in Figure 6.5, the electrical conductivity of an oil sand sample held at a constant temperature of 100°C does not change significantly with time. For the sample measured, the electrical conductivity remains constant for 140 hours (6 days), then slowly declines by 4% over the next 380 hours (15 days). When the sample was cooled back to room temperature, the conductivity returned to its initial value.

The results of the experiments where the oil sand sample was held at a constant temperature of 150°C are shown on Figure 6.6. When low and medium grade oil sand samples were heated to 150°C and held at that temperature, their electrical conductivities declined, over a period of time, by between 13% and 26% of the sample's initial value at 150°C. The usual decline was between 16% and 19% of the initial value. Most of the change in electrical conductivity occurred during the period from 24 hours (1 day) to 96 hours

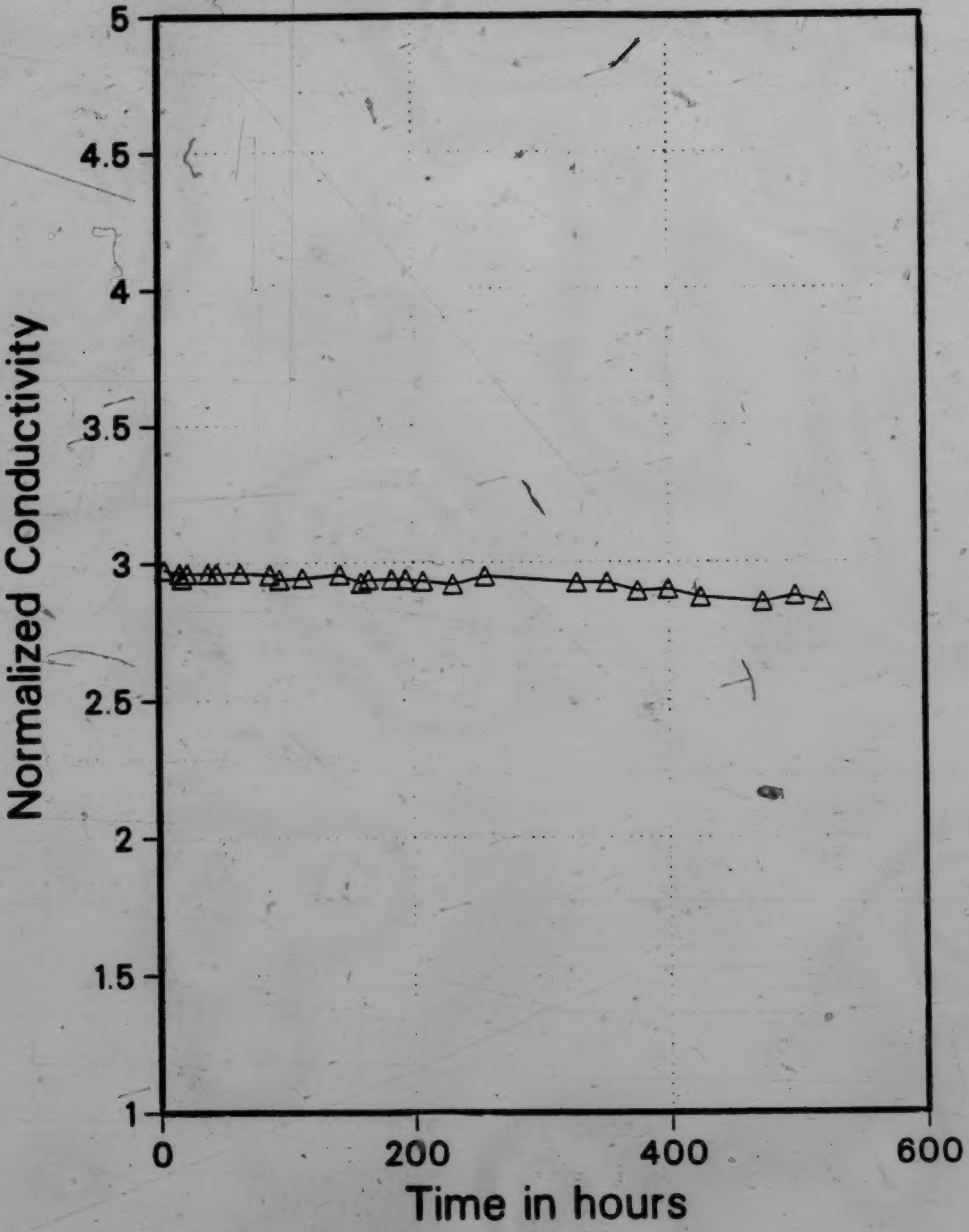

Figure 6.5 The normalized electrical conductivity versus time for an oil sand sample held at 100°C.

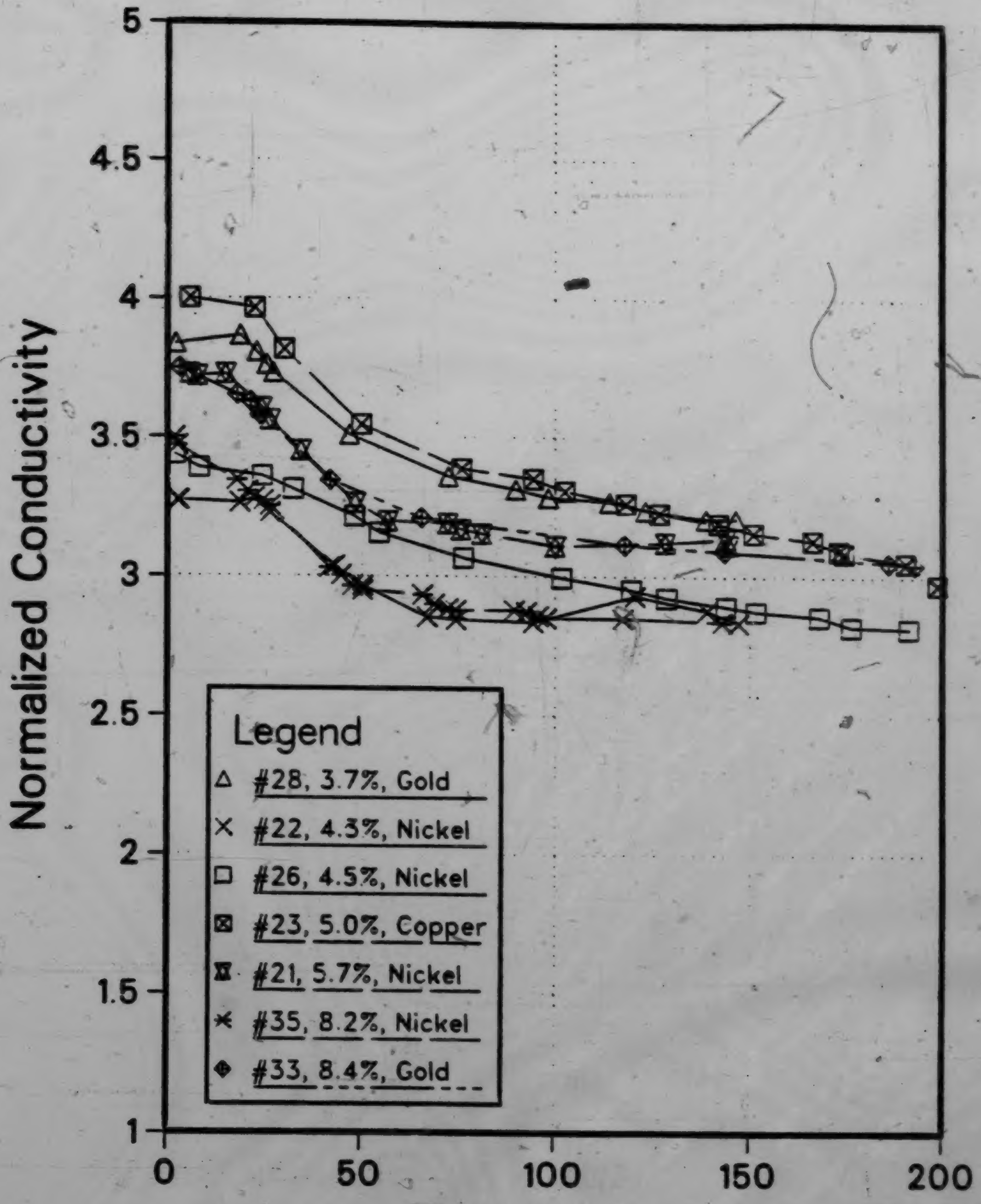

Figure 6.6 The normalized electrical conductivity versus time for oil sand samples held at 150°C. The experiment number, weight percent of water, and electrode type are given for each set of results.

(4 days) after the constant temperature of 150°C had been reached. When the samples were cooled back to room temperature, the measured electrical conductivities were all from 0% to 10% less than the original values at room temperature, with one exception which was 19% less than its original value.

The results of experiments where the oil sand samples were held at 200°C are given on Figure 6.7. Here the decline in conductivity occured more rapidly, with most of the change in conductivity occuring in the first 24 hour period. A correlation between the weight percentage of water in the sample and the amount of decrease in electrical conductivity with time was noted. The high water content samples (low grade oil sands) had a final average normalized electrical conductivity of 2.7, which is substantially lower than the average of 3.2 for the medium grade oil sand samples.

Results of the experiments where the samples were maintained at a constant temperature of 240°C are given in Figure 6.8. Here the results are somewhat erratic and it is difficult to draw any conclusions from them. Two of the experiments follow a behavior which would be expected from the results of the 150°C and 200°C experiments. In these two experiments, numbers 30 and 43, the conductivity initially declines rapidly from it's peak value and reaches a steady state value sooner than in the 200°C experiments. As in the 200°C experiments the final value of the normalized conductivity of the low grade oil sand (high water content)

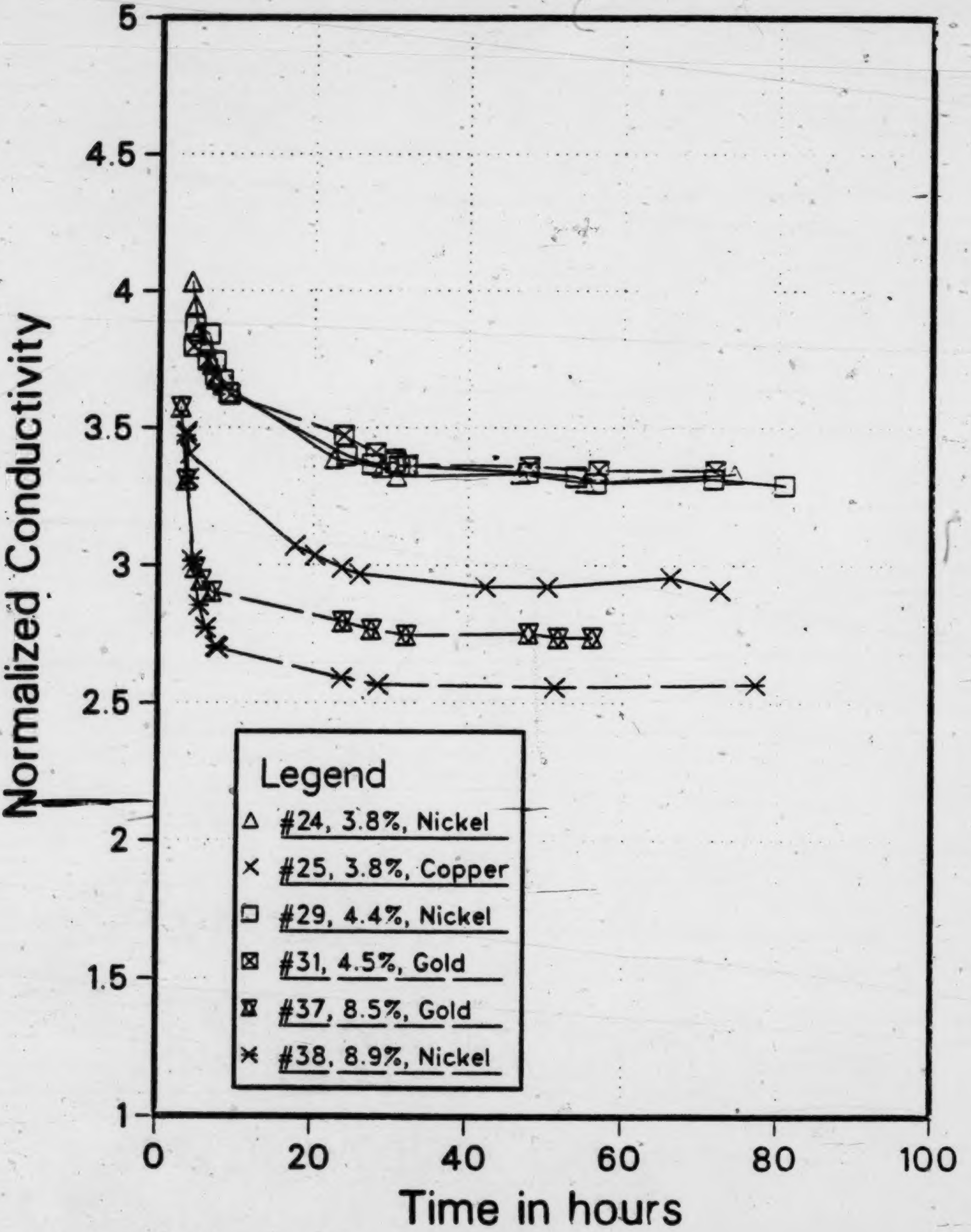

Figure 6.7 The normalized electrical conductivity versus time for oil sand samples held at 200°C. The experiment number, weight percent of water, and electrode type are given for each set of results.

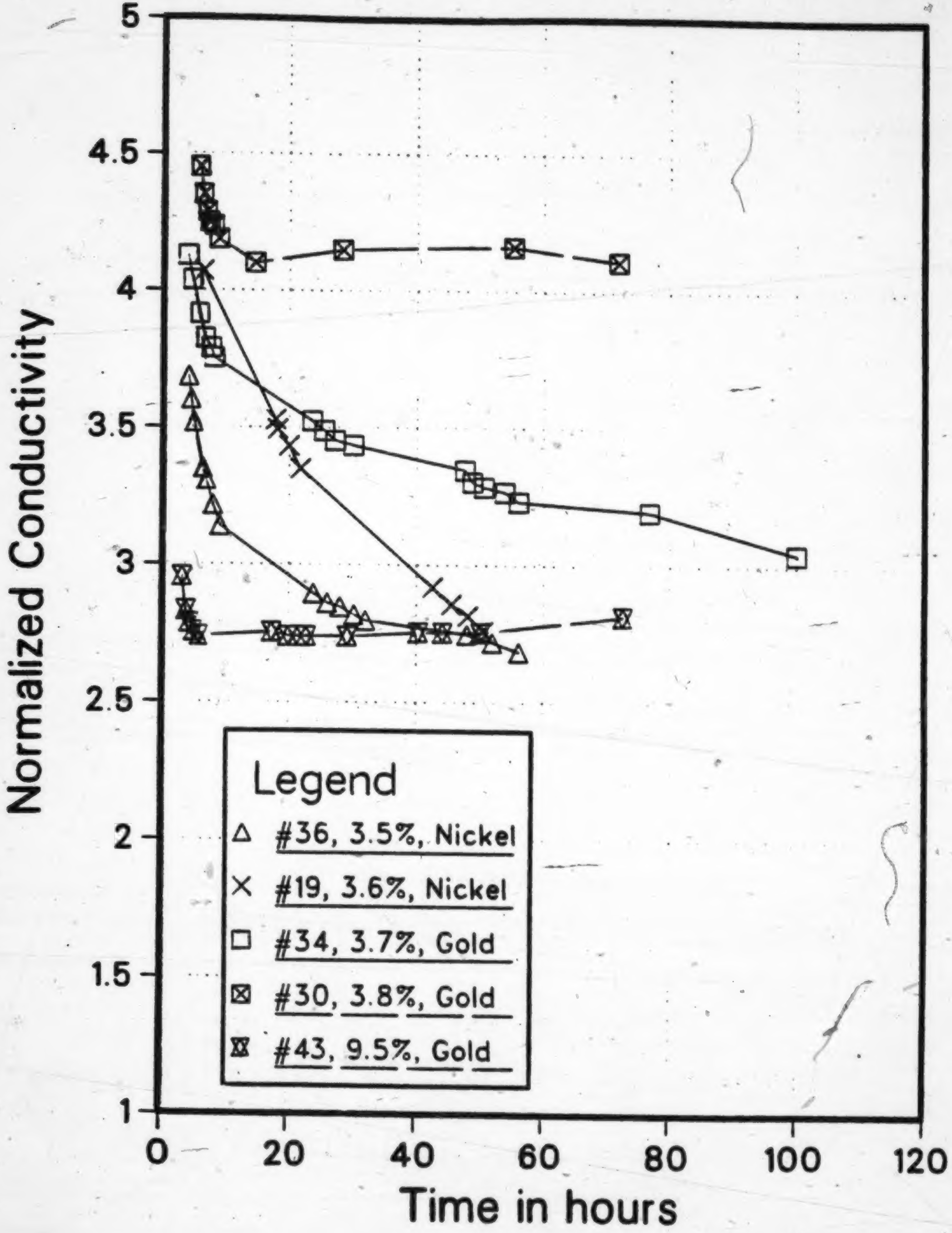

Figure 6.8 The normalized electrical conductivity versus time for oil sand samples held at 240°C. The experiment number, weight percent of water and electrode type are given for each set of results.

was lower than that of the oil sand with lower weight percentage of water.

Some of the experiments at 240°C did not reach any steady state value, but continued to decline, even after 60 or 100 hours at the higher temperature. The cause of this behavior has not been determined.

6.5.3 Results of Experiments using High Grade Oil Sands

High grade oil sand is characterized by having a high weight percentage of bitumen and a low weight percentage of water. The high grade oil sand used in the present experiments was obtained from the Alberta Research Council Oil Sand Sample Bank in a barrel labeled '14% Bitumen Athabasca Oil Sand - 1982'. Actual weight analysis (by the toluene extraction method) done on samples from the barrel yielded weight percentages of bitumen in the range 13.7% to 15.4%, and weight percentages of water in the range 0.9% to 2.4%. Experiments number 42, 44, and 45 were performed using the high grade oil sand. The results of these three experiments are shown on Figure 6.9.

Several major differences should be noted between the results of these experiments and those involving medium and low grade oil sand. The sample density obtained in packing the high grade oil sand was, on the average, lower than that obtained with the other grades of oil sand. The high grade samples all had a very low initial electrical conductivity, approximately 2.5×10^{-4} S/m. As the samples were heated, the

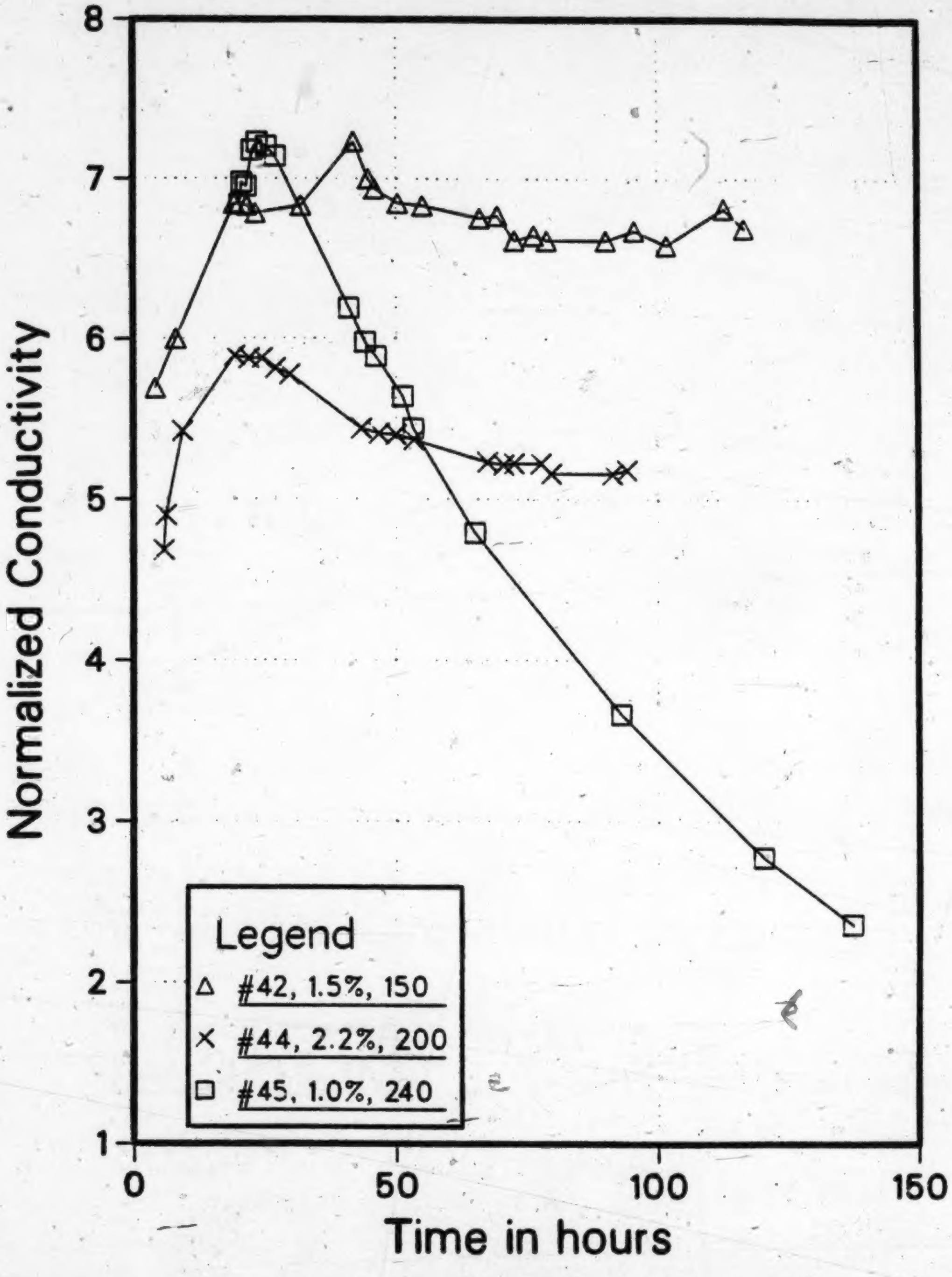

Figure 6.9 The normalized electrical conductivity versus time for oil sand samples with very low water contents. Three experiments, one each at 150°C, 200°C, and 240°C are shown.

conductivity increased much more rapidly than in the other grades of oil sand. Finally, the electrical conductivities of the samples when they were returned to room temperature were three to five times higher than their initial values. These final higher conductivity values were used to normalize the results on Figure 6.9, and in Tables A.29, A.31, and A.32.

The mechanism involved in the very large increase in electrical conductivity, and it's subsequently having a higher than initial value at room temperature, is not clear. The high grade samples have a very low water content. It may be that in mining, breaking up, and repacking the oil sand, the contact between the water layers around the sand grains is largely lost. As the oil sand is heated, the mobility of the bitumen and the water is increased, and capillary and fluid expansion forces may reestablish contact between the water layers around the individual sand grains. As the electrical conduction is almost entirely through the water, this would lead to a large increase in the electrical conductivity. When the sample is cooled all of these water contacts would not be lost and the electrical conductivity would remain higher than it's initial value.

It was noted that the peak value of normalized electrical conductivity obtained in each of the three experiments was higher for the samples with lower water contents. Experiments number 42 and 45, with water contents of 1.5 and 1.0 weight percent respectively, have peak conductivities of over seven times their final conductivities. Experiment 44, with a water content of 2.2 weight percent, had a peak of slightly less than six times its final conductivity. This trend of having a lower normalized peak conductvity with a higher water content is also observed for medium and low grade oil sands.

No results on the temperature dependence of high grade oil sands at low frequencies were published in the earlier study by Chute et al. (1979,1978). However, unpublished results from that study gave a value of α of .042 $°C^{-1}$, on the basis of two samples. As was the case in the current study, the electrical conductivity of the samples at room temperature was higher after the samples had been heated, then returned to room temperature.

Much work remains to be done in characterizing and understanding the electrical conductivity of the high grade oil sands.

6.5.4 The Variation of Electrical Conductivity with Pressure

No significant variation of the electrical conductivity of oil sand with fluid pressure was found, as long as the fluid pressure was maintained above the saturated steam pressure. This is consistent with the literature on the variation of the electrical conductivity of salt water solutions, where the electrical conductivity varied with the pressure only very near the saturated steam pressure (Ucok, Ershaghi, and Olhoeft, 1980).

During one experiment, the fluid pressure in the pressure vessel was accidentally allowed to fall below the saturated steam pressure for the temperature of the middle of the core. Immediately upon this occurring, the measured electrical conductivity of the sample decreased considerably and remained low after the sample was cooled. This sharp decrease of the electrical conductivity is the expected behavior if the water in the sample had flashed to steam and escaped from the sample.

6.5.5 The Variation of Electrical Conductivity with Current Density

For all of the electrical conductivity readings, the value of the conductivity was calculated from the average of readings for three different current densities. The usual variation in calculated conductivity for the different current densities (the highest current density being three times the lowest) was less than 1%.

For some samples particular note was made of the variation with current density. In these cases the current density was varied from 2 A/m^2 to 170 A/m^2. At the lowest current density, the calculated conductivity was at most 5% lower than at the higher current densities. However, at these low current densities the applied voltage was so low (about 10 V) that there were significant errors caused by the resistor divider network used in the present experimental system to measure the current.

6.5.6 The Variation of Electrical Conductivity at Ambient Temperatures with Water Saturation

The initial electrical conductivities of the oil sand samples in the current study were corrected for differences in the densities (i.e. for the difference between the actual density of the packed sample and the average in situ density of 2.1 g/cm³) by using the correlation of Chute et al. (1979). A least squares fit of the variation with the square of the weight percentage of water was then undertaken. The curve that best fits the data is

$$\sigma(24°C,\ 2.1\ g/cm^3,\ w) = 8.8x10^{-4}\ w^2 \qquad (6.2)$$

where w is the weight percentage of water in the sample. The multiplying constant ($8.8x10^{-4}$) is about 12% higher than a similar multiplying constant obtained by Chute et al., when the results of Chute et. al. have been corrected for their average sample density of 1.93 g/cm³. Given the errors involved in correcting both sets of data for differences in density, the two different values obtained for the multiplying constant are judged to be in good agreement.

The data obtained from each of the experiments in the current study was reviewed to determine for which packed samples a porosity and water saturation calculation could be performed with confidence. The initial (ambient temperature) electrical conductivity of these samples was plotted against their calculated water saturations in Figure 6.10. The geometric least squares fit for the data is

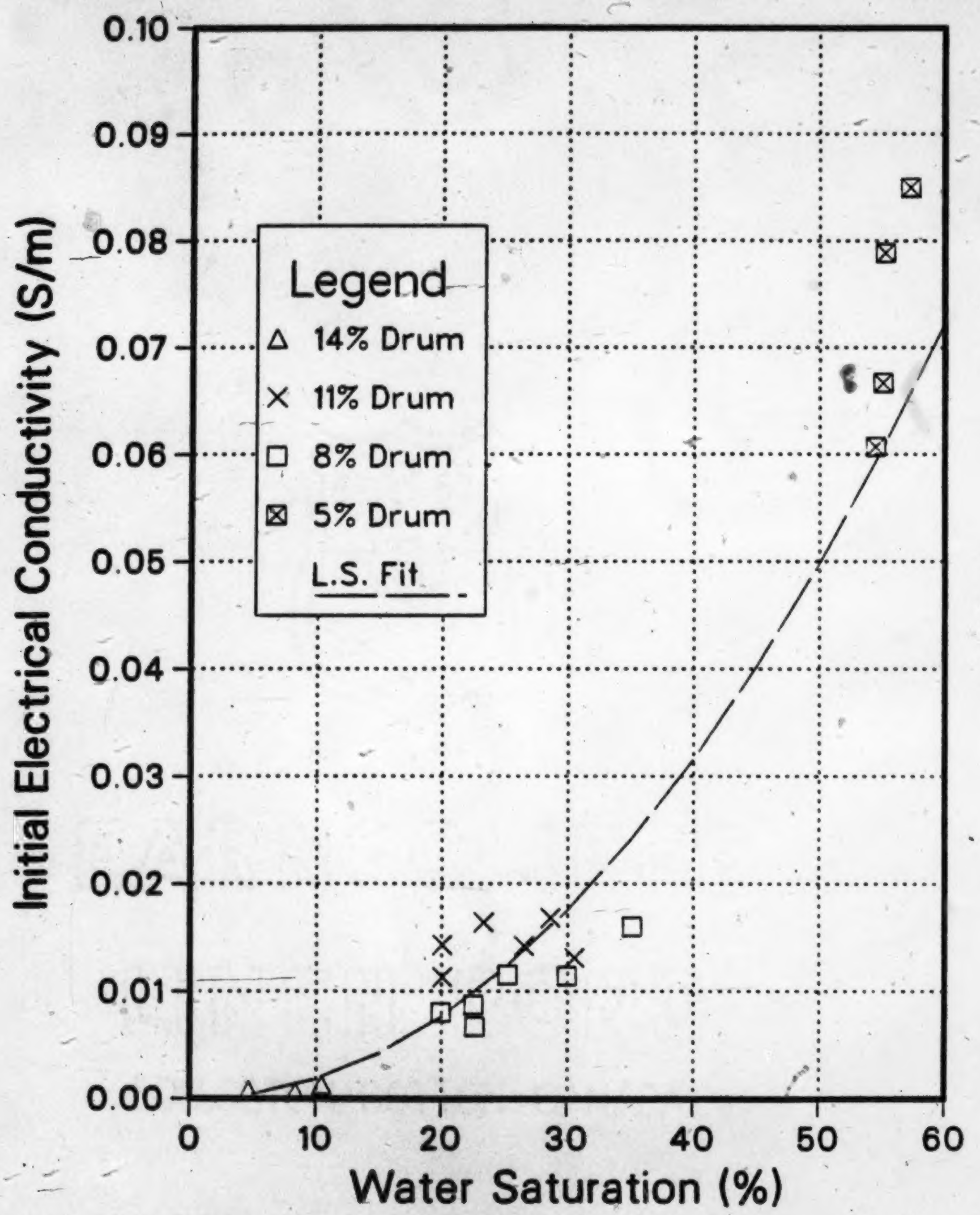

Figure 6.10 The initial electrical conductivity versus water saturation for oil sand samples.

$$\sigma_{24} = 0.205\ (Sw)^{2.05} \tag{6.3}$$

Common practice in well log interpretation makes use of the Archie Equation (Anon., 1972) in correlating the resistance of a clean sand and sandstone formation to the formation properties. This empirical formula may be applied to oil sand in the form

$$\sigma_{24} = \frac{\phi^m\ Sw^2\ \sigma w}{a} \tag{6.4}$$

where ϕ is the porosity (the fraction of the bulk volume occupied by fluids, including both liquids and gases), Sw is the water saturation (fraction of the fluid volume occupied by water), σw is the electrical conductivity of the connate water. The exponent m and the constant a are found empirically, and may vary depending on the type of rock. In particular, the value of m may vary from 1.3 for packed sands to 2.3 in tightly-cemented clastic rocks, with a also varying. For uncemented sands values of m equal to 1.37 and a equal to .88 have been found (Wait, 1971).

Note from Figure 6.10 that, while the samples from the 8% drum have the same range of water saturations as those from the 11% drum (both are considered medium grade oil sands in this study), the samples from the 11% drum have a consistently higher electrical conductivity for the same water saturation. Using Equation 6.4, with m equal to 1.37 and a equal to .88, the electrical conductivity of the connate water in individual samples may be estimated. Note that this equation assumes a clean sand with no clay or shale present. The average value of the calculated electrical conductivity of the connate water in all the samples of Figure 6.10 is .8 S/m. When the average values of the conductivities of the connate water for each of the sample drums are calculated separately, the values are 1.0 S/m for the 5% drum, .61 S/m for the 8% drum, .93 S/m for the 11% drum, and .33 S/m for the 14% drum. The range for all the samples was from .33 S/m to 1.35 S/m.

According to Takamura (1982), the connate water in oil sands is similar to a NaCl solution with a concentration in the range 30 mM to 100 mM. The electrical conductivities of NaCl solutions in this range are from .52 S/m to 1.1 S/m. Hitchon (1977) reports that the measured conductivity of the connate water from one well in the Athabasca Oil Sand deposit is 0.84 S/m. Thus, the calculated connate water conductivity values for the current study appear to be in the range reported in the literature - adding a measure of confidence that the experimental method of repacking mined oil sand yields samples that have initial electrical conductivities which agree with those present in situ.

6.5.7 The Variation of Electrical Conductivity with Temperature in the Range of 24°C to 100°C

A measurement of the electrical conductivity with the sample at a temperature of near 100°C was taken for all the experiments, both those using the Rapid Measurement Procedure, and during the heating of the samples for the Constant Temperature Procedure experiments. These measurements were all normalized by dividing the measured conductivity at 100°C by the initial measurement at 24°C. The normalized values of the electrical conductivities at 100°C varied between 2.43 and 3.14. If a linear change in electrical conductivity with temperature is assumed between 24°C and 100°C (equation 6.1), the temperature coefficient for electrical conductivity, α, can be calculated. For the low grade oil sand samples, the average value of α was .027 $°C^{-1}$, on the basis of five samples, and with a standard deviation of .0005. For the medium grade samples, the average value of α was .026 $°C^{-1}$, on the basis of twenty samples, and with a standard deviation of .003. In view of the spread of the data and the minor difference between the two averages, an overall average value of α of .026 $°C^{-1}$ may be used. This result may be compared with the result reported by Chute et al. (1979,1978), for measurements taken at 100 Hz, of .023 $°C^{-1}$, on the basis of four samples (two low grade and two medium grade).

6.6 Discussion of the Results

The electrical conductivity of the connate water in the oil sand is orders of magnitude higher than that of either the bitumen or sand. Thus, the electrical conductivity of bulk oil sand is essentially only dependent on the properties and amount of connate water and the ionic species in the connate water. It should also be noted that the volume of water will change with temperature and that the ionic species in the water may react with the sand grains, clays or fines, and the bitumen as higher temperatures are reached.

According to the current literature, the connate water in oil sand appears in two configurations: as pendular rings at grain to grain contact points, and as a roughly 10 nm thick film which covers the sand surface. This thin aqueous film exists due to double layer repulsive forces between the bitumen and sand surfaces (Takamura, 1982; Hall, Collins, and Melrose, 1983). A good explanation of the mechanisms which govern the change in the electrical conductivity of ionic solutions with temperature is given by Quist and Marshall (1968). For the temperature and pressure range used in the current study, the change in the electrical conductivity of an NaCl solution, in the concentration range of 30 mM to 100 mM (similar to the connate water in oil sand (Takamura, 1982)), as temperature increases, is due to a decrease in the water viscosity, which leads to an increase in ionic mobility. The electrical conductivity of the solution will be independent of the pressure, provided the pressure is maintained above the saturated steam pressure.

Athabasca Oil Sands consists of 2 to 3 percent mica flakes and clay mineral, with the clay minerals consisting of kaolinite and illite, with minor amounts of montmorillite

(Mossop, 1980). The low grade oil sands have a higher clay and fines content than the high grade oil sands. A discussion on the electrical conductivity of shaly sands, and of the temperature dependence of that conductivity, may be found in papers by Waxman and Thomas (1974) and Clavier, Coates, and Dumoir (1984). The paper by Waxman and Thomas includes the results from some experiments on resaturated shaly sand cores, with the temperature varied from 22°C to 200°C. The time period of the experiments was usually short, somewhat similar to the rapid measurement procedure described in section 6.3, although some of the samples were held at a constant temperature for periods of up to 48 hours. Waxman et al. do not report any of the time dependent features found in the current study. For samples resaturated with water of approximately the same salinity as oil sands, the measured electrical conductivity in the region 22° to 80°C increases linearly with temperature with a value of α (for equation 6.1) of 0.032 $°C^{-1}$. This compares to the results of the current study (for less shaly samples) of α equal to 0.026 $°C^{-1}$.

In reviewing the results of the rapid heating experiments, it was noted that the increase in the electrical conductivity of the oil sand samples with temperature was greater than the increase with temperature reported for NaCl solutions. In understanding this behavior, it should be recalled that the volume of water in the oil sand sample will increase with temperature. The volume of the water in the oil sand will increase by about 20% between 24°C and 240°C. The electrical conductivity of a solution, such as the NaCl solution mentioned above, is measured for a specific volume. Thus, the effect of increasing volume is not taken into account in reporting the change in electrical conductivity of a solution with temperature. This would explain the greater increase with temperature of the electrical conductivity of oil sand, compared with an NaCl solution, that was noted above. In addition, the studies on the electrical conductivity of shaly sand (Waxman et al., 1974; Clavier et al., 1984) noted that the presence of clay leads to a more rapid increase of the electrical conductivity with temperature than if the clays were not present.

An examination of the results of four experiments (Numbers 6, 40, 4, and 16) illustrates the effects of clays and bitumen on the electrical conductivity of oil sand. In the first two of these experiments a clean, clay free sand was partially saturated with a salt water solution to form the test sample, while in the last two experiments the samples were made by resaturating tailings pond sand (including clays and fines) and by resaturating sand after using a toluene extraction to remove the bitumen and water from oil sand. The results of these four experiment may be compared with each other and with experiments using oil sand samples to determine the effects of both clays and bitumen.

In the first experiment (Experiment 6, see Table A.2) washed tailings pond sand (clays and fines removed) was mixed with a salt water solution. Measurements were taken following the rapid measurement procedure (section 6.4.3), and repeated on the following day. According to the literature (Anon., 1972; Wait, 1971), the ratio of the electrical conductivity of the sand - salt water mixture to the electrical conductivity of the salt water used should remain constant. In other words, the temperature variation of the electrical conductivity of the sand, salt water mixture is due solely to the temperature variation of the salt water. The results of the experiment described above were plotted against the temperature variation of a 20 wt.% NaCl solution as reported by Ucok, Ershaghi, and Olhoeft (1980). (Prior to plotting, both sets of data were normalized to the value of conductivity at 22°C.) The results of the comparison are shown in Figure 6.11. Note that no hysteresis appears between the heating and cooling curves, contrary to the usual results for oil sand (as shown on Figure 6.3).

In the second experiment (Experiment No. 40, Table A.28) a second sand, salt water mixture was prepared, similar to that of Experiment 6, except that a well sorted silica sand was used. The sample was heated to 200°C, and the temperature was held constant for a period of 163 hours, with the conductivity measured at regular intervals. During this period, no significant change in the conductivity was

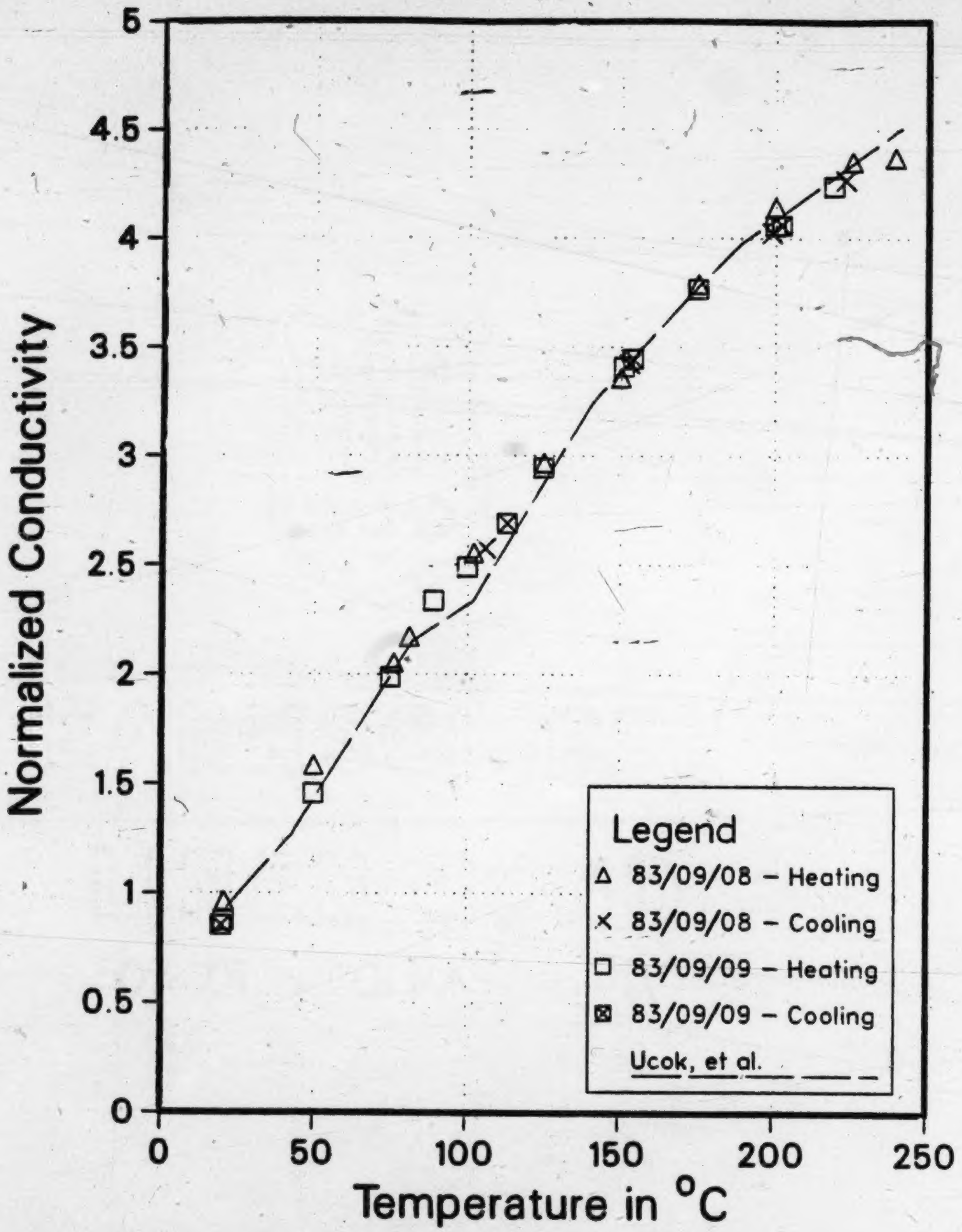

Figure 6.11 The normalized electrical conductivity of a mixture of sand and a 20 wt.% NaCl solution versus temperature, compared to the normalized results of Ucok. et al. for a 20 wt.% NaCl solution.

noted. Measurements taken during the heating and cooling of the sample indicated that the normalized conductivity followed the same curve versus temperature as Experiment 6. The actual (as well as normalized) results of the two experiments agreed to within 5%.

The sample for Experiment 4 (Table A.1) was prepared from a mixture of unwashed tailings pond sand and a 50 mM NaCl solution. The electrical conductivity versus temperature results, using the Rapid Measurement Procedure, for this experiment are compared with similar experiments using oil sand samples on Figure 6.4. Note that the change in electrical conductivity with temperature, when using a mixture of tailings pond sand and salt water, is similar to when using an oil sand sample. The normalized conductivity change with temperature, recorded in Experiment 4, while slightly lower than that recorded in the runs involving oil sand, tracks the results of these experiments. As the sand used in preparing the sample for Experiment 4 was not washed, it would contain most of the clays present in oil sand.

In Experiment 16 (Table A.7), the sand remaining after a toluene extraction had removed the bitumen and water from oil sand was used. This sand was resaturated with distilled water so that the sample contained 3.5 weight percent water. The initial electrical conductivity of this sample was similar to oil sand samples with the same weight percentage of water. This sample was heated to 150°C and held at that temperature in a similar manner to the constant temperature experiments. The peak value of normalized electrical conductivity was 2.86, which is lower than that of the oil sand experiment, but the amount of decline to the steady state value (9%) and the time to reach the steady state value (70 hours) was about the same as for the oil sand experiments.

The lower conductivity values obtained for Experiments 4 and 16, involving resaturated sand with no bitumen present, could be due to the liquid water lost in producing the vapor partial pressure of water in the pore space. In the experiments using oil sand samples, the bitumen occupies most of the pore space not occupied by the liquid water. In the experiments with no bitumen in the sample, some of the water in the sample will evaporate and occupy the gas saturated portion of the pore space. Increasing the fluid pressure of the sample will not reduce the amount of evaporation occurring, as, at the pressures obtainable in the equipment used, the partial pressure of water vapor will be almost independent of the nitrogen gas pressure in the pore space. A calculation of the amount of liquid water saturation that is lost to vapor may be done. This calculation indicates that at 150°C, the electrical conductivity would be about 3% lower than if no evaporation had taken place. The decrease at higher temperatures would be much greater.

The presence of clays and a high fines content may have a large effect on the high temperature properties of the electrical conductivity of oil sands. A paper by Hiltabrand, Ferrell, and Billings (1973) reports the results of a series of experiments where sea bed sediments were heated to temperatures of either 100°C or 200°C and held at that temperature for periods of 18 to 150 days. The changes in pH, various ion concentrations, and mineralogy were measured on a regular basis throughout the experiments. While the sediments in these experiments contained primarily the same types of clays as in oil sand (illite, kaolinite, and montmorillonite), they were present in different relative amounts. In addition, the fluid to sediment ratio was higher in these experiments than in oil sand samples. However, the results reported by Hiltabrand et al. give some indications of the changes which will occur in the clay and water system of oil sand. Hiltabrand et al. found a decrease in the pH of the fluid, over a period of less than a day, as the fluid and sediment samples were heated. The changes in ion concentration and minerals occured less rapidly. Feldspar, kaolinite, and mixed-layered montmorillonite were destroyed, or decreased in relative amounts, while montmorillonite and quartz remained, but underwent volumetric changes.

A study of the mineral changes in the Cold Lake oil sands deposits, under the conditions of steam stimulation, has been made. The porosity of the oil sand can be dramatically reduced by the crystallization of new minerals

(Lennox, 1981). However, these studies include not only the effects of temperature, but also the effects of the fresh water (from condensed steam) on the formation clays and minerals. Thus, they are not directly applicable to the electrical heating of oil sand, where little fluid movement occurs.

The electrical conductivity will be affected by the changes in the concentrates and types of ions in the connate water, and also by volume changes in the clays present. Different ionic species have different mobilities, due to differences in size. Therefore, if one ionic species is partially replaced by a different species, the average mobility of the ions in the connate water will change. The clays, and in particular their size and shape, will affect the ease with which the ions can move through the connate water. These two factors, the changing mobility of the ions and the changing effective viscosity of the water, will combine to change the bulk electrical conductivity of the oil sand.

The interpretation of the results of experiments where the oil sand was heated over 150°C is extremely difficult. A large number of physical and chemical changes can take place in the complex microenvironment of oil sands at these higher temperatures. An additional complication of interpreting the experimental results obtained in this study at these higher temperatures is due to the large fluid losses from the samples which occured in the 200°C and 240°C experiments. As pointed out in section 6.4.1, the fluids present in the oil sand will expand faster with an increase in temperature than will the sand grains. If the sand grains are maintained in close contact, the additional fluid volume must move out of the sand matrix. In the experimental apparatus described in this study, this additional fluid volume was lost from the sample. For the higher temperature experiments, significant volumes of fluid were lost, and the changes in the measured conductivity of the oil sand sample could not be unambiguously interpreted. The improved resolution of this experimental difficulty has been left to a future study.

6.7 Electrical Conductivity Formulas for use in the Computer Simulation of Electrical Heating of Oil Sand Formations

The typical time period for electrically heating an oil sand formation prior to a steam drive would likely be on the order of several months to several years. Thus, the final values obtained for electrical conductivity in the constant temperature experiments are preferred over those obtained in the rapid heating experiments. If, however, a computer simulation of a high temperature physical model was being done, where oil sand had been used as the model medium in the physical model, care would have to be taken that the conductivity values used in the simulation be correct for the actual time period involved in the physical model. If a high temperature physical scale model were run in an (unscaled) time period of only several hours, then the conductivity values obtained in the rapid heating experiments should be used in any computer simulation of the model.

To obtain an accurate, statistically valid correlation between the electrical conductivity of oil sand and temperature for the range above 150°C many more measurements would have to be performed. However, on the basis of the current work, formulas for the variation of electrical conductivity with temperature are developed for use until a more complete characterization of the higher temperature behaviour is available.

For low and medium grade oil sands, the electrical conductivity was always observed to increase linearly with temperature in the range from in situ temperature to 100°C. The conductivity remained constant with time for samples held at this temperature. Thus, for temperatures less than 100°C, the formula cited in the literature (equation 6.1) may be used with confidenc~~e, with~~ a value of α obtained in the current work of 0.026 $^{\circ}C^{-1}$ for low and medium grade oil sand.

For low and medium grade oil sand, the average final value of the normalized conductivity for samples held at 150°C, for more than 150 hours, is 2.95 (see Figure 6.6). This is almost the same as the value of normalized conductivity obtained for 100°C. Thus, for the experiments which were performed using the constant temperature procedure, the average value of electrical conductivity is almost the same for both 100°C and 150°C. Above 150°C, it is difficult to draw any conclusions from the current experimental data. It is therefore recommended by the author that it be assumed that the electrical conductivity remain constant above 100°C at a value of 2.98.

Thus, the following formulas are recommended for use when modelling low or medium grade oil sands:

$$\sigma = \sigma_{24}[1 + 0.026(T - 24)] \qquad T \leq 100°C$$

$$\sigma = 2.98\sigma_{24} \qquad T > 100°C \qquad (6.5)$$

In view of the limited data available at the present time, it is not clear how the electrical conductivity will vary with temperature for high grade oil sand. From the three experiments performed, it appears that the increase in electrical conductivity will be greater for a given increase in temperature than for other grades of oil sand. However, it is not clear whether this difference is due to the experimental method of using repacked oil sands for these measurements. Until more data is obtained, it is suggested that Equation 6.5 also be used for high grade oil sand.

6.7.1 Effect of the New Formulas

To get a first order estimate of how much of an effect the new equations for electrical conductivity would have on the results of computer simulation runs, a simulation previously done (using equation 6.1 with the conductivity continuing to increase linearly with temperature, and α equal to 0.023) was repeated with the new formulas (Equation 6.5). This simulation, described in detail in Appendix II, involved a multilayered oil sand reservoir, with the property data and lithology obtained from the logs and core data of an actual oil sand reservoir. The electrodes were completed in the middle of the oil sand reservoir, with the predominant current flow being radially outward from the electrode into the oil sand reservoir. A more detailed description of the simulation run and the final temperature contour plot are given in Appendix II.

A simulation of this electrode configuration was chosen to study the effects of the new electrical conductivity formulas as the maximum temperature occurs in the oil sand. In some other electrode configurations, such as the two electrode, "top-bottom", configuration, the maximum temperature will be reached in the adjacent shale and limestone formation. As the current study deals with the high temperature electrical conductivity of oil sand, and does not address the problem of determining suitable electrical properties for shale or limestone, an electrode configuration with the electrical current flow and heating occuring almost entirely in the oil sand is appropriate.

As this simulation involved constant power heating of the formation, the voltages of the electrodes were automatically adjusted during the simulation run to maintain a constant power into the formation. Thus, the same amount of energy was input to the formation during both runs, even though the electrical conductivity of the oil sands (and hence the resistance between the electrodes) was assumed to vary differently with temperature in the two runs.

Using the new equations, the maximum temperature (which occured near the electrode) was 215°C as compared to 195° when using the old equations. Farther away from the electrodes, the formation temperature was cooler using the new equations (74°C compared to 78°C at 14 m from the electrode). The formation resistance at the end of heating was also higher using the new equations. To maintain a constant power into the formation, the voltage in the run using the new equations was 9% higher at the end of the simulation.

One must be careful when generalizing from a single example. However, in view of the minor differences obtained in the results of the simulation using the new conductivity equations, further refinement of the electrical conductivity equations for low and medium grade oil sands will likely have only a slight effect on simulation results. The conclusions derived from the large amount of computer simulation work which has been done to date (assuming the electrical conductivity continues to rise linearly with temperature up to over 250°C) have not been invalidated by this study.

6.8 Conclusions and Recommendations for Further Study

In the temperature range from in situ temperatures to 100°C, the electrical conductivity will increase linearly with temperature for low and medium grade oil sand samples. This study confirmed the earlier results of Chute et al., but vastly increased the number of measurements taken in this temperature range. On the bases of the new measurements, the value of the temperature dependence parameter, α, of 0.023 obtained in the earlier study has been changed to 0.026.

The electrical conductivity of oil sand will decline with time when it is raised to, then held at a constant temperature of 150°C or above, until a steady state value is reached. The amount of decline and the length of time to reach steady state are dependent on the temperature the sample is being held at, and the amount of clay present in the sample. In particular, the decline is greatest for those samples with higher fines content. For samples involving clean sand and salt water solutions no decline is observed.

Formulas were developed to calculate the change in electrical conductivity with temperature, for low and medium grade oil sands, to be used in computer simulations of electrical heating of oil sand reservoirs.

Work remains to be done in the area of electrical conductivity measurements at 60 Hz. Further conductivity measurements using high grade oil sand should be performed. Different packing methods (pounding, vibration table) should be tried to examine if any of these packing methods lower the difference between the initial conductivity and the final conductivity.

More conductivity measurements should be performed using core samples. The cores should be obtained without freezing, and be stored at near the in situ temperature in sealed containers until the experiments are done.

Conductivity measurements with long time durations should be carried out. The samples should be heated very slowly, using low current densities, to approximate the actual field heating rates and current densities away from the electrodes. These runs would only have to be done up to a temperature of 100°C, but would take several months. Similarly, experiments involving higher current densities and temperatures should be conducted to simulate near electrode regions of an actual electrical heating process.

In view of the minor changes in simulation results which would occur with further refinement of the electrical conductivity equations from low and medium grade oil sands, immediate future efforts should be concentrated on the above mentioned work and on studying the electrical conductivity of shales and limestones rather than on further study of the electrical conductivity of low and medium grade oil sands.

7. Conclusions and Recommendations for Further Study

Specific conclusions dealing with topics of particular chapters of this thesis have been placed at the end of these chapters. The purpose of this chapter is to consider the overall state of numerical modelling of the electric pre-heat and steam drive process, and to make recommendations concerning this general topic.

Several areas for future study regarding the numerical modelling of the electric pre-heat and steam drive process exist. Primary among these is the development of electrode models where the electrode is small in size compared to the grid block size. In the work done in this thesis, one or more grid blocks were used to represent a single electrode, and the grid blocks surrounding an electrode had to be similar in size to the electrode grid blocks. In the simulation of fluid flow in reservoirs, well models are used so that the well diameter can be only a fraction of the grid block size. This allows the use of bigger grid blocks and hence fewer grid blocks are necessary. Once similar models are developed for electrodes, the same grid could be used for the solution of the electrical and fluid flow equations. While these electrode models will likely result in less accurate near-electrode temperature calculations, they will reduce computational requirements and make it possible to accurately predict temperature changes in the bulk of the volume being electrically heated. Thus, a simulator incorporating such electrode models would be suitable for performing initial studies on determining the best method to electrically heat a particular formation. Once the general aspects of an electric pre-heat had been established, more detailed simulations on the temperatures near the electrodes could be conducted.

Two areas for future study arise from the discussion, in Chapters 4 and 5, of the two formulations used in Model 2. One of these formulations treated the electrical conductivity and heating rate as implicit properties, while the other formulation treated these two properties explicitly. First, the timestep selection criteria could be reevaluated using the two formulations to see if it is overly conservative, that is, can larger timesteps be used in the simulation of the electric pre-heat. Second, a simulator could be developed to use the average value of the electrical heating rates at the beginning and the end of the timestep. Such a simulator would be able to take larger timesteps without introducing additional errors. However, it must be remembered that the outer iteration loop necessary to obtain the electrical heating rates at the end of the timestep requires additional computation. An area of research then would be whether the use of larger, but more computationally expensive, timesteps results in an overall computational saving.

While it was shown in this thesis that fluid flow and thermal expansion may be neglected in the modelling of certain types of electrical pre-heat processes, the need still exists for an integrated electrical heating and fluid flow simulator. Such a simulator could model some processes, such as fluid injection during electrical heating, which cannot be accurately or easily modelled if fluid flow is not incorporated into the simulator. There are also less obvious cases where the modelling of fluid flow is needed. If significant heating occurs in regions where both water and oil are mobile, fluid expansion will occur and some fluid will be driven out of the heated region. If both water and oil can move, the water may be more mobile than the oil. In this situation, sufficient water may be driven out of the region to significantly change it's electrical conductivity, affecting the heating rates for the entire reservoir. To be truly useful in modelling the wide range of electric pre-heat processes, a simulator should be able to model the salt concentration of the reservoir water, so water of a different salinity than that of the original connate water could be injected. It would also be useful to incorporate a more complex model of the changes in electrical conductivity with temperature and time in the simulator.

The area of high temperature, high pressure electrical properties of oil sands has only begun to be explored by the experimental work in this thesis. A great deal more experimental and theoretical work is needed in this area. In particular, a detailed study of the high temperature clay - connate water interaction is needed.

No study of the high temperature, high pressure electrical properties of the shales adjacent to the oil sand formations has been published. This information is needed for accurate simulation of many electric pre-heat configurations, in particular for the "Top-Bottom" electrode configuration where electrodes are actually placed in the adjacent shale formations.

It has been shown that an electric pre-heat can be used to establish a fluid communication path in a very heavy oil reservoir, such as an Athabasca oil sand reservoir. Research is now most urgently needed in the field of electrode design and placement. The types and sizes of electrodes that are technically and ecomonically feasible must be established before large amounts of detailed work into optimizing the electric pre-heat and steam drive process can confidently be done.

Bibliography

Abou-Kassen, J.H., 1981. Investigation of Grid Orientation in a Two-Dimensional, Compositional, Three-Phase Steam Model. Ph.D. Thesis, University of Calgary, 287 pages.

Ames, W.F., 1977. Numerical Methods of Partial Differential Equations. Academic Press.

Amyx, J.W., Bass, D.M. Jr., Whiting, R.L., 1960. Petroleum Reservoir Engineering. McGraw-Hill Book Company, New York.

Anbah, S.A., Chilingar, G.V., and Bessor, C.M. 1965. Application of Electrical Current for Increasing the Flow Rate of Oil and Water in a Porous Medium. J. Can. Petroleum Tech., May-June 1965, pp 81-88

Anon., 1969. Thermal Recovery System Uses Electricity. Petroleum Engineering, July 1969. pp. 44

Anon., 1970. A.C. Current Heats Heavy Oil for Extra Recovery. World Oil, 170(4) pp. 83-86.

Anon., 1972. Log Interpretation, Volume I - Principles, Schlumberger Limited, New York. 113 pages.

Aziz, K., and Settari, A., 1979. Petroleum Reservoir Simulation. Applied Science Publishers, New York.

Barnes, A.L., 1978. Method of Heating a Subterranean Formation. Canadian Patent No. 1031694. 15 pages.

Buchanan, W.L., 1985. Simulating Steam Additive EOR Processes. SPE Paper 13522, presented to the SPE 1985 Reservoir Simulation Symposium, Dallas, Texas.

Camp, F.W., 1976. The Tar Sands of Alberta, Canada. 3rd Ed. Cameron Engineering, Inc., Denver, Colorado.

Carnahan, B., Luther, H.A., and Wilkes, J.O., 1969. Applied Numerical Methods. John Wiley and Sons Inc. Chapter 7.

Cassis, R., Fuller, N., Hepler, L.G., McLean, R.J., Skauge, A., Srinivasan, N.S., and Yan, H., 1985. Specific Heat Capacities of Bitumen and Heavy Oils, Reservoir Minerals, Clays, Dehydrated Clays, Asphaltenes, and Cokes. AOSTRA Journal of Research, 1(3).

Cervenan, M.R., Vermeulen, F.E., and Chute, F.S. 1981. Thermal Conductivity and Specific Heat of Oil Sand Samples. Can. J. Earth Sciences, 18(5), pp. 926-931.

Christiansen, J.P., and Roberts, K.V., 1974. Olympus - A Standard Control and Utility Package for Initial-Value Fortran Programs. Computer Physics Communications, 7, pp. 245-270.

Chute, F.S, Vermeulen, F.E., and Cervenan, M.R., 1978. Physical Modelling of the Electrical Heating of the Oil Sand Deposits. AOSTRA Agreement No. 31.

Chute, F.S., Vermeulen, F.E., Cervenan, M.R., and McVea, F.J., 1979. Electrical Properties of Athabasca Oil Sands. Can. J. Earth Sci. 16(10). pp. 2009-2021.

Chute, F.S., Vermeulen, F.E., and Cervenan, M.R., 1981. On the electromagnetic heating of low loss materials using induction coils. Can. Elec. Eng. J., 6(1), pp. 20-28.

Chute, F.S., and Vermeulen, F.E., 1985. Private Communication.

Clavier, C., Coates, G., and Dumanoir, J., 1984. Theoretical and Experimental Bases for the Dual-Water Model for Interpretation of Shaly Sands. SPEJ, 24(2), pp. 153-168.

Coats, K.H., 1978. A Highly Implicit Steamflood Model. SPEJ, 18(5), pp. 369-383.

Coats, K.H., 1980. In-Situ Combustion Model. SPEJ, 20(6), pp. 533-554.

Coats, K.H., 1982. Simulation of Gas Condensate Reservoir Performance. SPE 10512, Sixth SPE Symposium on Reservoir Simulation, New Orleans.

Craft, B.C., and Hawkins, M.F., 1959. Applied Petroleum Reservoir Engineering. Prentice-Hall, Inc., Englewood Cliffs, New Jersey.

Crookston, R.B., Culham, W.E., and Chen, W.H., 1979. A Numerical Simulation Model for Thermal Recovery Processes. SPEJ 19(1), pp. 37-58.

de la Cruz, V., and Spanos, T.J.T., 1983. Mobilization of Oil Ganglia. AIChE Journal, 29(5), pp. 854-858.

Darcy, H., 1856. Les Fontaines de la ville de Dijon. Paris: Victor Dalmont.

Das, M., Thapar, R., Rajeshwar, K., and DuBow, J., 1981. Thermophysical characterization of oil sand: Electrical Properties. Can. J. Earth Sci., 18, pp. 742-750.

Dey, A., and Morrison, H.F., 1979. Resistivity modelling for arbitrarily shaped three dimensional structures.

Geophysics, 44(4), pp. 753-780.

Dietrich, J.K., 1981. Relative Permeability During Cyclic Steam Stimulation of Heavy-Oil Reservoirs. JPT, 33(10), pp. 1987-1989.

Dorn, W.S. and McCracken, D.D., 1972. Numerical Methods with FORTRAN IV Case Studies. John Wiley & Sons, Inc., New York. Chapter 5.

Edmunds, N.R., 1984. A Model of the Steam Drag Effect in Oil Sands. JCTP, Septemtber-October, pp. 30-39.

El-Feky, S.A., 1977. Theoretical and Experimental Investigation of Oil Recovery by the Electrothermic Technique. Ph.D. Disertation, University of Missouri-Rolla.

Farouq Ali, S.M. and Redford, D.A., 1977a. Physical Modelling of In Situ Recovery Methods for Oil Sands. The Oil Sands of Canada-Venezuela 1977, CIM Special Vol. 17, pp.319

Farouq Ali, S.M., 1977b. Multiphase, Multidimensional Simulation of In Situ Combustion. SPE Paper no. 6896, 52nd Annual Technical Conference of SPE, Denver. 11 pages.

Farouq Ali, S.M., 1980. Elements of Thermal Oil Recovery. Lecture notes for MNL E 568, University of Alberta.

Ferrer, J. and Farouq Ali, S.M., 1977. A Three-Phase, Two Dimensional Compositional Thermal Simulator for Steam Injection Processes. JCPT, 16(1), pp. 78-90.

Fitzgerald, J.J., 1978. Black Gold with Grit. Grey's Publishing Ltd., Sidney, B.C..

Flock, D.L., and Tharin, J., 1975. Unconventional Methods of Recovery of Bitumen and Related Areas Particular to the Oil Sands of Alberta. JCPT, 14(3), pp. 17-27.

Forsyth Jr., P., Rubin, B., and Vinsome, P.K.W., 1981. The elimination of the constraint equation and modelling of problems with a non-condensable gas in steam simulation. JCPT, 20(4), pp. 63-68.

Gill, W., 1979. The Electrothermic System for Enhanced Oil Recovery. International Conf. on the Future of Heavy Oil and Tar Sands. McGraw-Hill Inc.. pp. 469-473.

Gilpin, R.R., and Gates, E.M., 1981. Jet piercing of Oil Sand. J. Energy Resources Tech., 103, pp. 330-335.

de Haan, H.J., and van Lookeren, J., 1972. Early Results of First Large-Scale Steam Soak Project in the Tia Juana Field. Thermal Recovery Techniques. SPE Reprint Series No. 10. pp. 279-288.

Hagedorn, A.R., 1978. Oil recovery by combining Steam Stimulation and Electrical Heating. Canadian Patent 1023657, 19 pages.

Hageman, L.A., and Young, D.M., 1981. Applied Iterative Methods. Academic Press.

Hall, A.C., Collins, S.H., and Melrose, J.C., 1983. Stability of Aqueous Wetting Films in Athabasca Tar Sands. SPEJ, 23(2), pp. 249-258.

Harvey, A.H. and El-Feky, S.A., 1978. Selective Heating Could Boost Oil Recovery. Oil and Gas Journal, 76(46), pp. 185-190.

Harvey, A.H, Arnold, D.M., and El-Feky, S.A., 1979. Selective Electrical Reservoir Heating. JCPT, 18(3), pp. 47-57.

Harvey, A.H., and Arnold, M.D., 1980. A Radial Model for Estimating Heat Distribution in Selective Electrical Reservoir Heating. JCPT, 19(4), pp. 37-41.

Harvey, A.H., 1982. Influence of Adjacent Conductive Formations on the Selective Electric Reservoir Heating Process. SPEJ, 22(5), pp. 750-754.

Hayt, W.H., Jr., and Kemmerly, J.E., 1978. Engineering Circuit Analysis, 3rd Edition. McGraw-Hill Book Company, New York.

Hermance, J.F., 1982. Refined finite-difference simulation using integral forms: Application of telluric fields in two dimensions. Geophysics, 47(5), pp. 825-831.

Hiebert, A.D., 1981. Computer Simulation of In Situ, Low Frequency, Electrical Heating of Oil Sand Formations. M.Sc. Thesis, University of Alberta.

Hiebert, A.D., Capjack, C.E., Chute, F.S., and Vermeulen, F.E, 1983. A simulation code for investigating 2D heating of material bodies by low frequency electric fields. Applied Mathematical Modelling, 7(5), pp. 366-371.

Hiebert, A.D., Vermeulen, F.E., Chute, F.S., and Capjack, C.E, 1986. Numerical Simulation Results for the Electrical Heating of Athabasca Oil Sand Formations. SPE Reservoir Engineering, 1(1), pp. 76-84.

Hiltabrand, R.R., Ferrell, R.E., and Billings, G.K., 1973. Experimental Diagenesis of Gulf Coast Argillaceous Sediment. American Assoc. of Petroleum Geologist Bull. 57(2), pp.338-348.

Hitchon, B., 1977. Geochemical Aspects of In-Situ Recovery. The Oil Sands of Canada-Venezuela, 1977, CIM Special Volume 17, pp. 80-86.

Hubbert, M.K., 1940. The Theory of Ground-Water Motion. The Journal of Geology,48(8), pp. 785-944.

Hunt, J.M., 1979. Petroleum Geochemistry and Geology. W.H. Freeman and Company, San Francisco. Chap. 3.

Jackson, J.D., 1975. Classical Electromagnetics. John Wiley and Sons Ltd., Chap. 1.

Kern, L.R., 1977. Method and Apparatus for Electrical Heating of Hydrocabonaceous Formations. Canadian Patent No. 1018255. 21 pages.

Khosla, A., and Towson, D.E., 1985. Application of Computer Modelling to the PCEJ Electric Preheat/Steamdrive Athabasca Pilot. Petroleum Society of CIM Paper No. 85-36-51. Presented fo the 36th Annual Technical Meeting of the Petroleum Society of CIM, Edmonton, June 2-5, 15 pages.

Landau, L.D., and Lifshitz, E.M., 1960. Electrodynamics of Continuous Media. Pergamon Press, Oxford. pp. 93.

Lennox, T.R., 1981. The Impact of Geology on the Design and Performance of In-Situ Projects. Advances in Petroleum Recovery and Upgrading, Calgary, Alberta.

Magid, L.D., 1972. Electromagnetic Fields, Energy, and Waves. John Wiley and Sons Ltd., Chap. 9.

Mathews, J. and Walker, R.L., 1970. Mathematical Methods of Physics, 2nd Edition. W.A. Benjamin, Inc., Melno Park. 501 pp.

McVea, F.J., 1978. Electrical Properties of Tar Sands. M.Sc. Thesis, University of Alberta.

Mossop, G.D., 1980a. Geology of the Athabasca Oil Sands. Science, 207(11), pp. 145-152.

Mossop, G.D., 1980b. Facies Control on Bitumen Saturation in the Athabasca Oil Sands. Facts and Principles of World Petroleum Occurances, A.D. Miall, Ed.. Can. Soc. Petrol. Geol. Memoir 6. pp. 609-632.

Nelson, H.W., and Glaister, R.P., 1978. Subsurface Environmental Facies and Reservoir Relationships of the McMurray Oil Sands, Northeastern Alberta. Bull. Can. Pet. Geologists, 26(2), pp. 177-207.

Newbold, F.R., and Perkins, T.K., 1977. Wellbore Transmission of Electrical Power. The Oil Sands of Canada-Venezuela 1977, CIM Special Vol. 17, pp. 631-647.

Nex, C.M.M., 1980. Computational Methods for Sparse Matrices. Computer Physics Communications, 20, pp. 7-10.

Nicholls, J.H., and Luhning, R.W., 1977. Heavy Oil Sand and Insitu Pilot Plants in Alberta (Past and Present). The Oil Sands of Canada-Venezuela 1977, CIM Special Vol. 17, pp. 528-540.

Orkiszewski, J., McReynolds, P.S., Boberg, T.C., and Hill, J.L., 1967. Method and apparatus for electrical heating of oil-bearing formations. Canadian Patent 761266, 13 pages.

Outtrim,C.P., and Evans, R.G., 1977. Alberta's Oil Sands Reserves and their Evaluation. The Oil Sands of Canada-Venezuela 1977, CIM Special Vol. 17, pp. 36

Patchett, J.G., 1975. An Investigation of Shale Conductivity. The Log Analyst, Nov.-Dec., pp. 3-20.

Patel, J.G., Hegde, M.G., and Slattery, J.C., 1972. Further Discussion of Two-Phase Flow in Porous Media. AIChE Journal, 18(3), pp. 1062-1063.

Peaceman, D.W., 1977. Fundamentals of Numerical Reservoir Simulation. Elsevier Scientific Publishing Company, Amsterdam. pp. 24.

Perkins, T.K., 1976. Production of Bitumen from a Tar Sand Formation. U.S. Patent 3 958 636.

Perkins, T.K., 1978. Method of Increasing Electrical Conductivity about a Well Penetrating a Subterranean Formation. Canadian Patent No. 1031689. 24 pages.

Potter, D., 1973. Computational Physics. John Wiley and Sons Ltd., Chichester, England. Chapter 9.

Pritchett, W.C., 1979. Method and Apparatus for Producing Fluid by Varing Current Flow through Subterranean Source Formation. Canadian Patent No. 1047396. 40 pages.

Quist, A.S., and Marshall, W.L., 1968. Electrical Conductances of Aqueous Sodium Chloride Solutions from 0 to 800° and at Pressures to 4000 Bars. J. Physical Chem., 72(2). pp. 684-703.

Ramo, S., Whinnery, J.R. and Van Duzer, T., 1965. Fields and Waves in Communication Electronics. John Wiley and Sons Ltd.. p. 234.

Ranney M.W., (ed.), 1979. Oil Shale and Tar Sands Technology. Noyes Data Corporation. pp. 326-340.

Reddy, G.S., Prowse, D.R., and Redford, D.A., 1980. Physical Modeling and Numerical Simulation of In Situ Recovery of Bitumen from Oil Sands by Steam Injection. 31st ATM of the Pet. Soc. of CIM, Calgary. Paper No. 80-31-10.

Redford, D.A., and Cotsworth, P.F., 1976. Development of Communication Paths Within a Tar Sand Bed. Shale Oil, Tar Sand and Related Fuels. pp. 112.

Roberts, K.V., 1974. An Introduction to the Olympus System. Computer Physics Communications,7, pp. 237-243.

Rubin, B. and Buchanan, W.L., 1985. A General Purpose Thermal Model. SPEJ, 25(2), pp. 202-214.

Sacuta, A., 1981. Enhansed Oil Recovery using Electrical Means. Canadian Patent 1099210, 15 pages.

Sokolnikoff, I.S., 1964. Tensor Analysis. John Wiley and Sons, Inc., New York.

Stratton, J.A., 1941. Electromagnetic Theory. McGraw-Hill Book Company. pp.37

Takamura, K., 1982. Microscopic Structure of Athabasca Oil Sand. Can. J. Chem. Eng.,60, pp. 538-545.

Thomas, G.W., 1982. Principles of Hydrocarbon Reservoir Simulation, 2nd Edition. Inernational Human Resources Development Corporation, Boston.

Todd, J.C., and Howell, E.P., 1977. Numerical Simulation of In Situ Electrical Heating to Increase Oil Modility. The Oil Sands of Canada-Venezuela 1977, CIM Special Vol. 17, pp. 477-486.

Todd, J.C., 1980. Method of Producing Viscous Materials from Subterranean Formations. Canadian Patent No. 1076474. 28 pages.

Towson, D.E., 1979. The Electric Pre-heat Recovery Process. First International Conf. on the Future of Heavy Crude and Tar Sands. McGraw-Hill Inc., pp. 410-412.

Towson, D., 1982a. The Electric Preheat Recovery Process. Second International Conference on Heavy Oil and Tar Sand, Caracas, Venezuela, Feb. 1982, UNITAR/CF10/IX/6, 9 pages.

Towson, D., 1982b. The Electric Pre-heat Recovery Process. CIM Preprint No. 82-33-80. 8 pages.

Ucok, H., Ershaghi, I., and Olhoeft, G., 1980. Electrical Resistivity of Geothermal Brines. JPT, 32(4), pp. 717-727.

Vermeulen, F.E, Chute, F.S., and Cervenan, M.R., 1979. Physical Modelling of the electromagnetic heating of oil sand and other earth-type and biological materials. Can. Elec. Eng. J., 4(4), pp. 19-28.

Vermeulen, F.E., Chute, F.S., Cervenan, M.R., and Fearn, J., 1982. Physical Modelling of the Electrical Heating of the Oil Sand Deposits. AOSTRA Agreement No. 58, 322 pages.

Vermeulen, F.E. and Chute, F.S., 1983. Electromagnetic Techniques in the In-Situ Recovery of Heavy Oils. Journal of Microwave Power, 18(1), pp. 15-29.

Wait, J.R., (ed.), 1971. Electromagnetic Probing in Geophysics. The Golem Press, pp. 37.

Waxman, M.H., and Thomas, E.C., 1974. Electrical Conductivity in Shaly Sands - I. The Relation Between Hydrocarbon Saturation and Resistivity Index; II. The Temperature Coefficient of Electrical Conductivity. J. Pet. Tech., 257, pp. 213-225.

Woo, P.T., 1979. Application of Array Processor on Sparse Elimination. SPE of AIME Symposium on Reservoir Simulation, Denver, Colorado.

Yanosik, J.L., and McCracken, T.A., 1979 A Nine-Point, Finite-Difference Reservoir Simulator for Realistic Prediction of Adverse Mobility Ratio Displacements. SPEJ 19(3), pp. 253-262.

Yasuda, S., 1978. Method and Equipment to Extract and Collect Petroleum Substance form Underground Tar Sands Stratum and Underground Petroleum Reservoirs. Canadian Patent 1034870, 29 pages.

Appendix I. Experimental Results

On the following pages are tables giving the results of the experimental runs preformed. Not included in this set of tables are the runs where the experimental method or equipment was being tested, or where equipment failure meant that no useful results were obtained.

Table A.1 Results of Experiment No. 4.

The sample for this run was a mixture of dried tailings pond sand and a 50 mM NaCl solution.

Date Packed:	83.07.20
Initial Analysis:	3.50 % salt solution, 96.5 % Sand.
Density:	1.63 g/cm^3
Sample Thickness:	7.4 cm
σ_{24}:	0.0087 S/m
Electrode Surface:	Copper
Sample Holder Tube:	Glass

Run Time (Hours)	Pressure (MPa)	Temperature (°C)	σ (S/m)	σ/σ_{24}
0.0	2.1	27.	0.0093	1.07
0.45	2.3	50.	0.0137	1.57
0.82	2.5	73.	0.0183	2.10
1.22	2.6	99.	0.0229	2.63
1.55	2.7	120.	0.0261	3.00
2.00	3.0	149.	0.0284	3.26
2.23	3.1	155.	0.0292	3.36
2.47	3.0	159.	0.0301	3.46
2.73	3.0	159.	0.0302	3.47
2.97	3.0	158.	0.0301	3.46
3.97	2.5	109.	0.0232	2.67
19.25	2.1	24.	0.0094	1.08
19.87	2.3	50.	0.0149	1.71
20.37	2.5	76.	0.0205	2.36
20.93	2.7	99.	0.0245	2.82
21.33	3.0	124.	0.0275	3.16
21.87	3.2	150.	0.0293	3.37
22.38	3.4	176.	0.0316	3.63
22.87	3.6	200.	0.0334	3.84
23.42	4.5	225.	0.0338	3.89
23.80	4.7	239.	0.0322	3.70
24.97	4.3	215.	0.0321	3.69
26.18	3.8	187.	0.0305	3.51
28.58	3.4	145.	0.0270	3.10
33.27	2.5	88.	0.0200	2.30
43.72	1.7	23.	0.0091	1.05

Table A.2 Results of Experiment No. 6.

The sample for this run was a mixture of 95 wt.% clean sand and a salt-water solution.

Date Packed: 83.09.06
Initial Analysis: 1. % NaCl, 3.96 % H_2O, 95. % Sand.
Final Analysis: 1. % NaCl, 3.71 % H_2O, 95.3 % Sand.
Density: 1.59 g/cm^3
Sample Thickness: 8.2 cm
σ_{22}: 0.204 S/m
Electrode Surface: Copper
Sample Holder Tube: Glass

Run Time (Hours)	Pressure (MPa)	Temperature (°C)	σ (S/m)	σ/σ_{22}
0.00	1.4	21.	0.201	0.99
0.62	1.5	50.	0.331	1.62
1.18	1.6	76.	0.429	2.10
1.63	1.8	102.	0.534	2.62
2.13	2.0	125.	0.620	3.04
2.75	2.2	150.	0.702	3.44
3.35	2.7	175.	0.792	3.88
4.08	3.3	200.	0.866	4.25
4.75	4.0	225.	0.910	4.46
5.25	4.3	239.	0.914	4.48
6.10	3.9	223.	0.892	4.37
6.98	3.0	199.	0.841	4.12
9.27	2.0	153.	0.715	3.50
11.85	1.5	106.	0.538	2.64
22.77	1.1	20.	0.181	0.89
22.83	1.4	21.	0.182	0.89
23.33	1.6	50.	0.304	1.49
23.73	1.7	75.	0.415	2.03
24.03	1.8	89.	0.488	2.39
~~24.33~~	1.8	100.	0.520	2.55
24.73	2.0	125.	0.615	3.01
25.22	2.4	151.	0.712	3.49
25.65	2.8	175.	0.787	3.86
26.17	3.4	200.	0.848	4.16
26.58	4.0	219.	0.886	4.34
27.87	3.5	202.	0.849	4.16
29.25	2.4	154.	0.720	3.53
30.85	1.8	113.	0.562	2.75
46.78	1.1	20.	0.178	0.87

Table A.3 Results of Experiment No. 7.

Date Packed: 83.09.20
Initial Analysis: Unknown
Final Analysis: 9.7 % Bitumen, 3.6 % H_2O, 86.7 % Sand
Density : 1.91 g/cm^3
Sample Thickness: 7.5 cm
σ_{25}: 0.0051 S/m
Electrode surface: Copper
Sample Holder Tube: Glass

Run Time (Hours)	Pressure (MPa)	Temperature (°C)	σ (S/m)	σ/σ_{25}
0.0	1.5	25.	0.0051	1.02
0.47	1.6	50.	0.0084	1.68
0.90	1.8	75.	0.0123	2.46
1.35	1.9	100.	0.0163	3.26
1.85	2.2	126.	0.0188	3.76
2.35	2.5	149.	0.0204	4.08
2.82	3.0	175.	0.0241	4.82
3.40	3.6	200.	0.0262	5.24
3.92	4.4	224.	0.0250	5.00
4.43	4.5	240.	0.0218	4.36
5.65	3.6	212.	0.0203	4.06
6.90	2.8	182.	0.0190	3.80
10.65	2.0	137.	0.0174	3.48
13.65	1.6	89.	0.0135	2.70
23.95	1.2	25.	0.0059	1.18
24.42	1.3	50.	0.0097	1.94
24.75	1.4	75.	0.0138	2.76
25.15	1.6	100.	0.0178	3.56
25.57	1.8	125.	0.0209	4.18
26.08	2.1	150.	0.0225	4.50
26.47	2.5	175.	0.0238	4.76
26.78	3.1	200.	0.0243	4.86
27.22	3.9	225.	0.0231	4.62
27.77	4.3	240.	0.0214	4.28
28.85	3.5	215.	0.0202	4.04
30.88	2.1	162.	0.0181	3.62
33.33	1.6	113.	0.0151	3.02
36.33	1.4	76.	0.0117	2.34
47.92	1.1	26.	0.0058	1.16

Table A.4 Results of Experiment No. 8.

Date Packed:	83.09.23
Initial Analysis:	Unknown
Final Analysis:	8.8 % Bitumen, 4.2 % H_2O, 87. % Sand
Density :	1.94 g/cm³
Sample Thickness:	7.5 cm
σ_{24}:	0.0079 S/m
Electrode surface:	Copper
Sample Holder Tube:	Glass

Run Time (Hours)	Pressure (MPa)	Temperature (°C)	σ (S/m)	σ/σ_{24}
0.0	0.0	26.	0.0081	1.03
0.23	1.2	27.	0.0080	1.01
0.53	1.4	27.	0.0080	1.01
2.62	1.4	54.	0.0135	1.71
4.12	1.4	60.	0.0148	1.87
6.15	1.4	54.	0.0134	1.70
12.18	1.4	55.	0.0136	1.72
24.52	1.5	72.	0.0171	2.16
36.25	1.8	110.	0.0248	3.14
46.40	1.8	125.	0.0270	3.42
49.82	2.2	155.	0.0284	3.59
54.02	2.2	157.	0.0289	3.66
69.78	2.1	157.	0.0289	3.66
71.00	2.4	170.	0.0298	3.77
73.32	2.5	177.	0.0299	3.78
75.00	2.5	177.	0.0299	3.78
80.90	2.5	177.	0.0302	3.82
83.05	3.4	205.	0.0335	4.24
93.48	3.3	211.	0.0353	4.47
94.92	4.4	234.	0.0326	4.13
95.28	4.5	237.	0.0323	4.09
95.92	4.6	240.	0.0323	4.09
96.43	4.6	241.	0.0322	4.08
97.52	4.6	241.	0.0323	4.09
97.90	4.6	241.	0.0318	4.03
100.38	4.5	239.	0.0311	3.94
104.60	4.6	243.	0.0311	3.94
117.28	3.5	222.	0.0322	4.08
120.10	2.9	203.	0.0296	3.75
120.72	2.9	202.	0.0295	3.73
122.32	2.9	201.	0.0298	3.77
124.72	2.9	201.	0.0302	3.82
141.12	2.9	201.	0.0322	4.08
142.37	2.9	201.	0.0322	4.08
146.25	2.9	201.	0.0322	4.08
168.12	2.5	175.	0.0295	3.73
172.55	2.5	175.	0.0297	3.76

Table 4. (continued)

Run Time (Hours)	Pressure (MPa)	Temperature (°C)	σ (S/m)	σ/σ_{24}
199.92	2.4	148.	0.0262	3.32
237.18	2.3	125.	0.0232	2.94
241.33	2.2	100.	0.0190	2.41
244.58	2.2	99.	0.0189	2.39
250.47	2.1	99.	0.0192	2.43
264.78	1.9	74.	0.0154	1.95
267.55	1.8	59.	0.0125	1.58
285.13	1.7	52.	0.0119	1.51
308.97	1.5	25.	0.0073	0.92
309.47	1.6	50.	0.0122	1.54
309.90	1.7	76.	0.0179	2.27
310.37	1.9	100.	0.0231	2.92
310.87	2.1	125.	0.0280	3.54
311.33	2.5	150.	0.0309	3.91
311.80	2.9	175.	0.0319	4.04
312.27	3.5	200.	0.0334	4.23
312.83	4.5	226.	0.0335	4.24
313.32	4.7	241.	0.0316	4.00
334.73	3.0	206.	0.0319	4.04
340.13	3.0	152.	0.0247	3.13

Table A.5 Results of Experiment No. 11.

Date Packed:	83.12.15
Initial Analysis:	unknown
Final Analysis:	10.1 % Bitumen, 2.95 % H_2O, 87. % Sand
Density :	2.04 g/cm³
Sample Thickness:	8.2 cm
σ_{24}:	0.0112 S/m
Electrode surface:	Nickel
Sample Holder Tube:	Glass

Run Time (Hours)	Pressure (MPa)	Temperature (°C)	σ (S/m)	σ/σ_{24}
0.0	1.1	24.	0.0112	1.00
0.53	1.1	50.	0.0185	1.65
0.95	1.2	75.	0.0262	2.34
1.40	1.3	100.	0.0346	3.09
1.87	1.5	125.	0.0406	3.63
2.35	1.7	150.	0.0416	3.71
2.87	2.1	175.	0.0424	3.79
3.40	2.7	199.	0.0435	3.88
3.95	3.4	224.	0.0458	4.09
5.07	4.5	246.	0.0452	4.04
7.17	4.1	234.	0.0425	3.79
8.77	3.6	224.	0.0413	3.69
12.88	3.7	225.	0.0416	3.71
32.93	3.7	225.	0.0414	3.70
39.25	2.8	202.	0.0390	3.48
50.00	1.9	160.	0.0337	3.01
55.38	1.2	111.	0.0265	2.37
55.80	1.2	123.	0.0293	2.62
56.30	1.5	150.	0.0342	3.05
56.83	1.9	175.	0.0364	3.25
57.28	2.3	200.	0.0375	3.35
57.90	3.2	225.	0.0391	3.49
64.22	1.1	114.	0.0251	2.24
73.15	0.6	27.	0.0092	0.82

Table A.6 Results of Experiment No. 12.

Date Packed: 83.12.23
Initial Analysis: 12.3 % Bitumen, 3.9 % H_2O, 83.8 % Sand
Final Analysis: 10.3 % Bitumen, 2.7 % H_2O, 86.9 % Sand
Density : 1.99 g/cm^3
Sample Thickness: 6.9 cm
σ_{24}: 0.0085 S/m
Electrode surface: Copper
Sample Holder Tube: Glass

Run Time (Hours)	Pressure (MPa)	Temperature (°C)	σ (S/m)	σ/σ_{24}
0.0	1.1	25.	0.0089	1.05
0.52	1.0	25.	0.0090	1.06
5.50	1.1	57.	0.0163	1.92
22.78	0.9	59.	0.0169	1.99
23.88	1.0	59.	0.0170	2.00
42.78	1.1	60.	0.0173	2.04
50.83	1.1	61.	0.0174	2.05
69.55	1.2	94.	0.0257	3.02
78.53	1.2	94.	0.0261	3.07
94.27	1.2	95.	0.0261	3.07
114.48	1.1	96.	0.0262	3.08
120.57	1.4	127.	0.0301	3.54
127.37	1.4	126.	0.0293	3.45
139.28	1.4	126.	0.0287	3.38
217.00	1.4	131.	0.0278	3.27
234.70	1.6	151.	0.0282	3.32
246.57	1.6	150.	0.0275	3.24
259.10	1.6	149.	0.0269	3.16
261.45	1.6	150.	0.0269	3.16
280.63	1.2	109.	0.0240	2.82
286.80	1.0	62.	0.0153	1.80
308.87	0.9	24.	0.0086	1.01
309.08	1.0	24.	0.0086	1.01
312.65	1.1	52.	0.0140	1.65
332.05	1.1	52.	0.0140	1.65
334.82	1.1	69.	0.0178	2.09
362.78	1.1	75.	0.0194	2.28
366.83	1.4	97.	0.0245	2.88
377.63	1.3	101.	0.0250	2.94
389.43	1.3	100.	0.0246	2.89
400.53	1.3	100.	0.0245	2.88
407.40	1.3	101.	0.0244	2.87
424.38	1.3	100.	0.0242	2.85
434.98	1.3	99.	0.0238	2.80
448.15	1.3	100.	0.0240	2.82
457.03	1.3	101.	0.0239	2.81
472.73	1.2	101.	0.0239	2.81
480.05	1.2	101.	0.0238	2.80

Table 6.(Continued)

Run Time (Hours)	Pressure (MPa)	Temperature (°C)	σ (S/m)	σ/σ_{24}
499.67	1.2	101.	0.0236	2.78
526.73	1.2	100.	0.0235	2.76
568.22	1.2	100.	0.0232	2.73
575.85	0.9	25.	0.0080	0.94
579.50	0.9	25.	0.0080	0.94
594.20	0.9	24.	0.0081	0.95
617.22	0.9	24.	0.0083	0.98
641.97	0.9	24.	0.0084	0.99
665.13	0.8	24.	0.0085	1.00
696.90	0.8	24.	0.0088	1.04
718.23	0.8	24.	0.0090	1.06
736.88	0.8	24.	0.0090	1.06
808.60	0.7	24.	0.0094	1.11
808.65	0.9	24.	0.0094	1.11
809.62	1.1	79.	0.0215	2.53
810.63	1.3	121.	0.0305	3.59
811.13	1.6	146.	0.0312	3.67
811.23	1.6	151.	0.0316	3.72
811.73	2.0	172.	0.0315	3.71
812.15	2.4	190.	0.0328	3.86
812.53	3.0	212.	0.0341	4.01
813.22	3.5	225.	0.0355	4.18
813.62	4.1	236.	0.0317	3.73
813.73	4.1	239.	0.0317	3.73
814.20	4.3	240.	0.0313	3.68
815.28	4.4	241.	0.0306	3.60
821.38	3.4	217.	0.0282	3.32
834.97	1.4	119.	0.0218	2.56
839.20	1.1	75.	0.0153	1.80
905.92	0.7	24.	0.0073	0.86
1147.90	0.2	25.	0.0071	0.84

Table A.7 Results of Experiment No. 16.

The sample for this experiment was made by mixing the sand from oil sand samples with the bitumen removed by toluene extraction with distilled water.

Date Packed: 84.05.11
Initial Analysis: 0.0 % Bitumen, 3.5 % H_2O, 96.5 % Sand
Final Analysis: Unknown
Density : 1.71 g/cm^3
Sample Thickness: 7.3 cm
σ_{24}: 0.0138 S/m
Electrode surface: Copper
Sample Holder Tube: Teflon

Run Time (Hours)	Pressure (MPa)	Temperature (°C)	σ (S/m)	σ/σ_{24}
0.0	0.1	22.	0.0114	0.81
0.38	0.1	22.	0.0122	0.87
1.75	0.1	23.	0.0139	0.99
4.17	0.1	23.	0.0138	0.99
4.25	1.0	23.	0.0138	0.99
4.75	1.1	50.	0.0219	1.56
5.25	1.3	85.	0.0338	2.41
5.75	1.4	110.	0.0400	2.86
6.58	1.8	147.	0.0400	2.86
7.25	1.8	149.	0.0400	2.86
7.50	1.9	150.	0.0396	2.83
29.22	1.8	153.	0.0380	2.71
60.03	1.8	153.	0.0372	2.66
71.50	1.8	152.	0.0371	2.65
73.92	1.8	153.	0.0370	2.64
76.63	1.8	153.	0.0367	2.62
78.52	1.8	153.	0.0365	2.61
87.12	1.8	152.	0.0368	2.63
94.17	1.8	23.	0.0115	0.82
125.50	0.1	23.	0.0121	0.86
143.17	0.1	22.	0.0122	0.87

Table A.8 Results of Experiment No. 18.

Date Packed:	84.05.24
Initial Analysis:	12.9 % Bitumen, 3.5 % H_2O, 83.5 % Sand
Final Analysis:	10.2 % Bitumen, 2.8 % H_2O, 87. % Sand
Density :	2.08 g/cm³
Sample Thickness:	7.9 cm
σ_{24}:	0.0132 S/m
Electrode surface:	Copper
Sample Holder Tube:	Teflon

Run Time (Hours)	Pressure (MPa)	Temperature (°C)	σ (S/m)	σ/σ_{24}
0.0	1.0	24.	0.0132	1.00
1.00	1.1	70.	0.0270	2.05
1.55	1.3	98.	0.0340	2.58
2.67	1.5	124.	0.0399	3.02
3.88	1.7	146.	0.0403	3.05
17.25	1.7	151.	0.0375	2.84
19.92	1.7	151.	0.0375	2.84
22.42	1.7	151.	0.0373	2.83
25.60	1.7	151.	0.0372	2.82
43.72	1.7	151.	0.0358	2.71
70.93	1.6	151.	0.0346	2.62
71.58	1.7	151.	0.0346	2.62
89.25	1.7	151.	0.0342	2.59
94.75	1.7	151.	0.0344	2.61
97.82	1.7	151.	0.0345	2.61
113.33	1.7	151.	0.0347	2.63
121.42	1.7	152.	0.0350	2.65
138.42	1.7	152.	0.0344	2.61
144.00	1.7	151.	0.0344	2.61
149.28	1.0	72.	0.0223	1.69
160.50	0.9	37.	0.0152	1.15
162.97	0.8	31.	0.0135	1.02
164.60	0.8	26.	0.0115	0.87
185.37	0.8	23.	0.0117	0.89
193.30	0.8	24.	0.0121	0.92
216.15	0.8	22.	0.0120	0.91
234.92	0.7	21.	0.0119	0.90
257.30	0.7	22.	0.0118	0.89
257.62	0.7	22.	0.0121	0.92
258.47	1.3	49.	0.0192	1.45
259.10	1.4	74.	0.0269	2.04
260.00	1.5	98.	0.0346	2.62
260.70	1.7	124.	0.0400	3.03
261.38	2.1	150.	0.0382	2.89
262.48	2.5	174.	0.0377	2.86
263.13	3.1	197.	0.0388	2.94
264.00	4.1	223.	0.0426	3.23
264.93	4.6	239.	0.0456	3.45

Table 8.(Continued)

Run Time (Hours)	Pressure (MPa)	Temperature (°C)	σ (S/m)	σ/σ_{25}
280.43	4.3	239.	0.0375	2.84
285.25	4.2	239.	0.0373	2.83
289.33	4.2	239.	0.0367	2.78
296.00	4.3	239.	0.0367	2.78
304.57	4.2	239.	0.0358	2.71
313.80	4.3	239.	0.0352	2.67
328.45	4.2	239.	0.0332	2.52
329.35	4.2	239.	0.0328	2.48
335.38	4.2	239.	0.0318	2.41
337.50	4.2	239.	0.0315	2.39
352.55	4.2	239.	0.0290	2.20
358.65	4.2	239.	0.0280	2.12

Table A.9 Results of Experiment No. 19.

Date Packed: 84.05.29
Initial Analysis: 11.3 % Bitumen, 3.1 % H_2O, 85.6 % Sand
Final Analysis: 7.5 % Bitumen, 3.6 % H_2O, 88.9 % Sand
Density : 2.09 g/cm^3
Sample Thickness: 7.4 cm
σ_{24}: 0.0146 S/m
Electrode surface: Nickel
Sample Holder Tube: Teflon

Run Time (Hours)	Pressure (MPa)	Temperature (°C)	σ (S/m)	σ/σ_{24}
0.0	0.1	25.	0.0149	1.02
0.17	1.0	25.	0.0149	1.02
1.63	1.0	49.	0.0253	1.73
2.15	1.1	73.	0.0400	2.74
2.73	1.3	99.	0.0506	3.47
3.33	1.5	125.	0.0601	4.12
3.97	1.8	150.	0.0643	4.40
4.58	2.1	173.	0.0685	4.69
5.28	2.7	199.	0.0692	4.74
6.00	3.9	224.	0.0645	4.42
6.47	4.1	237.	0.0594	4.07
17.88	4.3	240.	0.0515	3.53
18.22	4.3	240.	0.0510	3.49
20.02	4.3	240.	0.0501	3.43
21.80	4.3	240.	0.0489	3.35
42.55	4.3	240.	0.0426	2.92
45.53	4.3	240.	0.0417	2.86
48.08	4.3	240.	0.0411	2.82
50.45	4.3	240.	0.0403	2.76
73.42	4.1	37.	0.0135	0.92
92.18	0.1	21.	0.0097	0.66
114.58	0.1	22.	0.0097	0.66

Table A.10 Results of Experiment No. 21.

Date Packed:	84.06.12
Initial Analysis:	9.1 % Bitumen, 5.2 % H_2O, 85.7 % Sand
Final Analysis:	8.6 % Bitumen, 5.7 % H_2O, 85.7 % Sand
Density:	2.10 g/cm^3
Sample Thickness:	8.0 cm
σ_{24}:	0.0138 S/m
Electrode surface:	Nickel
Sample Holder Tube:	Teflon

Run Time (Hours)	Pressure (MPa)	Temperature (°C)	σ (S/m)	σ/σ_{24}
0.0	1.0	24.	0.0138	1.00
1.12	1.3	98.	0.0416	3.01
2.12	1.8	147.	0.0506	3.67
3.25	1.8	149.	0.0510	3.70
5.78	1.8	151.	0.0514	3.72
7.80	1.8	151.	0.0513	3.72
14.90	1.8	151.	0.0514	3.72
24.22	1.8	151.	0.0497	3.60
26.28	1.8	151.	0.0491	3.56
34.30	1.8	151.	0.0476	3.45
48.38	1.8	151.	0.0450	3.26
56.75	1.8	151.	0.0441	3.20
72.35	1.8	151.	0.0440	3.19
75.80	1.8	151.	0.0437	3.17
81.20	1.8	151.	0.0435	3.15
100.08	1.8	151.	0.0429	3.11
128.35	1.8	151.	0.0431	3.12
143.78	1.8	151.	0.0433	3.14
144.60	1.8	151.	0.0430	3.12
153.10	1.0	27.	0.0162	1.17
168.10	0.1	22.	0.0150	1.08

Table A.11 Results of Experiment No. 22.

Date Packed: 84.06.19
Initial Analysis: 9.6 % Bitumen, 4.3 % H_2O, 86.1 % Sand
Final Analysis: 9.6 % Bitumen, 4.3 % H_2O, 86.1 % Sand
Density : 2.02 g/cm³
Sample Thickness: 7.4 cm
σ_{24}: 0.0115 S/m
Electrode surface: Nickel
Sample Holder Tube: Teflon

Run Time (Hours)	Pressure (MPa)	Temperature (°C)	σ (S/m)	σ/σ_{24}
0.0	1.0	24.	**0.0218	****
1.35	1.3	97.	0.0326	2.83
2.65	1.8	148.	0.0376	3.27
3.15	1.8	149.	0.0376	3.27
18.63	1.8	151.	0.0375	3.26
22.23	1.8	151.	0.0377	3.28
26.28	1.8	151.	0.0371	3.23
43.00	1.8	150.	0.0349	3.03
50.25	1.8	150.	0.0341	2.97
66.97	1.8	150.	0.0328	2.85
74.53	1.8	150.	0.0327	2.84
94.47	1.8	150.	0.0326	2.83
120.48	1.8	150.	0.0337	2.93
139.03	1.8	150.	0.0331	2.88
147.10	1.8	151.	0.0326	2.83
162.70	1.0	24.	0.0115	1.00

** It is believed that this measurement was incorrect. The results were normalized using the final electrical conductivity measurement.

Table A.12 Results of Experiment No. 23.

Date Packed: 84.06.21
Initial Analysis: 9.3 % Bitumen, 5.0 % H_2O, 85.7 % Sand
Final Analysis: 9.1 % Bitumen, 5.0 % H_2O, 85.9 % Sand
Density : 2.04 g/cm^3
Sample Thickness: 7.9 cm
σ_{24}: 0.0114 S/m
Electrode surface: Copper
Sample Holder Tube: Teflon

Run Time (Hours)	Pressure (MPa)	Temperature (°C)	σ (S/m)	σ/σ_{24}
0.0	1.0	25.	0.0117	1.03
1.28	1.3	98.	0.0347	3.04
2.28	1.8	147.	0.0437	3.83
5.70	1.9	151.	0.0456	4.00
22.30	1.9	151.	0.0452	3.96
29.95	1.9	150.	0.0435	3.82
49.90	1.9	150.	0.0404	3.54
75.92	1.9	150.	0.0386	3.39
94.42	1.9	150.	0.0382	3.35
102.55	1.9	150.	0.0377	3.31
118.15	1.9	150.	0.0372	3.26
126.73	1.9	150.	0.0368	3.23
141.78	1.9	150.	0.0364	3.19
150.77	1.9	150.	0.0360	3.16
166.15	1.9	150.	0.0357	3.13
172.87	1.9	150.	0.0353	3.10
174.30	1.9	150.	0.0352	3.09
190.40	1.9	150.	0.0348	3.05
198.73	1.9	150.	0.0339	2.97
218.08	1.9	150.	0.0332	2.91
285.82	0.1	21.	0.0103	0.90

Table A.13 Results of Experiment No. 24.

Date Packed:	84.06.27
Initial Analysis:	9.5 % Bitumen, 4.3 % H_2O, 86.2 % Sand
Final Analysis:	9.4 % Bitumen, 3.8 % H_2O, 86.8 % Sand
Density :	2.09 g/cm^3
Sample Thickness:	7.0 cm
σ_{24}:	0.0093 S/m
Electrode surface:	Nickel
Sample Holder Tube:	Teflon

Run Time (Hours)	Pressure (MPa)	Temperature (°C)	σ (S/m)	σ/σ_{24}
0.0	1.0	25.	0.0095	1.02
1.47	1.3	100.	0.0278	2.99
2.42	1.8	148.	0.0328	3.53
4.12	2.9	198.	0.0375	4.03
4.52	2.9	200.	0.0367	3.95
4.95	2.9	200.	0.0358	3.85
5.83	2.9	200.	0.0353	3.80
6.67	2.9	200.	0.0347	3.73
7.25	2.9	200.	0.0342	3.68
22.70	2.9	200.	0.0315	3.39
28.80	2.9	200.	0.0312	3.35
30.83	2.9	200.	0.0309	3.32
46.72	2.9	200.	0.0310	3.33
55.07	2.9	200.	0.0307	3.30
74.40	2.9	200.	0.0310	3.33
142.33	0.9	21.	0.0092	0.99

Table A.14 Results of Experiment No. 25.

Date Packed:	84.07.03
Initial Analysis:	9.7 % Bitumen, 3.4 % H_2O, 86.9 % Sand
Final Analysis:	9.1 % Bitumen, 3.8 % H_2O, 87.1 % Sand
Density :	2.09 g/cm^3
Sample Thickness:	8.2 cm
σ_{24}:	0.0087 S/m
Electrode surface:	Copper
Sample Holder Tube:	Teflon

Run Time (Hours)	Pressure (MPa)	Temperature (°C)	σ (S/m)	σ/σ_{24}
0.0	1.0	24.	0.0087	1.00
1.25	1.3	98.	0.0211	2.43
2.35	1.8	149.	0.0252	2.90
3.60	2.9	197.	0.0303	3.48
4.05	2.9	199.	0.0296	3.40
17.73	2.9	201.	0.0267	3.07
20.32	2.9	201.	0.0264	3.03
23.78	2.9	201.	0.0260	2.99
26.13	2.8	201.	0.0258	2.97
42.30	2.8	200.	0.0254	2.92
50.30	2.8	200.	0.0254	2.92
66.18	2.8	200.	0.0257	2.95
72.65	2.8	200.	0.0253	2.91
94.60	0.8	21.	0.0084	0.97

Table A.15 Results of Experiment No. 26.

Date Packed:	84.07.04
Initial Analysis:	11.5 % Bitumen, 4.5 % H_2O, 84.0 % Sand
Final Analysis:	10.0 % Bitumen, 4.5 % H_2O, 85.5 % Sand
Density :	2.11 g/cm³
Sample Thickness:	8.2 cm
σ_{24}:	0.0168 S/m
Electrode surface:	Nickel
Sample Holder Tube:	Teflon

Run Time (Hours)	Pressure (MPa)	Temperature (°C)	σ (S/m)	σ/σ_{24}
0.0	1.0	23.	0.0165	0.98
1.08	1.3	98.	0.0473	2.82
2.10	1.9	149.	0.0577	3.43
8.18	1.9	151.	0.0569	3.39
24.27	1.9	150.	0.0564	3.36
32.25	1.9	150.	0.0556	3.31
48.17	1.9	150.	0.0540	3.21
54.65	1.9	150.	0.0530	3.15
76.38	1.9	150.	0.0515	3.07
101.77	1.9	151.	0.0503	2.99
119.57	1.9	151.	0.0496	2.95
128.72	1.9	151.	0.0491	2.92
143.78	1.9	151.	0.0486	2.89
151.63	1.9	151.	0.0483	2.87
167.98	1.9	151.	0.0480	2.86
176.28	1.9	151.	0.0474	2.82
191.28	1.9	151.	0.0473	2.82
216.13	1.9	151.	0.0466	2.77
224.57	1.9	151.	0.0469	2.79
244.17	1.9	151.	0.0458	2.73
269.93	1.9	151.	0.0443	2.64
287.28	0.5	24.	0.0136	0.81

Table A.16 Results of Experiment No. 28.

Date Packed:	84.07.12
Initial Analysis:	9.6 % Bitumen, 3.7 % H_2O, 86.7 % Sand
Final Analysis:	7.8 % Bitumen, 3.7 % H_2O, 88.5 % Sand
Density :	2.04 g/cm^3
Sample Thickness:	7.9 cm
σ_{24}:	0.0067 S/m
Electrode surface:	Gold
Sample Holder Tube:	Teflon

Run Time (Hours)	Pressure (MPa)	Temperature (°C)	σ (S/m)	σ/σ_{24}
0.0	1.0	29.	0.0075	1.12
1.15	1.3	100.	0.0209	3.12
2.12	1.8	149.	0.0257	3.84
18.58	1.8	151.	0.0259	3.87
22.77	1.8	151.	0.0255	3.81
25.45	1.8	151.	0.0252	3.76
27.10	1.8	151.	0.0250	3.73
46.82	1.8	151.	0.0235	3.51
72.45	1.8	151.	0.0225	3.36
89.95	1.8	151.	0.0222	3.31
98.35	1.8	151.	0.0220	3.28
113.95	1.8	151.	0.0219	3.27
123.08	1.8	151.	0.0217	3.24
138.57	1.8	151.	0.0215	3.21
146.33	1.8	151.	0.0215	3.21
161.82	1.0	22.	0.0066	0.99

Table A.17 Results of Experiment No. 29.

Date Packed:	84.07.17
Initial Analysis:	10.9 % Bitumen, 5.0 % H_2O, 84.1 % Sand
Final Analysis:	11.2 % Bitumen, 4.4 % H_2O, 84.4 % Sand
Density :	2.08 g/cm^3
Sample Thickness:	7.8 cm
σ_{24}:	0.0131 S/m
Electrode surface:	Nickel
Sample Holder Tube:	Teflon

Run Time (Hours)	Pressure (MPa)	Temperature (°C)	σ (S/m)	σ/σ_{24}
0.0	1.0	25.	0.0134	1.02
1.02	1.3	97.	0.0360	2.75
1.97	1.8	149.	0.0464	3.54
3.52	2.9	199.	0.0495	3.78
4.55	2.9	200.	0.0507	3.87
6.43	2.9	200.	0.0503	3.84
7.22	2.9	200.	0.0490	3.74
8.12	2.9	200.	0.0481	3.67
8.87	2.9	200.	0.0475	3.63
24.35	2.9	200.	0.0445	3.40
27.58	2.9	200.	0.0441	3.37
30.62	2.9	200.	0.0442	3.37
31.08	2.9	200.	0.0440	3.36
32.12	2.9	200.	0.0440	3.36
47.75	2.9	200.	0.0437	3.34
53.92	2.9	200.	0.0435	3.32
56.53	2.9	200.	0.0432	3.30
71.73	2.9	200.	0.0434	3.31
80.92	2.9	200.	0.0431	3.29
100.28	0.7	22.	0.0099	0.76

Table A.18 Results of Experiment No. 30.

Date Packed: 84.07.20
Initial Analysis: 10.2 % Bitumen, 3.6 % H_2O, 86.2 % Sand
Final Analysis: 9.5 % Bitumen, 3.8 % H_2O, 86.7 % Sand
Density : 1.98 g/cm³
Sample Thickness: 7.4 cm
σ_{24}: 0.0080 S/m
Electrode surface: Gold
Sample Holder Tube: Teflon

Run Time (Hours)	Pressure (MPa)	Temperature (°C)	σ (S/m)	σ/σ_{24}
0.0	1.0	24.	0.0080	1.00
1.47	1.3	99.	0.0251	3.14
2.87	1.8	147.	0.0315	3.94
4.48	2.8	197.	0.0363	4.54
5.72	4.4	237.	0.0356	4.45
6.32	4.5	238.	0.0348	4.35
6.90	4.5	239.	0.0343	4.29
7.40	4.5	239.	0.0340	4.25
8.13	4.5	239.	0.0339	4.24
8.90	4.6	239.	0.0335	4.19
14.57	4.6	239.	0.0328	4.10
28.28	4.5	239.	0.0332	4.15
55.17	4.4	239.	0.0333	4.16
71.77	4.4	239.	0.0329	4.11
95.77	0.1	23.	0.0075	0.94

Table A.19 Results of Experiment No. 31.

Date Packed: 84.07.24
Initial Analysis: 12.0 % Bitumen, 4.4 % H_2O, 83.6 % Sand
Final Analysis: 13.4 % Bitumen, 4.5 % H_2O, 82.1 % Sand
Density : 2.08 g/cm^3
Sample Thickness: 8.4 cm
σ_{24}: 0.0142 S/m
Electrode surface: Gold
Sample Holder Tube: Teflon

Run Time (Hours)	Pressure (MPa)	Temperature (°C)	σ (S/m)	σ/σ_{24}
0.0	1.0	25.	0.0145	1.02
1.03	1.3	98.	0.0384	2.70
1.90	1.7	148.	0.0501	3.53
2.92	2.8	198.	0.0501	3.53
3.60	2.9	199.	0.0528	3.72
4.27	2.9	200.	0.0539	3.80
6.10	2.9	200.	0.0532	3.75
7.10	2.9	200.	0.0524	3.69
8.12	2.9	200.	0.0519	3.65
9.08	2.9	200.	0.0514	3.62
23.90	2.9	200.	0.0493	3.47
27.98	2.9	200.	0.0484	3.41
30.53	2.9	200.	0.0481	3.39
32.07	2.9	200.	0.0478	3.37
47.90	2.9	200.	0.0477	3.36
56.78	2.9	200.	0.0475	3.35
71.87	2.9	200.	0.0475	3.35
95.67	0.5	27.	0.0125	0.88

Table A.20 Results of Experiment No. 32.

Date Packed: 84.07.26
Initial Analysis: 10.4 % Bitumen, 5.8 % H_2O, 83.8 % Sand
Final Analysis: 11.1 % Bitumen, 5.6 % H_2O, 83.4 % Sand
Density : 2.08 g/cm^3
Sample Thickness: 7.9 cm
σ_{24}: 0.0160 S/m
Electrode surface: Nickel
Sample Holder Tube: Teflon

Run Time (Hours)	Pressure (MPa)	Temperature (°C)	σ (S/m)	σ/σ_{24}
0.0	1.0	28.	0.0175	1.09
1.05	1.3	97.	0.0470	2.94
2.05	1.8	149.	0.0660	4.12
3.03	2.9	199.	0.0655	4.09
4.27	4.5	237.	0.0373	2.33
4.78	4.6	238.	0.0346	2.16
5.90	4.6	239.	0.0335	2.09
6.38	4.6	239.	0.0334	2.09
6.93	4.6	239.	0.0333	2.08
7.78	4.6	239.	0.0335	2.09
8.77	4.6	239.	0.0336	2.10
23.97	4.6	239.	0.0374	2.34
24.55	4.6	239.	0.0374	2.34
25.40	4.6	239.	0.0375	2.34
27.12	4.6	239.	0.0377	2.36
28.05	4.6	239.	0.0378	2.36
29.45	4.6	239.	0.0382	2.39
56.63	4.6	239.	0.0431	2.69
95.65	4.6	239.	0.0465	2.91
120.15	1.0	28.	0.0116	0.73

Table A.21 Results of Experiment No. 33.

Date Packed: 84.07.30
Initial Analysis: 4.8 % Bitumen, 8.5 % H_2O, 86.7 % Sand
Final Analysis: 5.1 % Bitumen, 8.4 % H_2O, 86.5 % Sand
Density : 2.07 g/cm^3
Sample Thickness: 8.3 cm
σ_{24}: 0.0607 S/m
Electrode surface: Gold
Sample Holder Tube: Teflon

Run Time (Hours)	Pressure (MPa)	Temperature (°C)	σ (S/m)	σ/σ_{24}
0.0	1.0	27.	0.0649	1.07
1.18	1.3	99.	0.1840	3.03
2.53	1.8	150.	0.2275	3.75
3.08	1.8	150.	0.2275	3.75
17.83	1.8	150.	0.2216	3.65
21.17	1.8	150.	0.2201	3.63
23.63	1.8	150.	0.2172	3.58
41.77	1.8	150.	0.2030	3.34
65.40	1.8	150.	0.1948	3.21
117.72	1.8	150.	0.1891	3.12
143.28	1.8	150.	0.1877	3.09
185.83	1.8	150.	0.1854	3.05
192.62	1.8	150.	0.1849	3.05
209.82	0.8	24.	0.0549	0.90

Table A.22 Results of Experiment No. 34.

Date Packed: 84.08.08
Initial Analysis: 13.4 % Bitumen, 3.6 % H_2O, 83.0 % Sand
Final Analysis: 12.9 % Bitumen, 3.7 % H_2O, 83.4 % Sand
Density : 2.03 g/cm^3
Sample Thickness: 6.6 cm
σ_{24}: 0.0113 S/m
Electrode surface: Gold
Sample Holder Tube: Teflon

Run Time (Hours)	Pressure (MPa)	Temperature (°C)	σ (S/m)	σ/σ_{24}
0.0	1.0	24.	0.0113	1.00
0.98	1.3	99.	0.0323	2.86
1.77	1.8	148.	0.0399	3.53
2.55	2.7	197.	0.0441	3.90
3.82	4.3	238.	0.0466	4.12
4.58	4.4	239.	0.0456	4.04
5.83	4.4	239.	0.0442	3.91
6.78	4.4	239.	0.0432	3.82
7.85	4.4	239.	0.0428	3.79
8.35	4.4	239.	0.0424	3.75
23.58	4.4	239.	0.0398	3.52
25.53	4.4	239.	0.0394	3.49
27.18	4.4	239.	0.0390	3.45
30.13	4.4	239.	0.0388	3.43
47.65	4.4	239.	0.0378	3.35
48.83	4.4	239.	0.0373	3.30
50.60	4.4	239.	0.0371	3.28
53.92	4.4	239.	0.0369	3.27
56.15	4.4	239.	0.0365	3.23
76.82	4.4	239.	0.0361	3.19
100.90	4.4	239.	0.0344	3.04
121.60	0.1	31.	0.0073	0.65

Table A.23 Results of Experiment No. 35

Date Packed: 84.08.13
Initial Analysis: 5.4 % Bitumen, 7.9 % H_2O, 86.7 % Sand
Final Analysis: 5.2 % Bitumen, 8.2 % H_2O, 86.6 % Sand
Density : 2.15 g/cm^3
Sample Thickness: 7.4 cm
σ_{24}: 0.085 S/m
Electrode surface: Nickel
Sample Holder Tube: Teflon

Run Time (Hours)	Pressure (MPa)	Temperature (°C)	σ (S/m)	σ/σ_{24}
0.0	1.0	28.	0.0931	1.09
0.95	1.3	97.	0.2531	2.97
2.02	1.8	149.	0.2982	3.50
2.60	1.9	151.	0.2957	3.47
17.77	1.9	150.	0.2851	3.34
20.62	1.9	150.	0.2817	3.30
24.53	1.9	150.	0.2788	3.27
26.28	1.9	150.	0.2772	3.25
41.67	1.9	150.	0.2584	3.03
44.73	1.9	150.	0.2561	3.00
47.73	1.9	150.	0.2528	2.96
50.27	1.9	150.	0.2515	2.95
65.83	1.9	150.	0.2501	2.93
68.92	1.9	150.	0.2473	2.90
72.45	1.9	150.	0.2459	2.88
74.45	1.9	150.	0.2454	2.88
89.63	1.9	150.	0.2455	2.88
92.68	1.9	150.	0.2450	2.87
95.83	1.9	150.	0.2438	2.86
97.78	1.9	150.	0.2430	2.85
117.43	1.9	150.	0.2430	2.85
142.87	1.9	150.	0.2420	2.84
161.58	1.0	21.	0.0714	0.84

Table A.24 Results of Experiment No. 36.

Date Packed:	84.08.21
Initial Analysis:	13.4 % Bitumen, 3.3 % H_2O, 83.3 % Sand
Final Analysis:	7.9 % Bitumen, 3.5 % H_2O, 88.6 % Sand
Density :	2.09 g/cm^3
Sample Thickness:	7.8 cm
σ_{24}:	0.0143 S/m
Electrode surface:	Nickel
Sample Holder Tube:	Teflon

Run Time (Hours)	Pressure (MPa)	Temperature (°C)	σ (S/m)	σ/σ_{24}
0.0	1.0	21.	0.0133	0.93
0.98	1.3	98.	0.0406	2.84
1.88	1.8	149.	0.0500	3.50
2.75	2.8	198.	0.0545	3.81
3.93	4.3	240.	0.0527	3.69
4.25	4.3	240.	0.0515	3.60
4.78	4.3	240.	0.0503	3.52
6.45	4.3	240.	0.0479	3.35
7.00	4.3	240.	0.0473	3.31
8.10	4.3	240.	0.0460	3.22
9.23	4.3	240.	0.0449	3.14
23.85	4.3	240.	0.0414	2.90
25.98	4.3	240.	0.0409	2.86
27.98	4.3	240.	0.0407	2.85
30.20	4.3	240.	0.0403	2.82
32.02	4.3	240.	0.0400	2.80
47.90	4.3	240.	0.0393	2.75
51.88	4.3	240.	0.0389	2.72
56.08	4.3	240.	0.0384	2.69
167.98	0.7	20.	0.0075	0.52

Table A.25 Results of Experiment No. 37.

Date Packed: 84.08.29
Initial Analysis: 5.2 % Bitumen, 8.4 % H_2O, 86.4 % Sand
Final Analysis: 3.8 % Bitumen, 8.5 % H_2O, 87.7 % Sand
Density : 2.09 g/cm³
Sample Thickness: 7.6 cm
σ_{24}: 0.0667 S/m
Electrode surface: Gold
Sample Holder Tube: Teflon

Run Time (Hours)	Pressure (MPa)	Temperature (°C)	σ (S/m)	σ/σ_{24}
0.0	1.0	20.	0.0605	0.91
1.02	1.3	99.	0.2064	3.09
1.87	1.8	149.	0.2498	3.75
2.78	3.0	199.	0.2383	3.57
3.58	3.0	200.	0.2206	3.31
4.77	3.0	200.	0.1993	2.99
5.58	3.0	200.	0.1963	2.94
7.03	3.0	200.	0.1935	2.90
23.92	3.0	200.	0.1863	2.79
27.60	3.0	200.	0.1844	2.76
32.08	3.0	200.	0.1830	2.74
47.88	3.0	200.	0.1835	2.75
51.72	3.0	200.	0.1824	2.73
56.10	3.0	200.	0.1825	2.74
77.00	3.0	200.	0.1832	2.75
95.95	0.8	19.	0.0494	0.74

Table A.26 Results of Experiment No. 38.

Date Packed: 84.09.05
Initial Analysis: 5.7 % Bitumen, 8.9 % H_2O, 85.4 % Sand
Final Analysis: 5.2 % Bitumen, 8.7 % H_2O, 86.1 % Sand
Density : 2.07 g/cm³
Sample Thickness: 8.4 cm
σ_{24}: 0.0789 S/m
Electrode surface: Nickel
Sample Holder Tube: Teflon

Run Time (Hours)	Pressure (MPa)	Temperature (°C)	σ (S/m)	σ/σ_{24}
0.0	1.0	24.	0.0789	1.00
0.97	1.3	99.	0.2446	3.10
2.03	1.7	148.	0.3001	3.80
3.47	3.0	200.	0.2740	3.47
3.92	3.0	200.	0.2614	3.31
4.43	3.0	200.	0.2378	3.01
5.25	3.0	200.	0.2250	2.85
6.22	3.0	200.	0.2185	2.77
7.47	3.0	200.	0.2133	2.70
7.83	3.0	200.	0.2128	2.70
23.75	3.0	200.	0.2043	2.59
28.55	3.0	200.	0.2024	2.57
51.30	3.0	200.	0.2017	2.56
77.23	3.0	200.	0.2025	2.57
102.63	1.0	25.	0.0621	0.79
313.57	0.7	24.	0.0637	0.81

Table A.27 Results of Experiment No. 39.

Date Packed: 84.09.09
Initial Analysis: 11.7 % Bitumen, 3.9 % H_2O, 84.4 % Sand
Final Analysis: 11.0 % Bitumen, 4.0 % H_2O, 85.0 % Sand
Density : 2.06 g/cm^3
Sample Thickness: 7.4 cm
σ_{24}: 0.0164 S/m
Electrode surface: Gold
Sample Holder Tube: Teflon

Run Time (Hours)	Pressure (MPa)	Temperature (°C)	σ (S/m)	σ/σ_{24}
0.0	1.0	24.	0.0164	1.00
0.45	1.1	47.	0.0258	1.57
1.52	1.4	101.	0.0480	2.93
4.38	1.4	102.	0.0488	2.98
17.10	1.4	102.	0.0486	2.96
19.05	1.4	101.	0.0483	2.95
23.12	1.4	101.	0.0486	2.96
39.58	1.4	101.	0.0486	2.96
46.10	1.4	101.	0.0486	2.96
64.70	1.4	101.	0.0486	2.96
88.05	1.4	101.	0.0485	2.96
95.65	1.4	100.	0.0482	2.94
113.63	1.4	101.	0.0483	2.95
142.62	1.4	101.	0.0485	2.96
159.60	1.4	101.	0.0480	2.93
165.42	1.4	101.	0.0482	2.94
183.55	1.4	101.	0.0482	2.94
194.48	1.4	101.	0.0482	2.94
208.12	1.4	101.	0.0481	2.93
231.45	1.4	101.	0.0479	2.92
256.33	1.4	102.	0.0484	2.95
327.92	1.4	101.	0.0480	2.93
351.63	1.4	102.	0.0480	2.93
375.50	1.4	101.	0.0475	2.90
399.45	1.4	101.	0.0476	2.90
424.70	1.3	102.	0.0471	2.87
473.02	1.3	102.	0.0468	2.85
498.37	1.2	101.	0.0472	2.88
519.65	1.2	102.	0.0468	2.85
524.93	1.0	54.	0.0270	1.65
546.80	0.9	25.	0.0167	1.02

Table A.28 Results of Experiment No. 40.

The sample used in this experiment was a mixture of clean silica sand, salt, and distilled water.

Date Packed: 84.09.24
Initial Analysis: 1.0 % NaCl, 4.0 % H_2O, 95.0 % Sand
Density : 1.82 g/cm^3
Sample Thickness: 8.8 cm
σ_{22}: 0.202 S/m
Electrode surface: Gold
Sample Holder Tube: Teflon

Run Time (Hours)	Pressure (MPa)	Temperature (°C)	σ (S/m)	σ/σ_{22}
0.0	1.0	22.	0.2000	0.99
1.70	1.3	101.	0.5100	2.52
2.97	1.6	149.	0.7000	3.47
4.58	2.6	200.	0.8200	4.06
5.10	2.7	201.	0.8440	4.18
5.87	2.6	200.	0.8300	4.11
7.02	2.5	199.	0.8300	4.11
7.97	2.7	200.	0.8300	4.11
9.13	2.6	200.	0.8300	4.11
12.32	2.5	199.	0.8350	4.13
23.88	2.5	199.	0.8320	4.12
27.07	2.5	200.	0.8300	4.11
29.55	2.5	200.	0.8300	4.11
32.05	2.5	200.	0.8300	4.11
47.80	2.5	200.	0.8400	4.16
52.75	2.5	200.	0.8300	4.11
73.08	2.5	200.	0.8300	4.11
121.37	2.5	200.	0.8400	4.16
146.75	2.5	200.	0.8850	4.38
168.02	2.5	200.	0.8700	4.31
173.20	1.1	101.	0.5350	2.65
195.17	0.8	26.	0.2150	1.06

Table A.29 Results of Experiment No. 42.

Date Packed:	84.10.22
Initial Analysis:	14.2 % Bitumen, 1.3 % H_2O, 84.5 % Sand
Final Analysis:	13.9 % Bitumen, 1.5 % H_2O, 84.6 % Sand
Density :	2.01 g/cm^3
Sample Thickness:	7.7 cm
σ_{24}:	0.00065 S/m
Electrode surface:	Gold
Sample Holder Tube:	Teflon

Run Time (Hours)	Pressure (MPa)	Temperature (°C)	σ (S/m)	σ/σ_{24}
0.0	0.0	26.	0.00022	0.34
0.07	1.0	26.	0.00021	0.32
0.15	1.0	26.	0.00022	0.33
1.90	1.4	99.	0.00157	2.42
2.18	1.4	101.	0.00163	2.51
4.10	1.9	155.	0.00370	5.69
8.10	1.9	152.	0.00390	6.00
19.27	1.8	151.	0.00445	6.85
21.68	1.8	151.	0.00444	6.83
23.30	1.8	151.	0.00441	6.78
31.87	1.8	151.	0.00444	6.83
41.93	1.8	151.	0.00470	7.23
44.70	1.8	151.	0.00455	7.00
45.90	1.8	151.	0.00451	6.94
50.33	1.8	151.	0.00445	6.85
54.98	1.8	151.	0.00444	6.83
65.90	1.8	151.	0.00439	6.75
69.28	1.8	151.	0.00440	6.77
72.65	1.8	150.	0.00430	6.62
76.32	1.8	151.	0.00432	6.65
78.78	1.8	151.	0.00430	6.62
90.08	1.8	151.	0.00430	6.62
95.58	1.8	151.	0.00434	6.68
101.83	1.8	151.	0.00428	6.58
112.90	1.8	150.	0.00443	6.82
116.78	1.7	151.	0.00435	6.69
122.82	0.9	25.	0.00063	0.97
145.52	0.9	23.	0.00063	0.97
162.05	0.9	23.	0.00065	1.00

Table A.30 Results of Experiment No. 43.

Date Packed: 84.10.25
Initial Analysis: 4.6 % Bitumen, 9.5 % H_2O, 86.0 % Sand
Final Analysis: 4.1 % Bitumen, 7.9 % H_2O, 88.0 % Sand
Density : 1.99 g/cm³
Sample Thickness: 8.2 cm
σ_{24}: 0.065 S/m
Electrode surface: Gold
Sample Holder Tube: Teflon

Run Time (Hours)	Pressure (MPa)	Temperature (°C)	σ (S/m)	σ/σ_{24}
0.0	0.0	25.	0.06650	1.02
0.08	1.0	25.	0.06650	1.02
1.13	1.3	101.	0.20100	3.09
3.02	4.4	239.	0.19200	2.95
3.57	4.5	239.	0.18400	2.83
4.13	4.5	239.	0.18100	2.78
4.93	4.5	239.	0.17900	2.75
5.87	4.5	239.	0.17800	2.74
17.43	4.6	239.	0.17900	2.75
19.98	4.6	239.	0.17800	2.74
22.85	4.6	239.	0.17800	2.74
29.17	4.6	239.	0.17800	2.74
40.27	4.6	239.	0.17900	2.75
44.10	4.6	239.	0.17900	2.75
50.07	4.6	239.	0.17900	2.75
72.62	4.6	239.	0.18300	2.82
93.13	1.1	25.	0.04170	0.64
97.53	1.1	24.	0.04100	0.63
99.35	1.1	24.	0.04100	0.63
99.55	0.0	24.	0.04240	0.65
113.20	0.0	24.	0.04360	0.67
113.92	0.0	24.	0.04100	0.63

Table A.31 Results of Experiment No. 44.

Date Packed: 84.10.29
Initial Analysis: 13.7 % Bitumen, 2.4 % H_2O, 83.9 % Sand
Final Analysis: 11.8 % Bitumen, 2.2 % H_2O, 86.0 % Sand
Density : 1.91 g/cm³
Sample Thickness: 7.3 cm
σ_{24}: 0.00128 S/m
Electrode surface: Gold
Sample Holder Tube: Teflon

Run Time (Hours)	Pressure (MPa)	Temperature (°C)	σ (S/m)	σ/σ_{24}
0.0	0.0	24.	0.00025	0.20
0.25	1.0	24.	0.00024	0.19
2.00	1.4	100.	0.00096	0.75
2.18	1.4	104.	0.00151	1.18
2.58	1.4	110.	0.00171	1.34
2.73	1.4	110.	0.00175	1.37
2.92	1.4	111.	0.00240	1.88
3.50	1.4	111.	0.00248	1.94
3.68	1.4	111.	0.00249	1.95
5.80	2.9	199.	0.00599	4.68
6.22	3.0	201.	0.00627	4.90
9.38	3.0	200.	0.00694	5.42
19.45	2.8	200.	0.00754	5.89
22.12	2.8	200.	0.00752	5.88
24.60	2.8	200.	0.00752	5.88
27.07	2.8	200.	0.00744	5.81
29.85	2.8	200.	0.00739	5.77
43.37	2.7	200.	0.00696	5.44
46.75	2.7	200.	0.00692	5.41
50.05	2.7	200.	0.00691	5.40
53.43	2.7	200.	0.00687	5.37
67.37	2.7	200.	0.00669	5.23
70.53	2.7	200.	0.00667	5.21
72.47	2.7	200.	0.00668	5.22
77.63	2.7	200.	0.00668	5.22
79.57	2.7	200.	0.00660	5.16
91.33	2.7	200.	0.00660	5.16
94.10	2.7	200.	0.00663	5.18
98.35	0.9	53.	0.00191	1.49
169.03	0.8	23.	0.00125	0.98

Table A.32 Results of Experiment No. 45.

Date Packed:	84.10.30
Initial Analysis:	15.4 % Bitumen, 0.9 % H_2O, 83.7 % Sand
Final Analysis:	12.5 % Bitumen, 1.0 % H_2O, 86.5 % Sand
Density :	1.93 g/cm³
Sample Thickness:	8.0 cm
σ_{24}:	0.0008 S/m
Electrode surface:	Gold
Sample Holder Tube:	Teflon

Run Time (Hours)	Pressure (MPa)	Temperature (°C)	σ (S/m)	σ/σ_{24}
0.0	1.0	24.	0.00026	0.32
3.45	1.1	52.	0.00118	1.47
17.67	1.7	102.	0.00152	1.90
20.40	4.3	237.	0.00547	6.84
20.85	4.4	238.	0.00558	6.98
21.57	4.4	239.	0.00556	6.95
22.73	4.5	239.	0.00574	7.18
23.68	4.5	239.	0.00578	7.22
25.45	4.5	239.	0.00576	7.20
27.15	4.5	239.	0.00571	7.14
41.10	4.6	239.	0.00495	6.19
44.18	4.6	239.	0.00478	5.97
46.17	4.6	239.	0.00471	5.89
51.27	4.6	239.	0.00451	5.64
53.28	4.6	239.	0.00435	5.44
65.05	4.6	239.	0.00383	4.79
92.92	4.7	239.	0.00293	3.66
120.17	4.6	239.	0.00222	2.77
137.30	4.6	239.	0.00189	2.36
161.92	0.1	22.	0.00077	0.96

Appendix II. Details of the Computer Simulation Run used to Compare the Old and New Conductivity Equations

The simulation run described in this appendix was developed in a paper by Hiebert, Vermeulen, Chute and Capjack entitled "Numerical Simulation Results for the Electrical Heating of Athabasca Oil Sand Formations" (1986). The paper is extensively quoted in this appendix.

The Athabasca oil sands cover a large area and the reservoir lithology can vary widely even over a short distance. Information on the reservoir used in this simulation, together with it's electrical properties and lithology was obtained from the work of H.W. Nelson and R.P. Glaister, ("Subsurface Enviromental Facies and Reservoir Relationships of the McMurray Oil Sand, Northeastern Alberta", Bull. Can. Petroleum Geology, V. 26, pp. 177-207) and well logs obtained from the Energy Resources Conservation Board of Alberta.

The thermal properties for the reservoir were obtained from the work of M.R. Cervenan, F.E. Vermeulen, and F.S. Chute ("Thermal conductivity and specific heat of oil sand samples", Can. J. Earth Sci., V. 18, 1981, pp 926-931) The electrical conductivity was assumed first to vary linearly with temperature change. A second, repeat, simulation run was later done where the conductivity varied according to the equations developed in Chapter 6 of this work (equation 6.5). It was further assumed that the formation pressure is maintained so that steam formation will not occur until well above 200°C.

The reservoir and electrode dimensions and electrical and thermal properties for the simulation are given in Figure A.1 and an areal view of the electrode placement is shown in Figure A.2. This run simulates a five spot pattern of electrodes of alternating polarity with a 50 m spacing between wells. There is only one electrode per well, and this electrode is completed in the middle of the oil sand zone.

As the problem exhibits a great amount of radial symmetry near the electrodes, it is well suited to simulation by the 2D radial (R,Z) version of MEGAERA. (For information on MEGAERA see A.D. Hiebert, C.E. Capjack, F.S. Chute, and F.E. Vermeulen, "A Simulation Code for Investigating the 2-D Heating of Material Bodies by the Action of Low Frequency Electric Fields", **Applied Mathematical Modelling**, V. 7, 1983, pp 366-371) By symmetry, the same heating will occur near each well, if an infinite array is assumed. An equi-potential (Dirichlet) boundary condition is imposed at a radius of 26 m, instead of using the actual square equi-potential boundary, as illustrated in Figure A.2. The electrode consists of 15 m of well casing, assumed to be .5 m (20 inches) in diameter, and two disks of 3 m diameter, which have been jet cut into the formation and propped with steel shot, near the two ends of the 15 m electrode region. The bottom of the electrode is positioned at the top of the rich oil sand zone, which comprises the

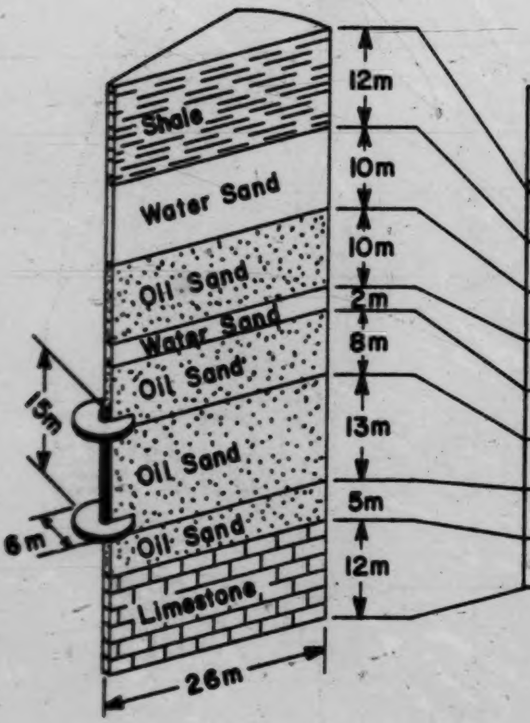
Shale
Water Sand
Oil Sand
Water Sand
Oil Sand
Oil Sand
Oil Sand
Limestone
12m
10m
10m
2m
8m
13m
5m
12m
15m
6m
26m

ρ_{24} $\Omega \cdot m$	M $10^6 J/m^3 \cdot K$	k $W/m \cdot K$
5.26	2.2	1.7
10.8	2.4	3.0
38.5	2.2	2.2
10.8	2.6	3.1
52.6	2.2	2.2
21.7	2.5	2.7
43.5	2.2	2.1
43.5	2.7	3.6

Figure A.1 The reservoir lithology and properties, and the electrode configuration for the simulation are shown

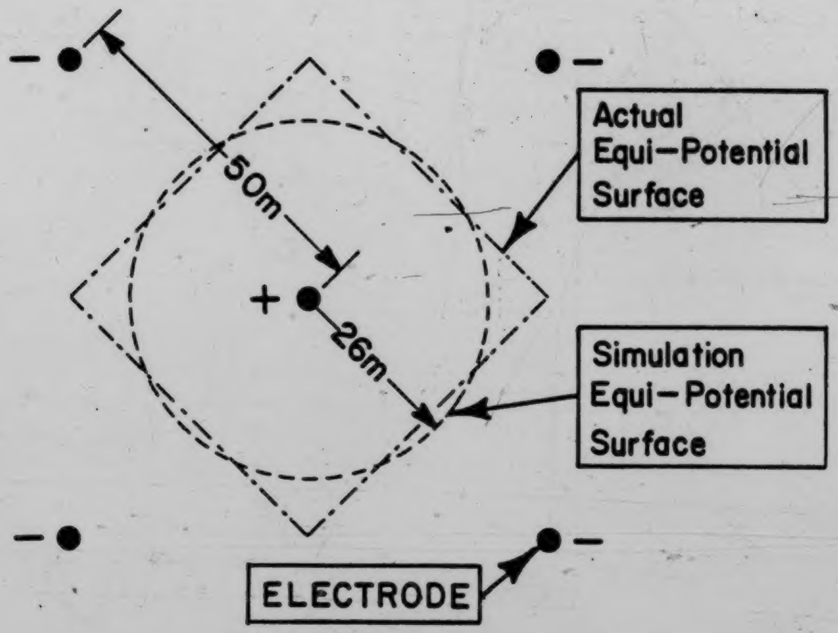

Actual
Equi–Potential
Surface
50m
26m
Simulation
Equi–Potential
Surface
ELECTRODE

Figure A.2 A plan view of the simulation electrode configuration

first 5 m above the underlying limestone formation. All of the casing from the top of the electrode to the surface is electrically insulated from the formation.

The voltage applied to the electrode is adjusted to maintain a constant power level of 250 kW input to the formation. After 59 days of heating, the temperature near the electrode has reached about 120°C. At this point the power level was raised to 300 kW and wellbore cooling was simulated, to maintain the wellbore at a constant temperature of 100°C for the remaining portion of the total heating time of one year. The jet cut disk portions of the electrode were not cooled. A contour plot of the temperature at the end of one year, in a vertical plane passing from one electrode to midway to another electrode, is given in Figure A.3. The solid contour lines give the temperature values obtained in the simulation when the old electrical conductivity formula is used. The dashed lines give the temperatures obtained when the new equations, developed in Chapter 6 of this work, are used in the simulation.

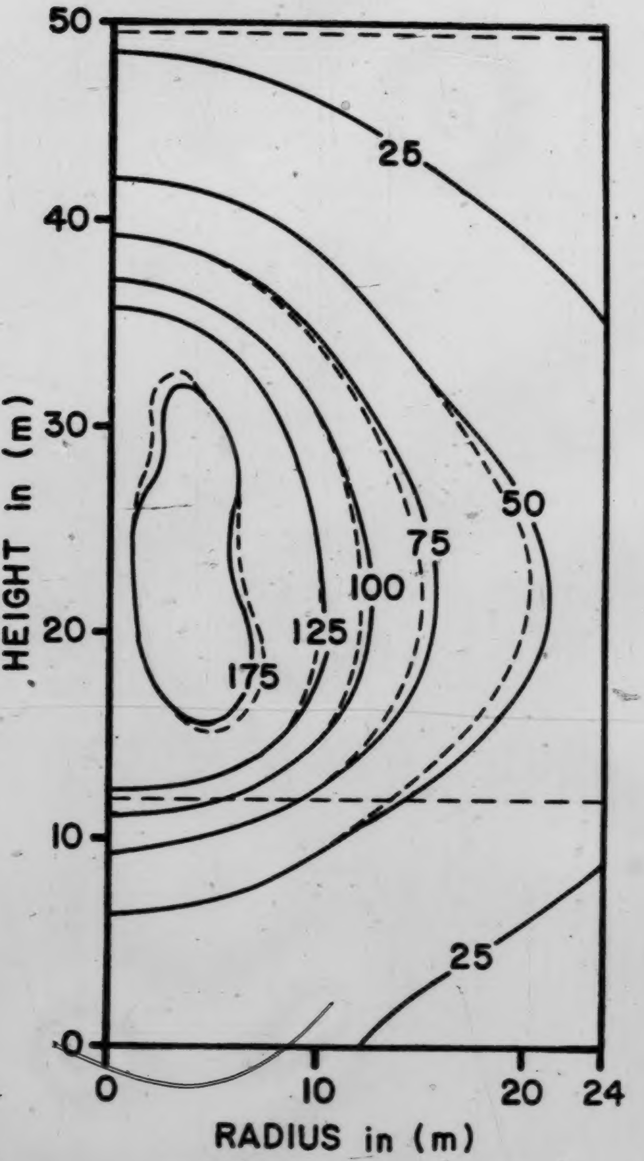

Figure A.3 A comparison between the temperature contours obtained using the old conductivity formula (solid lines) and those from the new formula (dashed lines). The horizontal dashed lines indicate the top and bottom of the oil sand zone.

Appendix III. EPEIOS User's Reference Manual

The purpose of this manual is to provide a reference guide to the program EPEIOS. It will be assumed that the reader is familiar with the finite difference method of finding approximate solutions to partial differencial equations, and is familiar with the equations and approximations used in EPEIOS. It will also be helpful if the reader is familiar with the MTS command language and the MTS command macros, and the IBM FORTRANVS language. Information on these is available from the Univeristy of Alberta bookstore and the computing services user reference room.

Namelist Data Input

The following namelists must be input, in order, into a single file. This file is attached to IO unit 5 in the $Run command. For information of namelist input see "VS FORTRAN Application Programming: Language Reference", IBM, page 137.

Namelist &INPUT1

This namelist is used to input flow control and output labeling variables.

MNSTEP - Type: Integer, Default: None.

MNSTEP specifies the maximum number of timesteps for the simulation run. If the simulation has not been completed by the MNSTEP timestep, the run will terminate with a return code of 50. Before termination, a printed output (and storage output if requested) will be produced for the last timestep.

CPUMAX - Type: Real, Default: 2000., Units: seconds.

At the end of every timestep, the program checks how many CPU seconds have been used to that point in the run. If this number is greater than CPUMAX, then the run will be terminated with a return code of 50. No checking of CPU usage is done during the timestep calculation, so the actual time used by the run termination will be somewhat greater than CPUMAX. A local or global time limit should be set, but, if this is reached, an error dump rather than a controlled termination will result. Before termination, a printed output (and storage output if requested) will be produced for the last timestep.

COSTMA - Type: Real, Default: 500, Units: dollars.

Similarly to CPUMAX, the program checks the cost of the run at the end of each timestep. If the cost excedes COSTMA, the program will be terminated with a return code of 50. A printout (and storage output if requested) will be produced for the last timestep.

LRESTA - Type: Logical, Default: .FALSE..

LRESTA must be set to .TRUE. for a restart run of a previously stored simulation run. By use of this control, the temperatures at some point in a previous run may be used as the start of the current run. The file containing the stored records of the previous run must be attached to IO unit 2 in the $Run command.

NREC - Type: Integer, Default: 1.

If LRESTA is set to .TRUE., the program will search the file attached to IO unit 2 for the storage record number NREC. The temperatures, etc., in this record will be used as the starting point for the current simulation run. When storage is specified for a simulation run (see the section on Namelist &INPUT3) the simulation time and record number of each stored record is printed on the printed output of the simulation run.

LABEL1, LABEL2, LABEL3, LABEL4 - Type: Character, Default: Blank.

The user may specified zero to four labels to be printed at the start of the simulation (LABEL1, LABEL2, LABEL3, and LABEL4). These 48 character maximum labels may be used to describe the simulation, indicate who set up the simulation, record the sequence number of the simulation, etc.

Namelist &INPUT2

This namelist is used to input basic geometric parameters, such as the dimensions of the problem domain, the number of regions and electrodes, and the initial temperature.

NX - Type: Integer, Default: None.

NX specifies the number of grid blocks that the problem domain is divided into in the X direction. The problem domain must be composed of a regular array of retangular prism shaped grid blocks.

NY - Type: Integer, Default: None.

NY specifies the number of grid blocks that the problem domain is divided into in the Y direction.

NZ - Type: Integer, Default: None.

NZ specifies the number of grid blocks that the problem domain is divided into in the Z direction.

DELTAX - Type: Real Array, Default: None, Units: meters.

This array specifies the X dimensions of the grid blocks, starting with the left most plane of grid blocks. The X dimension of each Y-Z plane of grid blocks must be specified, so there must be at least NX elements in DELTAX.

DELTAY - Type: Real Array, Default: None, Units: meters.

This array specifies the Y dimensions of the X-Z planes of grid blocks. It must contain NY elements.

DELTAZ - Type: Real Array, Default: None, Units: meters.

This array specifies the Z dimension of the X-Y planes of grid blocks. It must contain NZ elements.

NREG - Type: Integer, Default: None.

NREG specifies the number of different regions that are in the problem domain, also indicating the number of &REGION namelists which follow immediately after namelist &INPUT2.

NELECT - Type: Integer, Default: None.

NELECT specifies the number of different electrodes in the problem domain. This may be less than the number of electrode regions if two or more electrode regions (adjacent, overlapping, or separate) are used to form a single, non-rectangular, electrode.

TINIT - Type: Real, Default: 24., Units: °C.

TINIT specifies the initial, uniform, temperature of the problem domain.

Namelist &REGION

These namelist regions (of which there numst be NREG in number) are used to specify the location and properties of different regions in the problem domain. All regions are rectangular prisms in shape, and more complicated shapes may be formed by adjacent or overlapping regions with the same properties. The regions are lain down in consecutive order as they are read in, and a later region may cover all or part of a previously read in region. The default region, Region 0, which initially contains the entire grid, is electrically and thermally insulating. Any portion of the grid which is not contained in one of the read in regions will remain electrically and thermally insulating.

The region may be either an electrically conducting region, an electrically insulating region, or an electrode. Insulating regions are modeled as perfect insulators, and no further properties are specified. Electrode regions are perfect conductors, and the voltage of each electrode region must be specified. This is done by assigning an electrode number to the electrode region. More than one electrode region may have the same electrode number. This allows electrodes with complex, non-rectangular, shapes to be modelled by several adjacent or overlapping electrode regions. For an electrically conducting region, the electrical conductivity must be specified. In EPEIOS, the only functional dependence of the electrical conductivity is on temperature. This dependence is modelled using a three section, continuous, piece-wise linear, fit. The equation is as follows:

$$\sigma = C24*[1+ALPHA1*(T-24)] \qquad T \le TB1$$

$$\sigma = C24*[1+ALPHA1*(TB1-24)+ALPHA2*(T-TB1)] \qquad TB1<T \le TB2$$

$$\sigma = C24*[1+ALPHA1*(TB1-24) +ALPHA2*(TB2-TB1)+ALPHA3*(T-TB2)] \qquad T>TB2$$

where T is the temperature in Celsius, σ is the electrical conductivity in S/m, and ALPHA1, ALPHA2, ALPHA3, TB1, TB2, and C24 are specified by the user. The values of the user specified parameters may be different from region to region. For regions with anisotropic electrical conductivity, if the principle axis of the conductivity tensor are parallel to the coordinate axis of the grid blocks, the anisotropic conductivity may be modelled by inputting C24Y and C24Z.

Regions may be either thermally insulating, constant temperature regions, or thermally conducting. If a region is electrically conducting, it should also be specified as thermally conducting, or a program error will result. Electrically insulating or electrode regions may be specified as any type of thermal region. If a region is thermally insulating, no further thermal properties are needed. If the region is a constant temperature region, the temperature of the region must be specified. If the region is a thermally conducting region, the volumetric heat capacity (THMM) and the thermal conductivity (THMK) must be specified.

MINX - Type: Integer, Default: None.

MINX specifies the minimum grid block number in the X direction for the region.

MAXX - Type: Integer, Default: None.

MAXX specifies the maximum grid block number in the X direction for the region.

MINY - Type: Integer, Default: None.

MINY specifies the minimum grid block number in the Y direction for the region.

MAXY - Type: Integer, Default: None.

MAXY specifies the maximum grid block number in the Y direction for the region.

MINZ - Type: Integer, Default: None.

MINZ specifies the minimum grid block number in the Z direction for the region.

MAXZ - Type: Integer, Default: None.

MAXZ specifies the maximum grid block number in the Z direction for the region.

ETYPE - Type: Character, Default: None.

ETYPE specifies the electrical type of the region. ETYPE must be one of 'COND' , indicating an electrical conducting region, 'ELEC' indicating an electrode region, or 'INSU' indicating an electrically insulating region.

ELENUM - Type: Integer, Default: None.

If the region is an electrode, the electrode number is specified by ELENUM. The voltages of the electrodes are input in namelist &INWELL. A single electrode may be made up of more than one region.

C24 - Type: Real, Default: None, Units: Siemens/meter.

For electrically conducting regions, C24 specifies the electrical conductivity at 24°C. For the case of anisotropic electrical conductivity (when C24Y and C24Z are specified), C24 specifies the conductivity in the X direction.

C24Y - Type: Real, Default: C24, Units: Siemens/meter.

For regions of anisotropic electrical conductivity, the conductivity (at 24°C) in the Y direction is specified by C24Y. (For isotropic regions, C24Y does not need to be specified.)

C24Z - Type: Real, Default: C24, Units: Siemens/meter.

For regions of anisotropical electrical conductivity, the conductivity (at 24°C) in the Z direction is specified by C24Z. (For isotropic regions, C24Z does not need to be specified.)

ALPHA1 - Type: [illegible]al, Default: 0., Units: °C^{-1}

ALPHA1 specifies the slope of the electrical conductivity vs. temperature curve to the first breakpoint temperature. For more information, see the paragraph at the start of this section.

TB1 - Type: Real, Default: 1.E10, Units: °C.

TB1 indicates the temperature of the first change of slope for the electrical conductivity vs. temperature curve (see above).

ALPHA2 - Type: Real, Default: 0.0, Units: $°C^{-1}$

ALPHA2 specifies the slope of the second portion of the electrical conductivity vs. temperature curve (see above).

TB2 - Type: Real, Default: 1.E10, Units: °C.

TB2 specifies the temperature of the second change of slope for the electrical conductivity vs. temperature curve (see above).

ALPHA3 - Type: Real, Default: 0.0, Units: $°C^{-1}$

ALPHA3 specifies the slope of the third portion of the electrical conductivity vs. temperature curve (see above).

TTYPE - Type: Character, Default: None.

TTYPE specifies the thermal type of the region and must be one of 'INSU' indicating this is an thermally insulating region, 'CTEM' indicating this is a constant temperature region, or 'COND' indicating this is a thermally conducting region.

TEMPER - Type: Real, Default: None, Units: °C

TEMPER specifies the temperature of a constant temperature region (i.e. if TTYPE is 'CTEM', TEMPER must be specified.)

THMM Type: Real, Default: None, Units: $J/m^3 \cdot K$.

For thermally conducting regions, THMM specifies the volumetric heat capacity of the region.

THMK Type: Real, Default: None, Units: $W/m \cdot K$

For thermally conducting regions, THMK specifies the thermal conductivity of the region.

Namelist &INPUT3

The namelist &INPUT3 is used to specify the printed and data storage output from the program. While electrical heating is taking place, the electrical potentials, heating rates, and temperatures will be printed as specified. If no electrical heating is taking place, only the temperatures will be printed. Each printed output also contains information such as the simulation time, CPU time used, current, voltage and power into the formation, and energy balance calculations.

The three dimensional field data (temperature, heating rates, and potentials) are printed out as several X-Y planes at different Z values. There are two ways to specify the points on the X-Y planes and the Z values of the planes. The first way is to specify the number of X, Y, and Z points, and the minimum and maximum values of the points. The program then creates a regular grid between the maximum and minimum points and interpolates and prints out the grid values. The second way to specify the points is to set LUSPL to .TRUE. and explicitly specify each of the X, Y, and Z points (in XP, YP, and ZP).

Printed outputs will occur for the first and last timesteps, and may also be specified to occur every NSPO timesteps, or at explicitly specified times (PTIMES). Data storage output, to magnetic tape or to a file, will occur for the first and last timesteps, every NSTO timesteps, and at times specified by PTIMES.

NSTO Type: Integer, Default: 10000.

If NSTO is greater than 99, no data storage will occur. If data storage is requested, a file or magnetic tape should be attached to IO unit 1 in the $Run command.

NSPO Type: Integer, Default: 10000.

Printed output will be produced for each timestep number which is evenly divisable by NSPO.

PTIMES Type: Real Array, Default: No Values, Units: seconds.

Printed and Storage output will be produced for each simulation time specified in PTIMES. WARNING: The number of PTIMES specified must be less than the maximum number of regions allowed in the program version that you are running.

NPX Type: Integer, Default: 10.

NPX specifies the number of X points in the print out grid for 3D field data (such as temperature).

NPY Type: Integer, Default: 5.

NPY specifies the number of Y points in the print out grid for 3D field data.

NPZ Type: Integer, Default: 3.

NPZ specifies the number of Z points in the print out grid for 3D field data.

LUSPL Type: Logical, Default: .FALSE.

If LUSPL is .FALSE., then the print out grid is a regularly spaced grid between the minimums and maximums specified by by XMIN, XMAX, YMIN, YMAX, ZMIN, and ZMAX. If LUSPL is .TRUE., the user must specify an irregularly spaced grid using XP, YP, and ZP.

XMIN Type: Real, Default: Middle of the first grid block, Units: meters.

This specifies the minimum X value for a regularly spaced print out grid.

XMAX Type: Real, Default: Middle of the last grid block, Units: meters.

This specifies the maximum X value for a regularly spaced print out grid.

YMIN Type: Real, Default: Middle of the first grid block, Units: meters.

This specifies the minimum Y value for a regularly spaced print out grid.

YMAX Type: Real, Default: Middle of the last grid block, Units: meters.

This specifies the maximum Y value for a regularly spaced print out grid.

ZMIN Type: Real, Default: Middle of the first grid block, Units: meters.

This specifies the minimum Z value for a regularly spaced print out grid.

ZMAX Type: Real, Default: Middle of the last grid block, Units: meters.

This specifies the maximum Z value for a regularly spaced print out grid.

XP Type: Real Array, Default: None, Units: meters.

XP is a vector specifying the X grid point values for 3D data print out. A total of NPX values must be specified if LUSPL is TRUE.

YP Type: Real Array, Default: None, Units: meters.

YP is a vector specifying the Y grid point values for 3D data print out. A total of NPY values must be specified if LUSPL is TRUE.

ZP Type: Real Array, Default: None, Units: meters.

ZP is a vector specifying the Z grid point values for 3D data print out. A total of NPZ values must be specified if LUSPL is TRUE.

Namelist &INWELL

The namelist &INWELL is used to specify the electrode voltages, wellbore resistances, type of heating, length of heating, and size of the timestep. Several &INWELL namelists may be included at the end of the input file and these will be read and executed in order.

ELEVOL Type: Complex Array, Default: 0.0+j0.0, Units: Volts.

ELEVOL specifies the voltages of the electrodes in order (i.e. electrode no. 1 is first, electrode no. 2 is second, etc.) Complex electrode voltages must be specified, even for single phase problems. (In this case, set the imaginary part to zero.) For constant current and constant power problems the voltages will be scaled from the specified values.

WRESIS Type: Complex Array, Default: 0.0+j0.0, Units: Ohms.

WRESIS specifies the complex impedences of the wellbores to the corresponding electrodes. This is used in calculations of the surface voltages and the electrical energy lost in the wellbores.

L1PHAS Type: Logical, Default: .FALSE.

If the problem being modelled is a single phase problem (the imaginary part of all the electrode voltages are zero) then computational time and print out space may be saved by specifying L1PHAS to .TRUE..

NTYPE Type: Integer, Default: 1 (Constant Voltage)

NTYPE is used to specify the electrical heating as Constant Voltage (NTYPE=1), Constant Current (NTYPE=2, and CCUR and NECUR must be specified), Constant Power (NTYPE=3, and CPOW must be specified) or no electrical heating (NTYPE=4).

CCUR Type: Real, Default: 0.0, Units: Amperes.

When modelling constant current heating, the magnitude of the current (CCUR) out of a specified electrode (NECUR) must be input.

NECUR Type: Integer, Default: none.

Specifies the electrode used when modelling constant current heating.

TTIME Type: Real, Default: None, Units: seconds.

TTIME specifies the time to the end of the simulation, or the time at which the next namelist &INWELL is to be read. If TTIME is less than the current simulation time, the next &INWELL namelist will be read.

DTIME Type: Real, Default: TTIME/10. or previous value, Units: seconds.

DTIME specifies the length of the first timestep after the namelist is read in. After the first timestep, the length of the timestep is automatically adjusted.

DTMAX Type: Real, Default: 0.1

DTMAX specifies the maximum relative change in temperature that may occur in one timestep. If the temperature change is found to be greater than DTMAX the timestep size is reduced and the temperature is recalculated.

DSIGMA Type: Real, Default: 0.05

DSIGMA specifies the maximum relative change in conductivity which may occur in one timestep.

DTIMAX Type: Real, Default: 1.E40, Units: Seconds

DTIMAX specifies the maximum time step size.

ITMAX Type: Integer, Default: 900.

ITMAX specifies the number of iterations of the potential solving point-wise successive overrelaxation routine which will be done before the program aborts if the convergence test has not been passed.

RESMAX Type: Real, Default: 5.E-6

RESMAX specifies the maximum relative residual of the finite difference equations for which the solution will be deemed to have converged.

LRESET Type: Logical, Default: .TRUE.

LRESET specifies whether the potential array is to be cleared after ~~reading in~~ the namelist &INWELL. Setting this to .FALSE. may save calculation time in some types of problems (i.e. a restart of a stored run) but for the first &INWELL namelist of a new run this must be .TRUE..

EPEIOS Input File Template

Following is a copy of an EPEIOS input file. This file was used in a simulation of a physical model run.

```
 &INPUT1
   LABEL1='EPEIOS Test Run. ET5 - Physical Model Case 8 ',
   LABEL2='Electrodes in both o.s. and o.b. and u.b. ',
   LABEL3='Constant voltage run, with storage          ',
   LABEL4='Geometry set up and entered by Allan Hiebert',
   MNSTEP=100,LRESTA=.FALSE.,COSTMA=350.,CPUMAX=550.,NREC=1
 &END
 &INPUT2      NX=21,NY=34,NZ=6,
   DELTAX=.006,3*.01,6*.02,.028,5*.02,4*.01,.006,
   DELTAY=3*.1,.05,2*.025,8*.01,6*.02,8*.01,2*.025,4*.05,
   DELTAZ=6*0.0125,
   NREG=4,NELECT=2,TINIT=22.5,
 &END
```

```
&REGION    MINX=1,MAXX=21,MINY=1,MAXY=34,MINZ=1,MAXZ=6,
   ETYPE='COND',ALPHA1=2.5E-2,C24=0.0079,
   TTYPE='COND',THMM=1.3E6,THMK=1.7,
&END
&REGION    MINX=1,MAXX=21,MINY=11,MAXY=24,MINZ=1,MAXZ=6,
   ETYPE='COND',ALPHA1=2.6E-2,C24=0.0014,
   TTYPE='COND',THMM=1.8E6,THMK=1.5,
&END
&REGION    MINX=1,MAXX=1,MINY=9,MAXY=13,MINZ=1,MAXZ=2,
   ETYPE='ELEC',ELENUM=1,
   TTYPE='COND',THMM=3.5E6,THMK=390.,
&END
&REGION    MINX=21,MAXX=21,MINY=22,MAXY=26,MINZ=1,MAXZ=2,
   ETYPE='ELEC',ELENUM=2,
   TTYPE='COND',THMM=3.5E6,THMK=390.,
&END
&INPUT3
   NSTO=10,NPX=4,NPY=5,NPZ=3,LUSPL=.TRUE.,
   XP=.0191,.0635,.1143,.1651,
   YP=.399,.4495,.4787,.542,.631,
   ZP=0.0,.0254,.0635,PTIMES=39.,607.,
&END
&INWELL
   TTIME=361.,NTYPE=2,ELEVOL=-500.,0.,500.,0.,
   WRESIS=0.,0.,0.,0.,
   DSIGMA=.10,ITMAX=800,DTMAX=.15,L1PHAS=.TRUE.,
   CCUR=.0825,NECUR=2,
&END
&INWELL
   TTIME=1253.,NTYPE=2,ELEVOL=-500.,0.,500.,0.,
   WRESIS=0.,0.,0.,0.,
   DSIGMA=.10,ITMAX=800,DTMAX=.15,L1PHAS=.TRUE.,
   CCUR=.0945,NECUR=2,LRESET=.FALSE.
&END
```

Running EPEIOS

EPEIOS is written in FORTRAN 77. The source code is in "APEM:EPEIOS.S". The COMMON blocks, in "APEM:EPEIOS.C", must be inserted using the Olympus Pre-processor. The COMMON block insertion and compilation procedure is contained in an MTS Command Macro in "APEM:MACROS". The macros are invoked by entering

```
$Source APEM:MACROS
```

To compile EPEIOS, issue the following command:

```
Compile NX=20 NY=20 NZ=15 NR=20
```

The values of NX, NY, NZ, and NR indicate the maximum number of grid blocks and regions for problems to be run on the object code produced. The compilation procedure costs about three dollars. For most problems, this amount will quickly be saved by dimensioning the program to the size needed in the problem. Note that NR should be at least 10, regardless of the number of regions required, and NX, NY, and NZ must be at least 2.

If the object code exists in the file "-EPEIOS" (as after the compile macro is used), the program is run by entering

```
$Run -EPEIOS 1=... 2=... 5=... 6=...
```

where IO unit 1 is attached to the file/tape to be used for data storage, IO unit 2 is attached to the file/tape containing the restart record (if needed), IO unit 5 is attached to the input file, and IO unit 6 is attached to the file/device to be used for the printed output (defaults to *SINK*). For non-batch jobs, some run progress indicators will be printed on the terminal during the run.

If another problem (with the same or smaller dimensions) is to be run later, the EPEIOS object code may be saved by renaming the temporary file "-EPEIOS" to a permanent file.

```
$Rename -EPEIOS to EP
```

To use PICASSO on the stored output from EPEIOS, enter the following command:

```
$Run APEM:PICASSO+APEM:P.EIN 1=...
```

where IO unit 1 is attached to the storage output from EPEIOS. For more information on PICASSO, see the PICASSO writeup. To save typing, invoke the macros in "APEM:MACROS", then enter

```
PE data
```

where "data" is replaced by the name of the EPEIOS storage file.

Other MTS command macros have been written for use with EPEIOS and PICASSO. These macros are stored in "APEM:MACROS" and are loaded by entering

```
$Source APEM:MACROS
```

The macros are:

PM data

This macro will run PICASSO for MEGAERA input, with the input data for PICASSO being in "data".

Calcomp pdf

When a plot has been created using PICASSO, it may be sent to the Calcomp plotter with this command. "pdf" here is the name of the plot description file, which defaults to "-pl" in PICASSO.

ESPP pdf

This macro will produce a plot on the Electro-static Printer Plotter, instead of the Calcomp.

Greyshade gsf

When a greyshade plot in produced using PICASSO, it may be set to the Electro-static Printer Plotter by using this macro. Here "gsf" is the greyshade plot file, which defaults to "-grey" in PICASSO.

Appendix IV. TCTM-EPEIOS User's Reference Manual

Introduction

The purpose of this manual is to provide a reference guide to the program combining EPEIOS and the Alberta Research Council's Two Component Thermal Model. It will be assumed that the reader is familiar with the finite difference method of finding approximate solutions to partial differential equations, and is familiar with the equations and approximations used in EPEIOS. Information on the ARC Two Component Thermal Model is available in various ARC documents. It will also be helpful if the reader is familiar with the MTS command language and the MTS command macros, and the FORTRANVS language. Information on these is available from the bookstore and the computing services user reference room at the University of Alberta.

Data Input

Data input for the TCTM is unaltered from that of the version which is implemented on the MTS system. All commands and variable inputs are available, and are unaltered. Thus, all data input pertaining to the reservoir properties, flow equations, energy equation, finite difference grid for the flow equations, injection and production wells, and output of results, are exactly as indicated in the ARC documents on the Two Component Thermal Model.

The electrical heating is controlled by an additional input file, to be attached to IO unit 3 in the $Run command. The following namelists must be input, in order, into this file. For information of namelist input see "VS FORTRAN Application Programming: Language Reference", IBM, page 137.

Namelist &INPUT1

This namelist is used to print run identifying labels at the start of the printout.

LABEL1, LABEL2, LABEL3, LABEL4 - Type: Character, Default: Blank.

The user may specify zero to four labels to be printed at the start of the simulation (LABEL1, LABEL2, LABEL3, and LABEL4). These 48 character maximum labels may be used to describe the simulation, indicate who set up the simulation, record the sequence number of the simulation, etc.

Namelist &INPUT2

This namelist is used to input basic geometric parameters, such as the dimensions of the problem domain and the number of regions and electrodes. Note that two different grids may be used for a problem. One grid is used in the TCTM, and is input as usual for that program. (i.e. Dimensions in feet, Z increasing downward.) The second grid is used by EPEIOS, and may be the same as, or finer than, the TCTM grid. However, the boundaries of the two grids must be identical, and each EPEIOS grid block must be contained entirely in only one TCTM grid block. The dimensions of the EPEIOS grid are specified in meters, and Z is increasing downward.

NX - Type: Integer, Default: None.

NX specifies the number of grid blocks that the problem domain is divided into in the X direction. The problem domain must be composed of a regular array of retangular prism shaped grid blocks.

NY - Type: Integer, Default: None.

NY specifies the number of grid blocks that the problem domain is divided into in the Y direction.

NZ - Type: Integer, Default: None.

NZ specifies the number of grid blocks that the problem domain is divided into in the Z direction.

DELTAX - Type: Real Array, Default: None, Units: meters.

This array specifies the X dimensions of the grid blocks, starting with the left most plane of grid blocks. The X dimension of each Y-Z plane of grid blocks must be specified, so there must be at least NX elements in DELTAX.

DELTAY - Type: Real Array, Default: None, Units: meters.

This array specifies the Y dimensions of the X-Z planes of grid blocks. It must contain NY elements.

DELTAZ - Type: Real Array, Default: None, Units: meters.

This array specifies the Z dimension of the X-Y planes of grid blocks. It must contain NZ elements. NOTE: DELTAZ(1) indicates the thickness of the top-most grid layer and DELTAZ(NZ) indicates the thickness of the bottom-most layer. In other words, z increases downwards. This is done to ensure compatability with TCTM and may be different than the ordering used in EPEIOS.

NREG - Type: Integer, Default: None.

NREG specifies the number of different regions that are in the problem domain, also indicating the number of &REGION namelists which follow immediately after namelist &INPUT2.

NELECT - Type: Integer, Default: None.

NELECT specifies the number of different electrodes in the problem domain. This may be less than the number of electrode regions if two or more electrode regions (adjacent, overlapping, or separate) are used to form a single, non-rectangular, electrode.

Namelist &REGION

These namelist regions (of which there numst be NREG in number) are used to specify the location and properties of different regions in the problem domain. All regions are rectangular prisms in shape, and more complicated shapes may be formed by adjacent or overlapping regions with the same properties. The regions are lain down in consecutive order as they are read in, and a later region may cover all or part of a previously read in region. The default region, Region 0, which initially contains the entire grid, is electrically insulating. Any portion of the grid which is not contained in one of the read in regions will remain electrically insulating.

The region may be either an electrically conducting region, an electrically insulating region, or an electrode. Insulating regions are modeled as perfect insulators, and no further properties are specified. Electrode regions are perfect conductors, and the voltage of each electrode region must be specified. This is done by assigning an electrode number to the electrode region. More than one electrode region may have the same electrode number. This allows electrodes with complex, non-rectangular, shapes to be modelled by several adjacent or overlapping electrode regions. For an electrically conducting region, the electrical conductivity must be specified. In addition, the functional dependence of the electrical conductivity with temperature must be specified. This dependence is modelled using a three section, continuous, piece-wise linear, fit. The equation is as follows:

$$\sigma = \mathrm{C24*[1+ALPHA1*(T-24)]} \qquad \mathrm{T \le TB1}$$

$$\sigma = \mathrm{C24*[1+ALPHA1*(TB1-24)+ALPHA2*(T-TB1)]} \qquad \mathrm{TB1<T \le TB2}$$

$$\sigma = C24 * \{1+ALPHA1*(TB1-24)+ALPHA2*(TB2-TB1)+ALPHA3*(T-TB2)\} \qquad T>TB2$$

where T is the temperature in Celsius, σ is the electrical conductivity of the connate water in S/m, and ALPHA1, ALPHA2, ALPHA3, TB1, TB2, and C24 are specified by the user. The values of the user specified parameters may be different from region to region. For regions with anisotropic electrical conductivity, if the principal axes of the conductivity tensor are parallel to the coordinate axes of the grid blocks, the anisotropic conductivity may be modelled by inputting C24Y and C24Z.

Once the electrical conductivity of the connate water is calculated, the bulk electrical conductivity is found using the so-called 'Archie Equation'.

$$\sigma = \frac{\phi^{1.37} Sw^{2}\, \sigma w}{0.88}$$

where ϕ is the porosity and Sw is the water saturation.

MINX - Type: Integer, Default: None.

MINX specifies the minimum grid block number in the X direction for the region.

MAXX - Type: Integer, Default: None.

MAXX specifies the maximum grid block number in the X direction for the region.

MINY - Type: Integer, Default: None.

MINY specifies the minimum grid block number in the Y direction for the region.

MAXY - Type: Integer, Default: None.

MAXY specifies the maximum grid block number in the Y direction for the region.

MINZ - Type: Integer, Default: None.

MINZ specifies the minimum grid block number in the Z direction for the region.

MAXZ - Type: Integer, Default: None.

MAXZ specifies the maximum grid block number in the Z direction for the region.

ETYPE - Type: Character, Default: None.

ETYPE specifies the electrical type of the region. ETYPE must be one of 'COND' indicating an electrical conducting region, 'ELEC' indicating an electrode region, or 'INSU' indicating an electrically insulating region.

ELENUM - Type: Integer, Default: None.

If the region is an electrode, the electrode number is specified by ELENUM. The voltages of the electrodes are input in namelist &INWELL. A single electrode may be made up of more than one region.

C24 - Type: Real, Default: None, Units: Siemens/meter.

For electrically conducting regions, C24 specifies the electrical conductivity of the connate water at 24°C.

For the case of anisotropic electrical conductivity (when C24Y and C24Z are specified), C24 specifies the conductivity in the X direction.

C24Y - Type: Real, Default: C24, Units: Siemens/meter.

For regions of anisotropic electrical conductivity, the connate water electrical conductivity (at 24°C) in the Y direction is specified by C24Y. (For isotropic regions, C24Y does not need to be specified.)

C24Z - Type: Real, Default: C24, Units: Siemens/meter.

For regions of anisotropical electrical conductivity, the connate water electrical conductivity (at 24°C) in the Z direction is specified by C24Z. (For isotropic regions, C24Z does not need to be specified.)

ALPHA1 - Type: Real, Default: 0., Units: $°C^{-1}$

ALPHA1 specifies the slope of ~~the~~ electrical conductivity vs. temperature curve to the first breakpoint temperature. For more information, see the paragraph at the start of this section.

TB1 - Type: Real, Default: 1.E10, Units: °C.

TB1 indicates the temperature of the first change of slope for the electrical conductivity vs. temperature curve (see above).

ALPHA2 - Type: Real, Default: 0.0, Units: $°C^{-1}$

ALPHA2 specifies the slope of the second portion of the electrical conductivity vs. temperature curve (see above).

TB2 - Type: Real, Default: 1.E10, Units: °C.

TB2 specifies the temperature of the second change of slope for the electrical conductivity vs. temperature curve (see above).

ALPHA3 - Type: Real, Default: 0.0, Units: $^{\circ}C^{-1}$

ALPHA3 specifies the slope of the third portion of the electrical conductivity vs. temperature curve (see above).

Namelist &INWELL

The namelist &INWELL is used to specify the electrode voltages, wellbore resistances, and type and amount of heating. Several &INWELL namelists may be included at the end of the input file and these will be read and executed in order.

ELEVOL Type: Complex Array, Default: 0.0+j0.0, Units: Volts.

ELEVOL specifies the voltages of the electrodes in order (i.e. electrode no. 1 is first, electrode no. 2 is second, etc.) Complex electrode voltages must be specified, even for single phase problems. (In this case, set the imaginary part to zero.) For constant current and constant power problems the voltages will be scaled from the specified values.

WRESIS Type: Complex Array, Default: 0.0+j0.0, Units: Ohms.

WRESIS specifies the complex impedences of the wellbores to the corresponding electrodes. This is used in calculations of the surface voltages and the electrical energy lost in the wellbores.

L1PHAS Type: Logical, Default: .FALSE.

If the problem being modelled is a single phase problem (the imaginary part of all the electrode voltages are zero) then computational time and print out space may be saved by specifying L1PHAS to .TRUE..

NTYPE Type: Integer, Default: 1 (Constant Voltage)

NTYPE is used to specify the electrical heating as Constant Voltage (NTYPE=1), Constant Current (NTYPE=2, and CCUR and NECUR must be specified), Constant Power (NTYPE=3, and CPOW must be specified) or no electrical heating (NTYPE=4).

CCUR Type: Real, Default: 0.0, Units: Amperes.

When modelling constant current heating, the magnitude of the current (CCUR) out of a specified electrode (NECUR) must be input.

NECUR Type: Integer, Default: none.

Specifies the electrode used when modelling constant current heating.

TTIME Type: Real, Default: None, Units: seconds.

TTIME specifies the time to the end of the simulation, or the time at which the next namelist &INWELL is to be read. If TTIME is less than the current simulation time, the next &INWELL namelist will be read.

ITMAX Type: Integer, Default: 900.

ITMAX specifies the number of iterations of the potential solving point-wise successive overrelaxation routine which will be done before the program aborts if the convergence test has not been passed.

RESMAX Type: Real, Default: 5.E-6

RESMAX specifies the maximum relative residual of the finite difference equations for which the solution will be deemed to have converged.

LRESET Type: Logical, Default: .TRUE.

LRESET specifies whether the potential array is to be cleared after reading in the namelist &INWELL. Setting this to .FALSE. may save calculation time in some types of problems (i.e. a restart of a stored run) but for the first &INWELL namelist of a new run this must be .TRUE..

Appendix V. Testing of EPEIOS and TCTM-EPEIOS

This appendix contains the details of the tests used to verify that the various parts of EPEIOS and TCTM-EPEIOS were working properly. Four tests are listed for EPEIOS and one test is listed for TCTM-EPEIOS. It should be recalled when reviewing these test results that the finite difference method only produces an approximate solution to a particular partial differential equation or set of equations. How close the approximation will be to an analytic solution will depend on a number of factors, the primary one of which is the size of the grid blocks used in regions where the variable being solved (e.g. potential) is varying rapidly in space.

Test No. 1

Purpose: To verify the correctness of the finite difference equations, and their implementation in EPEIOS, for solving a simple one dimensional problem. Several aspects of EPEIOS are tested, including the calculation of the finite difference equation coefficient for the current continuity equation, the solution of the current continuity equation, the calculation of the heating rates, the electrode current calculation, the constant power scaling option and the solution of the energy (temperature) equation for a problem involving no heat flow.

Problem Description: Illustrated in Figure A.4 (a), Test No. 1 consists of passing an electrical current through three media, with different electrical conductivities, located in series. On either end of the three media is a parallel plate electrode to which a voltage is applied, causing a uniform electrical current flow through each of the three media. The conductivity of Medium #1 was 2.0 S/m, the conductivity of Medium #2 was 10.0 S/m, and the conductivity of Medium #3 was 100.0 S/m. As each medium has a different electrical conductivity, each will have a different electic field strength (or rate of voltage drop). A voltage of 50 volts r.m.s. at a phase angle of 45° was applied to Electrode #1, while a voltage of 50 volts r.m.s. at a phase angle of 225° was applied at Electrode #2. This resulted in the testing of the calculation of both the real and the imaginary parts of the potential.

The analytic solution for the magnitude of the potential is given by:

$\psi = 50.0 - 16.394 \cdot x$ Region #1
$\psi = -31.97 - 3.2787 \cdot (x - 5)$ Region #2
$\psi = -48.36 - 0.3279 \cdot (x - 10)$ Region #3

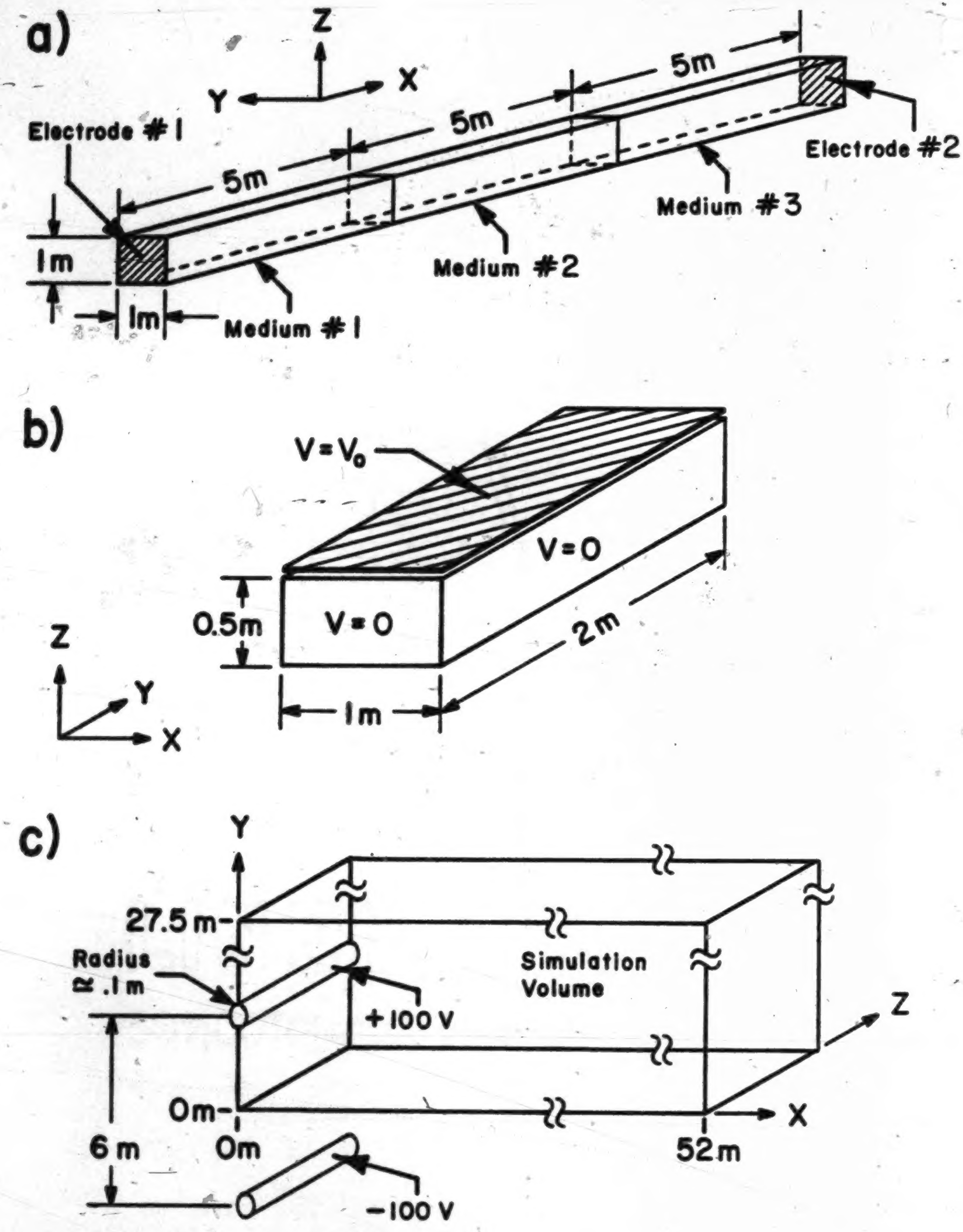
a)
Z
Y
X
Electrode #1
5m
5m
5m
Electrode #2
Medium #3
Medium #2
Medium #1
1m
1m
b)
V=V₀
V=0
V=0
0.5m
2m
1m
Z
Y
X
c)
Y
27.5 m
Radius
≃ .1 m
Simulation
Volume
+100 V
Z
Om
Om
X
6 m
52m
−100 V

Figure A.4 The geometries used by some of the test problems. Diagram (a) shows the geometry used for Tests #1 and #4. Diagram (b) shows the geometry used for Test #2. Diagram (c) shows the geometry used for Test #3.

where ψ is the potential in volts and x is the distance in meters measured from Electrode #1. The total heating rate (due to both the real and imaginary electric fields) is:

$Q = 537.5$	Region #1
$Q = 107.5$	Region #2
$Q = 10.75$	Region #3

where Q is the volumetric heating rate (W/m^3).

In the second stage of Test No. 1, the applied voltage was scaled to maintain a constant power into the problem domain. The initial heating rate of the problem presented thus far is 3278.7 W. If the electrode voltages were held fixed the heating rate would change due to the changing temperatures and hence changing electrical conductivities of the three media. However, EPEIOS can automatically scale the electrode voltages to maintain a constant electrical heating rate. Further, the heat capacities of each of the three media were set proportional to the heating rate in that medium so that a uniform rate of temperature increase would occur in all three media. The rate of temperature increase for the entire problem domain should be 0.1 °C per second.

EPEIOS Input File: Test No. 1 was run a number of times using EPEIOS. The problem was run three times, once with the current flow and three media aligned with each of the X, Y, and Z axis. This was to test the finite difference equation coefficient calculation in each of the three directions. The problem was also run using both uniform and variable grid block sizes. The particular input file listed below uses variable grid block sizes and constant power scaling.

```
&INPUT1
  LABEL1='EPEIOS Test No. 1  -  One Dimensional,',
  LABEL2='Three Media, Multiphase Heating   ',
  LABEL3='Configuration, Analytically Soluble.  ',
  LABEL4='Problem Designed By Allan Hiebert.',
  MNSTEP=100, LRESTA=.FALSE., NREC=1,
  CPUMAX=20., COSTMA=20.
&END
&INPUT2
  NX=25, NY=2, NZ=2,
  DELTAX=.01,.5,4*1.0,.5,2*.25,.5,3*1.0,.5,
         4*.25,.5,3*1.0,2*.5,.01,
  DELTAY=2*.5, DELTAZ=2*.5,
  NREG=5, NELECT=2, TINIT=24.,
&END
&REGION   MINX=2,MAXX=7,MINY=1,MAXY=2,MINZ=1,MAXZ=2,
   ETYPE='COND',ALPHA1=2.E-2,C24=2.0,
   TTYPE='COND',THMM=5375.,THMK=1.0,
&END
&REGION   MINX=8,MAXX=16,MINY=1,MAXY=2,MINZ=1,MAXZ=2,
   ETYPE='COND',ALPHA1=2.E-2,C24=10.,
   TTYPE='COND',THMM=1075.,THMK=1.0,
&END
&REGION   MINX=17,MAXX=24,MINY=1,MAXY=2,MINZ=1,MAXZ=2,
   ETYPE='COND',ALPHA1=2.E-2,C24=100.,
   TTYPE='COND',THMM=107.5,THMK=1.0,
&END
&REGION   MINX=1,MAXX=1,MINY=1,MAXY=2,MINZ=1,MAXZ=2,
   ETYPE='ELEC',ELENUM=1,
   TTYPE='INSU',
&END
&REGION   MINX=25,MAXX=25,MINY=1,MAXY=2,MINZ=1,MAXZ=2,
   ETYPE='ELEC',ELENUM=2,
   TTYPE='INSU',
&END
&INPUT3
   NSPO=2,NSTO=10000,NPX=4,NPY=1,NPZ=1,LUSPL=.TRUE.,
   XP=1.,4.,7.5,14.,YP=.5,ZP=.5,
&END
&INWELL
  DTIME=20.,TTIME=500.,NTYPE=3,RESMAX=5.E-6,
  DSIGMA=.03,ITMAX=300,L1PHAS=.FALSE.,CPOW=3278.7,
  ELEVOL=35.355,35.355,-35.355,-35.355,
  WRESIS=0.,0.,0.,0.,
&END
```

Results: EPEIOS performed very well in predicting the analytic solution to this problem. Results for all the test runs were similar. For the particular case of the input file given above some of the results were as follows.

Distance in meters from Electrode #1	1.0	4.0	7.5	12.5
Potential in volts				
Analytic	23.76	-11.01	-28.40	-35.12
EPEIOS	23.88	-10.89	-28.37	-35.12
Heating rate in watts per cubic meter				
Analytic	537.50	537.50	107.50	10.75
EPEIOS	537.35	537.33	107.50	10.91

Electrode currents in amperes	
Analytic	23.184 + j23.184
EPEIOS Electrode #1	23.181 + j23.181
EPEIOS Electrode #2	-23.413 - j23.413
Temperature change in Celsius after 500 seconds heating	
Analytic	50.0
EPEIOS	49.70 to 50.32

Test No. 2.

Purpose: To test the electrical potential calculation in a three dimensional anisotropic medium.

Problem Geometry: Test No. 2 consisted of calculating the electric potentials at various points in an enclosed, rectangular prism of a homogeneous but anisotropic conducting medium. One face of the prism was held at a potential of V_0, while the other five faces were held at ground (reference) potential, as illustrated in Figure A.4 (b).

An analytic solution to this problem may be found using the Separation of Variables Method. (See Ramo, Whinnery, and Van Duzer, pp. 201-203.) The analytic solution is not in closed form, but is an infinite series of sine and hyperbolic sine functions. A FORTRAN program was written to sum the first several hundred terms of the series, producing the analytical solution results shown below. The solution is given by the series

where a, b, and c are the X, Y, and Z dimensions, respectively, of the retangular prism as shown on Figure A.4(b).

EPEIOS Input File: The diagonal tensor electrical conductivity used for the medium in the rectangular prism was σ_x= 0.001, σ_y= 0.002, and σ_z= 0.005. The applied voltage, V_0, was set to 100 volts. The actual dimensions of the prism used are shown on Figure A.4(b). The input file was as follows:

```
&INPUT1
  LABEL1='Test No. 2 -  3 Dimensional, One medium',
  LABEL2='Rectangular Box with one side at 100 V.',
  MNSTEP=1, LRESTA=.FALSE., NREC=1,
  CPUMAX=200., COSTMA=200.,
&END
&INPUT2
  NX=11, NY=21, NZ=12,
  DELTAX=.001,10*.05,
  DELTAY=.001,20*.05,
  DELTAZ=.001,10*.05,.001,
  NREG=3, NELECT=2, TINIT=24.
&END
&REGION MINX=1,MAXX=11,MINY=1,MAXY=21,MINZ=1,MAXZ=11,
  ETYPE='ELEC',ELENUM=1,
   TTYPE='INSU',
 &END
 &REGION MINX=2,MAXX=11,MINY=2,MAXY=21,MINZ=2,MAXZ=11,
   ETYPE='COND',ALPHA1=2.E-2,
   C24=.002,C24Y=.003,C24Z=.004,
   TTYPE='COND',THMM=1.5E6,THMK=1.0,
 &END
 &REGION MINX=1,MAXX=11,MINY=1,MAXY=21,MINZ=12,MAXZ=12,
    ETYPE='ELEC',ELENUM=2,
    TTYPE='INSU',
 &END
 &INPUT3
    NSPO=1,NSTO=1000,NPX=3,NPY=3,NPZ=3,LUSPL=.TRUE.,
    XP=.101,.251,.491, YP=.251,.501,.951,
    ZP=.101,.251,.451,
 &END
 &INWELL
   DTIME=10.,TTIME=50000.,NTYPE=1,RESMAX=5.E-6,
   DSIGMA=.03,ITMAX=900,L1PHAS=.TRUE.,
   ELEVOL=0.,0.,100.,0.,
   WRESIS=0.,0.,0.,0.,
 &END
```

Results: Table A.33 compares the analytic and EPEIOS calculated potentials at various points in the rectangular prism. In general, good agreement between the EPEIOS results and the analytic calculations was obtained. Near the edges of the prism where the face held at 100 volts contacted one of the other grounded faces, agreement between EPEIOS results and the analytic calculation was not as good. In this region, the potential is changing very rapidly, and it is to be expected that the finite difference method will not perform as well as in regions where the potential is changing more slowly.

Table A.33 A comparison of the analytically calculated potentials with EPEIOS results for Test Problem #2. Columns headed "AN" indicate analytic solution while thoses headed "EP" indicate EPEIOS result.

Plane Z = 0.49 m

X (m)	0.10		0.30		0.49	
Y (m)	AN	EP	AN	EP	AP	EP
0.95	96.61	96.33	97.90	97.87	97.97	97.93
0.40	96.47	96.29	97.73	97.79	97.79	97.85
0.20	96.04	95.90	97.10	97.19	97.15	97.23

Plane Z = 0.4 m

X (m)	0.10		0.30		0.49	
Y (m)	AN	EP	AN	EP	AP	EP
0.95	68.66	67.78	79.44	79.37	79.93	79.93
0.40	68.33	67.43	78.78	78.69	79.23	79.19
0.20	65.28	64.20	73.91	73.61	74.21	73.96

Plane Z = 0.3 m

X (m)	0.10		0.30		0.49	
Y (m)	AN	EP	AN	EP	AP	EP
0.95	44.25	43.86	59.09	59.00	59.89	59.88
0.40	43.72	43.30	58.05	57.91	58.77	58.71
0.20	39.33	38.79	50.84	50.58	51.33	51.13

Plane Z = 0.2 m

X (m)	0.10		0.30		0.49	
Y (m)	AN	EP	AN	EP	AP	EP
0.95	26.40	26.32	39.10	39.02	39.89	39.88
0.40	25.89	25.77	38.07	37.94	38.78	38.73
0.20	22.01	21.86	31.54	31.40	32.02	31.94

Plane Z = 0.1 m

X (m)	0.10		0.30		0.49	
Y (m)	AN	EP	AN	EP	AP	EP
0.95	12.37	12.37	19.45	19.40	19.93	19.93
0.40	12.06	12.06	18.82	18.74	19.25	19.22
0.20	9.87	9.85	15.06	15.00	15.36	15.33

Test No. 3

Purpose: To test the potential calculation for a two dimensional problem with a single homogeneous isotropic medium.

Problem Geometry: As shown on Figure A.4(c), the problem consisted of finding the potential between two infinitely long wires, one held at a potential of 100 volts and the other held at a potential of -100 volts. The problem is symmetric about the plane intersecting the two wires and is antisymmetric about the plane midway between the two wires. The problem includes the effects of the finite wire diameter. An analytic solution to this problem is given on pages 186 to 188 of Ramo, Whinnery, and Van Duzer. For the dimensions shown on Figure A.4(c), the analytic solution for the potential is

$$\psi = 12.213 \ln\left[\frac{(y + 2.9983)^2 + x^2}{(y - 2.9983)^2 + x^2}\right]$$

EPEIOS Input File: Distances for this test problem are measured from an origin located midway between the two wires. The Y direction pointed upward through one of the wires and the X direction is perpendicular to the plane intersecting the two wires. The use of the finite difference method in EPEIOS requires that a no-flow boundary be imposed enclosing the problem domain at a finite distance. For the test run, this outer boundary was set at a distance of 27.5 m in the Y direction and 52 m in the X direction. The one half of the circular wire cross-section that was in the problem domain was represented by a structure of six square grid blocks. The input file was as follows:

```
 &INPUT1
   LABEL1='Two Dimensional Cartesian Potential Test',
   LABEL2='Two Line Voltages Sources - One Quadrant',
   MNSTEP=3, LRESTA=.FALSE., NREC=1
 &END
 &INPUT2     NX=40,NY=40,NZ=4,
  DELTAX=4*.05,4*.1,4*.2,4*.4,4*.8,2*1.6,18*3.0,
  DELTAY=.001,.399,3*.4,4*.2,4*.1,8*.05,2*.1,2*.2,
         2*.4,2*.8,2*1.6,2*3.0,7*4.0,
  DELTAZ=4*.25,
  NREG=4, NELECT=2, TINIT=24.,
 &END
 &REGION MINX=1,MAXX=40,MINY=2,MAXY=40,MINZ=1,MAXZ=4,
   ETYPE='COND',ALPHA1=2.E-2,C24=2.,
   TTYPE='COND',THMM=1.5E6,THMK=2.,
 &END
 &REGION MINX=1,MAXX=2,MINY=17,MAXY=18,MINZ=1,MAXZ=4,
   ETYPE='ELEC',ELENUM=1,
   TTYPE='INSU',
 &END
```

```
&REGION MINX=1,MAXX=1,MINY=16,MAXY=19,MINZ=1,MAXZ=4,
  ETYPE='ELEC',ELENUM=1,
  TTYPE='INSU',
&END
&REGION MINX=1,MAXX=40,MINY=1,MAXY=1,MINZ=1,MAXZ=4,
  ETYPE='ELEC',ELENUM=2,
  TTYPE='INSU',
&END
&INPUT3
   NSPO=10, NSTO=1000, NPX=5, NPY=5, NPZ=2,
   XMIN=.025, XMAX=3.4,
   YMIN=.6,YMAX=5.8,ZMIN=.25,ZMAX=.50
&END
&INWELL
   DTIME=1.E-2,TTIME=2.E5,NTYPE=1,
   DSIGMA=.01,L1PHAS=.TRUE.,RESMAX=1.E-5,
   ELEVOL=100.,0.,0.,0.,
&END
```

Results As shown below, the maximum error in calculated potential was 0.4 volts, which represents a relative error of 1.6%. The columns below headed "AN" are the analytic solution and the columns headed "EP" are EPEIOS results.

X(m)	.025		.869		1.712		2.556		3.40	
	AN	EP	AN	EP	AN	EP	AN	EP	AN	EP
Y(m)										
5.8	27.9	27.9	26.9	26.9	24.5	24.5	21.5	21.5	18.6	18.5
4.5	39.3	39.3	35.9	35.8	29.7	29.5	24.0	23.9	19.4	19.2
3.2	83.5	83.5	47.6	47.2	32.2	31.9	23.5	23.4	17.8	17.6
1.9	36.5	36.2	31.0	30.7	22.9	22.7	16.8	16.7	12.5	12.3
0.6	9.9	9.8	9.1	9.0	7.4	7.3	5.6	5.6	4.2	4.2

Test 4

Purpose: To verify that the energy equation was solved correctly for heat conduction in a multiple media problem, and to verify that the calculation of the heat lost to constant temperature surfaces was done correctly.

Problem Geometry: This test problem is a heat conduction analog to the current conduction problem of Test #1. The problem geometry is that shown in Figure A.4(a), with the exception that the electrodes are replaced with two constant temperature surfaces. The first constant temperature surface was placed in the position of Electrode #1 on Figure A.4(a), and was held at a constant temperature of 120°C. The second constant temperature surface was placed in the position of Electrode #2, and was held at a constant temperature of 20°C. The initial temperature of the three heat conducting media in the problem was 24°C. Medium #1 had a thermal conductivity of 2.0 W/m·K, Medium #2 had a thermal conductivity of 10.0 W/m·K, and Medium #3 had a thermal conductivity of 100.0 W/m·K. A steady state analytical solution to this problem may be obtained in a manner similar to that used to solve the current conduction problem (Test #1).

$T = 120. - 16.393 \cdot x$ Region #1
$T = 38.03 - 3.279 \cdot x$ Region #2
$T = 21.64 - 0.328 \cdot x$ Region #3

EPEIOS Input File: The EPEIOS input file for this problem was as follows.

```
 &INPUT1
   LABEL1='Test No. 7  -  One Dimensional, Three Media',
   LABEL2='Constant Temperature Surfaces',
   LABEL3='Analytically Solvable.        ',
   MNSTEP=140, LRESTA=.FALSE., NREC=1,
   CPUMAX=20., COSTMA=20.
 &END
 &INPUT2
   NX=25, NY=2, NZ=2,
   DELTAX=.01,.5,4*1.0,.5,2*.25,.5,3*1.0,.5,
           4*.25,.5,3*1.0,2*.5,.01,
   DELTAY=2*.5,
   DELTAZ=2*.5,
   NREG=5, TINIT=24.,
 &END
 &REGION   MINX=2,MAXX=7,MINY=1,MAXY=2,MINZ=1,MAXZ=2,
    ETYPE='COND',ALPHA1=2.E-2,C24=2.0,
    TTYPE='COND',THMM=1.5E6,THMK=2.0,
 &END
 &REGION   MINX=8,MAXX=16,MINY=1,MAXY=2,MINZ=1,MAXZ=2,
   ETYPE='COND',ALPHA1=2.E-2,C24=10.,
   TTYPE='COND',THMM=1.5E6,THMK=10.0,
&END
&REGION   MINX=17,MAXX=24,MINY=1,MAXY=2,MINZ=1,MAXZ=2,
   ETYPE='COND',ALPHA1=2.E-2,C24=100.,
   TTYPE='COND',THMM=1.5E6,THMK=100.0,
&END
&REGION   MINX=1,MAXX=1,MINY=1,MAXY=2,MINZ=1,MAXZ=2,
   ETYPE='INSU',
   TTYPE='CTEM',TEMPER=120.,
&END
&REGION   MINX=25,MAXX=25,MINY=1,MAXY=2,MINZ=1,MAXZ=2,
   ETYPE='INSU',
   TTYPE='CTEM',TEMPER=20.,
&END
&INPUT3
   NSPO=120,NSTO=10000,NPX=6,NPY=1,NPZ=1,LUSPL=.TRUE.,
   XP=1.,4.,6.,9.,11.,14.,YP=.5,ZP=.5,
   PTIMES=1.E6,1.E7,1.5E7,2.5E7
&END
&INWELL
  TTIME=5.E7,NTYPE=4,
  DTMAX=.1,
&END
```

Results: The simulation was run to a time of 1.5×10^{7} seconds at which point a steady state temperature distribution had been obtained. The analytic and EPEIOS temperatures are as follows.

Distance from Constant Temperature Surface #1 in meters	1.0	4.0	6.0	9.0	11.0	14.0
Temperatures in Celsius						
Analytic	103.6	54.43	34.75	24.92	21.31	20.33
EPEIOS	103.6	54.20	34.53	24.85	21.28	20.33

When these steady state temperatures had been reached, the thermal energy of the problem domain had increased by 4.3×10^{8} Joules from its inital state. EPEIOS predicted that during the transient period prior to steady state a total of 4.1×10^{8} Joules more energy had entered the problem domain from the hotter Constant Temperature Surface #1, than were lost from the cooler Constant Temperature Surface #2. A comparison between the increase in thermal energy and the net heat inflow indicates the accuracy of the heat loss to constant temperature surfaces calculation.

TCTM-EPEIOS Test

As both the ARC Two Component Thermal Model and EPEIOS had been tested separately, only minimal testing was necessary to ensure that the coupling between the two programs was correct.

Test No. 5

Purpose To verify that the proper values of temperatures, porosities, and saturations were passed from TCTM to EPEIOS, that the proper conductivity calculations occurred, and that the proper conversion of the heating rates was made before they were returned to TCTM.

Problem Geometry This problem considers the electrical heating of two media located adjacent to one another between two parallel plate electrodes, as shown in Figure A.5. The current in each will flow independently of the current in the other, and there will be a uniform voltage drop across both media. However, as the two media had different electrical conductivities, there were different heating rates in each medium. By adjusting the electrical conductivities to be proportional to the heat capacities of the media, the same temperature increase occurred in each medium. If the electrical conductivity does not vary with temperature, the temperature at a time t is given by

$$T = T_0 + 4.63x10^{-4} \cdot t$$

where t is measured in seconds.

The properties of the two media are as follows.

Property	Material #1	Material #2
Density (g/cm*3)	2.1	2.1
Porosity	0.332	0.340
Water Saturation	0.443	0.124
Oil Saturation	0.557	0.876
Gas Saturation	0.0	0.0
Permeability (darcies)	1.0	3.0
Connate Water Electrical Conductivity (S/m)	0.0724	0.8
Heat Capacity (MJ/m*3K)	2.28	2.04
Heating Rate (W/m*3)	1055.6	944.6

Note that in TCTM-EPEIOS the volumetric heat capacity is not input, but rather is calculated from the porosity, saturations, densities, and specific heat capacities of each of the oil, water, gas, and rock phases. Similarly, the heating rates shown on the above table were not input but were calculated.

Results: After a period of slightly more than one day of

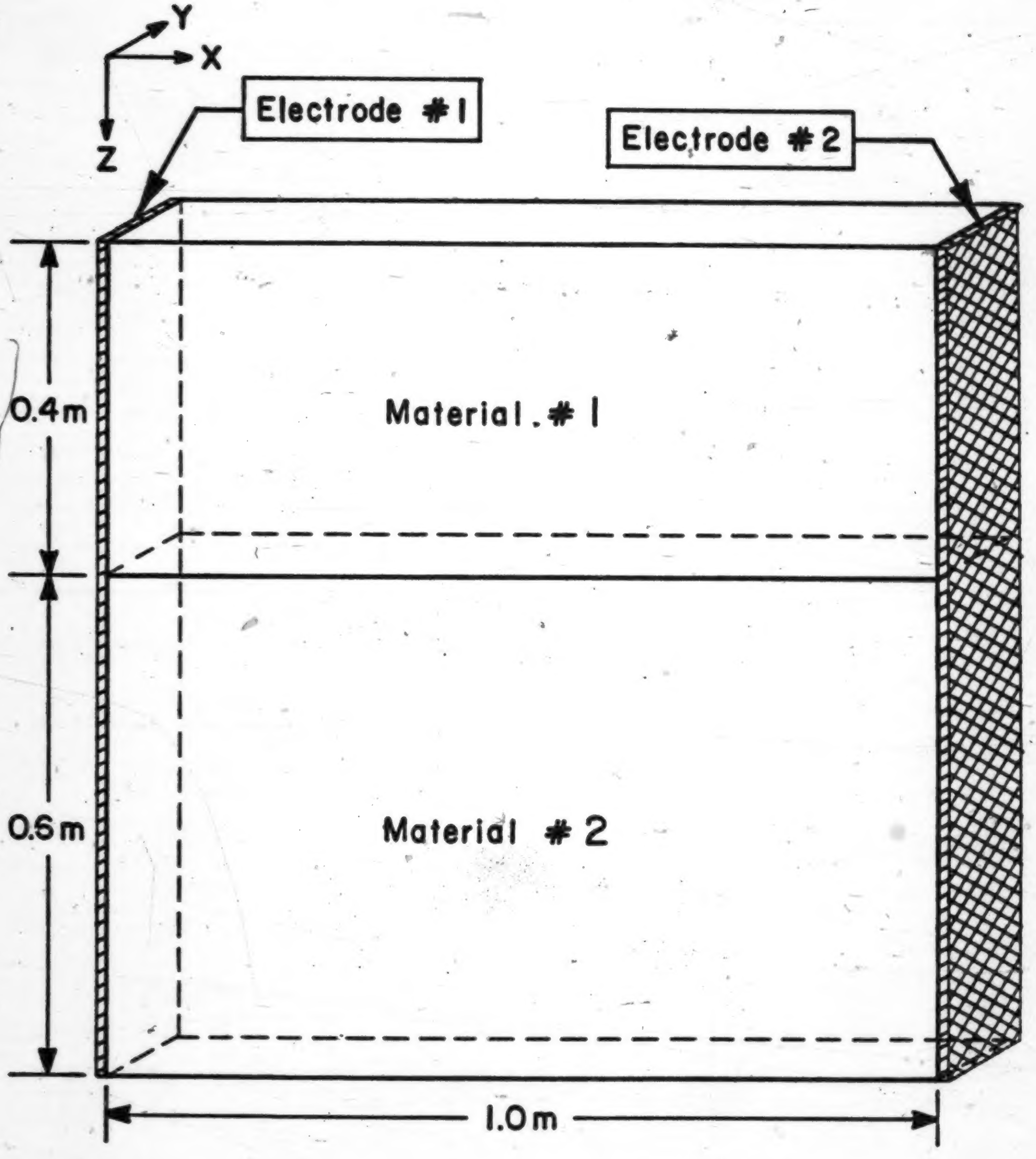
Y
X
Z
Electrode #1
Electrode #2
0.4m
0.6m
Material. #1
Material #2
1.0m

Figure A.5 The geometry used by Test No. 5.

heating, the analytic solution for the temperature gave a uniform temperature increase in both media of 41.1°C. The results produced by TCTM-EPEIOS showed temperature increases at the grid block centers of between 41.8°C and 42.8°C.